Interactions of Quinolinols, Peptides and SNAP-25 with the Protease Domain of Botulinum Neurotoxin A

A dissertation
submitted to the Faculty of the
Graduate School of Arts and Sciences
of Georgetown University
in partial fulfillment of the requirements for the
degree of
Doctor of Philosophy
in Chemistry

By

Huiguo Lai, M.S.

Washington, DC

September 21, 2010

INTERACTIONS OF QUINOLINOLS, PEPTIDES AND SNAP-25 WITH THE PROTEASE DOMAIN OF BOTULINUM NEUROTOXIN A

Huiguo Lai

Thesis Advisor: David C. H. Yang, Ph.D.

ABSTRACT

SNAP-25, an intrinsically disordered protein, assembles with syntaxin and synaptobrevin to form a SNARE (soluble N-ethylmaleimide-sensitive factor attachment protein receptor) complex, a four-helix bundle that plays a key role in the exocytosis of synaptic vesicles. Botulinum neurotoxins specifically cleave one of the SNARE proteins, resulting in the inhibition of membrane fusion. Small molecule inhibitors are being evaluated as potential therapeutic counter-measurement to the toxin's deleterious action on the neuromuscular junctions.

In order to understand the conformational changes exhibited by SNAP-25 prior to and during SNARE complex formation, and its biological function, we developed a method of investigating the conformational changes of SNAP-25 in the absence and presence of Zn^{2+}-depleted BoNT/A LC (botulinum neurotoxin A light chain), using FRET (fluorescence resonance energy transfer) between EGFP (enhanced green fluorescent protein) and CCPGCC-ReAsH fused to SNAP-25 at specific locations. The apparent distances between the C-terminus and the N-terminus, the C-terminus and the D140, and the N-terminus and the D140 of the SNAP-25 protein were determined based on the FRET efficiency in the absence and presence of Zn^{2+}-depleted BoNT/A LC. Various mutants of SNAP-25(A195S) were genetically engineered and used to measure the tertiary structures of SNAP-25(A195S) in the absence and presence of active BoNT/A

LC. Shorter apparent distances in the presence of BoNT/A LC suggest that the SNAP-25 folds around BoNT/A LC in the binary complex. FRET is a useful tool to investigate the conformational changes of other intrinsically disordered proteins.

The secondary structures of the full length SNAP-25(1-206), the N-terminal SNAP-25(1-140), and the C-terminal SNAP-25(141-206) and their corresponding N-terminal CCPGCC modified fragments were measured by CD. The results suggest that SNAP-25 and its N-terminal and C-terminal domains are intrinsically disordered proteins. Higher α-helical content was observed when the N-terminal and the C-terminal domains of the SNAP-25 bound to BoNT/A LC. We found that not only the C-terminal domain of SNAP-25(141-206), but also the N-terminal domain of SNAP-25(1-140) specifically bound to BoNT/A LC by means of a slow and tight binding.

Quinolinol derivatives were found to be effective inhibitors of botulinum neurotoxin serotype A (BoNT/A). Studies of the inhibitors and binding of 7-phenyl(8-quinolinylamino)-8-quinolinol (QAQ) to BoNT/A LC demonstrated that QAQ is a non-competitive inhibitor of zinc protease activity. Binding and molecular modeling studies revealed that QAQ binds to a hydrophobic pocket near the active site. A 24-mer SNAP-25 peptide, containing E183 to G206, with a Q197C mutation (Peptide C), binds to BoNT/A LC with an unusually slow second order binding rate constant of 76.7 $M^{-1}\cdot s^{-1}$. QAQ binds to Zn^{2+}-depleted BoNT/A LC with a K_D of 0.67 μM and to the Peptide C-BoNT/A LC complex with a K_D of 2.33 μM. Insights into the interactions between the quinolinols and peptides and the zinc protease of BoNT/A should aid in the development of metalloprotease inhibitors.

ACKNOWLEDGEMENTS

I wish to express my thanks to my thesis advisor, David C. H. Yang, for his guidance and wisdom throughout my thesis design and composition. He has helped me with dedication, consistent encouragement and infinite patience. Dr. Yang has been a father figure and a close friend, assisting me throughout this process whenever necessary.

I thank Leonard A. Smith and his group members, especially Virginia Roxas-Duncan, for the partial financial support and huge contribution to the study's outline. I am also grateful to his suggestions and discussions during the course of developing my experimental design and writing the thesis.

In addition to thanking the faculty members and staff of the chemistry department at Georgetown University, I would like to thank Dr. Yang's research group members for their help throughout my thesis, especially Minghao Feng for his cooperation and daily computer assistance.

I would like to thank my parents, Mingzao Lai and Mingfang Dong, for their kind encouragement and support of everything I have set out to accomplish, particularly with regard to the completion of this thesis. In addition, I thank my wife, Haojin Zhang, who is carrying our unborn baby at the time of this writing for her understanding and support.

Finally, I would like to express my gratitude to the thesis committee members for reviewing my thesis and providing suggestions during my defense.

TABLE OF CONTENTS

Page

LIST OF TABLES

LIST OF EQUATIONS

LIST OF FIGURES

ABBREVIATIONS

BAPQ: 7-((2-bromoaminlino)(8-quinolinylamino)methyl)-8-quinolinol, NSC 84086;

BoNT: botulinum neurotoxin

BoNT/A: *Clostridium botulinum* neurotoxin serotype A

BSA: bovine serum albumin

CAPQ, 7-((4-chloroanilino)(phenyl)methyl)-8-quinolinol, NSC 84090

CD: circular dichroism

DTT: dithiothreitol

CT: carboxyl-terminus of the SNAP-25

EDT: 1,2-ethanedithiol

EDTA: ethylenediaminetetraacetic acid

EGFP: enhanced green fluorescent protein

ELISA: enzyme-linked immunosorbent assay

FlAsH: fluorescein arsenic hairpin

FRET: fluorescence resonance energy transfer

GST: glutathione S-transferase

HC: heavy chain

IPTG: isopropyl-β-D-1-thiogalactopyranoside

K_d: dissociation constant

LC: light chain

NAPQ, 7-((4-hydroxy(oxido)amino)amilino)(phenyl)methyl)-8-quinolinol, NSC 1010

NEM: N-ethylmaleimide

NSC: national statics clearinghouse

NSF: NEM-sensitive fusion; N-ethylmaleimide sensitive fusion

NT: amino-terminus of the SNAP-25; NH_2-terminus of the SNAP-25

ORF: open reading frame

PAR: 4-(2-pyridylazo)resorcinol

10× PBS: phosphate buffer saline (80 g NaCl; 2.0 g KCl; 14.4 g Na_2HPO_4 (anhydrous); 2.4 g KH_2PO_4 (anhydrous) in 1.0 liter distilled H_2O, pH 7.4)

PCR: polymerase chain reaction

PMSF: phenylmethylsulfonyl fluoride

QAQ: 7-(phenyl(8-quinolinylamino)-8-quinolinol

ReAsH: resorufin arsenic hairpin

RT-PCR: reverse transcription polymerase chain reaction

Sb: synaptobrevin

SDS-PAGE: sodium dodecyl sulfate-polyacrylamide gel electrophoresis

SNAP: soluble NSF attachment protein

SNAP-25: synaptosomal-associated protein of 25 kDa

SNARE: soluble NSF attachment protein receptor

SNARE: soluble N-ethylmaleimide-sensitive factor attachment protein receptor

Sx: syntaxin

TC: tetracysteine tag, CCPGCC

TCEP: tris(2-carboxyethyl)phosphine

TMR: transmembrane region

VAMP: vesicle-associated membrane protein (synaptobrevin)

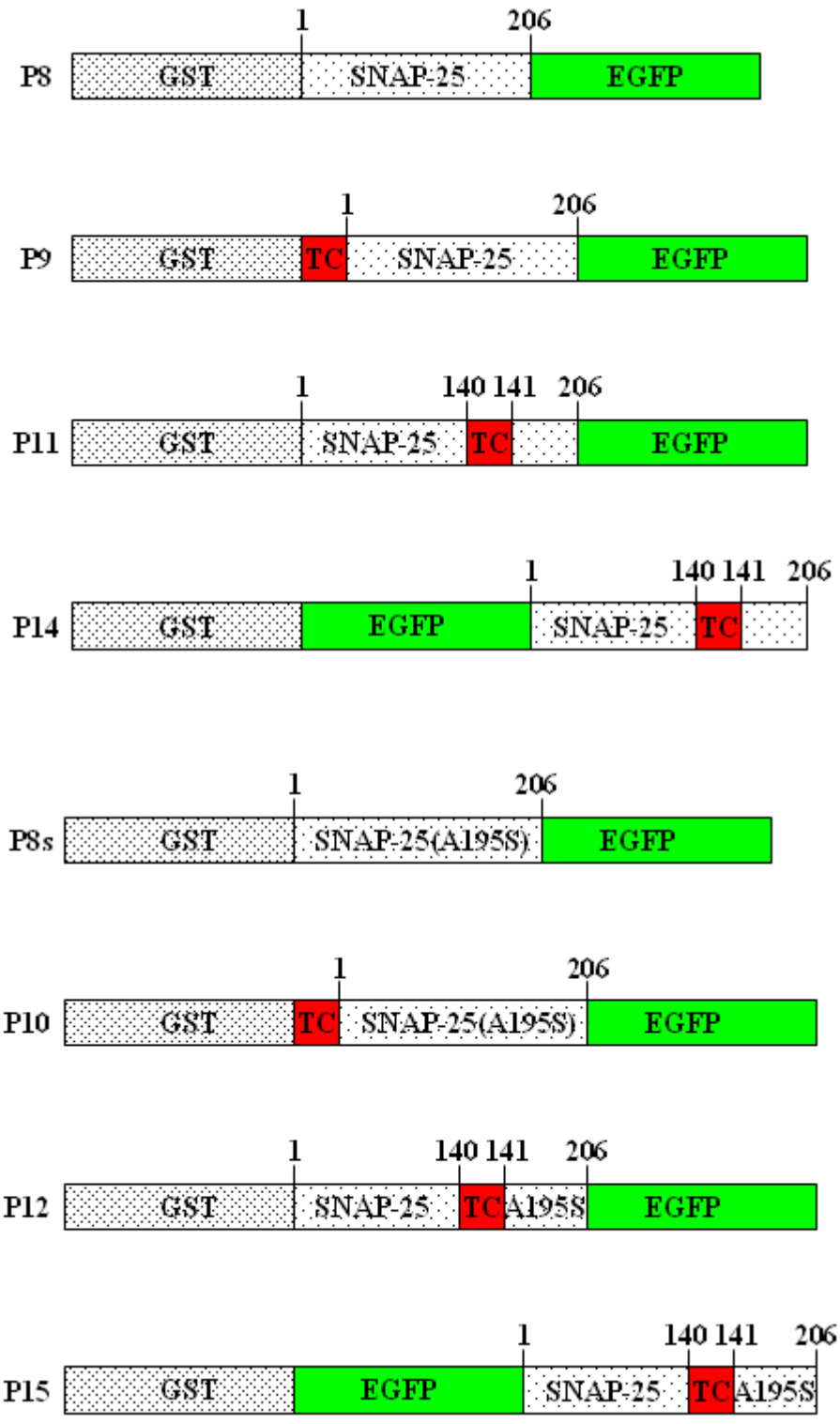
P8
1
206
GST
SNAP-25
EGFP
P9
1
206
GST
TC
SNAP-25
EGFP
P11
1
140 141
206
GST
SNAP-25
TC
EGFP
P14
1
140 141
206
GST
EGFP
SNAP-25
TC
P8s
1
206
GST
SNAP-25(A195S)
EGFP
P10
1
206
GST
TC
SNAP-25(A195S)
EGFP
P12
1
140 141
206
GST
SNAP-25
TC
A195S
EGFP
P15
1
140 141
206
GST
EGFP
SNAP-25
TC
A195S

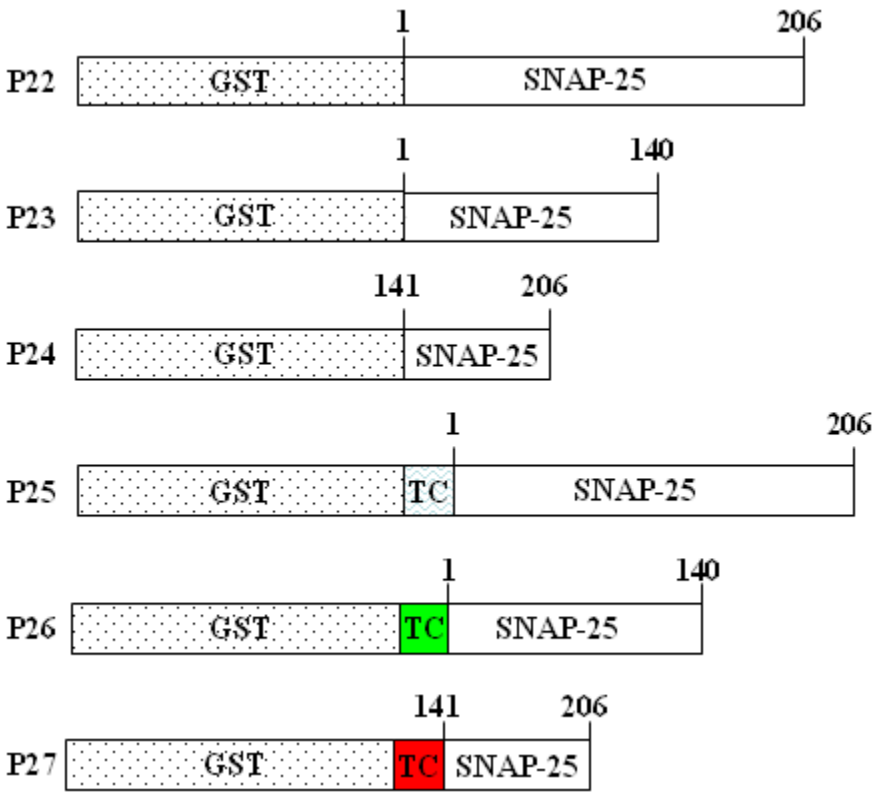

P8, **P9**, **P10**, **P11**, **P12**, **P14** and **P15** represent the proteins corresponding to plasmid **8**, **9**, **10**, **11**, **12**, **14** and **15**, respectively. When GST was removed, the proteins were named as **P22R**, **P23R**, **P24R**, **P25R**, **P26R** and **P127R** corresponding to the GST-tag proteins **P22**, **P23**, **P24**, **P25**, **P26** and **P27**, respectively. EGFP indicates the enhanced green fluorescent protein. TC represents tetracysteine (CCPGCC) motif. When FlAsH or ReASH was labeled in an individual protein, a fluorescent probe of green (CCPGCC-FlAsH) and red (CCPGCC-ReAsH) was coded. For example, **P27R-ReAsH** represents CCPGCC(ReAsH)-SNAP-25(141-206, A195S)

Chapter 1. Introduction

The neuronal system performs numerous functions through an orderly execution of membrane fusion, which is precisely timed communication among all the complex compartments (1). The complicated processes of membrane fusion occur in a short amount of time. The SNARE (Soluble N-ethylmaleimide-sensitive factor attachment protein receptors) proteins play a key role in membrane fusion. Botulinum neurotoxins can specifically cleave the SNARE proteins to block the neurotransmission, resulting in muscular paralysis. Inhibitors are developed to eliminate the protease activity facilitating the restoration of membrane fusion.

1.1 Membrane fusion

Intracellular membrane fusion is a fundamental cellular process in which vesicles from one compartment fuse with their target compartments. Soluble N-ethylmaleimide sensitive fusion (NSF) attachment receptor (SNARE) proteins are essential for various types of intracellular membrane fusion in eukaryotes. There are three proteins in the SNARE complex: synaptosome-associated protein 25 kD (SNAP-25), syntaxin, and synaptobrevin, which is a vesicle-associated membrane protein (VAMP). SNARE proteins assemble into a four-helix bundle and mediate membrane fusion, which plays a central role at the synapse. The SNARE proteins can mediate synaptic vesicle docking and fusion with the presynaptic membrane (2). Cleavage at any one of the three proteins in the SNARE complex by BoNTs inhibits exocytosis (3).

1.2 Classification of SNAREs

The SNARE proteins can be classified according to their locations they are found before and after membrane fusion.

1.2.1 *t*-SNAREs and *v*-SNAREs

SNAREs have been studied extensively in neurons and other secretory cells. SNARE proteins help secretory vesicles to fuse with the plasma membrane (1). SNAREs can be divided into two categories according to the localization of their homologues within nerve terminal membranes. When two membranes fuse, SNAREs related to synaptobrevin on the vesicle membrane are called *v*-SNAREs, whereas SNAREs related to syntaxin and SNAP-25 in the target membrane are called *t*-SNAREs.

1.2.2 *trans*-SNAREs and *cis*-SNAREs

The *v*-SNAREs and *t*-SNAREs intertwine by pulling their individual membranes closer to form a tight complex. The *t*-SNAREs are on the plasma membrane and the *v*-SNAREs are on the vesicle membrane. They are anchored in different membranes before membrane fusion, when they are called *trans*-SNAREs. When the vesicle membrane is trying to fuse with plasma membrane, SNARE proteins are involved to form a four-helix bundle complex during the membrane fusion (1, 2). Once the vesicle membrane and plasma membrane are close enough, the two membranes fuse together to form one membrane. The *v*-SNAREs and *t*-SNAREs reside in the same resultant membranes, which are called *cis*-SNAREs. The SNARE complexes are extremely stable and energy is required to disassemble the SNAREs during membrane recycling. The energy can be

provided by hydrolysis of ATP, which comes from the protein called NSF (N-ethylmaleimide-sensitive factor).

1.2.3 *R*-SNAREs and *Q*-SNAREs

R-SNAREs and *Q*-SNAREs are named such based on the components in the formation of the *zero ionic layer* (2). *R*-SNAREs and *Q*-SNAREs provide one arginine (R) residue and three glutamine (Q) residues, respectively, in the formation of the *zero ionic layer* in the assembled core SNARE complex. For example, synaptobrevin belongs to *R*-SNAREs, which are also called *v*-SNAREs because of their location in the synaptic vesicles. *Q*-SNAREs are syntaxin and SNAP-25, which are located in the plasma membranes. *Q*-SNAREs belong to *t*-SNAREs in the target membrane.

1.3 Structure of SNAREs

SNARE proteins are abundant in neuronal cells. Each SNARE protein provides a *SNARE motif*, which consists of 60-70 amino acids and forms a long range of α-helical component. In neuronal exocytosis, syntaxin and synaptobrevin are anchored in their respective membranes by their C-terminal domains, whereas SNAP-25 is tethered to the plasma membrane via several cysteine-linked palmitoyl chains. The core SNARE complex is a four-α-helix bundle (2), where one α-helix is contributed by syntaxin-1A, one α-helix by synaptobrevin, and two α-helices are contributed by SNAP-25. Each protein has different subdomains, except for the SNARE motif. The domain diagram of the proteins is shown in **Figure 1**.

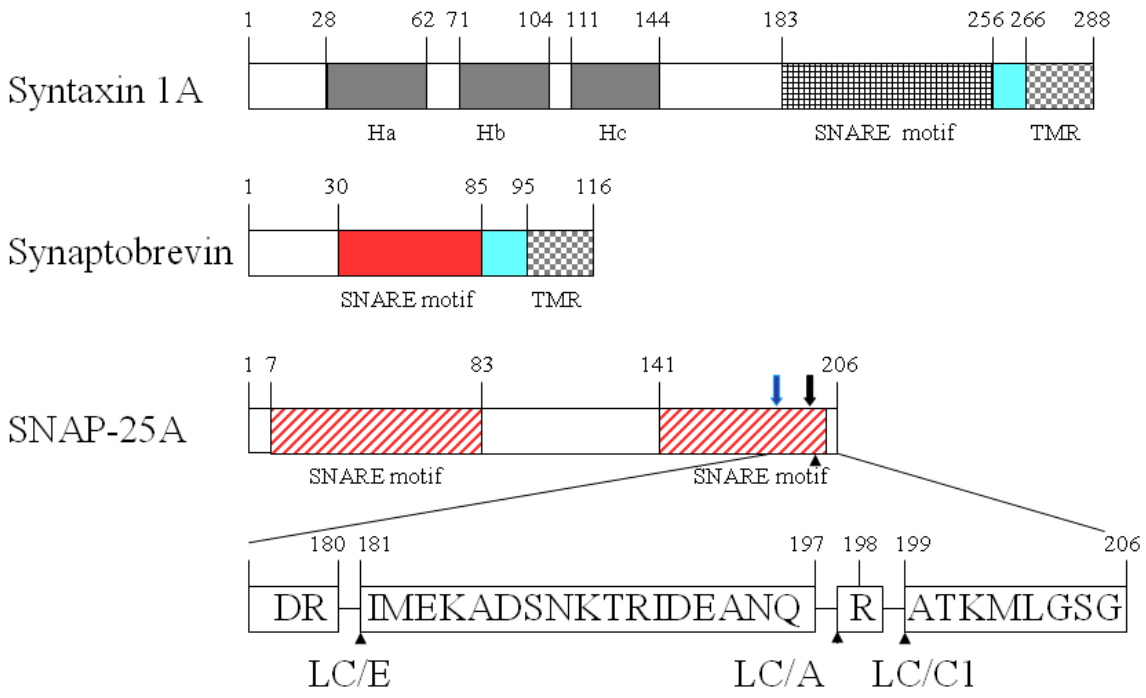

Figure 1. Schematic representation of SNARE complex. Domain diagrams of syntaxin 1A, synaptobrevin and SNAP-25A are shown in **Figure 1** above. TMR indicates the trans-membrane region, which is embedded in the membrane and maintains a helical conformation inside the membrane. SNARE motifs are the domains that form the helical bundle. The numbers on top of the boxes indicate the amino acid residue number corresponding to each protein. H_a, H_b and H_c refer to the subdomains of three consecutive helical components in syntaxin 1A. The arrows near the C-terminus of the SNAP-25A indicate the cleavage sites by the light chains of botunilum neurotoxins: BoNT/E LC specifically cleaves between R180 and I181, BoNT/A LC specifically cleaves between Q197 and R198 and BoNT/C1 LC specifically cleaves between R198 and A199.

1.3.1 Structure of the *zero ionic layer*

The core of the SNARE complex contains a four-α-helix bundle. Synaptobrevin and syntaxin contribute one α-helix each, while SNAP-25 participates with two α-helices (abbreviated as SN1 and SN2). The amino acid residues forming SNARE complex can be grouped into layers, which are clearly visible from the direction along the bundle. Each layer contains four amino acids, which are provided by four different SNARE motifs in the bundle. At the center of the complex is the *zero ionic layer*, composed of one arginine (R) and three glutamine (Q) residues (2). For example, in **Figure 2**, R56 of VAMP-2, Q226 of syntaxin-1A, Q53 of SNAP-25 (SN1 region) and Q174 of SNAP-25 (SN2 region) can form the *zero ionic layer* in a stable SNARE complex. All the layers are flanked by leucine zippering. The *zero ionic layer* is completely buried within the leucine-zipper layers. The positively charged guanidinum groups of the arginine (R) residue interacts with the carboxyl group of the glutamine (Q) residue and each glutamine provides one carboxylgroup. The R-Q_a-Q_b-Q_c residues form a *zero ionic layer* that has the largest diameter in the bundle. From the N-terminal to the C-terminal of the four-helical-bundle structure, 16 layers are composed of the bundle, which is labeled from -7 to +8 consecutively. Layers "-1", "+1" and "+2" at the center of the complex are near the *zero ionic layer*, which act as a water-tight seal to protect the *zero ionic layer* interactions from the surrounding solvent. The flanking leucine-zipper can be disassembled by α-SNAP and NSF in order to recycle SNARE proteins after the completion of synaptic vesicle exocytosis. A diagram of the *zero ionic layer* is shown in **Figure 2**.

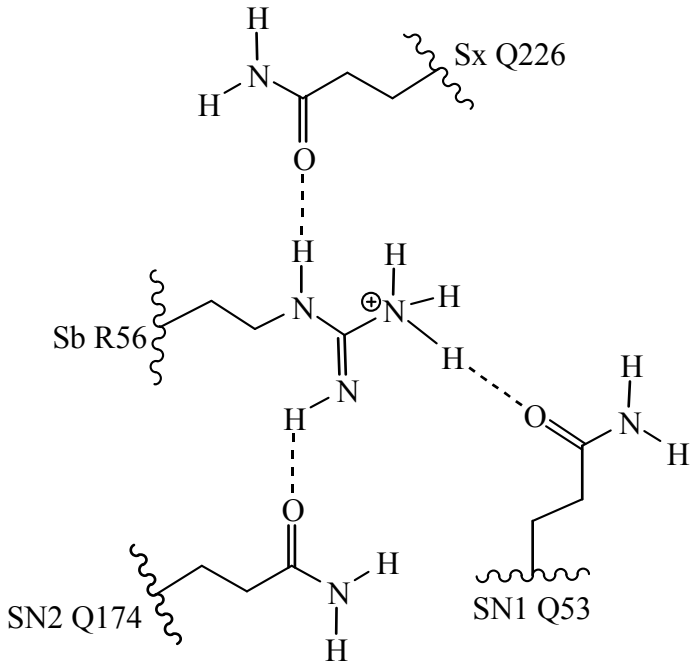

Figure 2. Diagram of *zero ionic layer* of the SNARE complex. The side chains are shown as solid lines; backbones are shown as curved lines; and the dotted lines indicate hydrogen bonds. Sx and Sb are abbreviations for syntaxin and synaptobrevin, respectively.

1.3.2 Structure of syntaxin

The syntaxins are a family of *Q*-SNARE proteins, which localize in the plasma membranes. Two isoforms have been identified, called syntaxin A and B (4). Syntaxin 1A, which contains 288 amino acid residues, plays an important role in neurotransmitter release through multiple protein-protein interactions (**Figure 1**). Three major parts include an N-terminal regulatory domain (Habc), a SNARE motif toward the C-terminus and a C-terminal transmembrane region (TMR). In the N-terminal, Habc domain contains three α-helices. The three-dimensional structure of Habc domain is demonstrated by NMR, and the crystal structure shows the three α-helices structures (5-7). Three helical

structures occupy the residue of 28 to 144. A helical structure (called H3 domain) at amino acid residues 183-266 constitutes a SNARE motif. In this region, the SNARE motif binds to both synaptobrevin and SNAP-25 to form the core of the SNARE complex, which is believed to generate the free energy required to initiate fusion between the vesicle membrane and plasma membrane (7). Trans-membrane segments of syntaxin play an important role in the Ca^{2+}-triggered exocytosis (8). The transmembrane region maintains a helical conformation inside the membrane (9).

1.3.3 Structure of synaptobrevin

Synaptobrevins have two isotypes, called synptobrevin-1 and synaptobrevin-2 (10). Synaptorevein-2 is the predominant form with 116 amino acid residues (**Figure 1**). The residues between 30 and 85 form the SNARE motif. The molecular weight of synaptobrevin is 18 kD. Synaptobrevin associates with SNAP-25 and syntaxin to form a stable four-helical bundle (2). In the presence of botulinum neurotoxin B, synaptobrevin is cleaved between Gln76 and Phe77. As the toxin active site is very deep, the cleavage is restricted to a single scissile bond of synaptobrevin. The botulinum neurotoxin B is unable to cleave the synaptobrevin substrate once the SNARE complex has formed. The C-terminus is a transmembrane region, which maintains an α-helical conformation inside the membrane (10).

BoNT/B cleaves the synaptobrevin, requiring a minimal nine residues and a proper sequence, which is termed the SNARE secondary recognition (SSR) sequence. The co-crystal structure of synaptobrevin peptide (Sb residue 33-88) and BoNT/B LC showed that the two proteins formed a stable Sb2-BoNT/B LC complex (11). However,

this report was retracted in July 2009 because of the lack of clear and continuous electron density for the peptide in the complex structure.

1.3.4 Structure of SNAP-25

SNAP-25 is an abbreviation for synaptosomal-associated protein 25 kD, which is a protein encoded by the *SNAP-25* gene. The *SNAP-25* gene in chicken contains 8 exons. Alternative usage of two variants of exon 5 accounts for the existence of two isoforms: SNAP-25A and SNAP-25B. The two isoforms differ in a nine-amino acid sequence containing the four central cysteine residues (12). SNAP-23 and Syndet, like SNAP-25, have regions with high probabilities of forming coiled coils, a cysteine rich-domain, and lack transmembrane domains (13).

The SNAP-25 provides two helices of the SNARE complex, which is believed to mediate membrane fusion. The SNARE complex directly executes fusion by forming a tight complex that brings the synaptic vesicle and plasma membranes together. SNAP-25 is a hydrophilic protein with 206 amino acid residues, which can be cleaved by botulinum neurotoxin serotype A, C1 and E (BoNT/A, C1 and E) near the C-terminus. BoNT/A specifically cleaves the peptide bond between Gln197 and Arg198 (14); BoNT/C1 specifically cleaves the peptide bond between Arg198 and Ala199 (14); and BoNT/E specifically cleaves between Arg180 and Ile181 (15). The details of cleavage sites are shown in **Figure 1**. Once the SNAP-25 is cleaved from any of these positions in the chain, the SNARE complex cannot be formed, resulting in the blockage of the neurotransmitter release at neuromuscular junctions. However, once the SNARE complex is formed, the SNAP-25 cannot be cleaved by botulinum neurotoxin.

In the SNARE complex, both syntaxin and synaptobrevin contain the C-terminal transmembrane domain, which is embedded in the membrane (9). However, SNAP-25 lacks a trans-membrane domain. It associates with membranes through palmitoyl chains that are thioester-linked to four closely spaced cysteine residues in the protein (16). The corresponding sequence is summarized in **Table 1**.

Table 1. Comparison of cysteine cluster

TYPE	Sequence
SNAP-25A	^{81}L G K **C** **C** G L F I **C** P **C** N K L K ^{97}S
SNAP-25B	^{81}L G K F **C** G L **C** V **C** P **C** N K L K ^{97}S
SNAP-23	^{76}L N K **C** **C** G L **C** V **C** P **C** N R T K ^{92}N
Syndet	^{76}L N K **C** **C** G L **C** I **C** P **C** N R T K ^{92}N

The four Cys of SNAP-25 are required for optimal palmitoylation, and each Cys may be a target for palmitoylation. It is interesting that the palmitoylation appears to be highly dependent on the presence of multiple Cys residues. Deletion of a 12 amino acid sequence containing the four Cys residues of SNAP-25 abolishes palmitoylation and membrane association of the protein, suggesting that palmitoylation is required for membrane fusion (17).

SNAP-25, a *Q*-SNARE protein, contributes two α-helices in the formation of the exocytotic fusion complex in neurons, where it assembles with syntaxin-1 and synaptobrevin. The N-terminal 7-83 of SNAP-25 provides a SNARE motif, and the C-terminal 141-204 of SNAP-25 provides another SNARE motif. The two SNARE motifs are connected with a flexible linker (residue 84-140). The linker might have evolved as an adaptation toward a high rate of execution of the fusion process (18). However, the

structures and functions of the linker domain are unknown. The linker domain is presumed to be exposed and disordered in the complex *in vitro* because of its susceptibility to proteolytic cleavage. In the linker region, the protein chain reorients to accommodate the parallel orientation of both SNAP-25 helices in the synaptic fusion complex. Various fragments of SNAP-25 fused with GFP were tested to define and characterize the plasma membrane-targeting domain of SNAP-25 (19). The 36 amino acids, between 85 and 120 of SNAP-25, are important residues in membrane targeting.

The N-terminal of SNAP-25 can specifically bind to syntaxin and induce a conformational change (20). The N-terminal of SNAP-25(7-83), referred to as SN1, forms a SNARE motif in the SNARE complex. Syntaxin and SNAP-25 form a stable complex that contains two syntaxin molecules, one of which occupies and possibly obstructs the binding site of synaptobrevin. The SNARE assembly begins with the slow and rate-limiting interaction of syntaxin and SNAP-25. The interaction is prevented by N-terminal, but not by C-terminal truncations. For productive assembly, all three participating helices must come together simultaneously (21). The binary complex of SNAP-25 and syntaxin is a dynamic acceptor for synaptobrevin binding, resulting in a ternary complex (22). The ternary complex formation can be the binary complex binds to another syntaxin to form a 1 : 2 helix-bundle or the binary complex binds to the VAMP to from a 1 : 1 : 1 bundle, and not affected by the presence of the regulatory domain (23).

The neuronal SNARE complex is a parallel four-helix bundle (24). The C-terminal of SNAP-25(141-204), referred to as SN2, forms a SNARE motif in the SNARE complex. However, the crystal structure showed that the SN2 region had two binding domains (α-exosite and β-exosite) with BoNT/A LC (E224Q, Y366F) (25). The results

indicate that the SN2 wraps around the globular BoNT/A LC. For BoNT/A, the minimum fragment 141-206 of SNAP-25 is required to retain most of the toxin sensitivity (26). The further cleavage-resistant region had been identified at the C-terminal residues (27). A unique substrate recognition by botulinum neurotoxins serotype A and E had been identified at the C-terminus (28). A fragment SNAP-25(141-206) linked with CFP and YFP was used as a fluorescent sensor to detect botulinum neurotoxin activity *in vitro* and in living cells. CFP-SNAP-25(141-206)-YFP appeared to be a poor toxin substrate in living cells. Incubation of BoNT/ A (50 nM) for 96 h exhibited a small (but significant) shift in the FRET ratio among the cell population, indicating the cleavage is inefficient in cells. Anchoring CFP-SNAP-25(141-206)-YFP sensor to the plasma membrane created a sensor that was efficiently cleaved by BoNT/A in cells (29). Janda developed an assay with SNAP-25 substrate using HPLC for analysis *in vitro*. The fragment had no structural modification and displayed the expected competitive mode of inhibition with a K_i of 300 ± 12 nM (30). Recently, tandem fluorescent proteins, as enhanced FRET-based substrates for botulinum neurotoxin activity, had been used to screen the inhibitors. YFP-SNAP-25(141-206)-CFP-SNAP-25(141-206)-YFP and CFP-SNAP-25(141-206)-YFP-YFP nearly doubled the fluorometric changes, as well as enhanced the ratio-metric changes in the BoNT/A cleavage assay (31). Other methods were used to test the activity based on the FRET method (32-33).

The C-terminal of SNAP-25 plays a key role in binding to BoNT/A LC and syntaxin. SNAP-25, with varying peptide length, has been reported in the literature as substrates for BoNT/Cl proteolysis, signifying the importance of remote exosites in BoNT/Cl required for activity. A 17-mer peptide corresponding to residues 187-203 of

SNAP-25 (32-33), which has been shown to be a substrate for BoNT/A, can be used as a substrate to quantify the activity of BoNT/Cl LC.

1.4 Botulinum neurotoxins

Botulinum neurotoxins (BoNTs) are the most potent toxins known to man (34). BoNTs are produced by *Clostridium botulinum*, which is an anaerobic, gram-positive bacterial species. The lethal dose is only 1 ng/kg of body weight for BoNT/A (35). Seven types of botulinum neurotoxins have been found, from types A to G.

The seven serotypes of BoNTs share a similar structure. The protein (150 kD) contains a catalytic domain, a translocation domain and a receptor binding domain. The catalytic domain is covalently linked with the other two domains by a disulfide bond. The protein can be cleaved to a light chain and a heavy chain by cleavaging from the disulfide bond. The catalytic domain is the light chain (50 kD), and the translocation and receptor binding domain form the heavy chain (100kD) (36). The general structure of BoNT/A is shown in **Figure 3**.

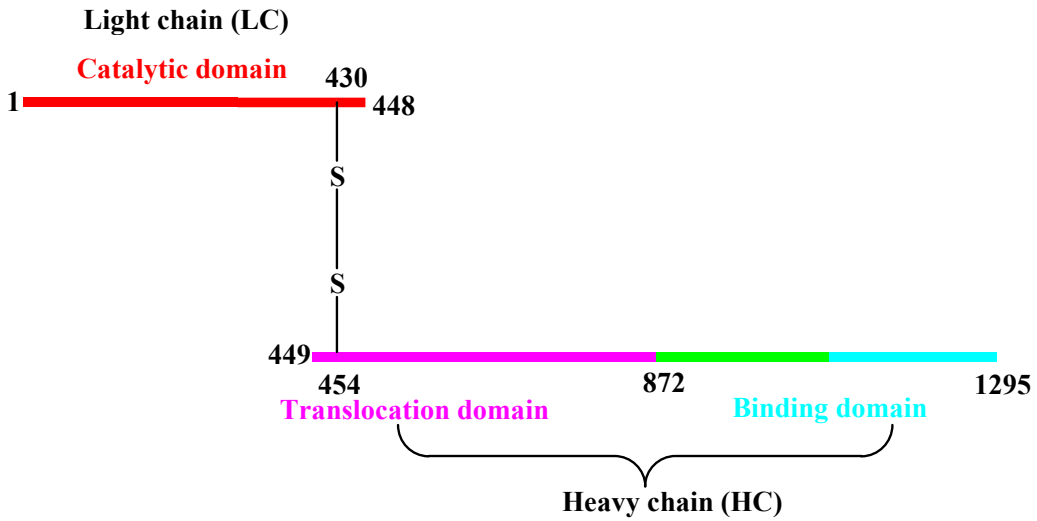

Figure 3. Structure of botulinum neurotoxin.

The crystal structures of BoNT/A (37-38), a catalytic intermediate (39) and a complex of BoNT/A LC with the C-terminal SNAP-25 (25), BoNT/B LC (11, 40), BoNT/C LC (41), BoNT/D LC (42), BoNT/E LC (43), BoNT/F LC (44) and BoNT/G LC (45) have been reported. The structures indicate that light chain (LC) is a zinc-dependent endopeptidase (46). The heavy chain (HC) contains two functional domains, each of approximately 50 kD. The translocation domain forms channels in the lipid bilayer, and the receptor binding domain plays a key role in binding to the target cell membrane and in internalizing the toxin molecules into cholinergic neurons.

Intracellular membrane fusion is a fundamental cellular process in which vesicles from one compartment fuse with their target compartments. Soluble NSF attachment receptor (SNARE) proteins are essential for various types of intracellular membrane fusion in eukaryotes. SNARE proteins assemble into a four-helix bundle and mediate membrane fusion. Cleavage at any one of the three proteins in the SNARE complex by BoNTs inhibits exocytosis. BoNT/A can recognize and specifically cleave SNAP-25 (14). After the cleavage from the holotoxin, the free LC maintains the same tertiary structure, and the protease activity is the same as the full-length toxin. Although LCs' structures from different serotypes are similar, the SNARE target selectivity is unique. Generally, the LCs do not recognize a consensus site. A particular side chain flanking the scissile bond is not required for the cleavage of the corresponding substrate. However, a long stretch of amino acids from their target proteins is necessary for an efficient cleavage. The LC's efficiency can be dramatically reduced by point mutations of substrate proteins far away from the scissile bond (47). The LC cleaves at specific sites of SNARE targets. For example, the BoNT/A LCs specifically cleave between Q197 and

R198 residue of the SNAP-25, while BoNT/C1 LC specifically cleaves between R198 and A199 of the SNAP-25. There is only one residue shift of the scissile bond for BoNT/A LC and BoNT/C1 LC. The results indicate the LC's cleavage site is highly specific. All seven types of Botulinum neurotoxins and their individual hosts are summarized in **Table 2**.

Table 2. List of the seven serotypes of the botulinum neurotoxin, the substrate cleavage sites and the affected hosts.

Serotype	Host	Target	Cleavage site	References
A	Human	SNAP-25	Gln197-Arg198	15
B	Human	VAMP	Gln76-Phe77	48
C	Animal	SNAP-25	Arg198-Ala199	15
		Syntaxin	Lys253-Ala254	49
D	Animal	VAMP	Lys59-Leu60	50
E	Human, fish	SNAP-25	Arg180-Ile181	15
F	Human	VAMP	Gln58-Lys59	51
G	Human	VAMP	Ala81-Ala82	52

1.5 Mechanism of BoNT/A LC cleavage

BoNTs cause botulism, which is characterized by descending flaccid paralysis as the result of the inhibition of acetylcholine release in neuronal transmission. The mechanism of action of botulinum neurotoxin (BoNT) is generally described in four steps: (1) the receptor binding domain of BoNT interacts with gangliosides and a protein

toxin receptor; (2) the toxin-receptor complex facilitates the formation of an endosome and the toxin is internalized into the nerve cell; (3) translocation—light chain endopeptidase is released from an acidic liposome into the cytosol; and (4) the light chain in cytosol cleaves one of the SNARE proteins.

All seven serotypes of botulinum neurotoxin have a homologous protein sequence between residues 200 and 250. The zinc chelation motif is HE××H. The protein sequences surrounding the Zn^{2+} binding motif are summarized in **Table 3**.

Table 3. Protein sequence comparison of the zinc binding motifs of the light chains of botulinum neurotoxin serotypes A to G

Serotype	Partial sequence																		
A	^{216}D	P	A	V	T	L	A	H	E	L	I	H	A	E	H	R	L	Y	^{234}G
B	^{222}D	P	A	L	I	L	M	H	E	L	I	H	V	L	H	G	L	Y	^{240}G
C	^{215}D	P	I	L	I	L	M	H	E	L	N	H	A	M	H	N	L	Y	^{233}G
D	^{222}D	P	V	I	A	L	M	H	E	L	T	H	S	L	H	Q	L	Y	^{240}G
E	^{205}D	P	A	L	T	L	M	H	E	L	I	H	S	L	H	G	L	Y	^{223}G
F	^{220}D	P	A	I	S	L	A	H	E	L	I	H	A	L	H	G	L	Y	^{238}G
G	^{223}D	P	A	L	T	L	M	H	E	L	I	H	V	L	H	G	L	Y	^{241}G
	*	*				*		*	*	*		*			*		*	*	*
								H	E	×	×	H							

BoNT/A LCs are highly specific to cleave SNAP-25. The metal ion (Zn^{2+}) plays a key role during the cleavage. Two Zn^{2+}-coordinated water molecules are important for enzymatic catalysis during the initial reaction. Before the cleavage, the zinc ion is five-member-chelation with H223, H_2O-E224, H227, E262 and H_2O-Y365 at the active site of

BoNT/A LC (53-55). The zinc coordinates with H223, H227, E262 and carboxyl oxygen at the scissile bond to form a tetrahedronal intermediate. The detailed mechanism is illustrated in **Figure 4**.

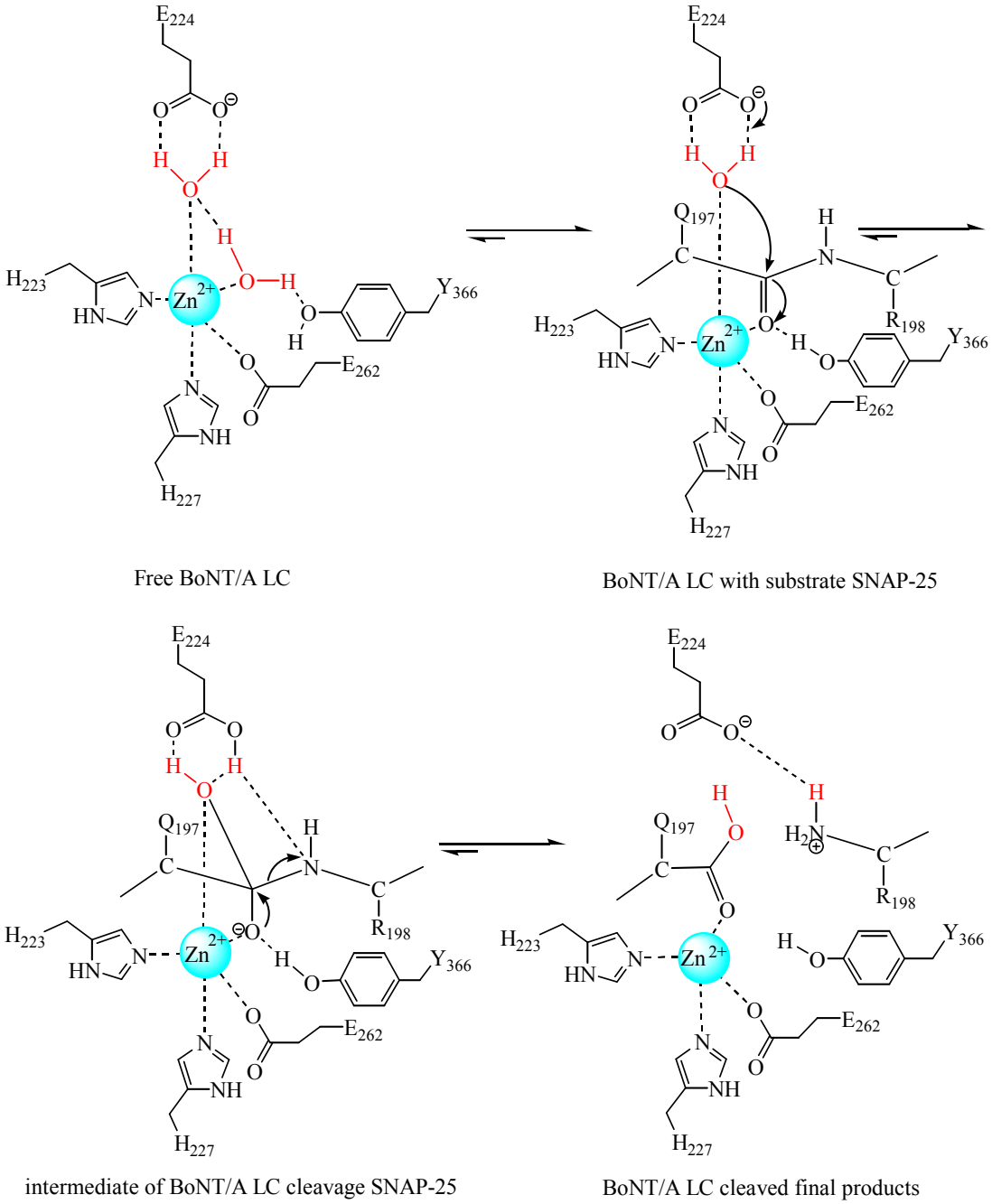

Figure 4. Mechanism of SNAP-25 cleavage by BoNT/A LC.

1.6 Inhibitors of BoNT/A LC

Cleaved SNARE proteins are not sufficient to dock the secretory vesicle to the synaptic membrane, so fusion of the vesicle to the plasma membrane is compromised. This in turn inhibits neurotransmitter release, which results in flaccid paralysis and potential death of the intoxicated human or animal (56).

Some antibodies and BoNT toxoid vaccines have been effectively used as therapy in the prevention of BoNT poisoning (57-59). The equivalent antibodies can cause severe side effects.

BoNT/A LC had been widely used as a drug target for the discovery and development of inhibitors of botulinum neurotoxins. Some peptide inhibitors (60-61), such as CRATKML, had been developed by Schmidt using an HPLC assay. Based on the peptide inhibitor CRATKML, more peptide inhibitors were screened by mRNA display (62). The peptidomimetic inhibitors of BoNT/A LC around the substrate SNAP-25 were developed (53). The pseudopeptide inhibitor that mimics the seven-residue ^{197}QRATKML^{203} sequence near the cleavage site of SNAP-25 showed a different conformation from the substrate. (DNP-DAB)-R-W-T-(DAB)-M-L is the most potent non-zinc-chelating inhibitor that has been reported and has a K_i = 41 nM. When this inhibitor was tested against LCs of BoNT/B, D, E, F, and thermolysin, it did not display any detectable inhibition, indicating that its inhibitory action is specific to BoNT/A. Surprisingly, the co-crystal structure (53) revealed a 3_{10} helical backbone conformation for the peptide inhibitor bound to the active site of BoNT/A LC, which is in sharp contrast to the extended conformation of bound SNAP-25 observed in the BoNT/A LC(E224Q, Y366F)-SNAP-25 complex (25). The inhibitor-binding pockets may change

due to the loop movements, resulting in a new binding surface for inhibitors. Molecular docking studies have been used to refine a common pharmacophore (63).

Previous studies have also provided reports of the co-crystal structures of BoNT/A LC with a weakly inhibiting (K_i = 1.9 μM) heptapeptide, N-Ac-CRATKML, and that of the weakly inhibiting peptide QRATKM and a better inhibitor RRATKM (64). In the N-Ac-CRATKML complex, the crystal structure (54) of CRATKML with BoNT/A LC indicates that the peptide is bound with the Cys Sγ atom, coordinating the metal ion Zn^{2+}.

With the BoNT/A LC as a zinc protease, small molecule inhibitors have been found by focusing on the zinc coordination. Small molecule and non-peptide inhibitors of BoNTs have been reviewed (84). A cinnamic acid hydroxamate was shown to inhibit BoNT/A LC by coordinating with the zinc ion at the active site (65). More hydroxamate derivatives were developed with better inhibition results (66-68). Researchers also created irreversible inhibitors based on the hydroxamate structure (69). Recently, it has been reported that the inhibitors' chirality may be an important factor for inhibiting the BoNT/A protease (70). A zinc chelator, bis(5-amidino-2-benzimidazoly)methane (BABIM) (71), binds to both the light chain and the holotoxin of BoNT serotype B, but very different inhibitory actions on the two forms of the protease were observed (72). The 4-aminoquinolines (73-75) have been identified as good inhibitors. Mercaptoacetamide inhibitors (76) against botulinum neurotoxin A have been developed with low micromolar potency. The pharmacophore-guided lead inhibitors (77-78) were used to develop the inhibitors. In addition, computer-aided lead optimization led to the pyrrole-substituted inhibitors (79-80). Structure- and substrate-based inhibitor designs were used

to screen the inhibitors (81). Preliminary structure-activity relationship studies based on the zinc-mediated inhibitors (82) were reported to chelate with Zn^{2+} to block the activity of BoNT/A LC. Various antagonists have been discovered to eliminate the activity of BoNT/A through *in vitro*, cell based and *ex-vivo* assays (83). However, the effective activity *in vitro* is comparable with the results *in vivo*. To reduce the LCs' activity is a direct and the most efficient method to screen inhibitors. Small molecules and peptides therapy for botulism is not effective so far, although some inhibitors have been developed.

1.7 Thesis aims

SNAP-25 is the natural substrate of BoNT/A LC. We screened for small molecule inhibitors for their ability to inhibit the protease activity of BoNT/A LC. We also investigated the conformational changes of SNAP-25 in the absence and presence of BoNT/A LC. For tertiary structural studies, SNAP-25 was labeled at two locations in SNAP-25 with different fluorescence probes, such as EGFP and ReAsH. GST was used as a tag for substrate purification. For secondary structure studies, unmodified SNAP-25 and its fragments were examined in the absence and presence of BoNT/A LC.

1.7.1 Design of inhibitors

Direct and efficient inhibitors are used to block the active site of the enzyme. The inhibitors are competitive with the corresponding substrates. For example, the inhibitors can specially chelate with zinc at the active site of BoNT/A LC. At the same time, the inhibitors can not affect the other's zinc proteases' activity. Some noncompetitive

inhibitors bind to the enzyme away from the active site and induce an overall conformational change of the enzyme, resulting in the loss of activity. Peptides, active site modification of the substrate, may be good candidates to screen inhibitors. However, peptides may be degraded *in vivo*. So, the small molecule inhibitors as candidates for potential drugs against BoNT/A LC were investigated in my thesis. Virtual screening was used in the initial search for inhibitors.

1.7.2 Glutathione *S*-transferases

Glutathione *S*-transferase (GST) was chosen as a tag for the expression and purification of SNAP-25 and its fragments. GST contains 239 amino acid residues, and its molecular weight is 26 kD. GST fusion proteins are readily purified by affinity chromatography using immobilized glutathione. The GST-tag can be cleaved by PreScission^{TM} protease (85). Unmodified SNAP-25 and its fragments can then be prepared. Other tags, such as 6×His and biotin, can be used to tag SNAP-25. However, in this thesis, BoNT/A LC, a zinc protease, was used in order to study the SNAP-25. The 6×His tag may bind to Zn^{2+} in the LC and introduce complications.

1.7.3 Green fluorescent protein

Enhanced green fluorescent protein (EGFP) is a red-shifted variant of wild-type green fluorescent protein (GFP), which is composed of 239 amino acids with a molecular weight of 27 kD. GFP has been extensively reviewed (86-87). Roger Tsien shared the 2008 chemistry Nobel Prize with Osamu Shimomura and Martin Chalfie for the discovery and development of GFP.

The EGFP has been optimized for brighter fluorescence and a higher expression level. Compared with the wild-type GFP, EGFP has substitutions of Phe-64 to Leu and Ser-65 to Thr. Val was inserted at the N-terminal following the Met. The crystal structure of GFP contains a central α-helix surrounded by an eleven-strand barrel of one anti-parallel β-sheet, and the fluorophore is located on a central helix. Most of the outer layer is composed of the β-sheet, so it is called "paint in a can" or "β can." The shape of GFP resembles a cylinder that has a diameter of 30 Å and a length of 40 Å (88).

The central fluorophore of GFP originates from the oxidation and autocatalytic cyclization of Ser65-Phe66-Gly67. The excitation maximum wavelength is 488 nm, and the emission maximum wavelength is 507 nm. The structure of the fluorophore is shown in **Figure 5**. GFP as a donor or an acceptor for energy transfer has been studied (89-90).

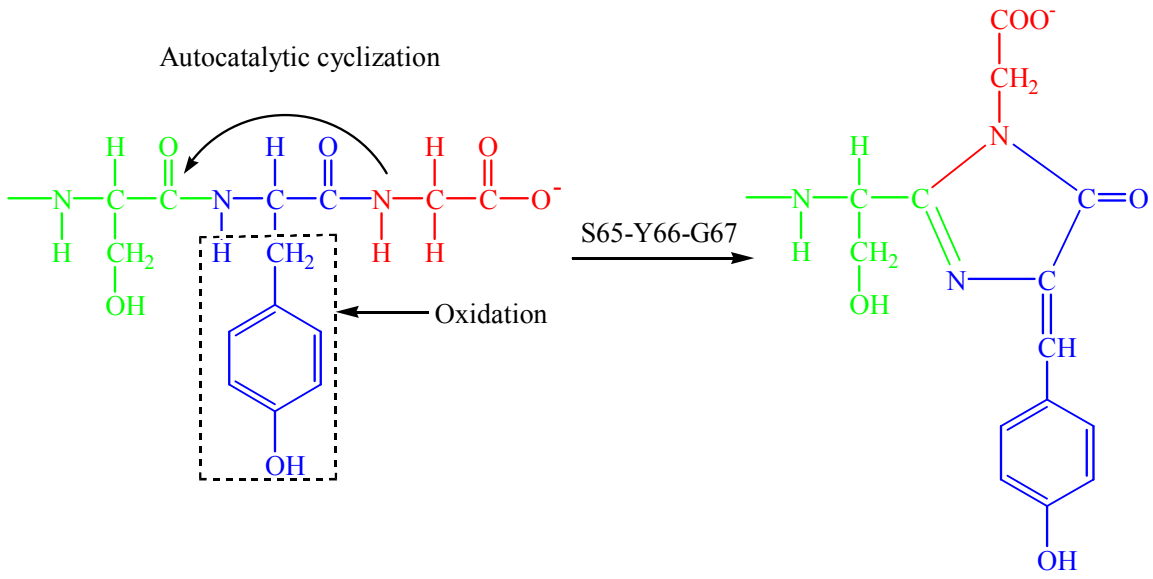

Figure 5. Structure of the fluorophore of GFP.

1.7.4 ReAsH covalently bound to CCPGCC as a fluorescent probe

The tetracysteine (TC, or CCPGCC) tag is a genetically encoded, small fluorescent tag. Biarsenical pro-fluorescent dyes 4, 5-bis(1, 3, 2-dithiasolan-2-yl)fluorescein (FlAsH) and 4, 5-bis(1, 3, 2-dithiarsolan-2-yl)resorufin (ReAsH) can covalently bind to the tetracysteine CCPGCC to form a hairpin and produce green (FlAsH) or red (ReAsH) fluorescence. In order to detect the interaction with FRET, ReAsH was chosen as a second labeling tag in the fusion protein. We selected the CCPGCC-ReAsH system as a fluorescent probe, since the CCPGCC can easily be inserted into SNAP-25 by means of mutagenesis at any specific location. Since CCPGCC (about 0.7 kD) is smaller than the fluorescent proteins, it introduces less distances than EGFP would.

Tetracysteine can be inserted into any location within a protein. ReAsH covalently binds to CCPGCC to form a fluorescent product, thereby providing a convenient *in vitro* and *in vivo* labeling method. The biarsenic dyes themselves are not fluorescent. Once ReAsH binds to the CCPGCC and a highly fluorescent complex is formed. The structure of ReAsH and its complex are shown in **Figure 6**.

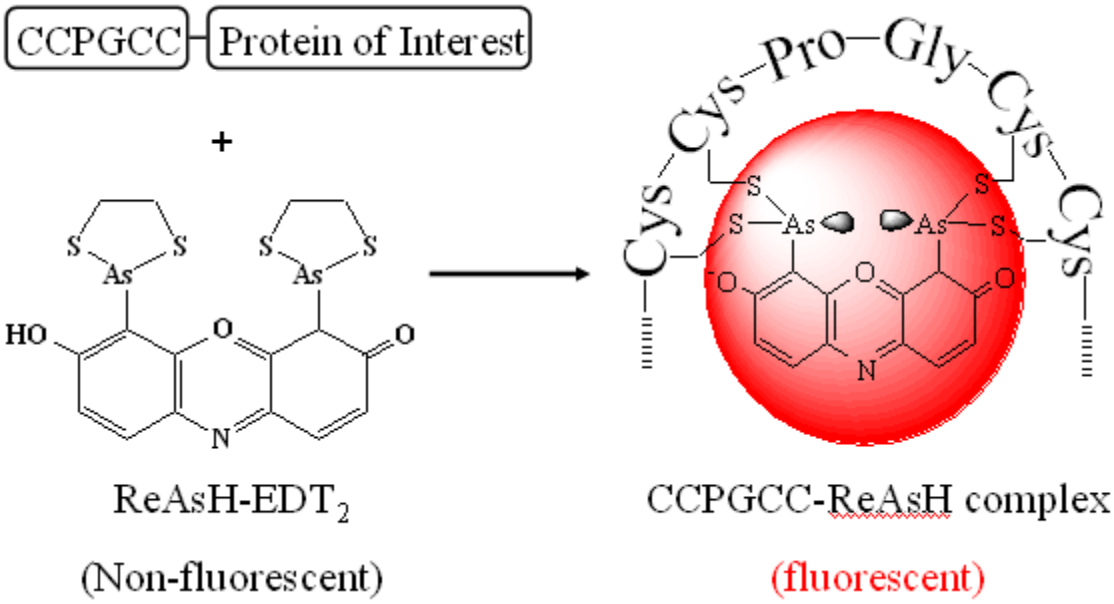

Figure 6. ReAsH and CCPGCC complex. The figure is modified by the CCPGCC-FlAsH complex from QIAGEN without permission.

The hairpin structure of CCPGCC with bound ReAsH was determined by NMR (90). The fluorescence specific to the hairpin structure has a number of applications. One of the approaches has been used to control labeling the protein tetracysteine tag with FlAsH (91). Hill (92) reported utilizing biarsenical-labeling to distinguish the α and β isoforms of prion proteins (PrP). Labeling the α-helical form of tetracysteine tagged PrP resulted in minimal fluorescence, whereas labeling the β-sheet form of tagged PrP yielded high fluorescence. The FlAsH binding tetracysteine motif can be used to probe protein stability and aggregation *in vivo* (93). As geometric constraints imposed upon tetracysteine thiol ligands by a native structure substantially lower the FlAsH quantum yield, fluorescence measurements may result in a useful fluorescence readout of the folded and unfolded populations. Krishnan (93) divided the binding motif into components that only accommodate FlAsH dye when the motif, referred to as a "split

tetra-Cys motif," is correctly arranged in space by a native protein structure. Chaumont (94) utilized tetracysteine tagging of the $P2X_2$ receptors' N and C-termini to generate CCPGCC-$P2X_2$ and $P2X_2$-CCPGCC receptors. It has been found that $P2X_2$ receptors carrying cytosolic domain 4C tags can be labeled with FlAsH, without affecting receptor function. In order to track HIV production, Turville (95) developed an infectious HIV construct bearing a dithiol-resistant tetracysteine motif (dTCM) at the C-terminus of the HIV p17 matrix protein within the HIV gag protein, resulting in restricted staining of the dTCM to de novo-synthesized un-cleaved gag in the dendritic cells (DCs). The β2 adrenoceptor (β_2-AR) is a well-characterized G protein-coupled receptor (GPCR), a versatile membrane protein that regulates a wide variety of physiological functions. Granier (96) introduced a CCPGCC motif at the proximal C-termini. FRET analysis has found that the structure and conformational changes in the C-terminal domains of the β_2-AR may be relevant to arrestin-dependent regulation and signaling. Hoffmann (97) has found that the conformational changes are functionally selective. Erster (98) developed a ligand interaction scan (LIScan) in TEM-1 β-lactamase by inserting a tetracysteine binding to FlAsH. Blommel (99) created a real-time protease assay by measuring anisotropy, using the CCPGCC attached to the N-terminal-modified maltose binding protein (MBP) as substrates for commonly used proteases. Griffin and Tsien (100) report of utilizing FlAsH obtain specific covalent labeling of recombinant protein molecules inside live cells. Luedtke (101) indicates that the intensity of the fluorescence of polypeptide-biarsenical complexes correlates with the thermodynamic stability of the protein fold or assembly.

The ubiquitin-proteasome pathway is the major non-lysosomal protein degradation pathway in eukaryotic cells. Archer (102-103) developed CCPGCC-Ub to detect the physical and functional interactions of monoubiquitylated trans-activators with the proteasome. Romantsov (104) used tetra-Cys and FlAsH to examine the subcellular locations of a target protein. The neuronal dopamine transporter (DAT) is a major determinant of extracellular dopamine (DA) levels and is the primary target for a variety of addictive and therapeutic psychoactive drugs. Navaroli (105) developed the CCPGCC-FlAsH into the DAT second extracellular loop, resulting in a functional transporter. The method holds promise for the use of biarsenic dyes in live DAT imaging studies.

Biarsenical dyes (106) have been used to study the dynamics of flagella in multicellular communities of *Escherichia coli*. Zhang (107) introduced FlAsH into protein tyrosine phosphatase (PTP) in order to make a potential "chemical switch" to control enzyme activity. The CCPGCC is inserted at site-directed positions in the catalytic domain of PTP that is essential for mammalian viability, T-cell PTP (TCPTP). Inserting CCPGCC had little to no affinity for wild-type TCPTP or other cellular proteins. However, when CCPGCC is embedded within the enzyme's catalytic domain, the conformation and activity may be changed after binding to FlAsH. The enzyme TCPTP exists in either the "open" or "closed" form, which differ predominantly in the conformation of the WPD loop. Shifting between the open and closed WPD loop conformations is critical for PTP activity. The substrates enter the active sites of open PTP domains, while the aspartic-acid residue (the "D" of WPD) can only perform its general-acid-base functions in the closed form. When CCPGCC is specifically targeted to the WPD-loop, the covalently bounded FlAsH inhibits the open/closed transition,

resulting in a shut-down of the enzyme activity (108). Bishop (109) introduced FlAsH into the antibiotic-resistance enzyme TEM-1. FlAsH has no significant affinity for wild-type TEM-1, which does not contain a CCPGCC motif. When TEM-1 is modified with CCPGCC, it becomes inactive. However, when FlAsH binds to the CCPGCC, TEM-1 activity can be restored. The mechanism is shown in **Figure 7**.

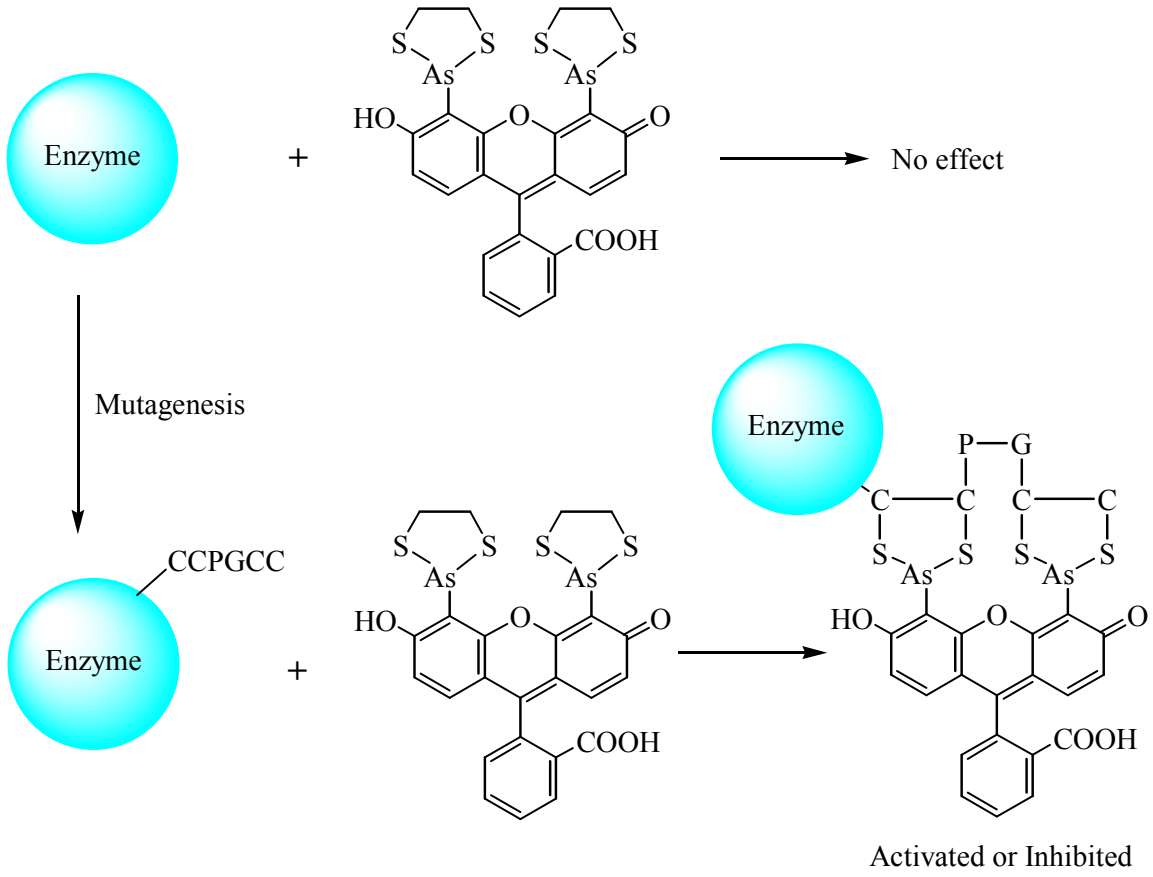

Figure 7. CCPGCC and the FlAsH complex affect the enzyme activity.

The tumor suppressor p53, labeled with FlAsH and having a C-terminal CCGPCC tetracysteine tag, can be used to study the DNA-binding specificity and oligomerization properties within the p53 family (110). Tetracysteine tags with the biarsenical complex can be used as fluorescent probes and for *in vivo* imaging. Andersen (111) developed 1×,

2×, and 3× CCPGCC at the C-terminal of Tub2 to obtain live cell imaging. Gaietta (112) introduced a short tetracysteine peptide tag, FLNCCPGCCMEP, to the Golgi resident enzyme α-Mannosidease II (MannII). The enzyme was found to have an increased affinity and improved ReAsH quantum efficiency compared with tetracysteine peptide CCPGCC. The ReAsH bound to the tetracysteine tag MannII-GFP-FLNCCPGCCMEP was used for the cell imaging.

Yan (113) reported that fluorophore-assisted light inactivation (FALI) permits the targeted inactivation of tagged proteins. Utilizing the calcium regulatory protein calmodulin (CaM) to regulate signal transduction, CCPGCC-CaM was used in the FALI.

A tetracysteine tag can be used to rapidly isolate protein complexes. Mayer (114) designed resin with a bis-arsenical dye to isolate the RNA polymerase A. The process can separate the intact multi-complex, thus providing a method to identify various changes in critical protein complexes over time modulated cell function (114). It can also be used to identify the specific bindings (115) and to identify the naturally occurring binding motifs for biarsenical probes in the proteome (116). The method is depicted in **Figure 8**.

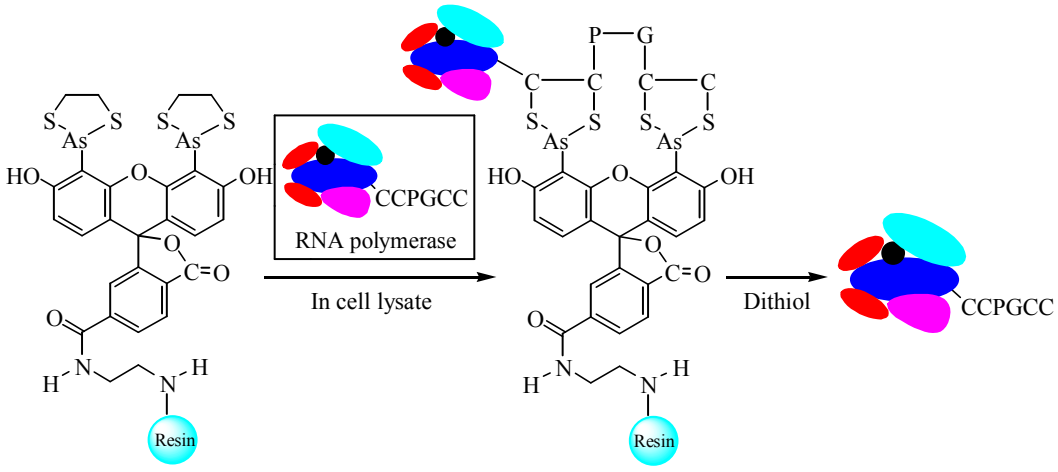

Figure 8. Diagram of complex separation by CCPGCC and FlAsH modified resin.

Hofmann (117) developed a method to monitor the protein-protein interactions of conformational changes of individual proteins. However, protein functions can be perturbed by the fusion of such large tags as CFP and YFP. G protein-coupled receptor (GPCR) activation was introduced in living cells as a model system by which to compare YFP with FlAsH targeted at CCPGCC. Various receptor constructs are based on the human A_{2A} adenosine receptor modified in different positions. A_{2A}-CFP, A_{2A}-CFP-CCPGCC, A_{2A}-CCPGCC-CFP, and A_{2A}-CFP-YFP were expressed, and the FlAsH-based FRET approach was used to determine GPCR activation in living cells. Maier-Peuschel (118) developed an M_2 muscarinic receptor sensor and used it for the FRET-based real-time monitoring of receptors to detect conformational changes.

In summary, the selective labeling of proteins by means of chemical probes has been widely used to detect conformational changes (119). The tetracysteine motif with FlAsH or ReAsH binding have been a valuable tool to evaluate the conformational changes of proteins (120) and protein locations (121) *in vivo* and may have other biological applications (122).

1.8 Thesis statement and significance

In the neuronal system, SNAP-25 associates with synaptobrevin and syntaxin to form a four-helix bundle, which plays a key role in membrane fusion. SNAP-25, a substrate of botulinum neurotoxins, cannot function once inactivated by BoNT. The C-terminal 64 amino acid residues of SNAP-25 wrap around BoNT/A LC to form a stable binary complex, displaying a totally different conformation from that of the natural four-helix bundle. However, the conformation of the N-terminus of SNAP-25 is unknown

when it interacts with BoNT/A LC. In order to understand the binding and inhibition mechanism between BoNT/A LC and SNAP-25, inhibitors are sought to block the protease activity and mechanism by which the inhibiton occurs investigated. The conformation of SNAP-25 may play a key role in the binding and folding processes during the four-helix SNAREs complex formation.

The objective of my thesis is to better understand the conformational changes of SNAP-25 in the absence and presence of BoNT/A LC. Specific aims include developing methods of introducing enhanced green fluorescence protein (EGFP) and a hairpin fragment CCPGCC at specific locations in SNAP-25. The apparent distances from the C-terminal to the N-terminal, the C-terminal to the residue D140, and the N-terminal to D140 are determined by fluorescence resonance energy transfer (FRET). The secondary structural changes of the full length SNAP-25 and the N-terminal and the C-terminal of SNAP-25 are determined by CD. The results suggest that both the N-terminus and the C-terminus of the SNAP-25 bind to BoNT/A LC and induce more helical moieties in the binary complex. In order to promote the membrane fusion, quinolinol-derived inhibitors are used to block protease activity. The binding and inhibition modes between BoNT/A LC and SNAP-25 are studied by means of fluorescence titration, computer modeling, and enzyme kinetics in the presence of a peptide from the C-terminal fragment of SNAP-25. The findings suggest that peptides are slow and that tightly binding inhibitors and quinolinol-derived inhibitors display a noncompetitive inhibition.

Chapter 2. Materials and methods

2.1 Materials

The inhibitors which passed the preliminary HPLC screening were custom synthesized to >98% purity by GLSynthesis, Inc. (Worcester, MA) and were then used in the subsequent assays. All the inhibitors structures are proved by NMR. Peptides, including Ac-CRATKML-NH_2, Peptide C (Ac-EKADSNKTRIDEANCRATKMLGSG-NH_2) and Peptide C1 (Ac-EKADSNKTRIDEANARATKMLGSG-NH_2), were prepared and purified by C. S. Bio. Co. (Menlo Park, CA). The purity was greater than 95% based on the HPLC chromatograms. SNAPtide (*o*-Abz-Dnp) was purchased from List Biological Laboratory and was used according to manufacture's instructions unless otherwise specified. Truncated BoNT/A LC(1-425) was a kind gift of J. Barbieri (Medical College of Wisconsin) and was used for fluorescence titration and for microtiter protease assays using full-length SNAP-25 as the substrate. Test compounds were stored at -20 ˚C until use. All other reagents and chemicals were from Sigma-Aldrich (St. Louis, MO) or standard sources.

1, 2-Ethanedithiol (EDT) was obtained from Aldrich. FLAs-EDT_2 and ReAsH-EDT_2 were synthesized as the literature reported methods. Ampicillin, kanamycin, adenosine triphosphate (ATP), isopropyl-β-D-1-thiogalactopyranoside (IPTG), biotin, Tris-HCl, Tris-base, ethylenediaminetetraacetic acid (EDTA), β-mercaptoethanol, dithiothreitol (DTT), ethidium bromide, agarose, glycerol, acetic acid, trichloroacetic acid (TCA), bromophenol blue, trypsin, L-glutathione (G4251), and Glutathione-agarose (G4510) were obtained from Sigma (St. Louis, MO). Coomassie brilliant blue, Tween 20, sodium dodecyl sulfate (SDS), and Bradford protein assay reagents, including Laemmli

sample buffer, were purchased from Bio-Rad (Hercules, CA). Tris(2-carboxyethyl)phosphine hydrochloride (TCEP) was purchased from Soltec Ventures in Massachusetts (M115). Ammonium bicarbonate (Fisher, A643-500) and NuPAGE® 4-12% Bis-Tris Gel were purchased from Invitrogen (Carlsbad, CA).

2.2 Molecular biology reagents

Expression vector pGEX-6P-3 was purchased from Amersham Biosciences (27-4599-01) and EGFP plasmid was from Clontech. Primers for vector construction were obtained from Operon (Huntsville, AL). TOPO TA cloning vector, competent cell DH5α™-T1^R and S.O.C. medium, electrophoresis reagents, including NuPAGE® Bis-Tris gels, were purchased from Invitrogen (Carlsbad, CA). Restriction enzymes, including BamHI and NotI, bovine serum albumin (BSA), and T4 DNA ligase, were purchased from NEB (Ipswich, MA) for construction of expression vectors. Chemicals for DNA sequencing were purchased from Applied Biosystems (Foster City, CA). Competent cell *E. coli* BL21(DE3)pLysS and QuickChange® II site-directed mutagenesis kit including Dpn1 were purchased from Stratagene (La Jolla, CA). QIAprep® spin miniprep kit and QIAquick® gel extraction kit were purchased from Qiagen (Valencia, CA). EDTA-free protease inhibitor tablets were obtained from Roche (Indianapolis, IN).

2.3. Buffers

Various buffers were used for DNA and protein purifications. Miller's LB broth and 1× Tris-Acetate-EDTA (TAE) buffer (pH 7.2) were purchased from Mediatech (Manassas, VA). 1 kb and 100 bp DNA ladder with 6× DNA loading buffer (pH 8.0) containing 10 mM Tris-HCl, 1mM EDTA were purchased from BioRad.

Lysis buffer and wash buffer containing 100 mM sodium phosphate (pH 7.4), 150 mM NaCl, 1 mM DTT, and 0.5% Triton X-100, and elution buffer containing 100 mM sodium phosphate (pH 7.4), 150 mM NaCl, 10 mM glutathione, 100 μM TCEP, and 1 mM EDTA were used for purification of GST-tag proteins.

Prestained SDS-PAGE standard (BioRad) containing 50% glycerol, 300 mM NaCl, 10 mM Tris, 2 mM EDTA 3 mM NaN_3, and purified proteins were loaded in the NuPAGE® 4-12% Bis-Tris gel (Invitrogen) with 1× Laemmli sample buffer (BioRad).

NuPAGE MOPS SDS running buffer (pH 7.0) was purchased from Invitrogen for SDS-PAGE. The gel was stained with coomassie staining solution containing 0.75% (w/v) coomassie brilliant blue R-250, 7.5% acetic acid, and 50% methanol followed by destaining solution containing 35% methanol and 10% acetic acid. Gel drying solution contains 20% methanol and 5% glycerol.

2.4 DNA sequencing

DNA sequencing was carried out at the Georgetown University Department of Biology core facility. The sequencing reaction was performed in 10 µl volume containing 5 µl of plasmid DNA (500 – 1000 ng), 2.5 µl of primer (3.2 pmol) and 2.5 µl of Terminator FS BigDye V3 (Applied Biosystems, Warrington, UK). Twenty five cycles of 96 °C for 10 sec, 50 °C for 5 sec, and 60 °C for 4 min were performed on a GeneAMP PCR 2700. Unincorporated deoxynucleotide triphosphates (dNTPs) were removed using BioMax Spin-50 Mini-column with collecting tubes (BIOMAX, Odenton, MD). Samples were dried using speed vac and stored at -20 ºC. Prior to sequencing, the samples were dissolved in 20 µl of formamide and denatured by heating to 95ºC for 2 min. Samples were incubated on ice for 5 min prior to sequencing.

2.5 Agarose gel electrophoresis

Gels were prepared by microwave heating 1% agarose in 1× TAE buffer (Mediatech, Manassas, VA) supplemented with 1 µg/mL ethidium bromide (Sigma). Gels were cast for use in a miniboat agarose gel unit from NAR Laboratories, Inc (Northborough, MA). DNA ladder (BioLabs) and samples were prepared in 6× DNA loading buffer (Promega) with blue and orange dyes at a 3:1 sample to buffer ratio. Electrophoresis was run at 100 voltages for 45 min. DNA bands were visualized by UV light and photographed with a Polaroid camera. The gel with expected DNA bands was collected and the DNAs were recovered and purified using QIAquick® gel extraction kit (Qiagen) following the manufacturer's instructions.

2.6 Expression and purification of recombinant proteins

pGEX plasmids were used to transform *E. coli* BL21(DE3)LysS for protein expression. Cells were grown at 37 ºC overnight in LB broth containing 100 μg/ml ampicillin. The overnight culture was diluted 1:100 with LB broth containing 100 μg/ml ampicillin and incubated at 37 ºC until OD_{600nm} reached 0.6. The cells were subsequently induced with 1 mM IPTG and incubated at 37 ºC for additional 4 h. The cells were pelleted by centrifugation at 6000 RPM for 10 min and suspended in lysis buffer (10 mM Tri·HCl, 200 mM NaCl, 1 mM DTT, and 0.5% Triton X-100, pH 7.5) supplemented with 1 mM PMSF (Sigma, P7626) and 5 mM benzamidine (Sigma, B-6506) as a protease inhibitor. The suspended cells were then lysed on ice by sonicating at 15 pulses with 15-second pauses following a 2 min sonicating, and then subsequently centrifuged at 6000 RPM for 10 min to pellet cell debris. The supernatant was applied to glutathione reduced agrose (Sigma Aldrich) column pre-equilibrated with lysis buffer. The column was thoroughly washed with wash buffer (10 mM Tri·HCl, 200 mM NaCl, 1 mM DTT, and 0.5% Triton X-100, pH 7.5) to remove the SNAP-25 and other proteins without GST-tag. The bound GST-SNAP-25 was eluted with elution buffer (10 mM Tris·Hcl, pH 7.5, 10 mM glutathione). Purified SNAP-25 with GST-tag was then dialyzed against 1× PBS (pH 7.5) for 3 h. The samples were analyzed by SDS-PAGE.

2.7 SDS—polyacrylamide gel electrophoresis (PAGE)

Proteins were analyzed on NuPAGE® 4-12% Bis-Tris gels (Invitrogen). Sample preparation and electrophoresis conditions were performed following the manufacturer's instructions. Prestained protein standard (BioRad) and protein samples were prepared

with 1× Laemmli sample buffer (BioRad) and denatured at 94 °C for 10 min. The denatured samples were gradually cooled to room temperature and loaded in the NuPAGE® 4-12% Bis-Tris gel (Invitrogen) and run at 200 voltages for 50 min in 1× NuPAGE MOPS SDS running buffer (Invitrogen). Gels were stained by incubating in 0.25% (w/v) Coomassie blue, 50% methanol, and 7.5% acetic acid for 1 h and then destained overnight in 35% methanol and 10% acetic acid. After destaining, gels were incubated in 20% methanol and 5% glycerol for 1 h and dried in DryEase Mini Cellophane (Invitrogen).

2.8 Site-directed mutagenesis

Site-directed mutagenesis was carried out using Quikchange® Mutagensis Kits (Stratagene) following the manufacturer's instructions. Mutagenesis reactions contained, in 50 µL, 100 ng of primer, 100 ng of template, 1 µl of dNTP, 5 µl of 10× reaction buffer (100 mM KCl, 100 mM $(NH_4)_2SO_4$, 200 mM Tris-HCl pH 8.8, 20 mM $MgSO_4$, 1% Triton X-100, and 1 mg/ml nuclease free bovine serum albumin (BSA)), 41 µl of de-ionized dH_2O, and 1 µl of *PfuTurbo* DNA polymerase (2.5 U/µl). Reactions were initially denatured at 95 °C for 2 min followed by 18 cycles with denature at 95°C for 30 s, annealing primer with single stranded DNA template at 55 °C for 1 min and extension at 68 °C for 8 min. Reactions were incubated with DpnI (20 U/µl) at 37 °C for 2 h to digest the original DNA template. The newly synthesized plasmids were transformed into DH5α supercompetent cells with standard transformation protocol. The transformed cells were grown overnight in LB broth supplemented with 100 µg/ml ampicillin. Plasmids were isolated and purified using Qiaprep® spin miniprep kit (Qiagen) following the

manufacturer's instructions. DNA sequences were confirmed using the sequence analysis located at the biology department of Georgetown University. Later, the samples were directly sent to Genewiz for sequencing.

2.9 Fluorescence measurements

All fluorescence measurements were made in phosphate buffer (10 mM sodium phosphate, 150 mM NaCl, 10 μM zinc acetate, pH 7.4) at 25 ˚C using SPEX Fluomax and 0.4 × 0.4 × 3 cm microcuvettes unless otherwise specified. The intrinsic fluorescence of the light chain was determined at 323 nm with an excitation wavelength at 280 nm. Samples with an absorbance at 280 nm greater than 0.05 were corrected for the inner filter effect. The intrinsic fluorescence of the light chain exhibited two exponential decays upon diluting the stock solution to the phosphate buffer (10 mM sodium phosphate, 150 mM NaCl, 10 μM zinc acetate, pH 7.4). The fluorescence decays consisted of two single exponentials and the rate constants were independent of the protein concentration. The fluorescence decreases were consistent with the dissociation of BoNT/A LC dimmers to monomers or conformational changes upon the dilution of BoNT/A LC. However, the exact cause was not clear. All light chain samples were thus pre-incubated in the phosphate buffer for 60 min at 25 ˚C before measuring fluorescence.

2.10 Zn^{2+} removal and Zn^{2+} assay

To remove the Zn^{2+} in the light chain, the protein was incubated in a buffer containing 10 mM EDTA and 150 mM sodium phosphate (pH 7.5), then dialyzed in the same buffer at 4 ˚C overnight to remove the zinc ions, and then re-dialyzed at 4 ˚C against 2500 volumes of 150 mM sodium phosphate (pH 7.5) pretreated chelex-100 with two changes overnight to remove the excess EDTA from the protein sample. The resulting light chain stripped of Zn^{2+} was stored at 4 ˚C and contained no detectable Zn^{2+} at 8 μM light chain as determined by the 4-(2-pyridylazo)resorcinol (PAR) indicator assay (**Appendix A5**). The sensitivity is less than μM range (131). Protein samples were incubated in 6 M guanidinium chloride, 30 mM sodium phosphate (pH 7.5), and 100 μ M PAR at 25 ˚C for 15 min. The absorbance of PAR in complex with Zn^{2+} at 500 nm was determined. The amounts of Zn^{2+} in the protein samples were obtained by interpolating onto a standard curve of zinc acetate with PAR in the same buffer.

2.11 Determination of the dissociation constants

The fluorescence of BoNT/A LC (0.2 μM) in 250 μl of 10 mM sodium phosphate (pH 7.4) and specified concentration of zinc acetate with an maximum wavelength at 323 nm (λ_{ex} at 280 nm) was monitored at varying concentrations of the test compound in the same buffer in a microcuvette (0.4 × 0.4 × 3 cm) by adding aliquots of 1 μl at an increment of 0.02 to 0.2 μM. The changes in the fluorescence (ΔF) and the extent of binding (α) were used to calculate the apparent dissociate constant based on the fluorescence quenching of the BoNT/A LC as the following **Equation 1** and **Equation 2**.

$$\alpha = \frac{\Delta F}{\Delta F_{\max}} = \frac{F_0 - F}{F_0 - F_{\max}} = \frac{x_b}{E_0} = \frac{(E_0 + x_0 + K_d) - \sqrt{(E_0 + x_0 + K_d)^2 - 4E_0 x_0}}{2E_0} \quad (1)$$

If $F_0 = 100$, $\alpha = \frac{\Delta F}{\Delta F_{\max}} = \frac{100 - F}{\Delta F_{\max}} = \frac{x_b}{E_0} = \frac{(E_0 + x_0 + K_d) - \sqrt{(E_0 + x_0 + K_d)^2 - 4E_0 x_0}}{2E_0}$

$$F = 100 - \Delta F_{\max} \cdot \left(\frac{(E_0 + x_0 + K_d) - \sqrt{(E_0 + x_0 + K_d)^2 - 4E_0 x_0}}{2E_0} \right) \quad (2)$$

where F_0, F, and $F_{\max}$ are the BoNT/A LC tryptophan emission intensities in the absence of the inhibitor, in the presence of limiting test compound, and in the presence of saturating concentration of the inhibitor, respectively. x_0 is the total concentration of the inhibitor, x_b is the concentration of the BoNT/A LC-bound inhibitor, and E_0 is the total BoNT/A LC concentration. The solution of the quadratic equation was obtained using the Scatchard equation and the equilibrium constant equation. The number of binding sites was assumed to be one for the monomeric light chain at low concentration. Curve fitting to the above equation using Sigmaplot gave the dissociate constant of the compound under the specified conditions.

2.12 Microtiter protease assay of BoNT/A LC

Purified GST-SNAP-25 (100 μg/ml) or GST-SNAP-25 in crude lysate from *E. coli* over-expressing GST-SNAP-25 was diluted 100 folds in wash buffer (phosphate buffered saline, pH 7.2, 0.05% Tween 20, 10 μM zinc acetate). The diluted GST-SNAP25 was applied to glutathione-coated microtiter plates (Pierce) and incubated at 25 °C for 1 h. The microtiter wells were washed three times (200 μl × 3) with wash buffer. BoNT/A LC (0.1μg/ml) in 10 mM potassium phosphate (pH 7.4), 10 μM zinc acetate, 150 mM NaCl, 5 mM DTT and 0.05% Tween 20, was incubated at 37 ºC for 2 h to cleave the immobilized GST-SNAP-25. The wells of the microtiter plates were washed three times (200 μl × 3) with wash buffer and incubated with 0.05 μg/ml anti-SNAP-25 rabbit polyclonal antibody (Stressgen Biotechnologies) for 1 h at room temperature. The plate was inverted to empty wells and blotted on stacked paper towels and the wells were washed three times (200 μl × 3) with the wash buffer. The wells were subsequently incubated with 10,000-fold dilution of donkey anti-rabbit IgG-horse radish peroxidase (Amersham Biosciences) at 25 °C for 1 h, emptied, and washed three times (200 μl × 3) with wash buffer. The wells were then incubated with Quantablu peroxidase substrate working solution (Pierce) for 30 min at 37 °C. The reactions were stopped by adding the Quantablu stop solution, and the fluorescence intensities in the wells were measured at the excitation maximum wavelength at 325 nm and the emission maximum wavelength at 420 nm using a Perkin Elmer LS50B luminescence spectrometer plate reader. Control wells had no light chain or light chain in the presence of excess protease inhibitor. The method is illustrated in **Figure 9**.

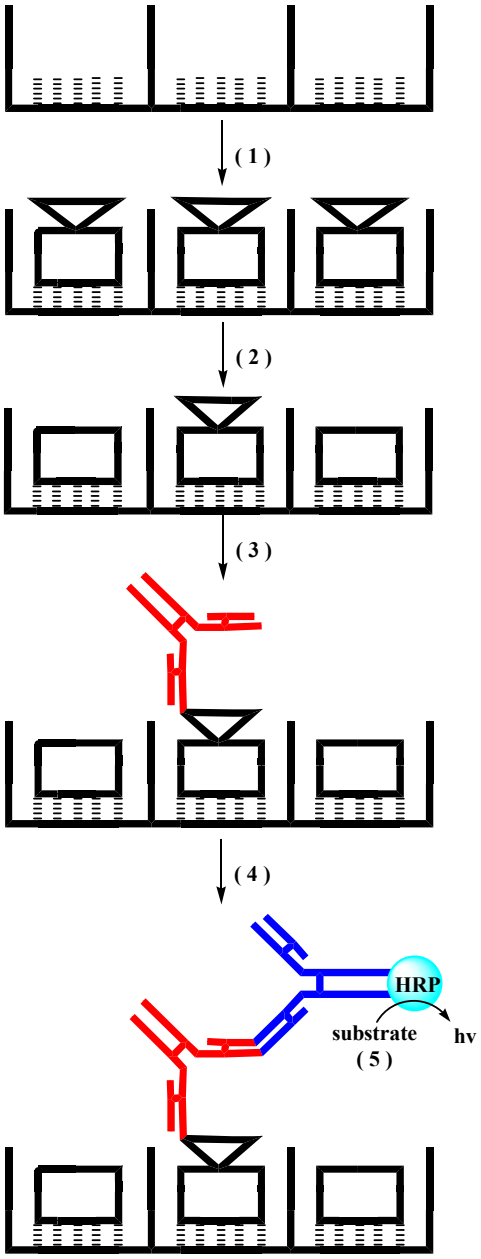

Figure 9. Method of ELISA. The dotted line represents the pre-coated gluotathione. The triangle and square indicate the C-terminal and the N-terminal of SNAP-25, respectively. The connection point is the cleavage site of BoNT/A LC. The red and the blue symbols represent the primary and secondary antibody, respectively. The secondary antibody is modified by horseradish peroxidase. Chemiluminescence was emitted with addition of substrates.

2.13 Determination of Michaelis-Menten kinetics constants

SNAPtide (*o*-Abz-Dnp) purchased from List Biological Laboratories (Campbell, CA) was used for analyzing the kinetics of protease inhibition. SNAPtide was incubated with the inhibitor in 10 mM potassium phosphate, pH 7.4, 150 mM NaCl, and 10 μM zinc acetate in the presence of varying concentrations of SNAPtide, and the reaction was initiated by the addition of BoNT/A LC. The protease activity was monitored by the increase of donor fluorescence intensity. The results were analyzed using Sigmaplot and Lineweaver-Burke plots. The cleavage of SNAP-25 is shown in **Figure 10**.

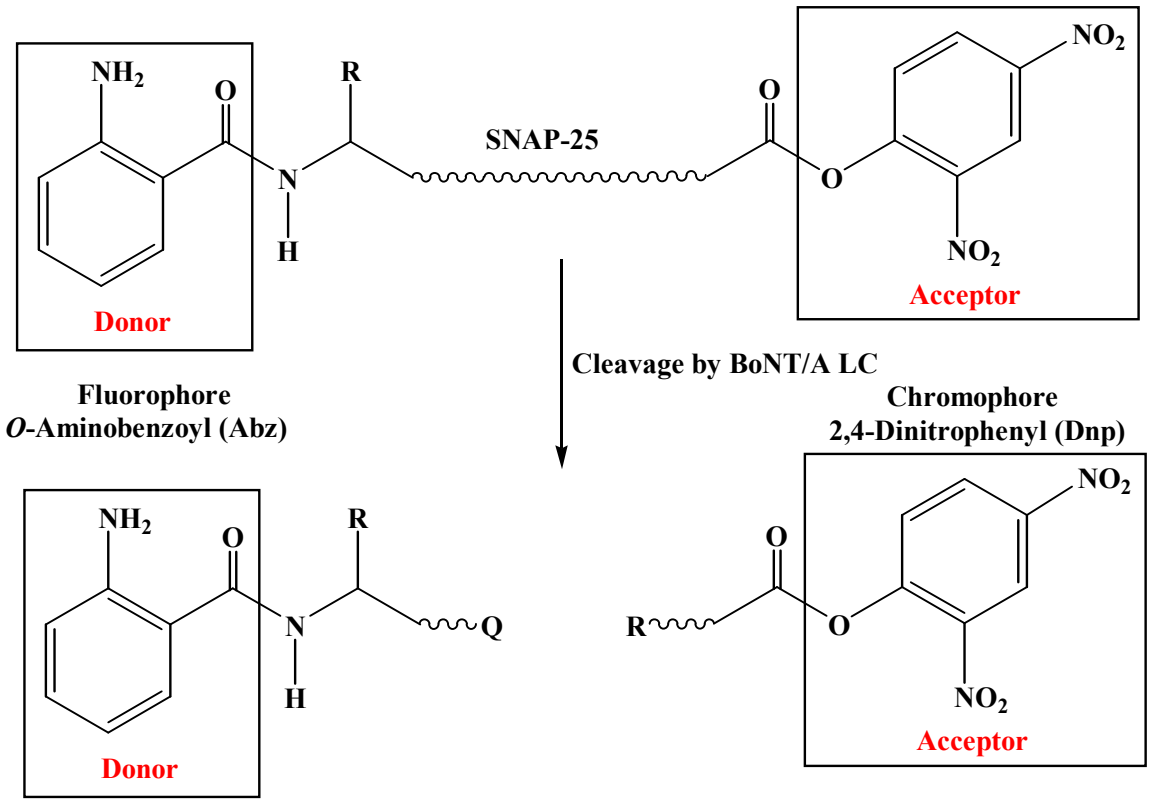

Figure 10. SNAPtide assay for cleavage by BoNT/A LC.

2.14. Fluorescence resonance energy transfer (FRET) measurements

Fluorescence resonance energy transfer is a distance-dependent interaction between two fluorophores, in which excitation from a fluorescent donor (EGFP) is resonant with an acceptor (ReAsH-CCPGCC). The efficiency of energy transfer (E) is related to R_0 (Förster radius) and R (apparent distance between donor and acceptor) by **Equation 3**:

$$E = \frac{{R_0}^6}{{R_0}^6 + R^6} \qquad (3)$$

R_0 represents the distance at which the transfer has 50% efficiency and is calculated (in centimeters) according to **Equation 4**:

$${R_0}^6 = \frac{9Q(\ln 10)\kappa^2 J}{128\pi^5 n^4 N_A} = 8.79\times10^{25}\left[n^{-4}Q\kappa^2 J\right] \qquad (4)$$

where, n is the refractive index (taken as 1.4) of the medium; Q is the quantum yield of the donor in the absence of acceptor (Q_{EGFP} = 0.6, Q_{ReAsH} = 0.6); κ^2 is the orientation factor for dipole coupling (assumed to be 2/3 for randomly oriented, mobile donor and acceptor); and $J(\lambda)$, the overlap integral between donor emission and acceptor absorption is calculated from the spectral data.

2.15 Calculation of overlap integral *J* between EGFP and ReAsH

The fluorescence emission of EGFP and the absorbance of ReAsH spectrum were measured at a specific concentration. After the normalization, the overlap between EGFP and ReAsH is shown in **Figure 11**. The J value can be obtained based on the previously reported method (123-124).

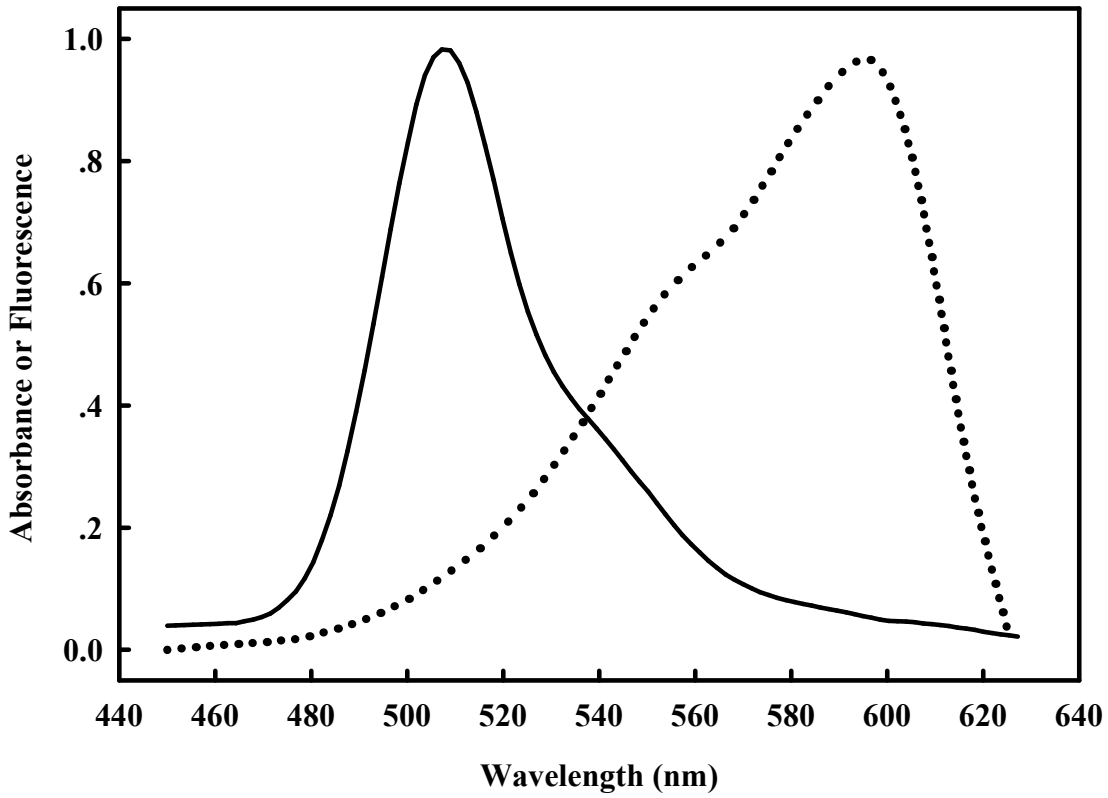

Figure 11. Spectral overlap integral between EGFP and ReAsH. The solid line indicates the fluorescence emission spectrum of EGFP with an excitation maximum wavelength of 488 nm, and the dotted line indicates the absorbance of ReAsH at the corresponding wavelength. The emission maximum wavelength of EGFP is 509 nm, which is the typical wavelength for EGFP. The spectra were subtracted from the buffer (10 mM potassium phosphate, pH 7.4, 150 mM NaCl, 100 μM TCEP, and 10 μM zinc acetate) background and normalized in order to show the same scale. The sample concentration is 0.2 μM EGFP, while the ReAsH concentration is 10.0 μM in order to decrease the background of detection error.

The spectral overlap was obtained by numerical integration using **Equation 5**.

$$J(\mathrm{M}^{-1}\cdot\mathrm{cm}^{-3}) = \frac{\int F_{\mathrm{d}}(\lambda)\varepsilon_{\mathrm{a}}(\lambda)\lambda^4 d\lambda}{\int F_{\mathrm{d}}(\lambda)d\lambda} = \frac{\sum_{\lambda=450}^{630} F_{\mathrm{d}}(\lambda)\cdot\frac{A_{\mathrm{a}}(\lambda)}{C_{\mathrm{a}}}\cdot\lambda^4\cdot 10^{-35}}{\sum_{\lambda=450}^{630} F_{\mathrm{d}}(\lambda)\cdot 10^{-7}} \quad (5)$$

where, J indicates the spectral overlap integral between the emission spectrum of the donor and the absorption spectrum of the acceptor; $F_{\mathrm{d}}(\lambda)$ indicates the fluorescence intensity of donor; $\varepsilon_A(\lambda)$ is the acceptor molar extinction coefficient in $cm^{-1}\cdot M^{-1}$ units; $A_{\mathrm{a}}(\lambda)$ indicates the absorbance of acceptor; C_{a} represents the molar concentration of acceptor for the determination of absorbance; and λ indicates wavelength. The J was found to be 2.1198×10^{-13} ($M^{-1}\cdot cm^{-3}$) and R_0 was measured to be 51.83 Å.

2.16 Fluorescence labeling with FlAsH or ReAsH

20 fold molar excess of the ReAsH-EDT_2 or FlAsH-EDT_2 was incubated overnight with the protein (10–100 μg) with CCPGCC at room temperature in the phosphate buffer (10 mM phosphate, 200 mM NaCl, 100 μM TCEP, and 1 mM β–mercaptoethanol, pH 7.2). The excess ReAsH (or FlAsH) and EDT were removed by two successive cycles of 50-fold dilution and concentration using Microcon filter (Millipore) with 30 kD molecular weight cut-off. The concentration of ReAsH was determined by UV-vis absorbance at 597 nm (ε = 63,000 $M^{-1}\cdot cm^{-1}$). The amount of EGFP was measured by fluorescence at 509 nm. The results indicate that all the proteins are labeled with ReAsH and the ratio of EGFP to CCPGCC(ReAsH) was 1 to 1.

Labeling of N-terminally FlAsH-tagged CCPGCC-SNAP-25, CCPGCC-SNAP-25(1-140), and SNAP-25(141-206) was performed in the phosphate buffer (10 mM

phosphate, 200 mM NaCl, 100 μM TCEP, and 1 mM β–mercaptoethanol, pH 7.2). The protein of CCPGCC-SNAP-25(141-206) was chosen to be labeled with ReAsH. Excess free dye (ReAsH and FlAsH) and EDT were removed by dialysis into 1× PBS buffer with 10% Polyethylene glycol (Mol. Wt 15,000-20,000). The concentration of labeled protein after the dialysis was determined from the absorbance measured at 508 nm, which the molar extinction coefficient (ε) for bounded FlAsH was 41,000 $M^{-1} \cdot cm^{-1}$ for all the proteins.

2.17 Circular Dichroism.

CD spectra were obtained on a Jasco J710 Spectropolarimeter equipped with a temperature control system (Model NESLAB). The CD spectra between 190 and 250 nm were recorded at 25 °C in a 0.1 cm path-length quartz cell using a protein concentration of 5.0 μM. The scan rate was 25 nm/min and the response time was 4 s. The width of the slit was set at 1.0 nm and sensitivity was 50 mdeg. All CD spectra were recorded based on an average for 3 accumulations. Equilibrated buffer was recorded for correction. All of the sample spectra were recorded after subtracting the background of the buffer.

2.18 Synthesis of ReAsH-EDT_2

ReAsH-EDT_2 was synthesized by Huiguo Lai, as described by Tsien (122, 125) with minor modifications. Resorufin was used as the starting material to synthesize intermediate **1**. After demercuration and addition with $AsCl_3$ in a specific condition, the final product **2** was obtained as a red solid. The synthesis scheme is shown in **Figure 12**. Similarly, FlAsH-EDT_2 was synthesized by using fluorescein as a starting material. The

intermediate **3** was synthesized as the previous reported method (122, 125). The final FlAsH-EDT_2 was obtained as a dark solid. The synthesis scheme is shown in **Figure 13**.

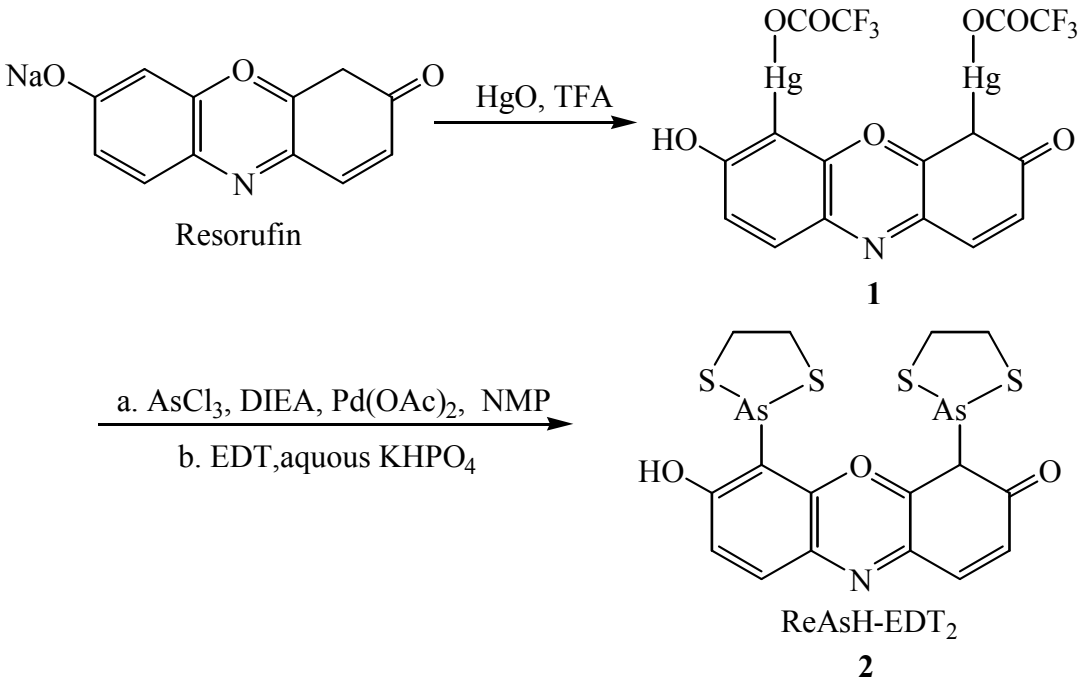

Figure 12. Synthesis route of ReAsH-EDT_2.

2.18A Synthesis of Resorufin 4,5-Bis(mercuric trifluoroacetate); Bis(trifluoroacetato-κO)[μ-(7-hydroxy-3H-phenoxazin-3-one-4,5-diyl)]dimercury (1).

To a solution of mercuric oxide (480 mg, 2.0 mmol) and trifuloroacetic acid (8.0 ml) at ambient temperature was added resorufin sodium salt (240 mg, 1.0 mmol) portion-wise during 5 min. After the addition of resorufin was completed, the reaction mixture was allowed to warm gradually to reflux overnight. The solvent was removed *in vacuo*. The solid was collected and washed with water (3 × 20 ml). The residue was dried for the next step reaction without further purification. Pure **1** (528 mg, 63 %) was thereby

obtained as a dark red powder. ^{1}H NMR (DMSO-d_6): δ7.59 (d, J = 8.7 Hz, 2 H), 6.94 (d, J = 8.7 Hz, 2 H), 3.46 (br, peak disappears when sample is shaken with D_2O, 1 H, OH).

2.18B Synthesis of ReAsH-EDT$_2$; 4, 5-Bis(1,3,2-dithiarsolan-2-yl)resorufin (2).

To the solution of **1** (168 mg, 0.2 mmol) and 1-methyl-2-pyrrolidinone (4.0 ml) at ambient temperature, arsenic trichloride (0.34 ml, 8.0 mmol), DIEA (0.28 ml, 3.2 mmol), and palladium acetate (10 mg) were added sequentially under the protection of N_2. The resulting mixture was heated at 60 ºC for 3 h. The reaction mixture was allowed to cool down gradually to room temperature and then poured into acetone and potassium phosphate (0.25 M, pH = 6.9) mixture (50 ml, 1:1 v/v). Excess of 1, 2- ethanedithiol (1.0 ml) was added portion-wise in 5 min into the mixture. Milky precipitation was observed during the addition of EDT. The mixture was stirred for 30 min. The reaction mixture was washed sequentially with ethyl acetate (3 × 25 ml), water (3 × 25 ml), and brine (3 × 25 ml). The organic layer (top layer) was collected and dried ($MgSO_4$). After filtration, the filtrate was concentrated *in vacuo*. The residue was purified via column chromatography on silica gel by eluting with 10% EtOAc-hexane. Pure **2** (85.0 mg, 77.8%) was thereby obtained as a dark red solid. ^{1}H NMR ($CDCl_3$): δ6.22 (d, J = 8.3 Hz, 2 H), 6.30 (d, J = 8.3 Hz, 2 H), 3.58 (br, peak disappears when sample is shaken with D_2O, 1 H, OH); 3.49 (m, 8 H, S-CH_2).

2.19 Synthesis of FlAsH-EDT$_2$

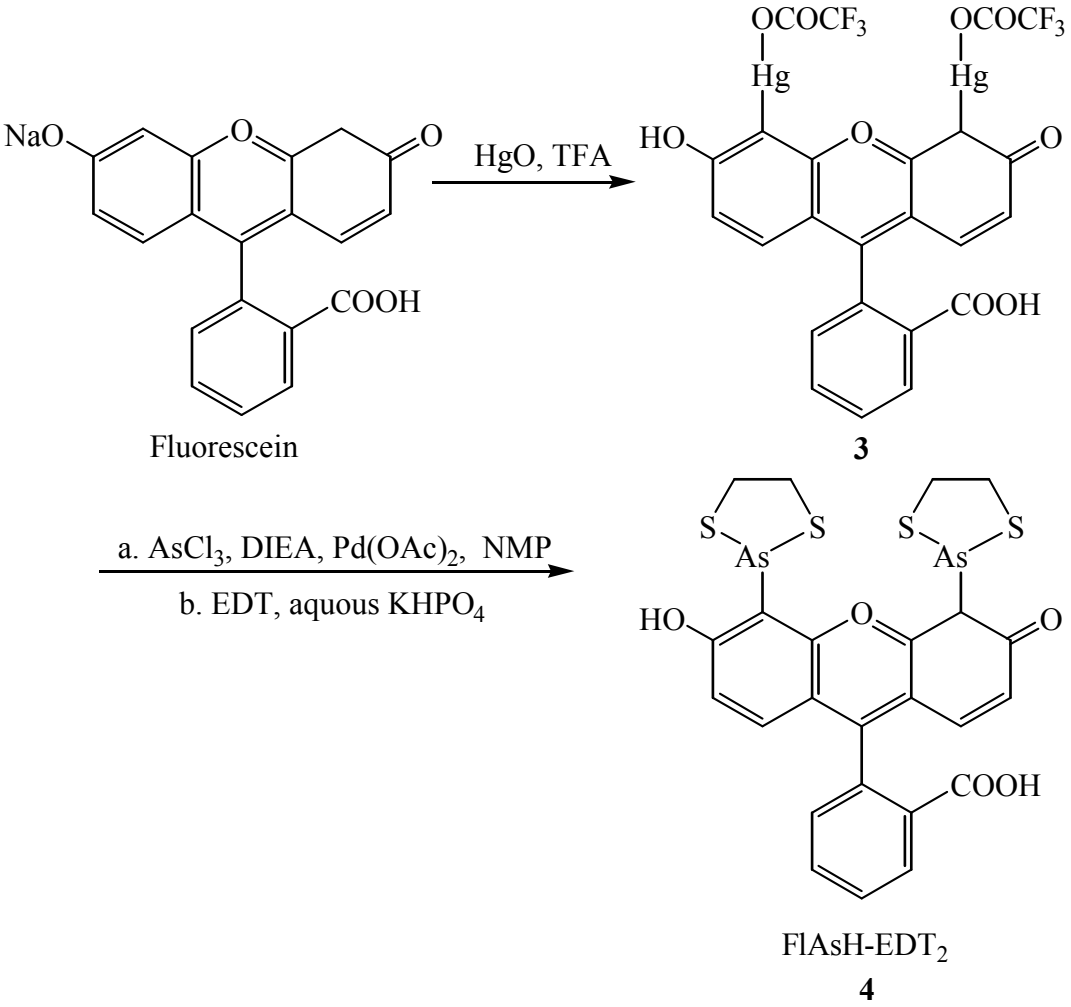

Figure 13. Synthesis route of FlAsH-EDT$_2$.

2.19A Synthesis of Fluorescein 4', 5'-Bis(mercuric trifluoroacetate); (3).

To the solution of mercuric oxide (480 mg, 2.0 mmol) and trifluoroacetic acid (8.0 ml) at ambient temperature was added fluorescein sodium salt (355 mg, 1.0 mmol) portion-wise during 5 min. After the addition of fluorescein had been completed, the reaction mixture was allowed to warm gradually to reflux overnight. The solvent was removed *in vacuo*. The solid was collected and washed with water (3 × 20 ml). The

residue was dried for the next step reaction without further purification. Pure **3** (769 mg, 80 %) was thereby obtained as a dark red powder. ^{1}H NMR (DMSO-d_6): δ4.48 (br, peak disappears when sample is shaken with D_2O, 1 H, OH), 6.46 (d, J = 8.7 Hz, 2 H, H-2'), 6.61 (d, J = 8.7 Hz, 2 H, H-1'), 7.39 (d, J = 7.5 Hz, 1 H, H-7), 7.84(m, 1 H, H-6), 7.88 (m, 1 H, H-5), 8.04 (d, J = 7.5 Hz, 1 H, H-7).

2.19B Synthesis of FlAsH-EDT$_2$; 4', 5' Bis(1, 3, 2-dithiarsolan-2-yl)-fluorescein (4).

To the solution of **3** (192 mg, 0.2 mmol) and 1-methyl-2-pyrrolidinone (4.0 ml) at ambient temperature, arsenic (III) chloride (0.34 ml, 8.0 mmol), DIEA (0.28 ml, 3.2 mmol), and palladium acetate (10 mg) were added sequentially under the protection of N_2. The resulting mixture was heated at 60 ºC for 3 h. The reaction mixture was allowed to cool down gradually to room temperature and then poured into an acetone and potassium phosphate (0.25 M, pH = 6.9) mixture (50 ml, 1:1 v/v). Excess of 1, 2- ethanedithiol (1.0 ml) was added portion-wise in 5 min into the mixture. Milky precipitations were observed during the addition of EDT. The mixture was stirred for 30 min. The reaction mixture was washed sequentially with ethyl acetate (3 × 25 ml), water (3 × 25 ml), and brine (3 × 25 ml). The organic layer (top layer) was collected and dried ($MgSO_4$). After filtration, the filtrate was concentrated *in vacuo*. The residue was purified via column chromatography on silica gel by eluting with 10% EtOAc-hexane. Pure **4** (118.0 mg, 89%) was thereby obtained as a dark solid. ^{1}H NMR ($CDCl_3$): δ3.08 (br, peak disappears when sample is shaken with D_2O, 1 H, OH), 3.67 (m, 8 H, -SCH_2CH_2S-), 6.48 (d, J = 8.7 Hz, 1 H, H-2'), 6.67 (d, J = 8.7 Hz, 1 H, H-1'), 7.09 (d, J = 8.7 Hz, H-7), 7.68 (m, 2H, H-5, 6), 8.09 (d, J = 8.7 Hz, 1 H, H-4).

Chapter 3. Slow and tight binding inhibitors of BoNT/A LC

3.1 Introduction

Botulinum neurotoxins (BoNTs) are the causative agents of botulism and have been recognized as the most toxic substances known to man (34). BoNTs have found broad clinical applications in an increasing number of neurological diseases, such as dystonia, migraine headache, and others (36). However, the potential nefarious misuse of these neurotoxins in a bioterrorist action could result in mass casualties requiring post-exposure therapy. Effective medical counter-measurements to treat victims after signs and symptoms of botulism have presented are limited, and therapies to target, inactivate and clear toxin from nerve cell are being actively sought worldwide.

Several "unusual" properties of the zinc protease in BoNTs have been discovered, such as their extraordinary substrate specificity, the extensive substrate-protease interactions in substrate recognition (25), the pivotal roles of amino acid residues distal from the active site in substrate binding and catalysis (28), and the PRIME and molten globular states during catalysis (126).

Recent progress in determining the three-dimensional structure of BoNTs has provided molecular insights about these neurotoxins and a computational basis for designing inhibitors based on the structure. Quinolinol-based compounds (127) were reported to effectively inhibit the protease activity of BoNT/A LC and BoNT/A holotoxin. These results raised the possibility that quinolinol derivatives can be used to against BoNT. Since the exact mechanism of inhibition by this class of compounds remains to be elucidated, we sought to study their mechanism of action (128). Preliminary studies revealed a disparate range between the concentrations for binding and

inhibition suggesting that the inhibition may be affected by the high concentration of peptide substrate, the zinc ions in the buffer and at the enzyme's active site as well as the temperatures and pH of the buffers.

In my thesis, we examined the binding and inhibition of BoNT/A LC with the quinolinol derivatives and peptide inhibitors by using enzyme kinetics and fluorescence titration in the absence and presence of Zn^{2+} from the active site of BoNT/A LC. Molecular modeling was used to evaluate the consistency with the experimental results. Here we show that the effective quinolinol inhibitors bind to Zn^{2+}-free BoNT/A LC and peptide-BoNT/A LC complexes. The results suggest that the inhibitory structure corresponds to the QAQ binding mode to the Peptide-BoNT/A LC complex. The model of QAQ inhibition has significant implications for their use and provides a rationalization for their different effects in various assays.

3.2 Results

3.2.1 Fluorescence quenching of BoNT/A LC

The concentration in the stock of BoNT/A LC(1-425), was 5.0 mg/ml. The fluorescence intensity of the LC decreased with time upon dilution. Three types of LCs (full length BoNT/A, truncated BoNT/A LC(1-425) and BoNT/B LC) were tested and all three showed a fluorescence gradually decrease upon dilution. The results are shown in **Figure 14**. The first order kinetic data of the time courses are consistent with either the dissociation of the dimmers in a high concentration of LCs or the conformational changes of the light chains upon dilution.

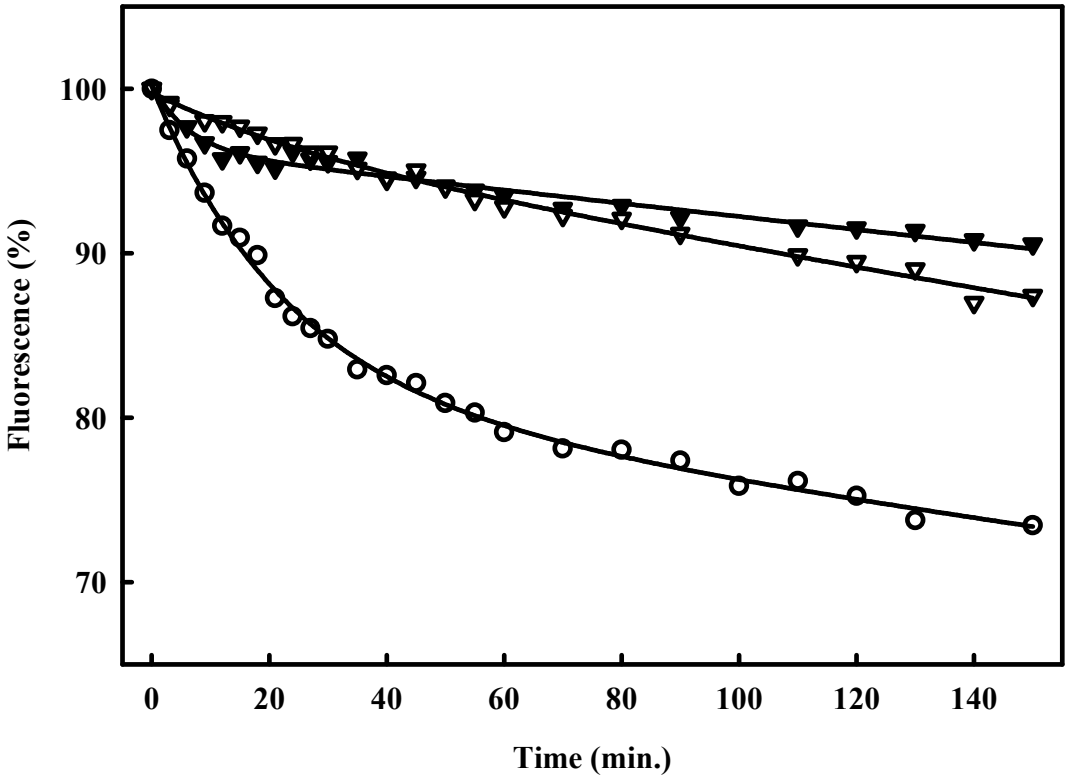

Figure 14. Time courses of fluorescence changes of full length BoNT/A LC, truncated BoNT/A LC1-425 and BoNT/B LC. 1.0 µl of BoNT/A LC(1-425) (5.0 mg / ml) was diluted into 500 µl buffer (10 mM phosphate, 150 mM NaCl, 10 µM zinc acetate, pH = 7.4). The fluorescence intensity gradually decreased with time. The time courses correspond to: (○) BoNT/A LC-full length; (▼) BoNT/B LC; (▽) BoNT/A LC(1-425). The solid lines are fitted curves to two exponential decays.

At the end of 2 h incubation, 20% fluorescence quenching for BoNT/A LC, but less than 10% quenching for BoNT/B LC and truncated BoNT/A LC1-425. The fluorescence intensity changes are relatively small after 1 h. All light chains were incubated at 25 ˚C for 1 h after dilution before binding studies.

3.2.2 Strategy of inhibitors screening

Virtual screening of the NCI database (http://cactus.nci.nih.gov/) was performed in collection with Istvan Enyedy at Lombadi Cancer Center of Georgetown University to initially sift through >250,000 compounds activities against BoNT/A LC. The binding pose (orientation and conformation) of each molecule was evaluated by the DOCK scoring function. Five hundred top scoring compounds were selected and visually inspected for best fit in the binding site. Following this initial screen, 100 compounds were tested for inhibition of the protease activities of BoNT/A LC using an HPLC-based assay. Three rounds of screening and synthesis of analogs were carried out in collaboration with Leonard A. Smith and Virginia Roxas-Duncan at U.S. Army Medical Research Institute of Infectious Diseases (USAMRIID). Four compounds (**Figure 16**) were selected and advanced to the *in vitro* and *ex vivo* bio-assays.

3.2.3 Quinolinol derivatives as lead inhibitors

To determine the effectiveness of the compounds initially identified by using the virtual screening, an HPLC-based enzymatic assay was performed in the presence and absence of inhibitor at 20 μM and 200 μM concentrations using a recombinant full-length BoNT/A LC in collaboration with Leonard A. Smith's research group at U.S. Army Medical Research Institute of Infectious Diseases (USAMRIID). Of the 100 compounds that were tested, 14 compounds were confirmed that inhibited BoNT/A LC by more than 60%. One of the compounds that showed high percent inhibition against BoNT/A LC in the assays was 7-(phenyl(8-quinolinylamino)-8-quinolinol (QAQ). Further research on this candidate demonstrated that QAQ was predicted to have quinolinol scaffold, and was non-toxic to mammalian cells. So a synthesized QAQ to >98% purity by LC-MS and NMR was chosen to re-tested in the HPLC assays, which showed 74% inhibition (20 μM) against BoNT/A LC. Hence, this particular compound became the basis for a second round of analog search. Additional inhibitors were screened based on the QAQ with quinolinol scaffold moieties. The structures of the inhibitors are shown in **Figure 15**. All molecules contain the quinolinol scaffold. These compounds were chosen to carry out additional biochemical studies by fluorescence titration and kinetics studies. The binding mode between the quinolinol moiety and BoNT/A LC was examined in collaboration with Minghao Feng and Sivanesan Dakshanamurthy. The quinolinol derivatives could be a good candidate for the future development as a drug against botulism.

3.2.4 Tight binding of quinolinol derivatives to BoNT/A LC

Four small molecule inhibitors (QAQ, BAPQ, CAPQ and NAPQ) were initially identified from the virtual screening and inhibition assays. The structures of these inhibitors are shown in **Figure 15**. The intrinsic fluorescence of BoNT/A LC was quenched by the small molecule inhibitors. The binding of the small molecule inhibitor was thus determined by fluorescence titration by monitoring the quenching of BoNT/A LC fluorescence at varying concentrations of the inhibitor. The apparent dissociation constants of QAQ, BAPQ, CAPQ and NAPQ were determined by fluorescence titration. These inhibitors showed binding to BoNT/A LC with dissociation constants ranging from 140 to 33 nM in the presence of 10 μM zinc acetate. The results are shown in **Figure 16**.

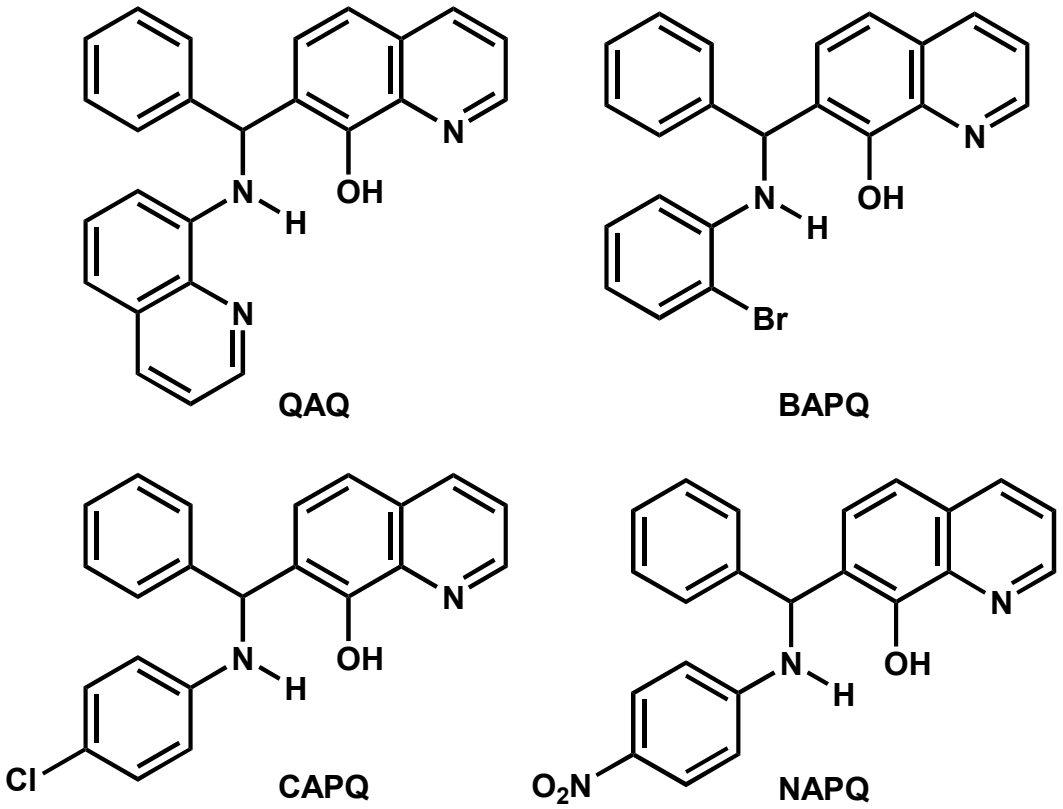

Figure 15. Structure of small molecule inhibitors. All the inhibitors contain quinolinol scaffold which is a strong Zn^{2+}-binding moiety. Abbreviations used: QAQ, 7-(phenyl(8-quinolinylamino)-8-quinolinol, NSC 84096; BAPQ, 7-((2-bromoaminlino)(8-quinolinylamino)methyl)-8-quinolinol, NSC 84086; CAPQ, 7-((4-chloroanilino)(phenyl) methyl)-8-quinolinol, NSC 84090; NAPQ, 7-((4-hydroxy(oxido)amino)amilino)(phenyl) methyl)-8-quinolinol, NSC 1010.

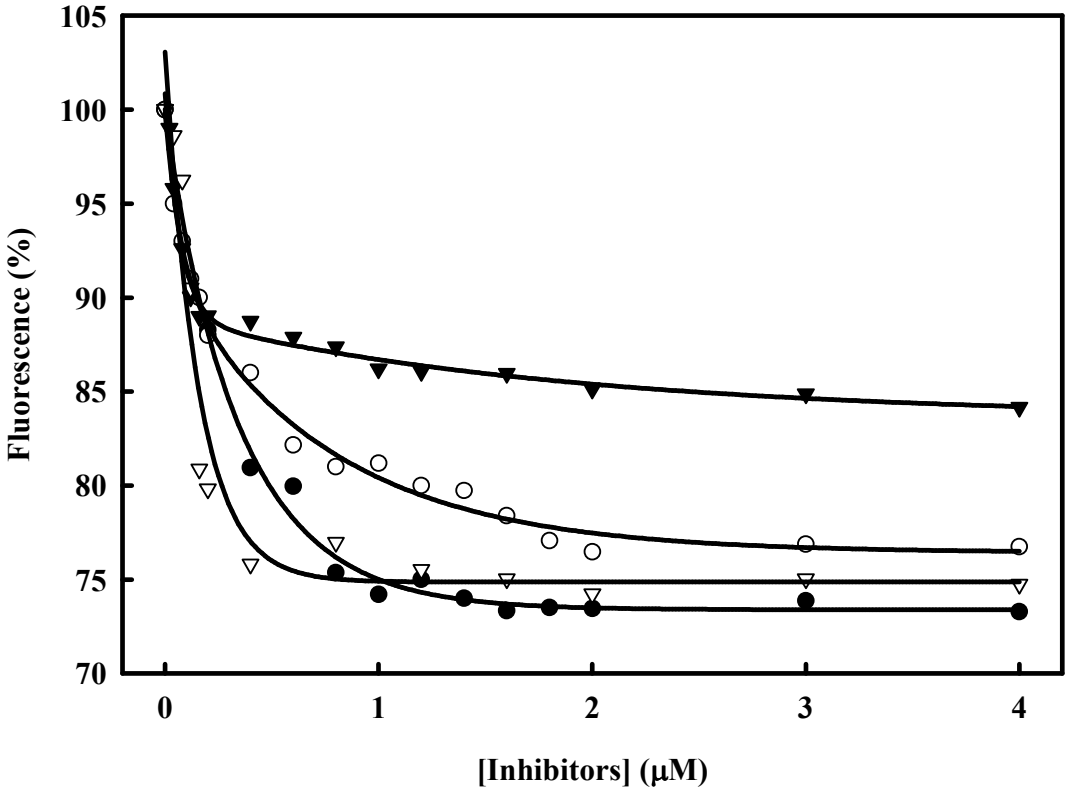

Figure 16. Fluorescence titration of BoNT/A LC with inhibitors. The BoNT/A LCs (0.1 μmol) were diluted with 500 μl of buffer (10 mM phosphate, 150 mM NaCl, 10 μM zinc acetate, pH = 7.4). Spectra were recorded at 25 ºC. The fluorescence intensity gradually decreased with addition of inhibitors was converted to the percentage of fluorescence. The inhibitors were as follows: (●) BAPQ; (○) CAPQ; (▼) NAPQ; (▽) QAQ. The solid line is the theoretical quenching curve calculated by the **Equation 2**. The fluorescence intensity was measured at 323 nm with excitation at 280 nm. All the spectra were shown after subtraction of the buffer spectrum. The apparent dissociation constants for BAPQ, CAPQ, NAPQ and QAQ were 0.142 ± 0.021, 0.127 ± 0.029, 0.114 ± 0.022 and 0.020 ± 0.013 μM, respectively.

3.2.5 Effect of zinc on the binding of quinolinol QAQ

BoNT/A LC is a zinc protease. Zinc ion is very important to maintain the LC activity. So the zinc concentration in the buffer may affect the inhibitors binding to the active sites of BoNT/A LC due to zinc chelation. The apparent dissociation constant of QAQ and the BoNT/A LC was 0.0301 ± 0.0032 μM in the presence of 10 μM Zn^{2+} in buffer, while the apparent dissociation constant was 0.215 ± 0.016 μM in the presence of 10 mM Zn^{2+} in buffer (**Figure 17**). The dissociation constant was 0.0186 ± 0.0041 μM if there was no zinc in buffer. The dissociate constant was less than two-fold difference (0.0301 to 0.019) at 10 μM Zn^{2+} and no zinc at all in buffer. The dissociation constant was about 10-fold difference (0.215 to 0.030) in 10 μM Zn^{2+} and 10 mM Zn^{2+} buffer.

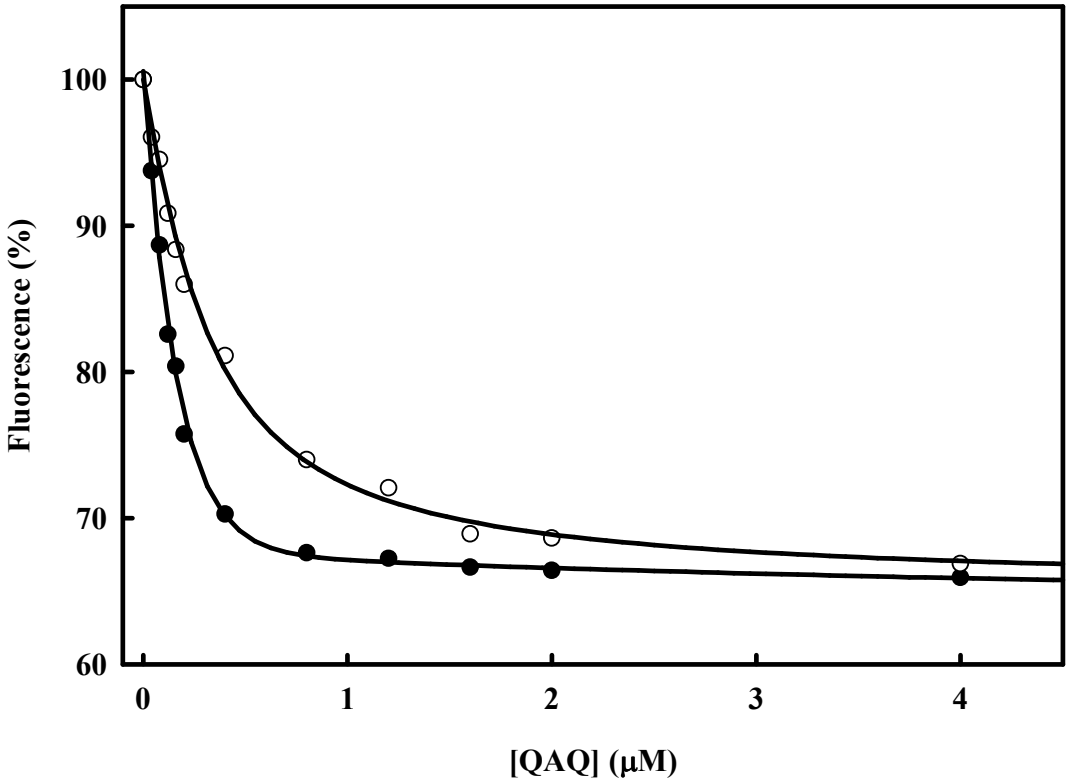

Figure 17. Fluorescence titration of QAQ with BoNT/A LC in the presence of different concentration of Zn^{2+} in phosphate buffer. The concentration of Zn^{2+} was: (●) 10.0 μM and (○) 10.0 mM. The obtained dissociation constants for **QAQ** in 10.0 μM and 10.0 mM Zn buffer were: 0.0301 ± 0.0032 μM and 0.2146 ± 0.0161 μM, respectively. The solid lines were the fitted curves using **Equation 2**. The percentages of maximal fluorescence changes at 10 μM and 10 mM Zn^{2+} were (34.50 ± 0.29)% and (34.79 ± 0.41)%, respectively. The standard devivation came from the vurve-fitting **Equation 1**.

3.2.6 Temperature effects on the binding of inhibitors to LC

The effects of experimental parameters such as temperature and pH on the inhibitor bindings were examined. The K_D of QAQ to BoNT/A LC increased from 0.016 ± 0.006 μM at 25 ˚C to 0.023 ± 0.0014 μM and 0.071 ± 0.002 μM at 37 ˚C and 42 ˚C, respectively. The decrease of the affinity of the BoNT/A LC corresponded to a decrease in the entropy of 135 $J \cdot mol^{-1} \cdot K^{-1}$ of the QAQ binding to LC suggesting hydrophobic interactions may be involved in the QAQ binding to the BoNT/A LC.

3.2.7 Effects of pH on the binding of inhibitors to BoNT/A LC

When the pH was reduced to 5.0, the affinity of QAQ to BoNT/A LC decreased slightly. The K_D at pH 5.0 were 0.04 ± 0.016 μM, 0.096 ± 0.0032 μM and 0.113 ± 0.048 μM at 27, 37 and 42 ˚C, respectively. The slight decrease in affinity could be partially attributed to protonation of the quinolinol amino group at the lower pH. The lack of a major change in the K_D in relation to temperature and pH suggested that high temperature and low pH were unlikely to drastically affect the affinity of QAQ to BoNT/A LC.

3.2.8 Stoichiometry of BoNT/A LC and CRATKML

CRATKML is a known inhibitor of BoNT/A LC with stoichiometric binding (60). To 0.02 μM BoNT/A LC, the short peptide CRATKML was added. The intrinsic fluorescence intensity was monitored based on the LC's fluorescence quenching of emission maximum wavelength at 323 nm with excitation at 280 nm at 25 °C. The results are shown in **Figure 18**.

Plotting the fluorescence changes against the ratio of free CRATKML and BoNT/A LC, the quenching curve was obtained. 35% fluorescence quenching observed when CRATKML and BoNT/A LC reached equilibrium. The obtained K_d of CRATKML to BoNT/A LC was 0.015 ± 0.006 μM based on the fluorescence titration. The intercept of the initial fluorescence intensity changes of CRATKML and the saturated conditions of the binary complex was extrapolated. The stoichiometry between CRATKML and BoNT/A LC was close to 1 (**Figure 18**). The results suggest that one molecule of CRATKML bound to one molecule of BoNT/A LC in the binary complex.

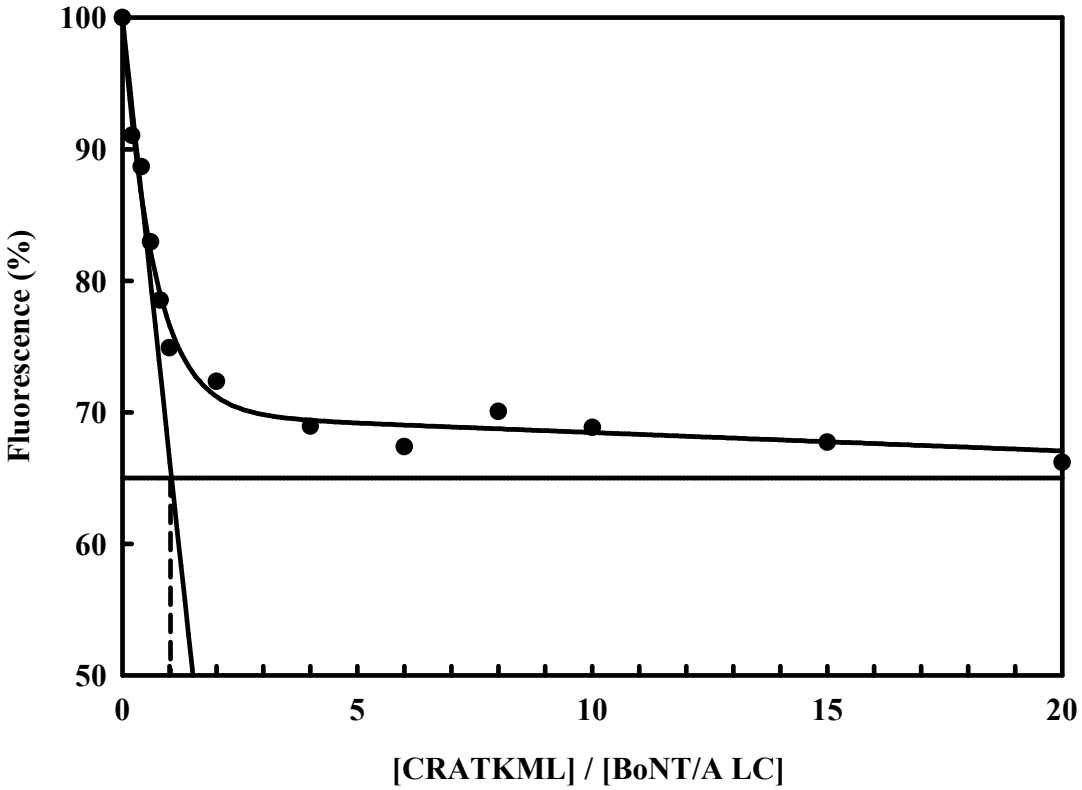

Figure 18 Stoichiometry of BoNT/A LC with short peptide CRATKML. The BoNT/A LCs (1.0 µl, 5.0 mg / ml) were diluted with 500 µl of buffer (10 mM phosphate, 150 mM NaCl, 10 µM zinc acetate, pH = 7.4). The fluorescence intensity was measured at 323 nm with excitation at 280 nm at 25 ºC. The fluorescence intensity gradually decreased with addition of CRATKML and the percent quenching of fluorescence was calculated. The dash indicated that the stoichiometry between CRATKML and BoNT/A LC was 1 to 1.

3.2.9 Interactions of QAQ to the CRATKML-BoNT/A LC

The peptide CRATKML was incubated with BoNT/A LC to form a binary of complex. QAQ was added to the binary complex. The fluorescence intensities were measured with addition of QAQ. The results are shown in **Figure 19**.

The results indicate that more binary complex formed between CRATKML and BoNT/A LC when the initial concentration of CRATKML was higher. When QAQ added to the binary complex, QAQ was competitive binding with CRATKML. Two kinds of binary complex (BoNT/A LC-CRATKML and BoNT/A LC-QAQ) provided the contribution of fluorescence intensity. The results suggested that QAQ might replace the CRATKML in order to bind to BoNT/A LC since QAQ and CRATKML bound to LC at the same binding site of BoNT/A LC.

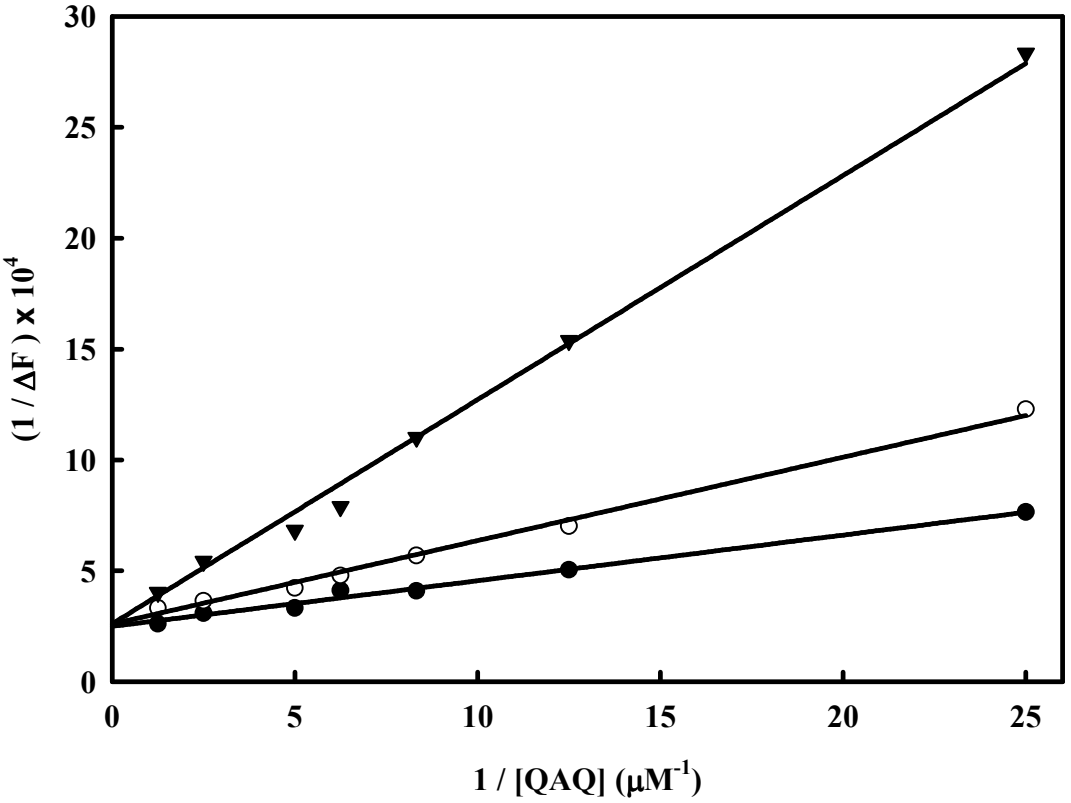

Figure 19. Double reciprocal plot of QAQ binds to the CRATKML-BoNT/A LC complex. The BoNT/A LCs (1.0 µl, 5.0 mg / ml) were diluted with 500 µl of buffer (10 mM phosphate, 150 mM NaCl, 10 µM zinc acetate, pH = 7.4). CRATKML in varying concentrations was incubated with LC for 1 h at 25 °C to form a binary complex. QAQ was added into the binary complex of BoNT/A LC-CRATKML. The fluorescence intensity was measured at 323 nm with excitation at 280 nm at 25 ºC. The fluorescence intensity gradually decreased with addition of QAQ and double reciprocal was plotted based on the direct fluorescence intensity changes of the complex. The concentrations of peptide CRATKML were: (●) 0.2 µM; (○) 1.0 µM; (▼) 2.0 µM. The solid lines were the theoretical fitting lines with a linear equation.

3.2.10 Binding of QAQ to the Peptide C-BoNT/A LC

To further probe the interaction of QAQ with BoNT/A LC, synthetic peptide with the amino acid sequence corresponding to SNAP-25 residues E183 to G206 but with a Q197C mutation, Ac-EKADSNKTRIDEANCRATKMLGSG-NH_2, abbreviated as Peptide C, was synthesized. The C197 in Peptide C was incorporated to prevent Peptide C from being cleaved by BoNT/A LC. After the binary complex of Peptide C and LC formation, QAQ was added into the binary complex of Peptide C-BoNT/A LC. The fluorescence intensities of BoNT/A LC were monitored with addition of QAQ. The results are shown in **Figure 20**.

The results indicate that more binary complex formed between Peptide C and BoNT/A LC when the initial concentration of Peptide C was high. When QAQ added to the binary complex, QAQ was noncompetitive binding to Peptide C to form a ternary complex. Two kinds of binary complex (Peptide C-BoNT/A LC and QAQ-BoNT/A LC) and ternary complex of Peptide C-BoNT/A LC-QAQ provided the contribution of fluorescence intensity. The results suggested that QAQ bound to free LC and the complex of Peptide C-BoNT/A LC. The difference of Peptide C and CRATKML might due to the non-specific binding of Peptide C with BoNT/A LC in addition to the specific binding with sequence of CRATKML.

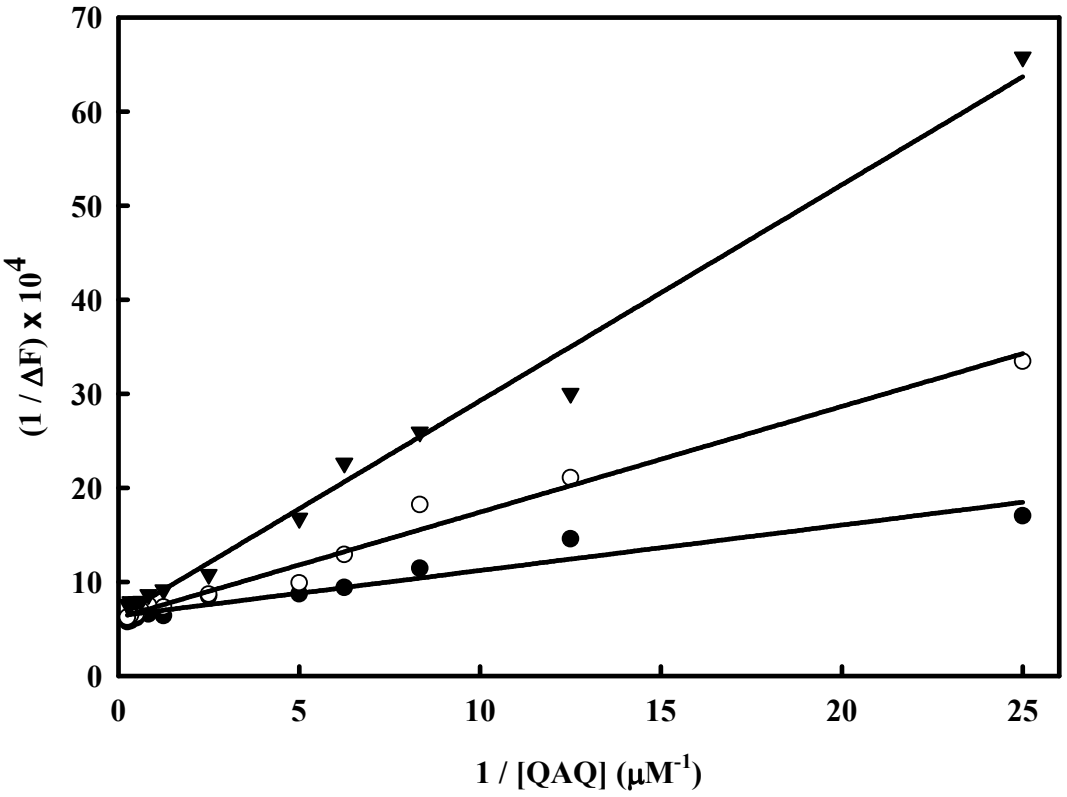

Figure 20. Double reciprocal plot of QAQ binds to the Peptide C-BoNT/A LC complex. The BoNT/A LCs (1.0 µl, 5.0 mg / ml) were diluted with 500 µl of buffer (10 mM phosphate, 150 mM NaCl, 10 µM zinc acetate, pH = 7.4). Peptide C in varying concentrations was incubated with LC for 1 h at 25 °C to form a binary complex. QAQ was added into the binary complex of Peptide C-BoNT/A LC to form a ternary complex. The fluorescence intensity was measured at 323 nm with excitation at 280 nm at 25 ºC. The fluorescence intensity gradually decreased with addition of QAQ and double reciprocal was plotted based on the direct fluorescence intensity changes of the complex. The concentrations of Peptide C were: (●) 0.2 µM; (○) 1.0 µM; (▼) 2.0 µM. The solid lines were the theoretical fitting lines with a linear equation.

3.2.11 IC_{50} of small molecule inhibitors

Inhibition of the metalloprotease activity of BoNT/A LC was determined using the intact GST-SNAP-25 fusion protein immobilized on glutathione microtiter plates at 37 ˚C. Under these conditions, up to 10 ng of GST-SNAP-25 per well was immobilized in a microtiter well. The obtained IC_{50} values for QAQ, CAPQ, NAPQ and BAPQ were 11.29, 0.29, 2.77 and 4.34 μM, respectively. The difference between IC_{50} and inhibition of the small molecule inhibitors might due to the difference of experimental conditions.

3.2.12 Non-competitive inhibition of BoNT/A LC by QAQ

The steady-state kinetics of QAQ inhibition of BoNT/A LC protease activity was examined using the FRET protease assay with SNAPtide as the substrate in the presence of excess zinc acetate (10 μM). The method is illustrated in **Figure 10**. Varying concentrations of SNAPtide with a specific concentration of QAQ in steady-state kinetic analysis gave nearly identical Michaelis-Menten constants of 42.3 ± 2.42, 42.7 ± 2.27 and 43.7 ± 3.76 μM SNAPtide at 0, 1 and 5 μM QAQ, respectively. Under the same conditions, the maximal velocities decreased from 5.64 to 4.2 μM/min and 3.3 μM/min for 0, 1 and 5 μM QAQ (**Figure 21**). Since QAQ affected the maximal velocity of SNAPtide cleavage catalyzed by BoNT/A LC without affecting the Michaelis-Menten constant for SNAPtide, QAQ appears to be a non-competitive inhibitor of BoNT/A LC. The corresponding inhibition constant, K_i, for QAQ was 1.84 ± 0.12 μM.

The inhibition of BoNT/A LC by QAQ was also examined by the microtiter assay using full-length SNAP-25. The IC_{50} of QAQ was 0.93 ± 0.032 and 1.21 ± 0.034 μM in the presence of 10 and 250 μM zinc acetate, respectively.

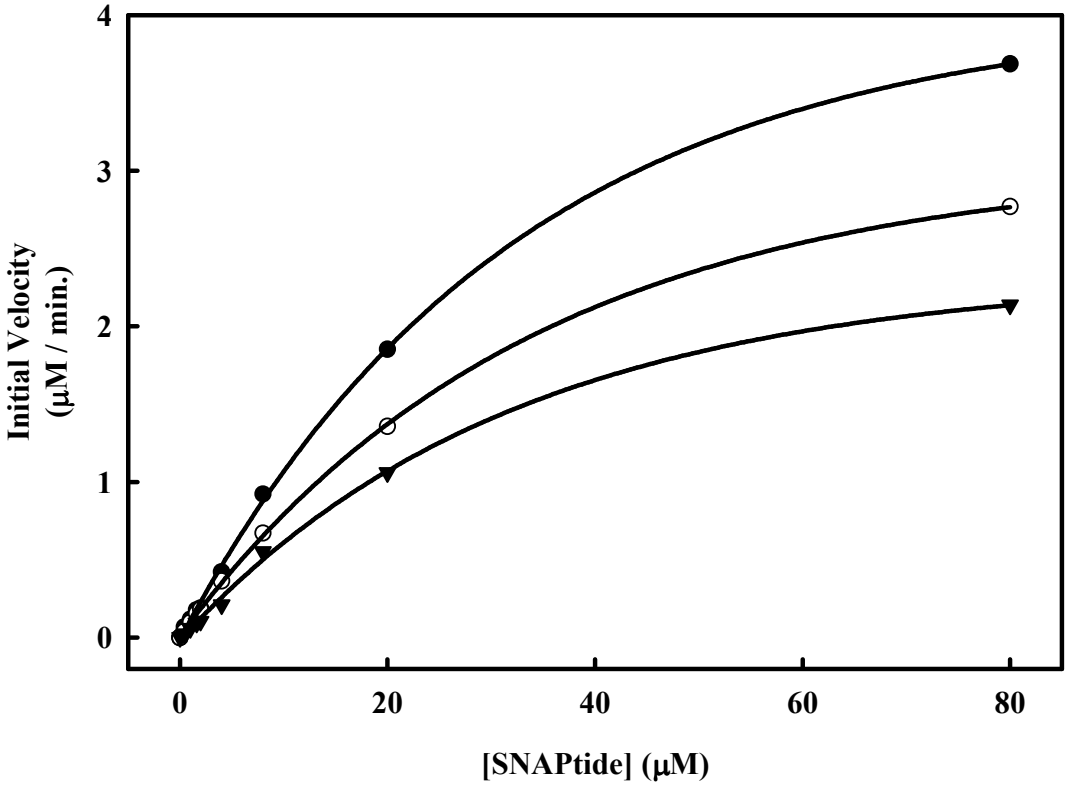

Figure 21. Inhibition of BoNT/A LC protease activity by QAQ. The initial rates of the SNAPtide cleavage catalyzed by 0.2 μM BoNT/A LC in 10 mM phosphate (pH 7.4), 150 mM NaCl, and 10 μM zinc acetate at 25 ºC. The concentrations of QAQ corresponded to: (●) 0 μM; (○) 1 μM; (▼) 5 μM. The reactions were initiated by the addition of BoNT/A LC and the fluorescence intensity at 420 nm was monitored with an excitation wavelength at 320 nm. Reactions were less than 5% complete in call cases to maintain valid steady-state measurements. The solid lines are fitted lines using the Michaelies-Menten equation.

Comparison of the K_D of QAQ to BoNT/A LC with the effective QAQ concentrations for protease inhibition of BoNT/A LC unexpectedly showed differences of nearly two orders-of-magnitude. These results are not likely to be due to the experimental parameters of the binding and protease assays, such as temperature (25 *vs.* 37 ˚C) and pH (5.0 *vs.* 7.4), since binding studies at various temperatures and pHs showed relatively small changes. The differences are most likely due to the different peptide concentrations. For binding studies, the dissociations constants were obtained in the absence of peptides, while inhibitions experiments were carried out in the presence of peptides which acted as the substrates of the enzyme. These results suggest that the interactions involved in QAQ binding and in peptide binding may be important in understanding the mechanism of QAQ inhibition.

3.2.13 Roles of Zn^{2+} chelation in quinolinol inhibition

Because quinolinols are known to chelate divalent cations (129), the potential roles of chelation on the inhibition of BoNT/A LC protease activity were examined. The Zn^{2+} in the light chain is required for catalysis. Whether QAQ inhibited the light chain protease activity by removing Zn^{2+} in the light chain was examined in collaboration with Minghao Feng. Zn^{2+} in the light chain was first stripped by incubating with 10 mM EDTA followed by dialysis against Chelex-100 pretreated buffer. The removal of Zn^{2+} from LC was confirmed using the chromogenic PAR assay (130). The light chain stripped of Zn^{2+} lost the protease activity as monitored by real-time SNAPtide protease assay. The protease activity of Zn^{2+}-depleted LC instantaneously restored to 80% activity by the addition of zinc acetate (128). Zn^{2+}-free BoNT/A LC (0.2 μM) was titrated with

QAQ in Chelex-100 pretreated buffer containing 10 mM phosphate (pH 7.4), 150 mM NaCl. Binding of QAQ was monitored by the change in the intrinsic fluorescent intensity of QAQ binding to Zn^{2+}-free BoNT/A LC and the dissociation constant was found to be 0.67 ± 0.05 μM, which indicated a tight binding to LC in the absence of Zn^{2+} at the active site. QAQ inhibited the protease activity of light chain with a K_i of 1.84 μM in the presence of an excess of Zn^{2+} relative to that of QAQ used. The fact that the value of K_i is similar to that of K_D for QAQ binding to the Zn^{2+}-free light chains suggests that QAQ inhibition of the light chain protease activity depends at least in part on the Zn^{2+}-independent binding pocket. The QAQ inhibition of the protease activity was unlikely due to the removal of Zn^{2+} by QAQ from the light chain since the protease activity could be immediately restored as the Zn^{2+} returned to the LC in the presence of excess Zn^{2+}.

3.2.14 Binding of Peptide C to BoNT/A LC

The binding of synthetic Peptide C to BoNT/A LC was examined using fluorescence titration by monitoring the intrinsic fluorescence intensity of BoNT/A LC upon addition of varying concentrations of Peptide C. The K_D of Peptide C-BoNT/A LC complex in PBS containing 10 μM zinc acetate was found to be 0.04 ± 0.01 μM as determined by monitoring the intrinsic fluorescence of BoNT/A LC. The IC_{50} of the Peptide C in PBS containing 10 μM zinc acetate was 3.4 ± 0.27 μM as determined by the SNAPtide protease assay.

3.2.15 BoNT/A LC binding of QAQ in the presence of Peptide C

The binding of QAQ to BoNT/A LC at indicated fixed concentrations of Peptide C was analyzed by monitoring the intrinsic fluorescence of BoNT/A LC. The K_Ds of QAQ to BoNT/A LC were 0.020 ± 0.0054, 0.066 ± 0.011, 0.124 ± 0.018, and 0.224 ± 0.034 μM in the presence of 0, 0.2, 1.0, and 2.0 μM Peptide C, respectively. Thus, the affinity of QAQ to BoNT/A LC was moderately affected by Peptide C.

The interactions of QAQ with BoNT/A LC were next examined in the presence of high concentrations of Peptide C (> 10 μM). **Figure 22** shows the QAQ binding curves with BoNT/A LC in the presence of 20, 40, and 60 μM Peptide C as determined by monitoring the intrinsic fluorescence of BoNT/A LC. The binding curves evidently consisted of two distinct phases. The binding at low concentrations of QAQ quenched the intrinsic fluorescence of BoNT/A LC and had a similar affinity as that observed in the absence of Peptide C, while the second phase showed fluorescence enhancement. The biphasic binding of QAQ in the presence of high concentrations of Peptide C suggested that the second phase of binding occurred at a much slower rate than the first phase such that second phase binding could not occur simultaneously with the first phase binding to give a smooth titration curve. Although it was an equilibrium measurement, the kinetic factors had to be considered in order to explain the biphasic curve. Peptide C appears to bind slowly to BoNT/A LC and the fluorescence increase was likely due to the binding of QAQ to the complex of BoNT/A LC and Peptide C. These findings led us to analyze the time courses for the kinetics of Peptide C binding to BoNT/A LC. The results are shown in **Figure 23**.

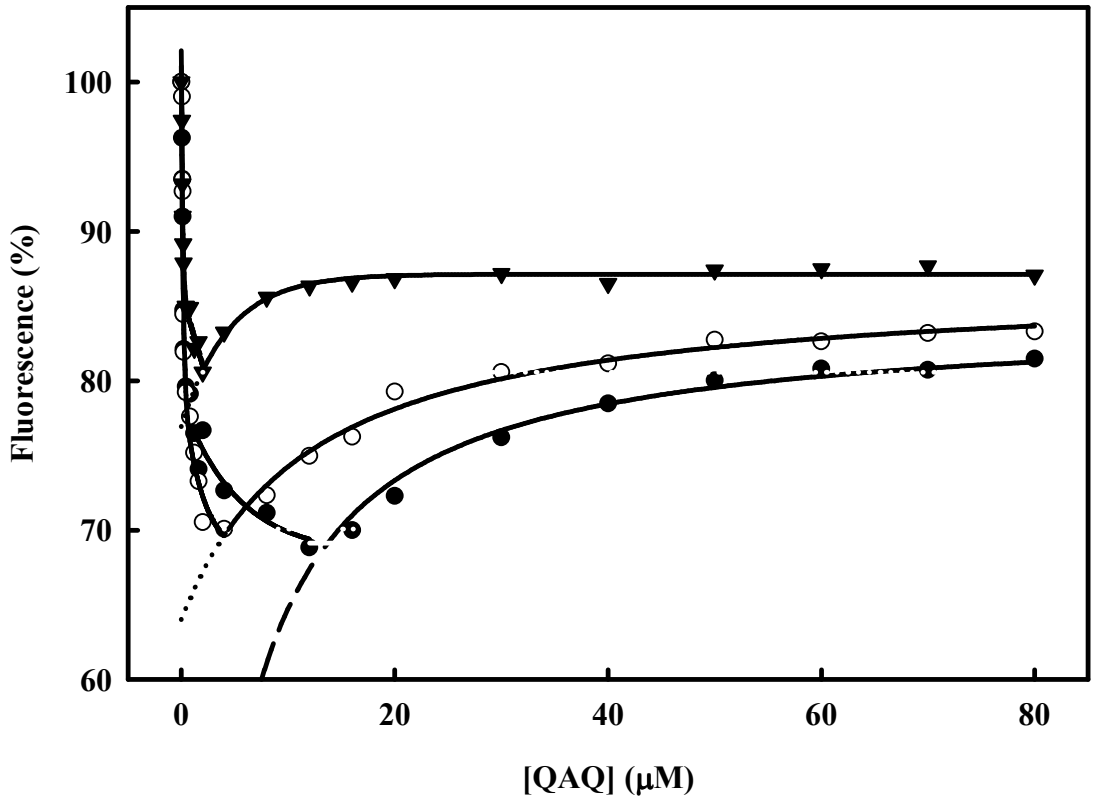

Figure 22. Fluorescence titration of BoNT/A LC with QAQ in the presence of Peptide C.

The intrinsic fluorescence of BoNT/A LC (0.2 μM) in 10 mM phosphate (pH 7.4), 150 mM NaCl and 10 μM zinc acetate was monitored with the addition of varying concentrations of QAQ in the presence of Peptide C. The concentration of Peptide C corresponded to: (●) 20 μM; (○) 40 μM; (▼) 60 μM. The fluorescence intensity was measured the emission maximum wavelength at 323 nm with the excitation maximum wavelength at 280 nm. The changes of the fluorescence intensity with the concentrations of the inhibitors were analyzed as described in Material and Methods. Solid lines are fitted curves of the K_Ds shown in the text using **Equation 2**.

3.2.16 Slow binding of Peptide C to BoNT/A LC

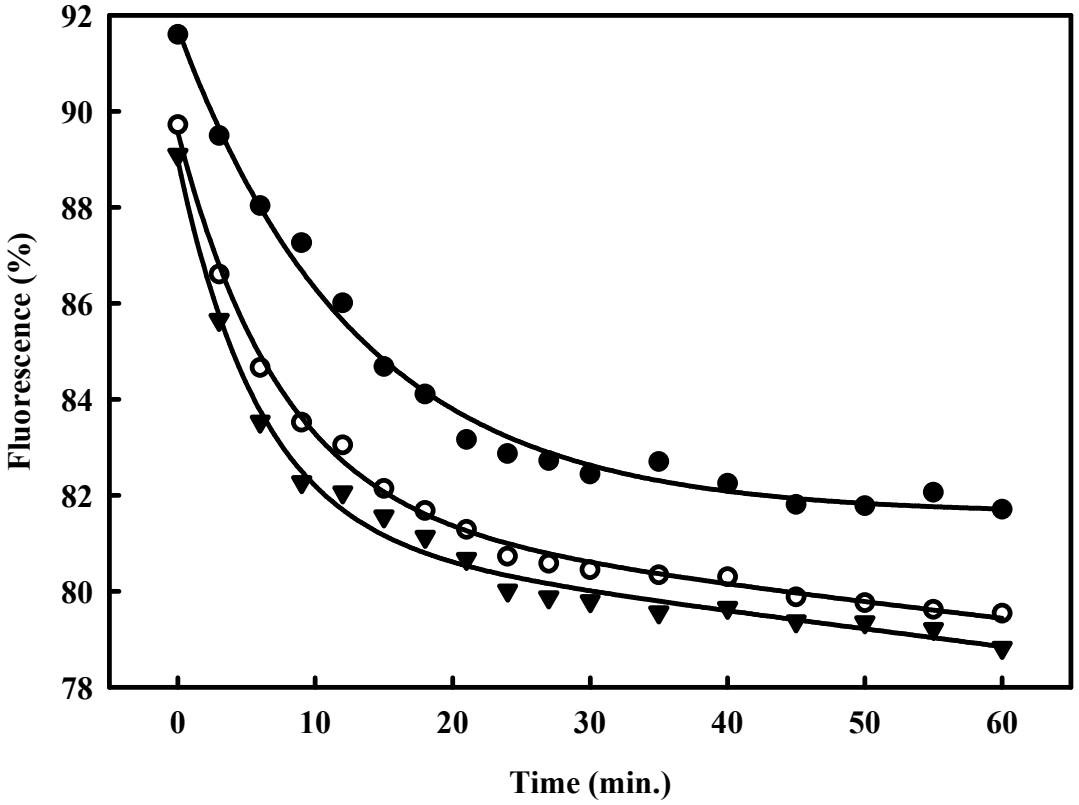

Figure 23. Time course of fluorescence changes of BoNT/A LC in the presence of Peptide C. The concentration of Peptide C was: (●) 1.0 μM; (○) 5.0 μM; (▼) 20.0 μM. The obtained binding rates for peptide C were: 0.077 ± 0.012, 0.103 ± 0.011 and 0.167 ± 0.016 min^{-1} at 1, 5, 20 μM Peptide C, respectively. The buffer background was subtracted;

BoNT/A LC (0.1 μmol) was diluted into 500 μl of PBS buffer containing 10 mM sodium phosphate (pH 7.4), 150 mM NaCl and 10 μM zinc acetate and incubated on ice for 1 h before the detection of fluorescence. The fluorescence intensity of LC was taken as 100 before the addition of Peptide C.

The time courses for the Peptide C binding to BoNT/A LC were determined by monitoring the time dependent changes in the intrinsic fluorescence immediately after incubating after the addition of Peptide C. The results are shown in **Figure 23.** Binding of the Peptide C to BoNT/A LC was slow and followed pseudo-first order reactions time courses in the presence of a 5-, 25-, and 100-fold excess of Peptide C in comparison to BoNT/A LC. The The second order rate constant for Peptide C binding to BoNT/A LC was determined from the observed pseudo-first order rate constants at varying concentrations of Peptide C and found to be 76.7 $M^{-1} \cdot s^{-1}$ (**Figure 24**).

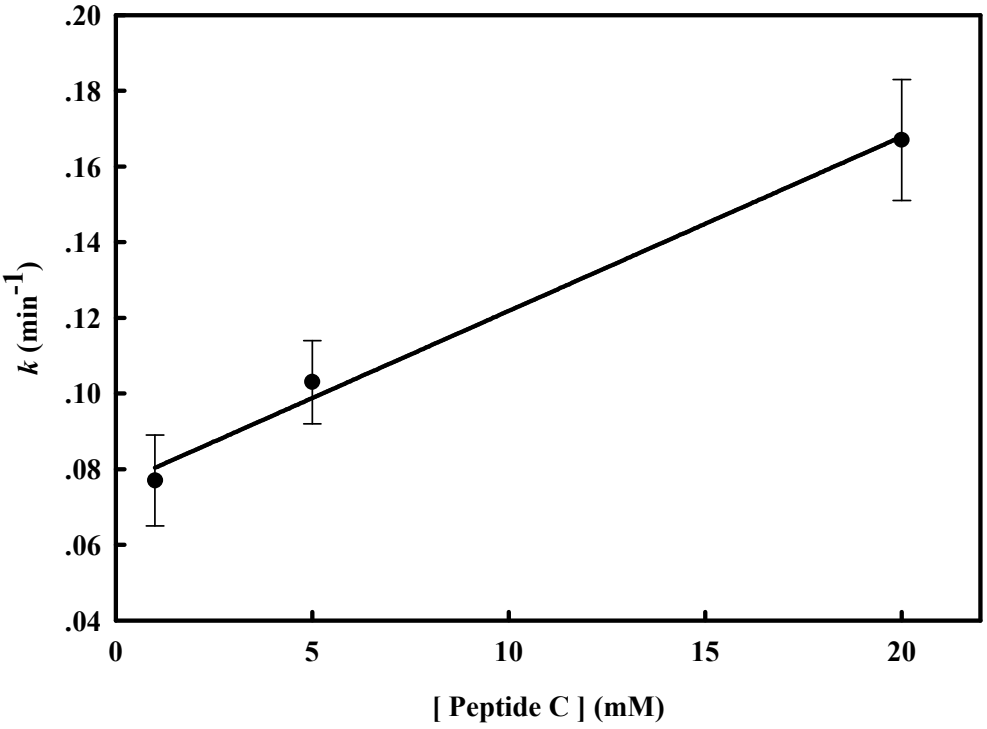

Figure 24. Derived k_{on} of Peptide C. The pseudo-first order constants from **Figure 23** fitted by linear regression with concentrations of Peptide C. The second order rate constant was found to be 76.7 $M^{-1} \cdot s^{-1}$.

3.2.17 Binding of QAQ to the Peptide C-BoNT/A LC complex

BoNT/A LC was pre-incubated at varying concentrations of Peptide C for 60 min at 25 ˚C to allow the formation of the Peptide C-BoNT/A LC complex. The Peptide C-BoNT/A LC complex remained intact based on the dissociation rate constant for the complex, which was calculated from the K_D and the observed second order rate constant for Peptide C binding to BoNT/A LC. When the Peptide C-BoNT/A LC complex was titrated with QAQ, BoNT/A LC showed additional quenching as monitored by the intrinsic fluorescence of BoNT/A LC. The results are shown in **Figure 25**. The K_Ds of QAQ to BoNT/A LC were 2.33 ± 0.14 and 4.63 ± 0.24 μM in the presence of 1 and 5 μM Peptide C, respectively.

The values of K_D thus obtained correlated with the values of IC_{50} of QAQ as determined by the HPLC and SNAPtide protease assay for BoNT/A LC, suggesting that the binding mode of QAQ to BoNT/A LC in the presence of Peptide C likely resembles its inhibition mode.

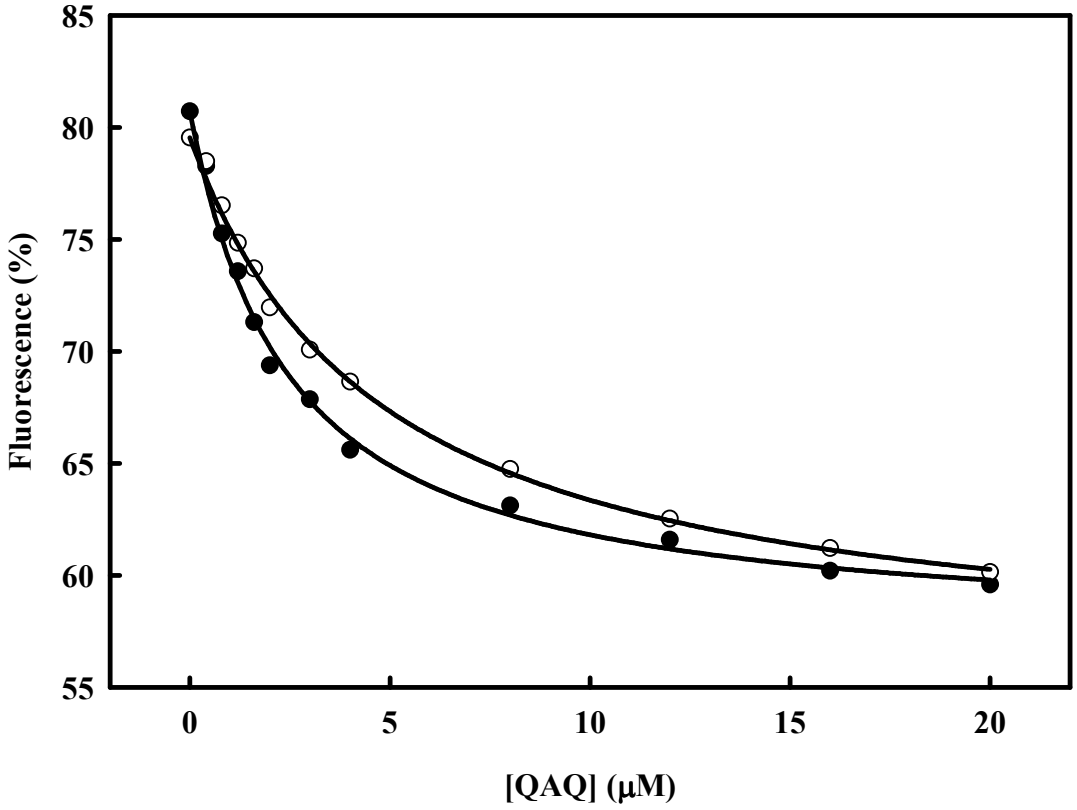

Figure 25. Fluorescence titration of QAQ with the Peptide C-BoNT/A LC complex. QAQ was added after the BoNT/A LC incubation 1 h with Peptide C, assuming that the Peptide C-BoNT/A LC formed a 1 : 1 complex. The concentrations of Peptide C were: (●) 1.0 μM; (○) 5.0 μM; The obtained K_d values for QAQ in the presence of 1.0 μM and 5.0 μM Peptide C were 2.33 ± 0.14 μM and 4.63 ± 0.24 μM, respectively.

3.2.18 Binding of Peptide C1 to BoNT/A LC

To further probe the interaction of QAQ with BoNT/A LC, a synthetic peptide, designated Peptide C1, was synthesized with the amino acid sequence corresponding to SNAP-25 residues E183 to G206 but with a Q197A mutation instead of Q198C in Peptide C, Ac-EKADSNKTRIDEANARATKMLGSG-NH_2. Unlike Peptide C, A197 in Peptide C1 can not coordinate to Zn^{2+} in the active site of BoNT/A LC. The binding of synthetic Peptide C1 was first examined using fluorescence titration by monitoring the intrinsic fluorescence intensity of BoNT/A LC upon addition of varying concentrations of Peptide C1. The K_D of Peptide C1 with BoNT/A LC in PBS containing 10 μM zinc acetate was found to be 0.34 ± 0.01 μM as determined by monitoring the intrinsic fluorescence intensity of BoNT/A LC. The IC_{50} of the Peptide C1 in PBS containing 10 μM zinc acetate was 3.6 ± 0.37 μM as determined by the SNAPtide protease assay. The fluorescence titration result is illustrated in **Figure 26**.

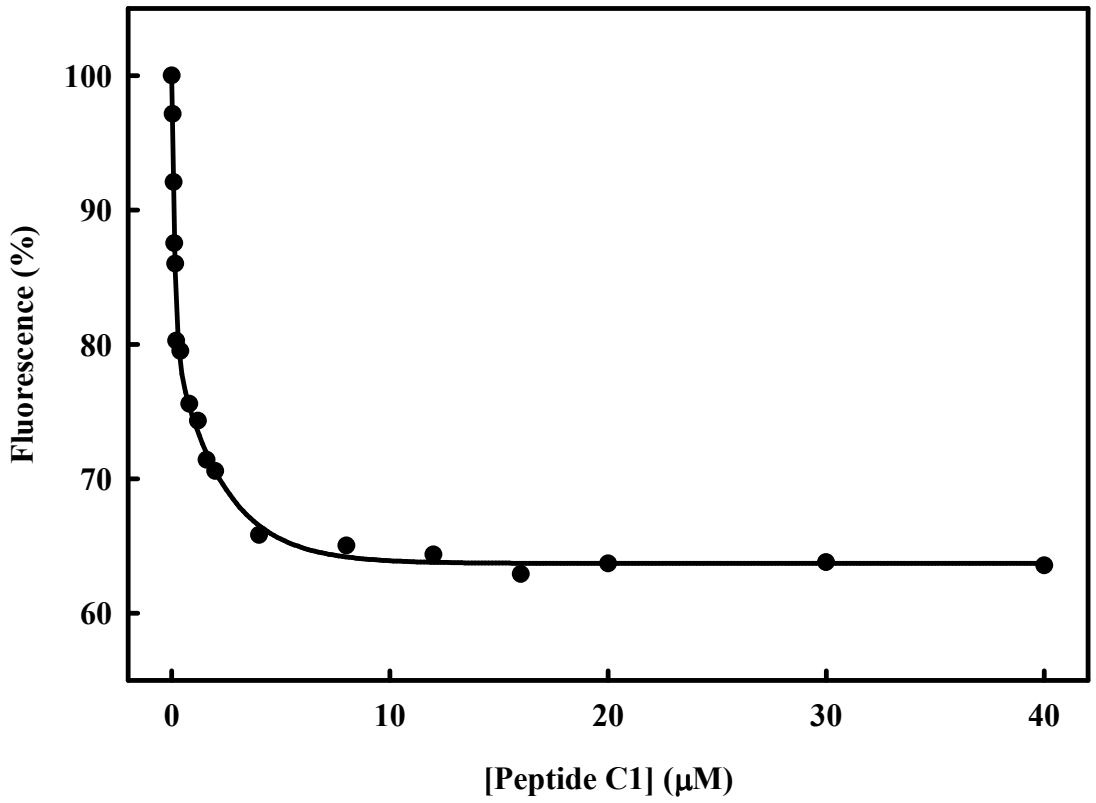

Figure 26. Interaction of BoNT/A LC with Peptide C1. The experiments were performed at 25 ˚C with pH 7.4. BoNT/A LC (1 μl, 5.0 mg / ml) was diluted into 500 μl of PBS buffer containing 10 mM sodium phosphate (pH7.4), 150 mM NaCl and 10 μM zinc acetate and incubated on ice for 1 h before the detection of fluorescence. Peptide C1 in varying concentrations was added to measure the fluorescence intensity, which was taken as 100 before the addition of Peptide C1. All the data were taken after the subtraction of the buffer background.

3.2.19 Time course of the BoNT/A LC binding to Peptide C1

Peptide C1 was used to analyze its effect on the binding of QAQ to BoNT/A LC. Unlike cysteine in Peptide C, Ala residue in Peptide C1 is unable to coordinate the Zn^{2+} in BoNT/A LC. The time course of the Peptide C1 binding to BoNT/A LC is shown in **Figure 27**. At 1.0 μM Peptide C1, BoNT/A LC exhibited a monophasic first order time course with a pseudo-first order rate constant of 0.128 min^{-1}. At higher concentrations of Peptide C1, binding to BoNT/A LC showed two exponential biphasic time courses. The fast phase had pseudo-first order rate constants of 0.263 and 0.515 min^{-1} at 5.0 and 20.0 μM Peptide C1, respectively. The second order rate constant for the Peptide C1 binding to BoNT/A LC was 323 $M^{-1}{\cdot}s^{-1}$ for the fast phase. The slow binding phase corresponded to pseudo-first order rate constants of 0.0936 and 0.0681, μM^{-1} at 5.0 and 20.0 μM Peptide C1, respectively. The slow phase in the time courses for Peptide C1 binding to BoNT/A LC could be due to non-specific binding to secondary binding sites in BoNT/A LC or to secondary slow conformational changes of the Peptide C1-BoNT/A LC complex.

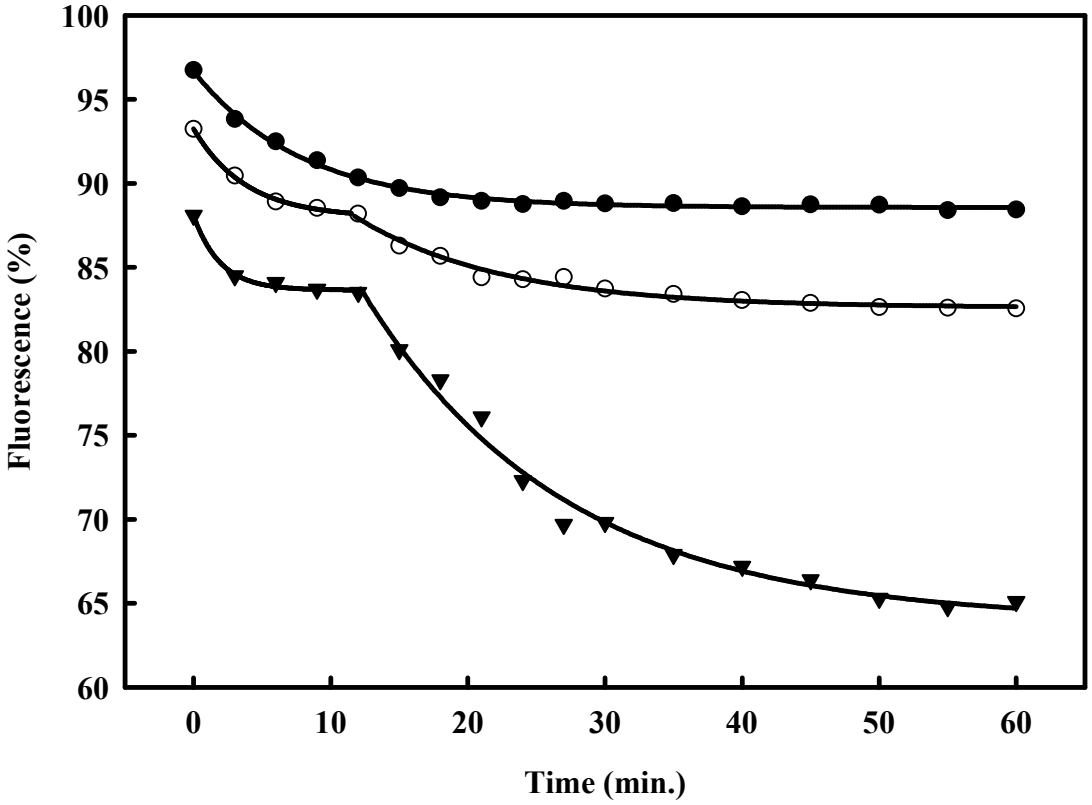

Figure 27. Time course of the fluorescence change of BoNT/A LC in the presence of Peptide C1. The concentrations of Peptide C1 were: (●) 1.0 μM; (○) 5.0 μM; (▼) 20.0 μM. For the fast phase, the pseudo-first order reaction kinetics binding rates for Peptide C1 were: 0.128 ± 0.005, 0.263 ± 0.025 and 0.515 ± 0.096 min^{-1} at 1, 5 and 20 μM Peptide C1, respectively. For the slow phase, the pseudo-first order rate constants for the second phases were 0.094 and 0.068 min^{-1} at 5.0 and 20.0 μM Peptide C1, respectively. The solid lines represent the fitted lines to two exponential time courses.

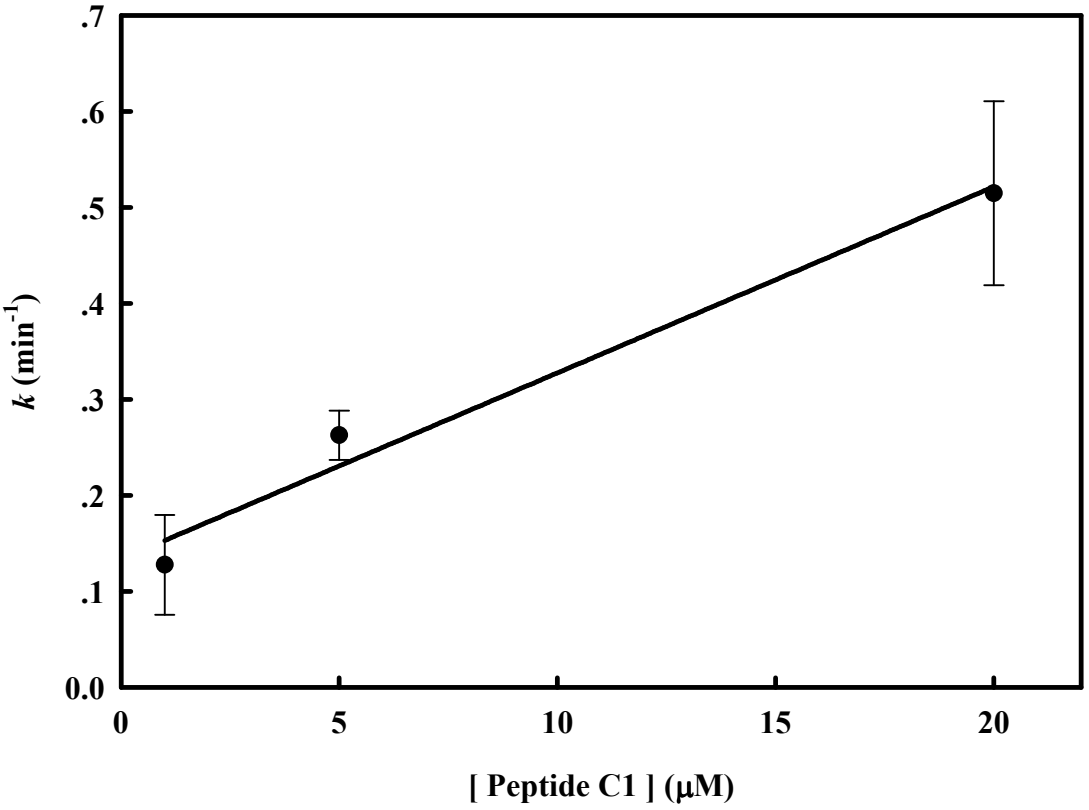

Figure 28. Derived k_{on} of Peptide C1. The pseudo-first order constants from the **Figure 27** fitted by linear regression with concentrations of Peptide C. The second order rate constant was found to be 323.33 $M^{-1} \cdot s^{-1}$.

3.2.20 Binding of QAQ to the Peptide C1-BoNT/A LC complex

The binding to QAQ to the Peptide C1-BoNT/A LC complex was next examined. BoNT/A LC (0.2 μM) and Peptide C1 (0.2 μM) were pre-incubated for 60 min to form the Peptide C1-BoNT/A LC complex. Addition of varying concentrations of QAQ to the Peptide C1-BoNT/A LC complex resulted in additional decrease of the intrinsic fluorescence intensity of BoNT/A LC. The K_Ds for QAQ to the Peptide C1-BoNT/A LC complex were 1.89 ± 0.18 and 3.13 ± 0.40 μM in the presence of 1 and 5 μM of Peptide C1, respectively. The similar values of K_D of QAQ to BoNT/A LC were obtained and had little affected by the substitution of Cys to Ala in Peptide C. The fluorescence titration results are shown in **Figure 29**.

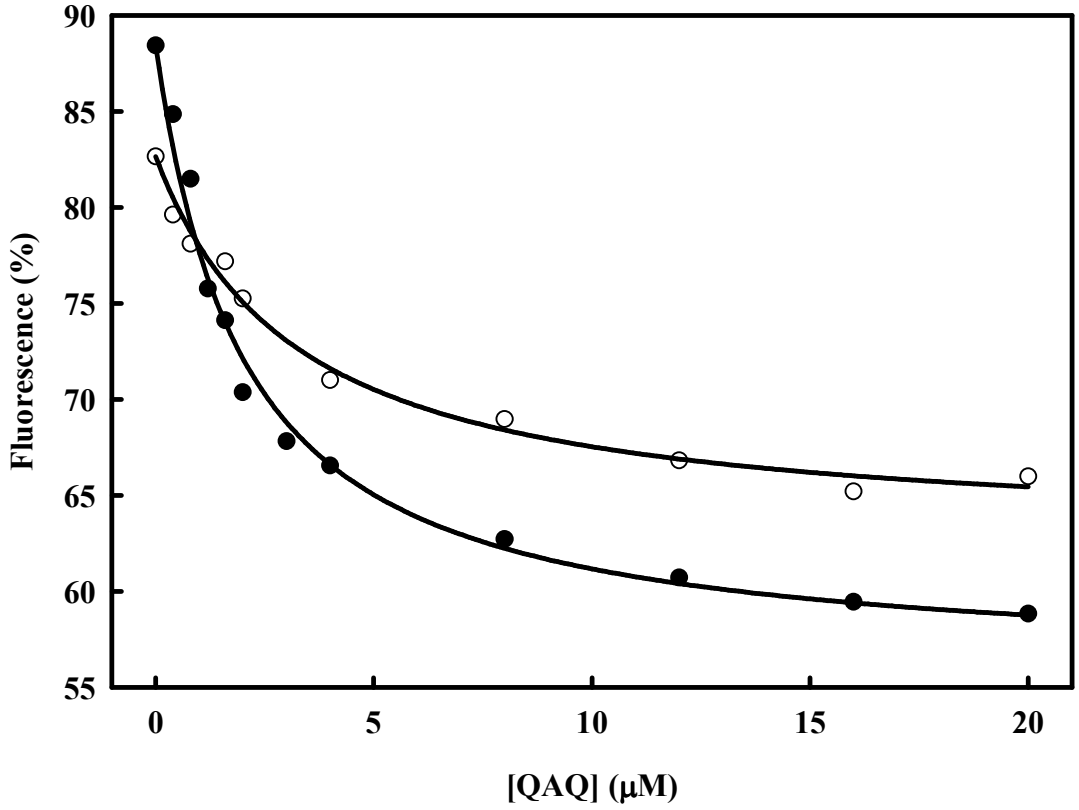

Figure 29. Fluorescence titration of QAQ with the Peptide C1-BoNT/A LC complex. QAQ was added after the BoNT/A LC incubation 1 h with Peptide C1, assuming that the Peptide C1-BoNT/A LC formed a 1 : 1 complex. The concentrations of Peptide C1 were: (●) 1.0 μM; (○) 5.0 μM; The obtained K_d values for QAQ in the presence of 1.0 μM and 5.0 μM Peptide C1 were 1.88 ± 0.18 μM and 3.13 ± 0.40 μM, respectively.

3.3 Discussion

QAQ was the first small molecule inhibitor of BoNT/A LC that was found to be effective in inhibiting the protease activity of BoNT/A by biochemical assay and in reducing the toxicity of BoNT/A by cell- and tissue-based assays (127). QAQ bound to native BoNT/A LC with a K_D of 0.02 μM as determined by monitoring the intrinsic fluorescence of BoNT/A LC, and that its affinity was reduced to a K_D of 0.214 μM at high concentrations of Zn^{2+} but was not significantly affected by temperature or pH. QAQ inhibited the protease activity with K_i of 1.84 μM. Removal of Zn^{2+} from BoNT/A LC reduced QAQ affinity to a K_D of 0.67 μM. Thus, the QAQ affinity to Zn^{2+}-free BoNT/A LC correlated with the K_i of QAQ as determined by the SNAPtide assay. Binding of QAQ to BoNT/A LC at 0.02 μM likely involves chelation of Zn^{2+} in the active site of BoNT/A LC, but did not inhibit the protease activity. QAQ inhibition of the protease activity could not be due to the removal of Zn^{2+} from the protease since the inhibition was observed with Zn^{2+} (10 μM) in excess of QAQ and Zn^{2+} re-binding to Zn^{2+}-free BoNT/A LC was instantaneous. Moreover, the inhibition was observed at concentrations much higher than the K_D expected for quinolinol chelation to Zn^{2+}. The binding of QAQ to Zn^{2+}-free BoNT/A LC demonstrated the presence of the Zn^{2+}-independent QAQ binding site in BoNT/A LC.

The three-dimensional structure of the BoNT/A LC remains the same after the depletion of Zn^{2+} (39, 54). It appears that QAQ binds to a hydrophobic pocket near the active site of Zn^{2+}-free BoNT/A LC (K_D of 0.67 μM), and chelates Zn^{2+} at the active site of BoNT/A LC in the presence of zinc (K_D of 0.02 μM).

The steady-state enzyme kinetic analysis of the QAQ inhibition of BoNT/A LC protease activity was consistent with non-competitive inhibition based on the results that the catalytic constant was reduced with increasing concentrations of QAQ and that the Michaelis-Menten constant did not change. The non-competitive inhibition pattern suggests QAQ binds to the enzyme-substrate complex and the free form of BoNT/A LC. The observation that QAQ bound to Zn^{2+}-free BoNT/A LC with a K_D of 0.67 μM and to the Peptide C-BoNT/A LC with a K_D of 2.33 μM was in agreement with that of the K_i of QAQ was 1.84 μM. The difference between the K_D and the K_i could be due to the differences in the types of assays.

Peptide C was able to bind to BoNT/A LC and inhibited BoNT/A LC protease activity. The slowness of the binding of long peptides such as Peptide C to BoNT/A LC was first observed based on the usual biphasic QAQ binding to BoNT/A LC in the presence of Peptide C. The slow binding of Peptide C to BoNT/A LC was contrast to the short peptide inhibition CRATKML, which did not show slow binding. Based on the observed second order rate constant (k_{on}) of 76 $M^{-1} \cdot s^{-1}$ and the K_D of 24.9 nM for Peptide C binding to BoNT/A LC, the dissociation rate constant of the Peptide C-BoNT/A LC complex was calculated to be 1.91×10^{-6} s^{-1}. The Peptide C-BoNT/A LC complexes would not dissociate in days based on the observed second order binding rate constant and K_D. Such slow dissociation allows a new approach of developing antagonists of BoNT/A similar to the very tight binding of naturally occurring protease inhibitors such as soybean trypsin inhibitor to trypsin.

The K_D of QAQ to BoNT/A LC in the presence of Peptide C, which contains a cysteine, was similar to that in the presence of C1, which replaces the cysteine with an

alanine, suggesting that QAQ coordination to the Zn^{2+} in BoNT/A LC did not play a major role in the QAQ binding to the peptide-BoNT/A LC complexes. The coordination of the cysteine in CRATKML covalently bound to Zn^{2+} in BoNT/A LC has been shown by X-ray crystallography (54). The cysteine in Peptide C, which contains this sequence of CRATKML, is likely to coordinate to the Zn^{2+} in BoNT/A LC. However, the potent peptidomimetic inhibitor in complex with BoNT/A LC adopts a helical instead of the extended conformation of bound SNAP-25 (53). The conformation that Peptide C and C1 adopt will alter the QAQ access to the Zn^{2+} in the active site. The present results suggest that Zn^{2+} in BoNT/A LC plays a minor role in the QAQ binding to the peptide-BoNT/A LC complexes.

The exact nature of the mechanism for the slow binding of long peptides is yet to be determined. The slow binding was at least in part likely due to the extensive interactions of peptides with BoNT/A LC. Long peptides could have more extensive interactions with BoNT/A LC than shorter peptides. The binding of long peptides to BoNT/A LC could necessitate BoNT/A LC undergo slow conformational changes and require the selection of specific conformers of the long peptides from large conformation ensembles before productive binding to BoNT/A LC can occur. The later scenario is plausible considering a potent peptidomimetic inhibitor adopts a very different conformation from that of SNAP-25 (53). Whether or not the release of natural substrate and product from the BoNT/A holotoxin resembles the release of long Peptides C and C1 from BoNT/A LC is not known. The slow release of long peptides observed in the present study raises the possibility that this event is one of the factors contributing to the prolonged action of BoNT/A *in vivo*.

Molecular modeling of the QAQ-BoNT/A LC complexes in the absence and in the presence of SNAP-25 suggested two different binding modes **(Appendix A3 and A4)**. QAQ bound to the active site by chelating the Zn^{2+} in the active site in the presence of Zn^{2+}. However, the QAQ bound to the hydrophobic pocket in the presence of bound peptide. The presence of two binding modes for an inhibitor of BoNT/A LC provides new insights towards protease-inhibitor design. The results suggest that the peptide substrate may play an important role in the action of the inhibitor and thus in the development of inhibitors.

Chapter 4. Tertiary structure of SNAP-25

4.1 Introduction

SNAP-25 is one of the components of the SNARE complex and can be cleaved by botulinum neurotoxin, which blocks the neurotransmitter release. The structure of the two helices of SNAP-25 in the SNARE complex has been reported. The results indicate that the N-terminal SNAP-25(7-83) and the C-terminal SNAP-25(131-204) are of α-helical conformation after the four-helix bundle has been formed (2). However, the C-terminal SNAP-25(141-204) in complex with BoNT/A LC(E224Q, Y366F) results in a coil-like molecule that wraps around the protease to form a binary complex (25). The two different crystal structures of the four-helix bundle and the complex of SNAP-25 with BoNT/A LC(E224Q, Y366F) are represented in **Figure 30A**.

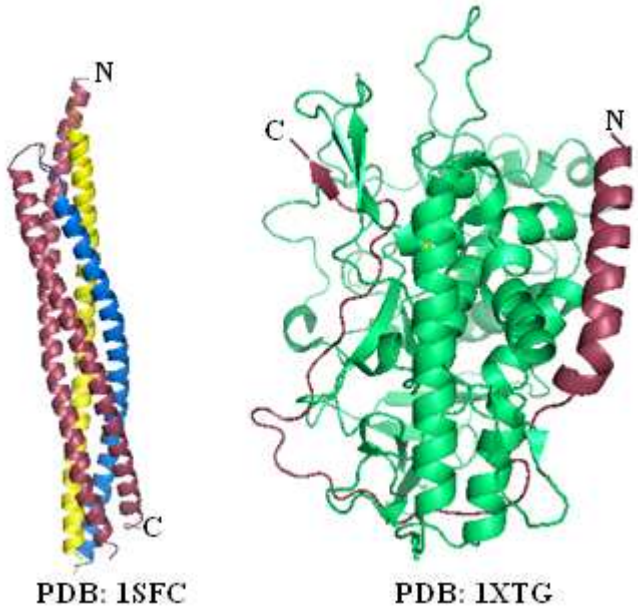

Figure 30A. Crystal structures of the four-helix bundle of the SNARE complex and binary complex of BoNT/A LC and SNAP-25. The pink helices indicate the SNAP-25 helices in the SNARE complex. The pink ribbon represents the C-terminal SNAP-25(141-204) in the binary complex with BoNT/A LC(E224Q, Y366F).

The different structures indicate that SNAP-25 can exist as a coil as well as in helical form in neuronal cytoplasm. SNAP-25 is an intrinsically disordered protein prior to the membrane fusion and folds into helices upon associating with VAMP and syntaxin (20). The tertiary structure of the full length SNAP-25 has not yet been elucidated. We used fluorescence resonance energy transfer (FRET) to examine the structural and conformational changes of SNAP-25 by introducing EGFP and tetracysteine CCCPGCC as fluorescence probes. The constructs are depicted in **Figure 30B**.

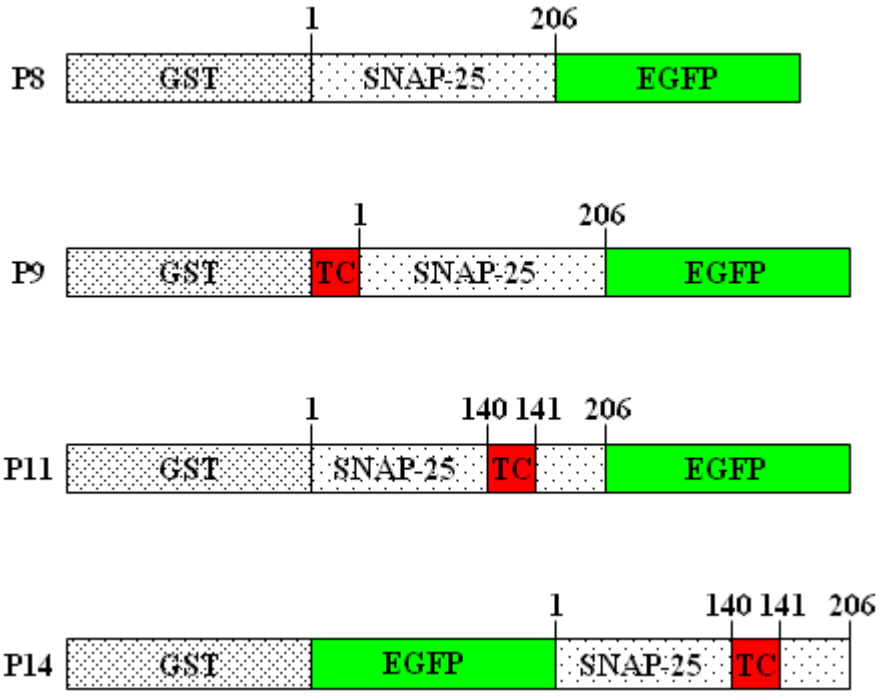

Figure 30B. Schematic representation of SNAP-25 with fluorescent probes. EGFP stands for enhanced green fluorescent protein and TC represents the tetracysteine motif, CCPGCC. The numbers on top of the box refer to the corresponding amino acid residues of the SNAP-25. **P8**, **P9**, **P11**, and **P14** are proteins corresponding to the plasmid **8**, **9**, **11**, and **14**, respectively.

When both fluorescence probes are attached to SNAP-25, EGFP and CCPGCC-ReAsH can act as a donor and an acceptor, respectively, in FRET. The method can be used to measure the apparent distances between the specific sites between the C-terminus and the N terminus (**P9**), between the C-terminus and the residue D140 (**P11**), and between the N-terminus and the residue D140 (**P14**) of SNAP-25. Based on the distances measured by FRET, a spatial model can be constructed indicating the conformational changes of SNAP-25 in the absence and presence of Zn^{2+}-depleted BoNT/A LC. A similar method can be used to measure the conformational changes of the inactive mutant SNAP-25(A195S) (**Figure 30C**) in the absence and presence of active BoNT/A LC.

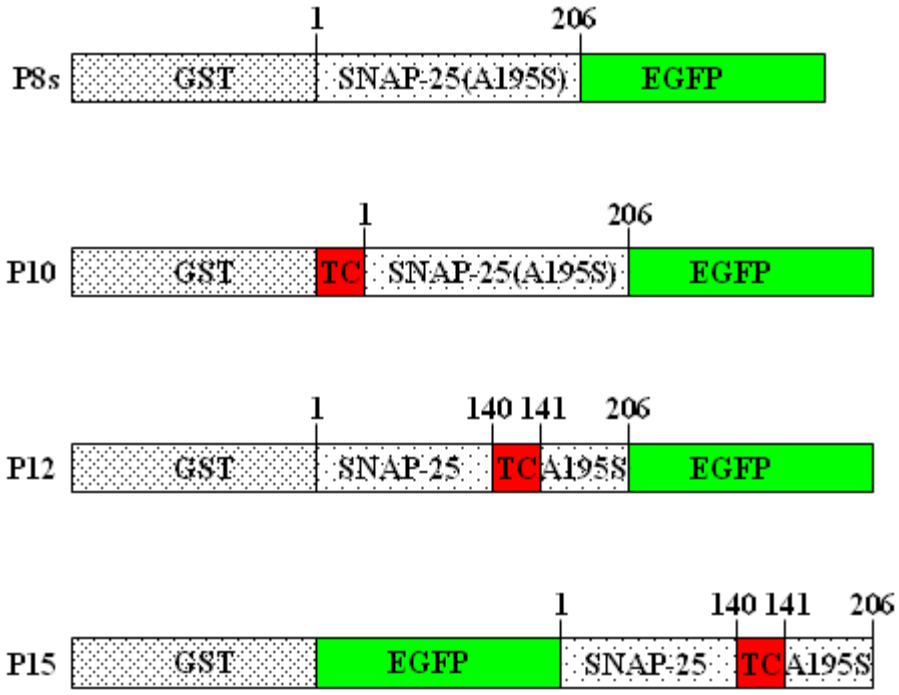

Figure 30C. Schematic representation of the mutant SNAP-25(A195S) with fluorescence probes. P8s, **P10**, **P12**, and **P15** are proteins corresponding to the A195S mutation plasmids **8**, **10**, **12**, and **15**, respectively.

4.2 Results

4.2.1 Construction of SNAP-25 cDNA plasmids with genetically encoded probes

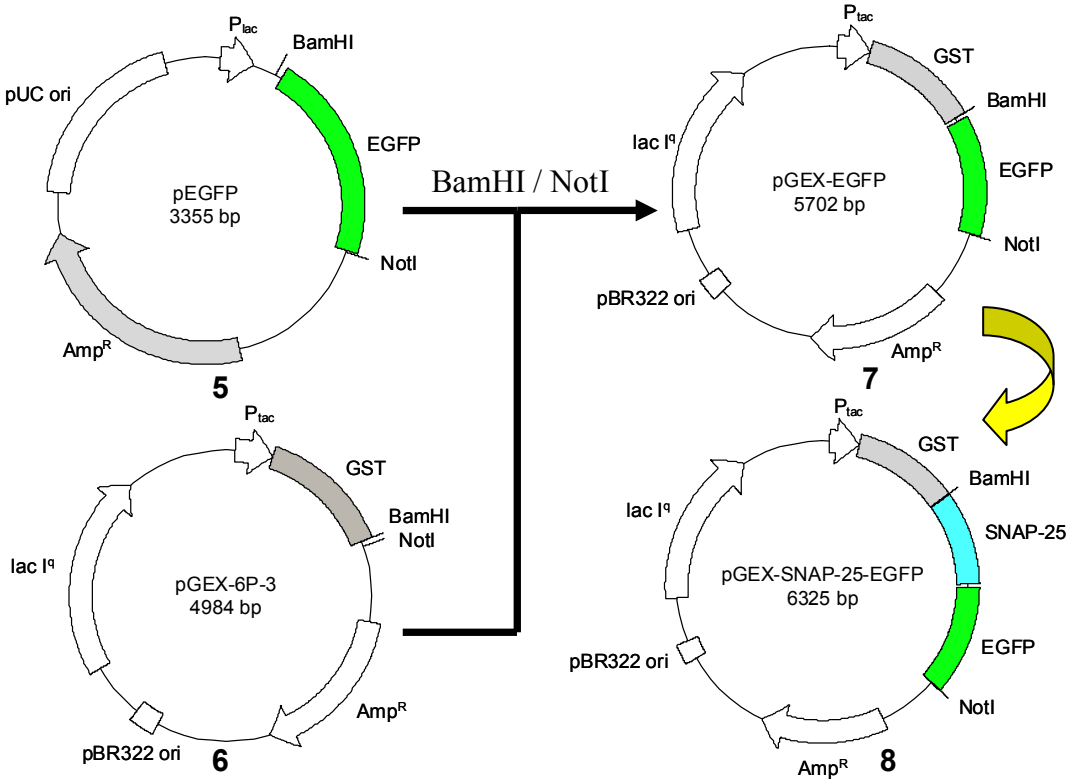

Figure 30D. Diagram of construct plasmid GST-SNAP-25-EGFP.

The plasmid pEGFP (Clontech) **(5)** was digested by BamHI/NotI and EGFP cDNA was inserted into pGEX-6P-3 (Amersham Biosciences) **(6)** pre-digested by BamHI/NotI, using T4 DNA ligase (**Figure 30D**). The resulting construct is designated as pGEX-EGFP **(7)**. cDNA encoding SNAP-25 was inserted into pGEX-EGFP **(7)**, resulting in the pGEX-SNAP-25-EGFP construct **(8)** (**Figure 30D**). 28 extra nucleotides TAAGGATCCCCGGGTACCGGTCGCCACC in plasmid **(8)** between SNAP-25 and EGFP were introduced. These included the stop codon (TAA) of SNAP-25 and the 5'

multi-cloning site in pEGFP. The protein could not be expressed because the reading frame shifted. Deletion of 4 bases, including the stop codon (TAAG), was accomplished by site-directed mutagenesis using Quickchange mutagenesis (Strategene) following the manufacturer's instruction, using pGEX-SNAP-25-(TAAGGATCCCCGGGTACCGGTC GCCACC)-EGFP as the template, the forward primer (5'-ATGCTGGGAAGTGGTGAT CCCCGGGTACCG-3'), and the reverse primer (5'-CGGTACCCGGGGATCACCACTT CCCAGCAT-3'). The underlined nucleotides indicate the Gly codon at the C-terminus of the SNAP-25. After the mutagenesis, the GST-SNAP-25-EGFP with correct open reading frame (ORF) was obtained. The construct was confirmed by DNA sequencing. The overall scheme is shown in **Figure 30D**. Eight amino acid residues expressed as Asp-Pro-Arg-Val-Pro-Val-Ala-Thr, corresponding to the linker nucleotides: GATCCCCGGGTAC CGGTCGCCACC.

The tetracysteine ReAsH- and FlAsH-binding motif, CCPGCC, was appended onto the N-terminus of the SNAP-25 by mutagenesis. Site-directed mutagenesis was performed by Quickchange mutagenesis (Strategene) following the manufacturer's instructions, using pGEX-SNAP-25 **(8)** as the template, the 46 nucleotide forward primer (5'-GGCCCCTGGGATCCTGTTGTCCTGGCTGTTGCATGGCCGAGGACGC-3') and the 46 nucleotide reverse primer (5'-GCGTCCTCGGCCATGGCAACAGCCAGGACA ACAGGATCCCAGGGGCC-3'). The underlined nucleotides indicate the bases, encoding CCPGCC. The plasmid GST-CCPGCC-SNAP-25-EGFP **(9)** was obtained after the mutagenesis (**Figure 31**).

The mutant SNAP-25(A195S) was constructed as a control for BoNT/A LC binding studies since A195S prevents the BoNT/A LC cleavage, while SNAP-

25(A195S)-LC binding remains tight. The A195S mutant was constructed using pGEX-CCPGCC-SNAP-25-EGFP **(9)** as the template, the 51 nucleotides forward primer (5'-CCAACAAAACCAG AATTGATGAATCCAACCAACGTGCAACAAAGATGCTGG-3') and the 51 nucleotides reverse primer (5'-CCCAGCATCTTTGTTGCACGTTGGTT GGATTCATC AATTCTGGTTTTGTTGG-3'). The underlined nucleotides indicate the Ser codon, resulting in the change from Ala to Ser at position 195 in SNAP-25. The plasmid GST-CCPGCC-SNAP-25(A195S)-EGFP **(10)** was obtained after the mutagenesis (**Figure 31**). The construct was confirmed by DNA sequencing.

The ReAsH- and FlAsH- binding motif, CCPGCC, was also inserted between D140 and A141 of the SNAP-25. Site-directed mutagenesis was performed by Quickchange mutagenesis (Strategene) following the manufacturer's instructions, using pGEX-SNAP-25-EGFP as the template, the 59 nucleotide forward primer (5'-CCGCAGGGTAACAAATGATTGTTGTCCTGGCTGTTGC*GCC*CGGGAAAATGAG ATGGATG-3') and the reverse primer (5'-CATCCATCTCATTTTCCCGGGCGCAAC AGCCAGGACAACAATCATTTGTTACCCTGCGG-3'). The underlined nucleotides correspond to the sequence encoding CCPGCC. The plasmid pGEX-SNAP-25(1-140)-CCPGCC-SNAP-25(141-206)-EGFP **(11)** was obtained after the mutagenesis. The construct was confirmed by sequencing.

The A195S mutant was constructed using pGEX-SNAP-25(1-140)-CCPGCC-SNAP-25(141-206)-EGFP as the template, the 51 nucleotide forward primer (5'-CCAACAAAACCAGAATTGATGAATCCAACCAACGTGCAACAAAGATGCT GG-3'), and the reverse primer (5'-CCCAGCATCTTTGTTGCACGTTGGTTGGATTCA TCAATTCTGGTTTTGTTGG-3'). The underlined residues indicate the A195S

mutation. The plasmid pGEX-SNAP-25(1-140)-CCPGCC-SNAP-25(141-206, A195S)-EGFP **(12)** was obtained after the mutagenesis. The construct is shown in **Figure 31**.

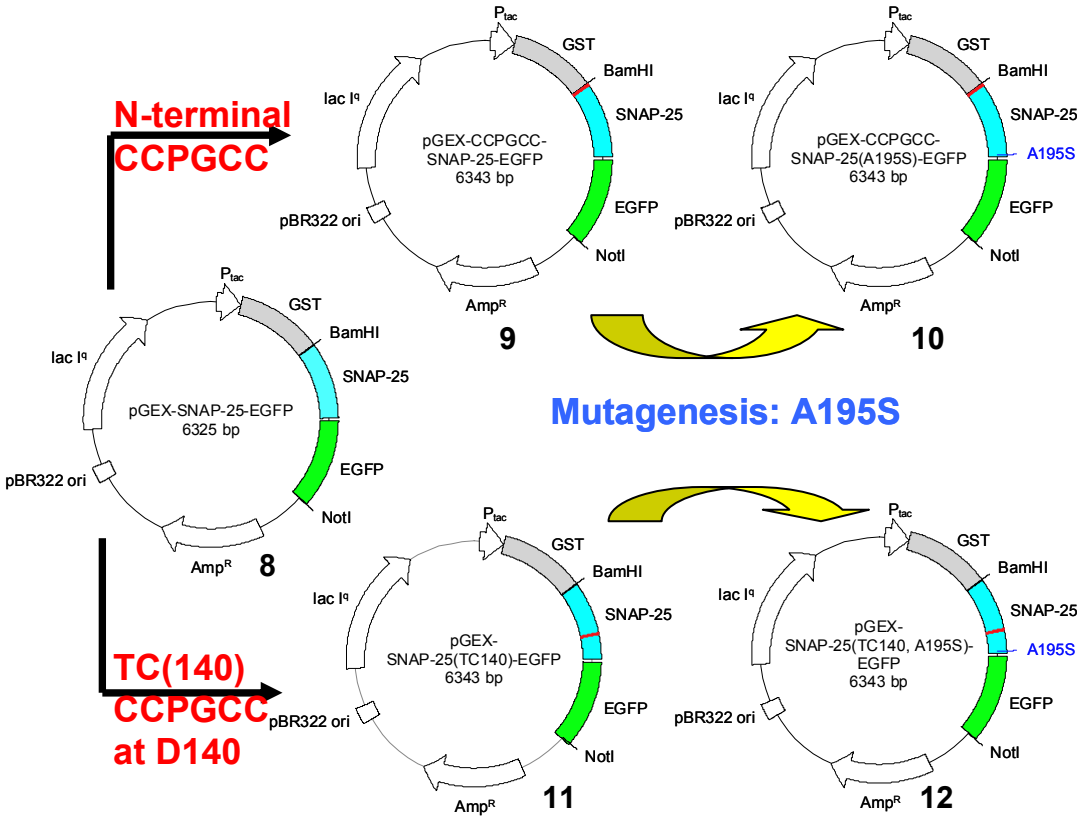

Figure 31. Construction of the mutant plasmids of GST-CCPGCC-SNAP-25-EGFP (9), GST-CCPGCC-SNAP-25(A195S)-EGFP (10), GST-SNAP-25(1-140)-CCPGCC-SNAP-25(141-206)-EGFP (11) and GST-SNAP-25(1-140)-CCPGCC-SNAP-25(141-206, A195S)-EGFP (12).

EGFP was fused to the N-terminus of the SNAP-25 by ligating the pGEX-EGFP and SNAP-25 cDNA, followed by the removal of the stop codon of EGFP.

The stop codon of EGFP in pEGFP was removed by PCR amplification using the 37 nucleotide forward primer (5'-CTCTAGAGGATCCCGGGTACCGGTCGCCACC ATGGTG-3') and the 38 nucleotide reverse primer (5'-GAGTCGCGGCCGC**T**CTTGTA CAGCTCGTCCATGCCGAG-3'). The underlined nucleotides indicate the N-terminal start codon and the C-terminus of the EGFP, respectively. The plasmid pGEX-EGFP **(13)** was obtained after the ligation of the amplified cDNA to pGEX using T4 DNA ligase. 18 nucleotides linker was introduced into the N-terminal of EGFP, encoding Arg-Val-Pro-Val-Ala-Thr (abbreviation as RVPVAT). The linker bases are from the 5'-multiple cloning site (5'MCS) corresponding to CGGGTACCGGTCGCCACC.

cDNA encoding SNAP-25(1-140)-CCPGCC-SNAP-25(141-206) was inserted into pGEX-EGFP **(13)** pre-digested by NotI, using T4 DNA ligase. The resulting construct was designated as pGEX-EGFP-SNAP-25(1-140)-CCPGCC-SNAP-25(141-206) construct **(14)**. PCR was performed using a 36 nucleotide forward primer (5'-AAGA*GCGGCCGC*ATGGCCGAGGACGCAGACATGCGC-3') and a 39 nucleotide reverse primer (5'-GTC*GCGGCCGC*TTTAACCACTTCCCAGCATCTTTGTTGC-3'). The underlined nucleotides indicate the N-terminal start codon and the C-terminal stop codon of the SNAP-25, respectively. The plasmid pGEX-EGFP-SNAP-25(1-140)-CCPGCC-SNAP-25(141-206) **(14)** was obtained after the ligation. 9 bases (AGCGGCCGC) from the NotI were introduced between the EGFP and the SNAP-25, encoding Ser-Gly-Arg. The scheme is shown in **Figure 32**.

The corresponding SNAP-25(A195S) was constructed as a control for BoNT/A LC binding studies. The A195S mutant was constructed using Quickchange mutagenesis (Strategene) using plasmid **14** as the template. After the mutagenesis, plasmid pGEX-EGFP-SNAP-25(1-140)-CCPGCC-SNAP-25(141-206, A195S) **15** was constructed as a mutated plasmid.

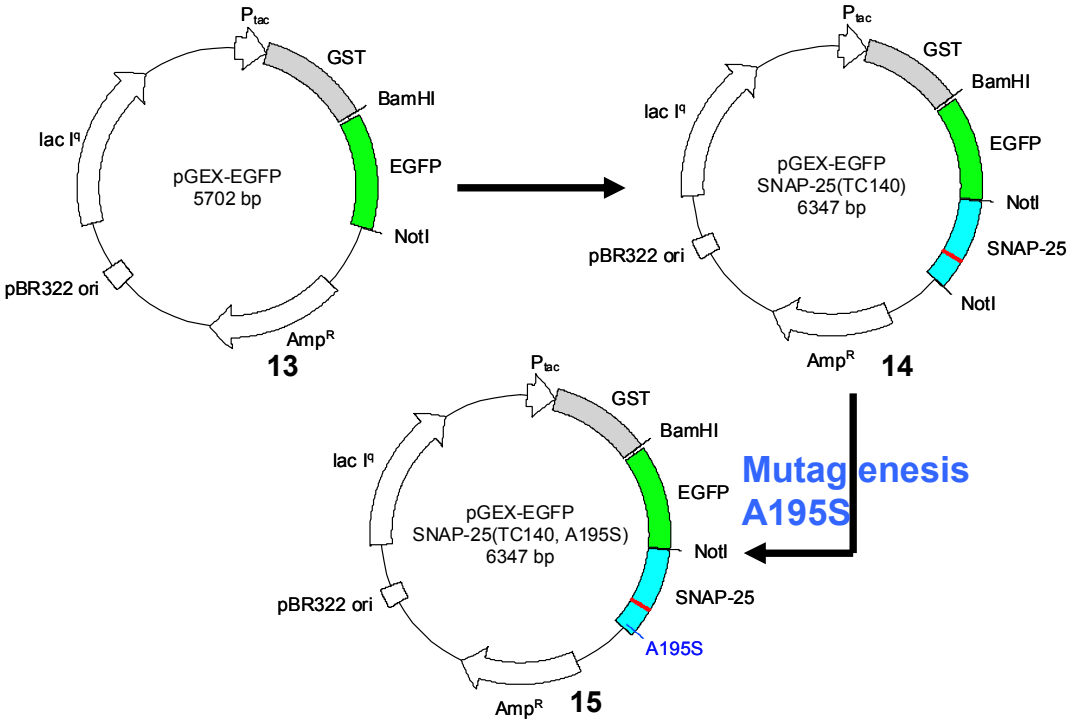

Figure 32. Construction of the plasmid GST-EGFP-SNAP-25(1-140)-CCPGCC-SNAP-25(141-206) (14) and GST-EGFP-SNAP-25(1-140)-CCPGCC-SNAP-25(141-206, A195S) (15).

4.2.2 Expression and purification of various SNAP-25(A195S)

The pGEX plasmids (**8-15**) in **Figure 30C** and **Figure 31,** which contain the cDNA coding for SNAP-25 and SNAP-25(A195S), were used for protein expression. The purified proteins were analyzed by SDS-PAGE. The results are shown in **Figure 33**.

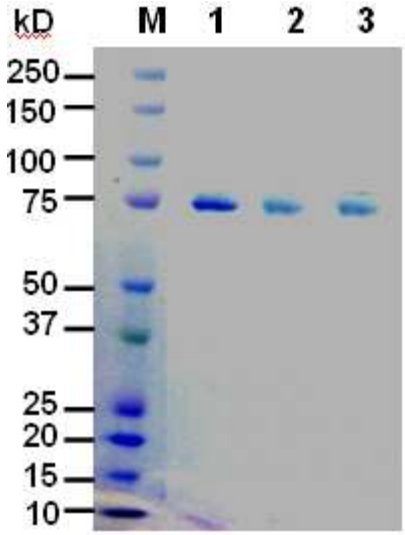

Figure 33. Various SNAP-25(A195S) with fluorescent probes. M indicates the protein maker (Bio-Rad). Lane 1 indicates the purified protein GST-CCPGCC-SNAP-25(A195S)-EGFP (**P10**); lane 2 indicates the purified protein GST-SNAP-25(1-140)-CCPGCC-SNAP-25(141-206, A195S)-EGFP (**P12**); and lane 3 indicates the protein GST-EGFP-SNAP-25(1-140)-CCPGCC-SNAP-25(141-206, A195S) (**P15**). The molecular weights of all three proteins are 76 kD.

4.2.3 Specific cleavage of GST-SNAP-25-EGFP by BoNT/A LC

In order to examine the substrate activity of SNAP-25 in the fusion proteins, BoNT/A LC was used to cleave SNAP-25 in GST-SNAP-25-EGFP. The LC's activity was comparable in the EGFP-fused and the wild-type SNAP-25. The EGFP in the C-terminus of the SNAP-25 is not expected to affect the SNAP-25 conformation. Only if the modified SNAP-25 exhibits a similar activity as the wild-type SNAP-25, the fusion protein could be used for further interaction studies.

BoNT/A LC specifically cleaved SNAP-25 between Q197 and R198 in GST-SNAP-25-EGFP (**P8,** from the plasmid **8**). Once the protein (**P8**) is cleaved by BoNT/A LC, two fragments are formed: GST-SNAP-25(1-197), with the molecular weight of 48 kD; and SNAP-25(198-206)-EGFP, with the molecular weight of 27 kD, as shown in **Figure 34**. The results indicate that SNAP-25 in fusion protein GST-SNAP-25-EGFP (**P8**) can be cleaved by BoNT/A LC, which suggests that the conformation of SNAP-25 in the fusion protein (**P8**) can be recognized by BoNT/A LC. The introduction of EGFP in the fusion protein does not significantly affect the conformation of SNAP-25 to prevent the cleavage by BoNT/A LC. The fused protein (**P8**) with EGFP could be used as a substrate of BoNT/A LC for our research to study the recognition of SNAP-25 by BoNT/A LC.

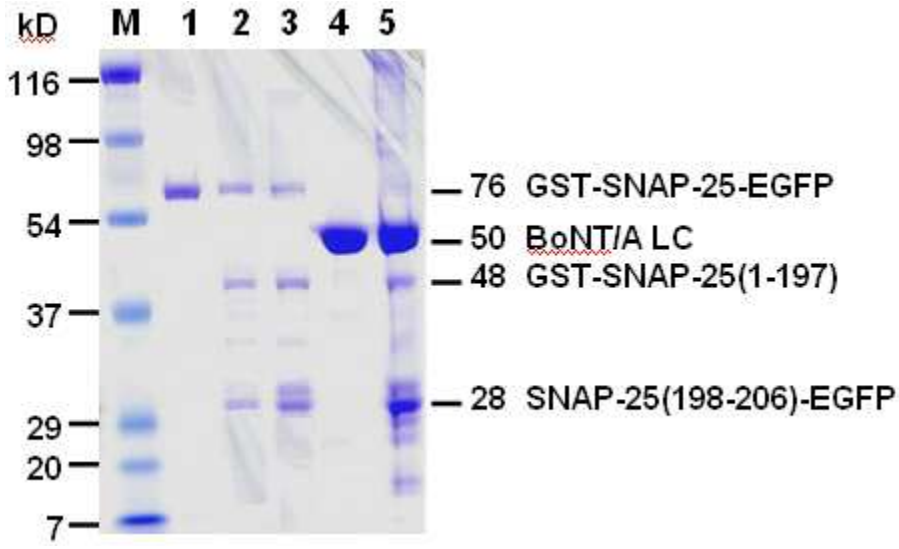

Figure 34. GST-SNAP-25-EGFP (P8) cleavage by BoNT/A LC. M indicates the protein standard marker; lane 1 represents 0.2 μM GST-SNAP-25-EGFP (**P8**); lane 2 represents the 10 min incubation of 0.2 μM GST-SNAP-25-EGFP (**P8**) in the presence of 2.0 nM BoNT/A LC; lane 3 represents the 30 min incubation of 0.2 μM GST-SNAP-25-EGFP (**P8**) in the presence of 2.0 nM BoNT/A LC; lane 4 represents the 2.0 μM BoNT/A LC; and lane 5 represents the 2 h incubation of GST-SNAP-25-EGFP (**P8**) in the presence of 2.0 μM BoNT/A LC.

The results suggested that SNAP-25 was cleaved by BoNT/A LC in the fusion protein GST-SNAP-25-EGFP (**P8**) and the two fragments were obtained: the 48 kD corresponded to the N-terminus of the fusion protein, GST-SNAP-25(1-197); the 28 kD corresponded to the C-terminus of the fusion protein, SNAP-25(141-206)-EGFP. The 76 kD was the intact protein GST-SNAP-25-EGFP (**P8**). The longer the incubation with the BoNT/A LC, the more cleavage of SNAP-25 occurred. More BoNT/A LCs were added, and the cleavage occurred faster, resulting in more fragments that were obtained. All of the fusion protein GST-SNAP-25-EGFP (**P8**) was cleaved by BoNT/A LC in the presence of excess BoNT/A LC (lane 5 in **Figure 34**).

4.2.4 Specific cleavage of GST-SNAP-25-EGFP by PreScission

Double-labeled fusion, GST-CCPGCC-SNAP-25-EGFP **(P9),** was expressed and purified. In the fusion protein, the N-terminus of the SNAP-25 was modified by CCPGCC and the C-terminus of the SNAP-25 was modified by EGFP. In order to determine if the CCPGCC affects the folding of SNAP-25, the substrate activity of SNAP-25 was determined by BoNT/A LC. In addition, the GST-tag could be removed by PreScission™ protease. The results are shown in **Figure 35**.

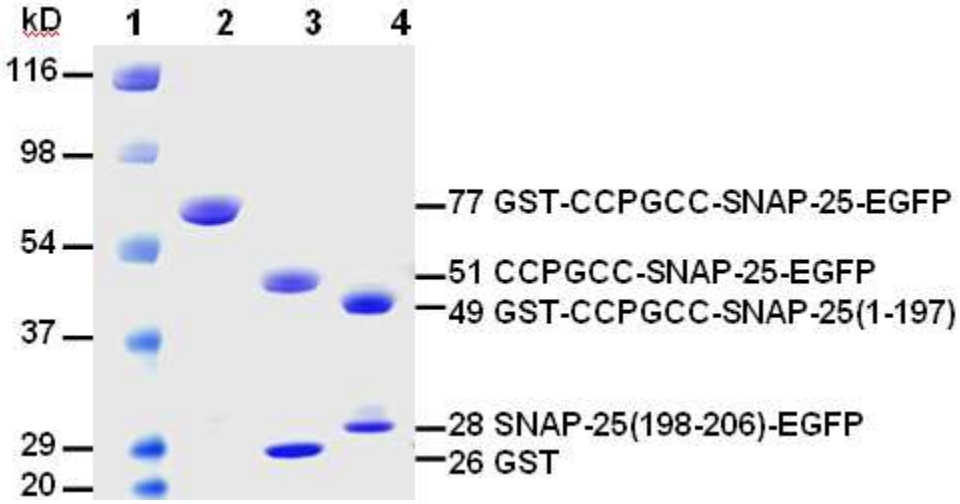

Figure 35. GST-CCPGCC-SNAP-25-EGFP (P9) cleavage by LC and PreScission. Lane 1 represents the protein ladder; lane 2 represents intact protein GST-CCPGCC-SNAP-25-EGFP (**P9**); lane 3 represents the protein after digestion with PreScission™ protease; lane 4 represents the overnight incubation of the protein after digestion with BoNT/A LC.

Lane 3 indicates that the GST-tag contains the LEVLFQGP sequence flanking SNAP-25 and can be cleaved by PreScission™ protease. GST-tag in GST-CCPGCC-SNAP-25-EGFP is shown in lane 3 in **Figure 35** to be cleaved by PreScission™ protease. The large fragment (51 kD) corresponded to CCPGCC-SNAP-25-EGFP and the small fragment (26 kD) corresponded to GST.

The results (lane 4) indicated that all of SNAP-25 was cleaved after incubation overnight in the presence of BoNT/A LC. The large fragment (49 kD) corresponded to GST-CCPGCC-SNAP-25(1-197), and the small fragment (27 kD) corresponded to SNAP-25(198-206)-EGFP.

The cleavage experiments suggest that the conformation of SNAP-25 is not significantly affected by introducing CCPGCC and EGFP. The modified SNAP-25 exhibits the similar substrate activity with the wild-type full-length SNAP-25.

4.2.5 Time course of the cleavage of GST-CCPGCC-SNAP-25-EGFP by BoNT/A LC

SNAP-25 in GST-CCPGCC-SNAP-25-EGFP (**P9**) could be completely cleaved in the presence of excess BoNT/A LC (**Figure 35**). The time course of the specific cleavage of GST-CCPGCC-SNAP-25-EGFP (**P9**) (5.0 μM) was monitored in the presence of 2.0 nM BoNT/A LC. The results are shown in **Figure 36**.

GST-CCPGCC-SNAP-25-EGFP (**P9**) (5.0 μM) was incubated with BoNT/A LC (2.0 nM) in 250 μl buffer (10 mM potassium phosphate, 150 mM NaCl, 10 μM zinc acetate, pH 7.4) at 25 ˚C. Aliquots (10 μl) were withdrawn at specified time points (0 ~ 2.5 h) and the reaction was stopped by adding 20 μl of Laemmli sample buffer (Bio-Rad) and denatured at 94 ˚C for 5 min following an analysis by SDS-PAGE. The 77 kD protein corresponded to the un-cleaved GST-CCPGCC-SNAP-25-EGFP (**P9**). The 49 kD protein corresponded to the large fragments of GST-CCPGCC-SNAP-25(1-197) and the 28 kD protein corresponded to the small fragment of SNAP-25(198-206)-EGFP.

The amounts of cleaved GST-CCPGCC-SNAP-25-EGFP (**P9**) were quantitatively determined using imageJ software, which was used to calculate the spot area and pixel value statistics of a specific area selection and intensity threshold marks. The results are shown in **Figure 37**. The results demonstrated that the SNAP-25 in GST-CCPGCC-SNAP-25-EGFP (**P9**) could be cleaved by BoNT/A LC.

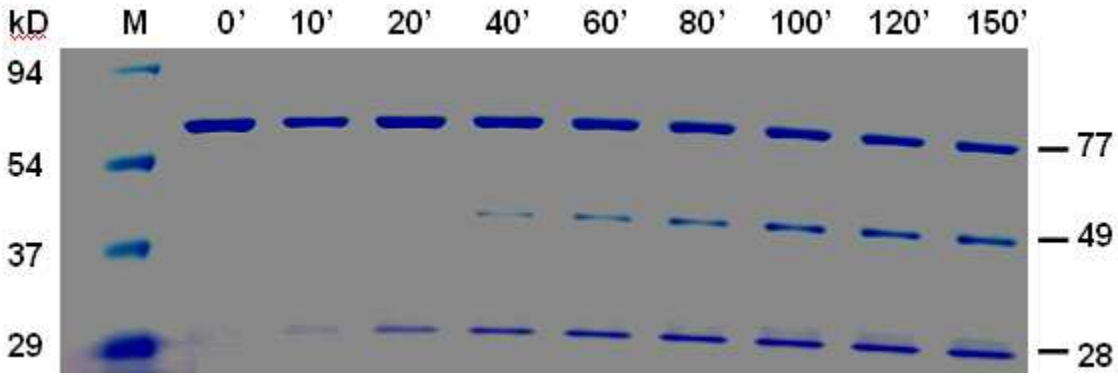

Figure 36. Time dependent cleavage of GST-CCPGCC-SNAP-25-EGFP (P9) by BoNT/A LC. The reactions were performed at 25 ˚C. The incubation time is labeled on top of the figure and M indicates the protein ladder (Bio-Rad). The concentrations of GST-CCPGCC-SNAP-25-EGFP (**P9**) and BoNT/A LC were 5.0 μM and 2.0 nM, respectively. The molecular weight of the large fragment was 49 kD, which corresponded to GST-CCPGCC-SNAP-25(1-197), and the small fragment weighed 28 kD, which corresponded to SNAP-25(198-206)-EGFP.

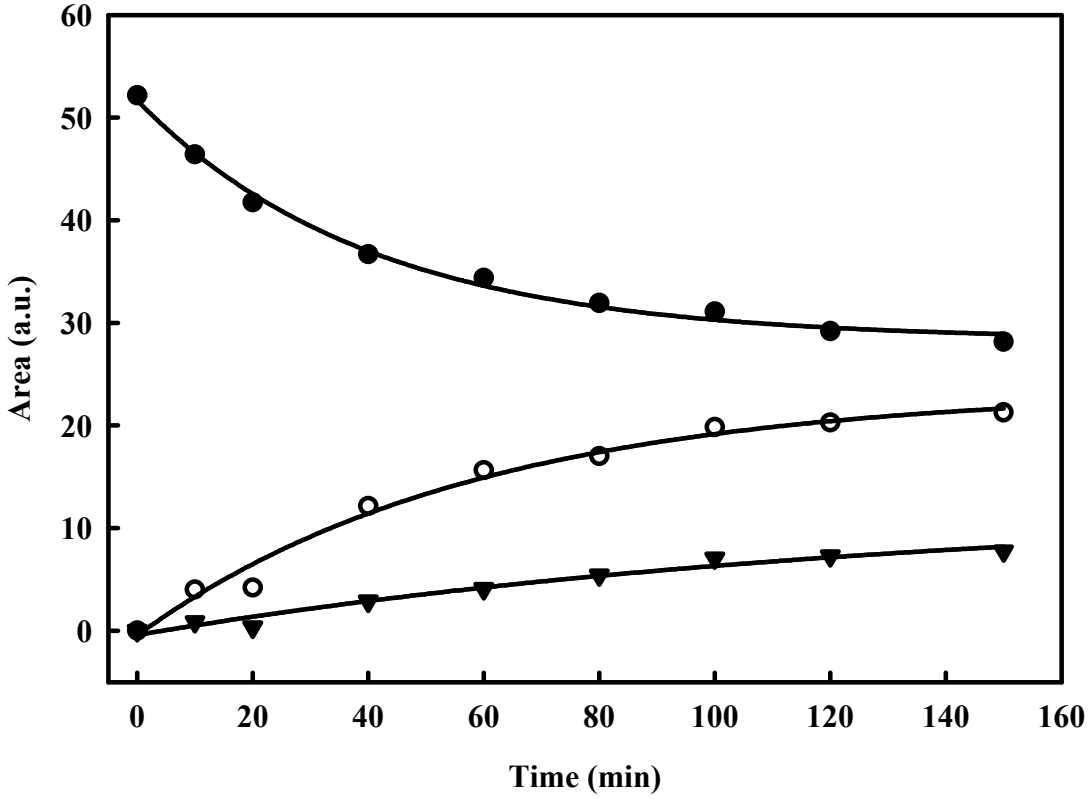

Figure 37. Time course of GST-CCPGCC-SNAP-25-EGFP (P9) cleavage by LC. The amount of intact GST-CCPGCC-SNAP-25-EGFP (**P9**) (●), the large fragment GST-CCPGCC-SNAP-25(1-197) (▼), and the small fragment SNAP-25(198-206)-EGFP (○) were obtained using imageJ based on the data in **Figure 36**. The solid line is the fitting curve based on exponential equation. The obtained pseudo-first order rate constants for the un-cleaved protein, the large fragment of GST-CCPGCC-SNAP-25(1-197), and the small fragment of SNAP-25(141-206) were 0.0248 ± 0.0023, 0.0076 ± 0.0023 and 0.0171 ± 0.0032 min^{-1}, respectively.

4.2.6 Time course of the cleavage of GST-CCPGCC-SNAP-25(A195S)-EGFP by BoNT/A LC

In order to reduce cleavage of SNAP-25, point mutation at P3 site was designed: the Ala was mutated to Ser at the 195 position in wild type SNAP-25. The mutated protein GST-CCPGCC-SNAP-25(A195S)-EGFP was expressed and purified to test the cleavage in the presence of BoNT/A LC. The results are shown in **Figure 38**.

The results suggested that the SNAP-25(A195S) could not be cleaved in the presence of 0.2 nM BoNT/A LC.GST-CCPGCC-SNAP-25(A195S)-EGFP (**P10**) and could not be cleaved or could only very slowly be cleaved by BoNT/A LC, although there was only one point mutation compared with the wild type of SNAP-25. But the binding to BoNT/A LC wasn't affected by the mutation since the K_m was similar compared with the wild-type SNAP-25. The catalysis was blocked because of the point mutation, resulting in the lack of detectable cleavage by BoNT/A LC. SNAP-25(A195S) was used in our binding studies with active BoNT/A LC.

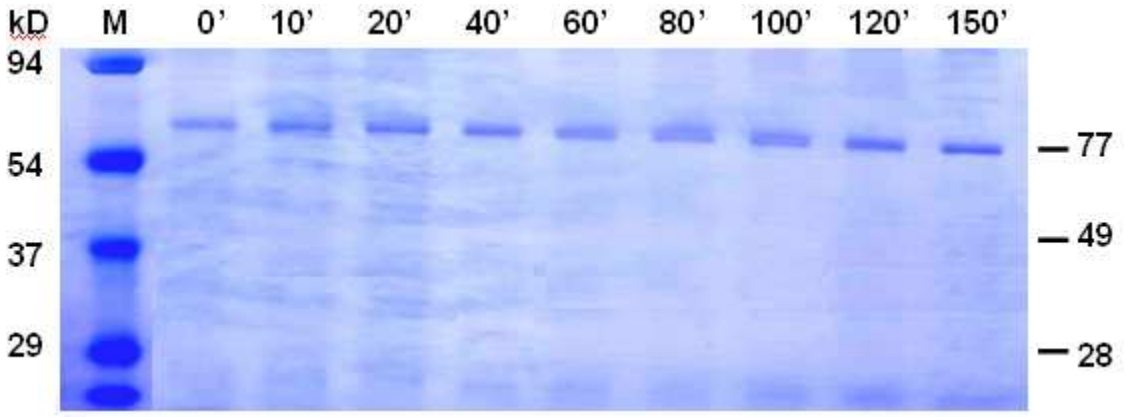

Figure 38. Time dependent cleavage of GST-CCPGCC-SNAP-25(A195S)-EGFP (P10) by BoNT/A LC. The purified GST-CCPGCC-SNAP-25(A195S)-EGFP (**P10**) (5.0 μM) was incubated with BoNT/A LC (2.0 nM) in 10 μl of buffer (10 mM Phosphate, 150 mM NaCl, 10 μM zinc acetate, pH 7.4). Reactions were kept at 37 ˚C for 2 h and then put in at 25 °C overnight. The reaction was stopped by adding the Laemmli sample buffer (Bio-Rad) and denatured 94 ˚C for 5 min following an analysis by SDS-PAGE. The incubation time was labeled on top of the figure. The cleaved fragments were not detectable at 49 and 28 kD under this condition.

4.2.7 Binding of ReAsH to GST-SNAP-25-EGFP

It was not clear weather the separated four cysteines (^{85}CGLCVCPC^{92}) in a short sequence, such as the case in SNAP-25B, bound to ReAsH or not. The fluorescence of EGFP was used to study the interactions between SNAP-25 and ReAsH. The fluorescence intensity of GST-SNAP-25-EGFP was determined at 25 ˚C. 20 fold molar excess of the ReAsH-EDT_2 reagent was added into the protein sample and incubated for 1 h at 25 ˚C in the phosphate buffer (10 mM potassium phosphate, 200 mM NaCl, 100 μM TCEP, and 1 mM β–mercaptoethanol, pH 7.2). For free resorufin, the excitation and emission maximum wavelengths were 571 and 585 nm, respectively. While the ReAsH bound to CCPGCC, the excitation and emission maximum wavelengths were 597 and 607 nm, respectively. In order to obtain the emission spectrum of EGFP and ReAsH, the excitation maximum wavelength was set at 460 nm and a continuous emission was scanned from 480 to 700 nm. The result is shown in **Figure 39**.

The fluorescence intensity of EGFP had no change, while the signal of ReAsH was not detectable even with excitation at 580 nm (data not shown). The results suggested that ReAsH did not bind to SNAP-25 nor affect the fluorescence intensity of EGFP. However, the baseline of fluorescence increased a little bit in the presence of ReAsH. For the un-bound ReAsH, there was no fluorescence contribution. Only ReAsH bound to CCPGCC, a strong fluorescence emission was obtained at 607 nm. A hydrolyzed resorufin from ReAsH may contribute a little bit of fluorescence.

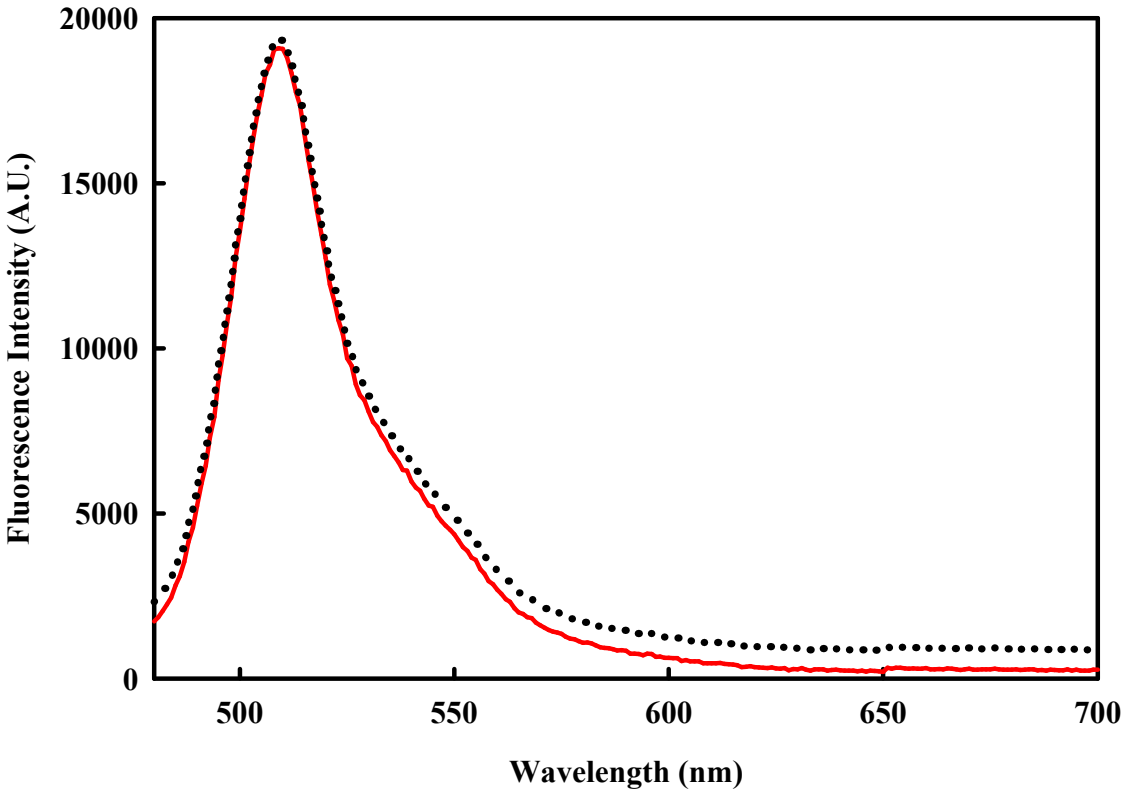

Figure 39. Emission spectra of GST-SNAP-25-EGFP (P8). The solid line represents the 0.2 μM GST-SNAP-25-EGFP (**P8**) and the dotted line represents the GST-SNAP-25-EGFP (**P8**) in the presence of ReAsH (0.2 μM). The excitation wavelength was 460 nm.

4.2.8 Excitation and emission of EGFP and ReAsH

The fluorescence of EGFP and ReAsH was determined in the phosphate buffer. For EGFP, the excitation maximum wavelength was 488 nm and the emission maximum wavelength was 509 nm, while for ReAsH bound to CCPGGCC, the excitation maximum wavelength was 597 nm and the emission maximum wavelength was 607 nm. The results are shown in **Figure 40**.

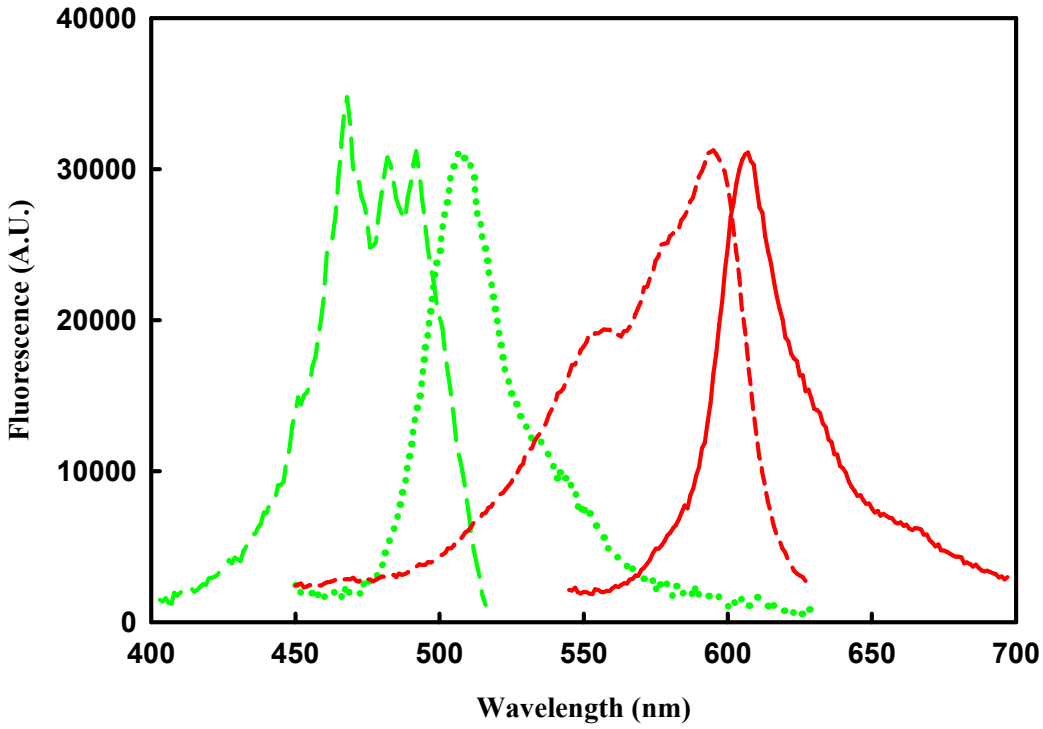

Figure 40. The excitation and emission spectra of EGFP and ReAsH. The spectra corresponded to the excitation (λ_{em} = 540 nm) (long dashed line) and the emission (λ_{ex} = 435 nm) (dotted line) spectra of EGFP; the excitation (λ_{em} = 640 nm) (short dashed line) and emission (λ_{ex} = 540 nm) (solid line) of ReAsH bound to CCPGCC in GST-CCPGCC-SNAP-25-EGFP (**P9**).

4.2.9 Transfer efficiency between donor and acceptor

In order to determine the energy transfer potentially occurring in the same molecule of GST-CCPGCC(ReAsH)-SNAP-25-EGFP (**P9-ReAsH**), a mixture of donor alone, with EGFP in GST-SNAP-25-EGFP, and acceptor alone, with ReAsH in GST-CCPGCC(ReAsH)-SNAP-25, was used as a control in our fluorescence studies.

Samples containing only EGFP or only ReAsH with SNAP-25 were used as controls. To the protein GST-SNAP-25-EGFP (**P8**) was added ReAsH-bound GST-CCPGCC-SNAP-25 in phosphate buffer containing 10 mM phosphate, pH 7.4, 150 mM NaCl, 0.1 mM TCEP, and 1 mM β–mercaptoethanol. The result is shown in **Figure 41**.

When the donor (EGFP) was excited at 488 nm, the fluorescence intensity was monitored between 495 nm and 700 nm. To confirm that FRET occurred between EGFP and ReAsH within the same protein in GST-CCPGCC(ReAsH)-SNAP-25-EGFP (**P9**), the spectra were obtained containing only donor or only acceptor after exciting at 488 nm.

The results indicate that there was no inter-molecule energy transfer between EGFP and ReAsH. The ReAsH itself was not fluorescent. When ReAsH bound to CCPGCC, the fluorescence intensity increased sharply at 607 nm when it was excited at 597 nm. However, the fluorescence intensity was very low when it was excited at 488 nm. So there should be little contribution from the ReAsH emission in our FRET studies.

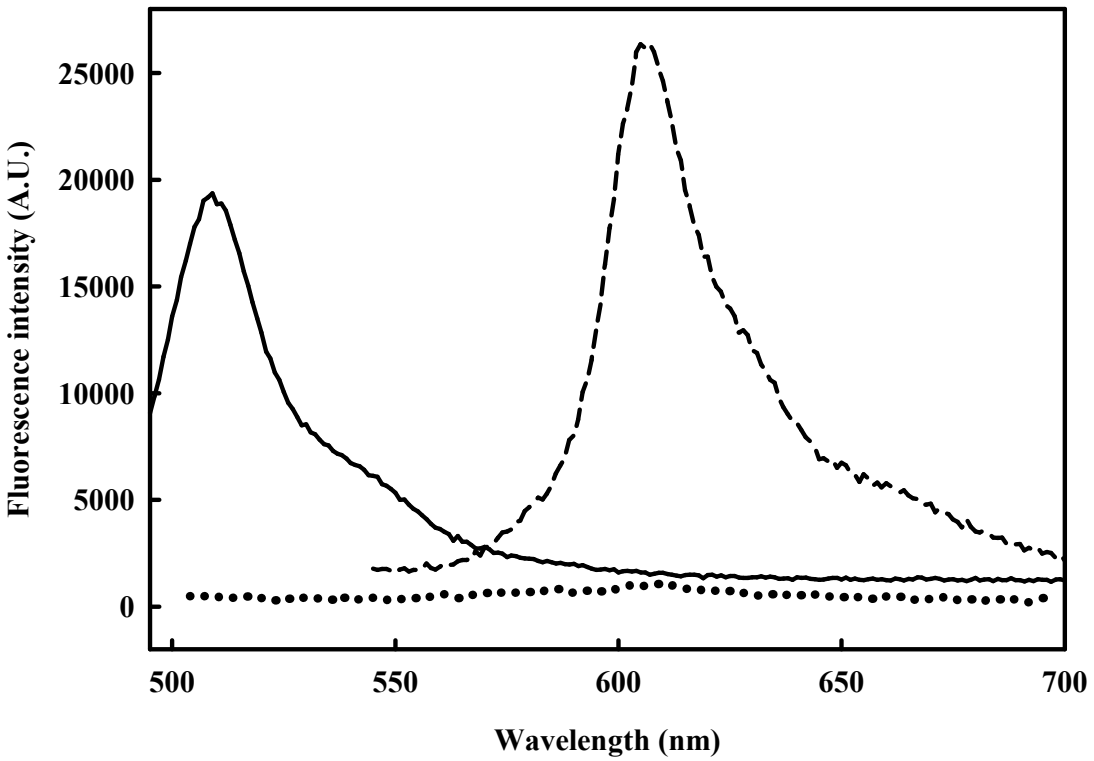

Figure 41. Fluorescence emission spectra of SNAP-25 with EGFP or ReAsH. The solid line represents the emission spectrum of a mixture of GST-SNAP-25-EGFP (**P8**) and GST-CCPGCC(ReAsH)-SNAP-25, excitation at 488 nm; the dotted line represents the GST-CCPGCC(ReAsH)-SNAP-25 with excitation at 488 nm, the emission of ReAsH is not prominent; the dashed line represents the GST-CCPGCC(ReAsH)-SNAP-25 with excitation at 530 nm and the maximal wavelength of ReAsH at 607 nm is prominent. All sample contained 0.2 μM proteins.

4.2.10 Time course of fluorescence changes of GST-CCPGCC-SNAP-25-EGFP in the presence of active BoNT/A LC

GST-CCPGCC-SNAP-25-EGFP (**P9**) was incubated with excess ReAsH at 25˚C overnight. The excess dye was removed by centrifugation and the ReAsH bound fusion protein was obtained.

When the fluorescence of the GST-CCPGCC-SNAP-25-EGFP (**P9**) was monitored with addition of active BoNT/A LC, two phases were observed in the time course. The results are shown in **Figure 42**.

An initial small decrease was followed by a slow large increase of fluorescence intensity. In the presence of active BoNT/A LC, the signal of EGFP decreased in the first 45 min, followed by an increase. The results suggest that BoNT/A LC binding to SNAP-25 dominated the process at the beginning. After 45 min, the binding process reached equilibrium, resulting in the cleavage process of SNAP-25 by BoNT/A LC domination. The total fluorescence intensity involved at least two processes: SNAP-25 binding to the BoNT/A LC and SNAP-25 cleaving by the BoNT/A LC.

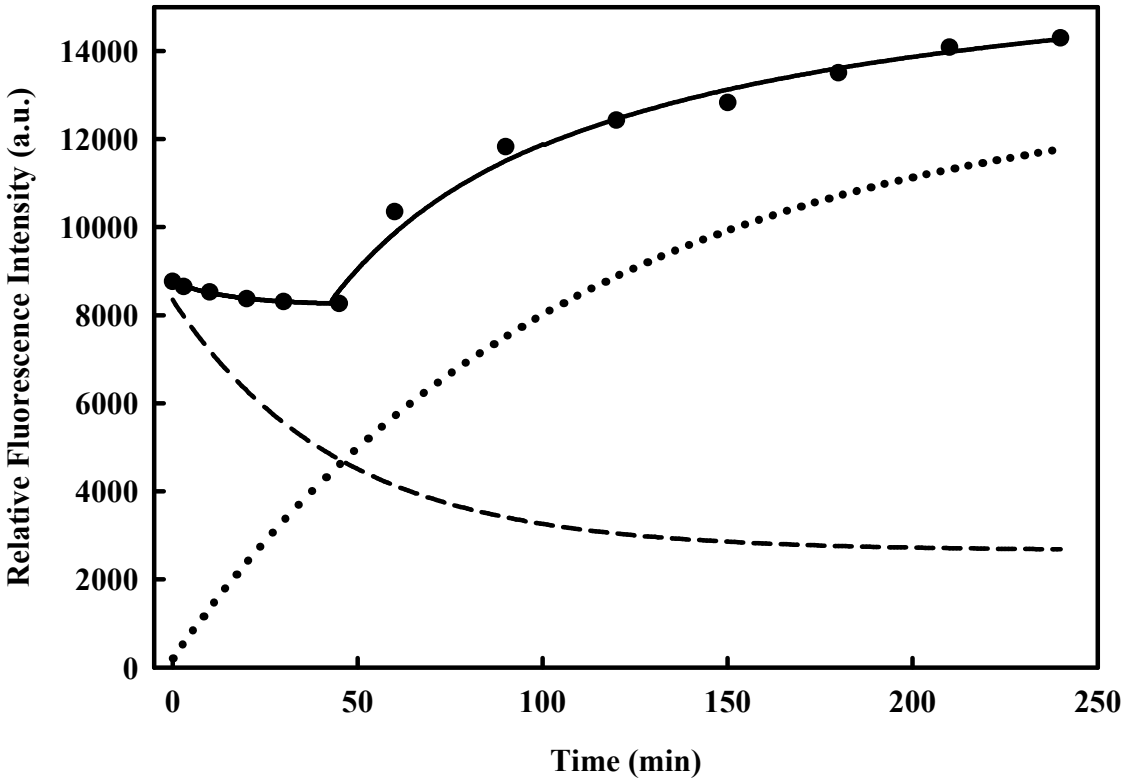

Figure 42. Time courses of BoNT/A LC cleavage of GST-CCPGCC-SNAP-25-EGFP (P9) at 509 nm. To the ReAsH modified protein of GST-CCPGCC-SNAP-25-EGFP (**P9**) (0.2 μM), BoNT/A LC (1 μl, 10 μM) was added to initiate the reaction in 500 μl phosphate buffer containing 20 mM phosphate, pH 7.4, 150 mM NaCl, 10 μM zinc acetate, 0.3 mM TCEP, and 1 mM β–mercaptoethanol. The time course was obtained by monitoring the emission of EGFP at 509 nm (●) with the excitation maximum wavelength at 488 nm at 25 °C. The biphasic time courses were the sum of two exponential fits, including a slow increase (cleavage) of EGFP emission (dotted line) and a fast decrease (binding) of EGFP emission (dashed line). The obtained cleavage rate of SNAP-25 by active BoNT/A LC was found to be 39.6 s^{-1} and the binding constants of SNAP-25 to BoNT/A LC were found to be1875 $M^{-1} \cdot s^{-1}$.

In the presence of BoNT/A LC, GST-CCPGCC-SNAP-25-EGFP (**P9**) wrapped around the active BoNT/A LC before the cleavage of substrate, resulting in a decrease of the distance between CCPGCC-ReAsH and EGFP. So, FRET between EGFP and ReAsH-CCPGCC increased. The pseudo-first order rate constant for the binding was 0.0225 ± 0.0006 min^{-1}. Since the amount of substrates (0.2 μM) was in a large excess of the amount of enzyme (2.0 nM), the concentration of the substrate could be consider as a constant. The binding constant was found to be 1875 $M^{-1} \cdot s^{-1}$.

However, binding to SNAP-25 and cleavage of SNAP-25 by BoNT/A LC occurred simultaneously. Once BoNT/A LC bound to SNAP-25, cleavage was expected to occur at the same time. After the cleavage of the SNAP-25 by BoNT/A LC, the fragments of GST-CCPGCC-SNAP-25(1-197) and SNAP-25(198-206)-EGFP were separated, resulting in a decrease of FRET between EGFP and ReAsH. The obtained cleavage rate constant was 39.6 s^{-1}.

The results suggested that the full length SNAP-25 in GST-CCPGCC-SNAP-25-EGFP (**P9**) could be cleaved by BoNT/A LC, which provided evidence of the correct folding of SNAP-25 in the fusion protein.

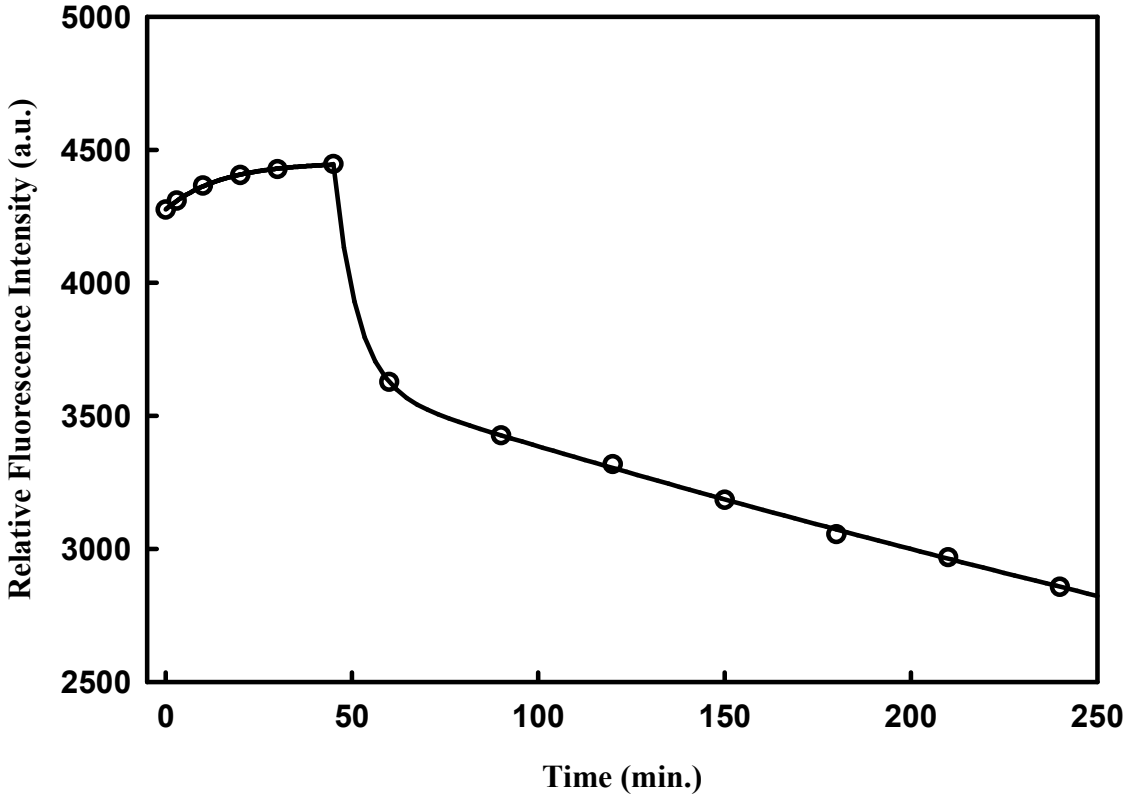

Figure 42B. Time courses of BoNT/A LC cleavage of GST-CCPGCC-SNAP-25-EGFP (P9) at 607 nm. The spectra were recorded at 25 ˚C. To the ReAsH modified protein of GST-CCPGCC-SNAP-25-EGFP (**P9**) (0.2 μM), BoNT/A LC (1 μl, 10 μM) was added to initiate the reaction in 500 μl phosphate buffer containing 20 mM phosphate, pH 7.4, 150 mM NaCl, 10 μM zinc acetate, 0.3 mM TCEP, and 1 mM β–mercaptoethanol. The time course was obtained by monitoring the emission of ReAsH at 607 nm (○) at 25 °C with the excitation maximum wavelength at 488 nm.

4.2.11 Trypsin digestion of GST-CCPGCC-SNAP-25-EGFP

Purified GST-CCPGCC-SNAP-25-EGFP (**P9**) was cleaved with trypsin for 3 h at 37 ºC. To 100 µl of buffer (100 mM MOPS, 10 mM Mercaptoethanol, 10 µM EDT, pH 7.2), 4.0 µl of protein GST-CCPGCC-SNAP-25-EGFP (**P9**) (10 µM) and 2.0 µl (1.0 µM) of trypsin (Sigma, T-0134) were mixed. The trypsin was freshly prepared (1.0 µM) and dissolved in aqueous ammonium bicarbonate (Fisher, A643-500). After the reaction, the mixture was diluted into 500 µl of buffer (100 mM MOPS, 10 mM β-Mercaptoethanol, 10 µM EDTA, pH 7.2). The signal of EGFP disappeared, which suggested that the EGFP had been cleaved away from the substrate.

ReAsH-EDT_2 (Invitrogen, 2. 0 µl, 250 µM in DMSO) was added into the mixture and used to detect the fluorescence intensity. The fragment of peptide containing CCPGCC bound to ReAsH to form a strong fluorescence complex, which had the emission maximum wavelength at 607 nm (excitation maximum wavelength at 595 nm). The results suggest that the fusion protein had ReAsH-CCPGCC and the cleaved CCPGCC fragment bound to ReAsH and emitted a strong fluorescence (Data was not shown). Later, GST-CCPGCC-SNAP-25 was constructed to be used as the positive control of the CCPGCC bound to ReAsH.

4.2.12 Preparation of Zn^{2+}-depleted BoNT/A LC

In order to remove trace amounts of cations, such as Zn^{2+} in the buffer, 5.0 g of Chelex® 100 (molecular biology grade, Bio-Rad) was added to 1.0 liter of buffer (10 mM phosphate, 200 mM NaCl, pH 7.2) for 24 h at 25 °C. The resin was removed by centrifuge at 13,000 RPM for 5 min prior to use. EDTA (20 ml, 0.5 M, pH 8.0) was diluted into 1 liter of buffer (10 mM sodium phosphate, 200 mM NaCl, pH 7.2). To remove Zn^{2+} in the light chain, the protein was incubated in a buffer (10 mM sodium phosphate, 200 mM NaCl, 10 mM EDTA, pH 7.2), and then dialyzed against the same buffer at 4 ºC overnight. The zinc-depleted protein was re-dialyzed at 4 ºC against 2500 volumes of 10 mM sodium phosphate (pH 7.2) pre-treated Chelex® 100 with three changes overnight to remove excess EDTA. The resulting light chain stripped of Zn^{2+} had no protease activity. The distance between the EGFP and ReAsH tags via FRET was determined after **P9-ReAsH** binding to Zn^{2+}-depleted BoNT/A LC. This method was first used by Minghao Feng in Dr. David Yang's lab.

4.2.13 FRET and determination of apparent distance between the C-terminus and the N-terminus of the SNAP-25

The double labeled protein SNAP-25 with N-terminal ReAsH and C-terminal EGFP in GST-CCPGCC-SNAP-25-EGFP (**P9**) was used for fluorescence resonance energy transfer (FRET) experiments.

GST-CCPGCC-SNAP-25-EGFP (**P9**) (0.2 μM) and GST-CCPGCC(ReAsH)-SNAP-25-EGFP (**P9-ReAsH**)(0.2 μM) were incubated in 10 mM MOPS buffer (pH 7.4), 150 mM NaCl, 100 μM TCEP, 1 mM β-mercaptoethanol, and 1 mM EDTA for 2 h at 25 ˚C. The fluorescence intensity was recorded from 495 nm to 700 nm with an excitation maximum wavelength at 488 nm. The results are shown in **Figure 43**.

Zn^{2+}-depleted BoNT/A LC was incubated with GST-CCPGCC-SNAP-25-EGFP (**P9**) for 2 h at 25 ˚C to determine the donor fluorescence quenching by BoNT/A LC in the presence of the acceptor. The results are shown in **Figure 44**.

The emission maximum wavelength of 509 nm and 607 nm is a characteristic peak for EGFP and ReAsH bound to CCPGCC, respectively. For the free ReAsH in the buffer, the maximal fluorescence is at 585 nm, but the intensity is negligible. In the fusion protein, CCPGCC residues are not fluorescence without labeling with ReAsH. So the donor emission in the absence of acceptor can be monitored from the EGFP in GST-CCPGCC-SNAP-25-EGFP (**P9**) in the absence of ReAsH. When CCPGCC was labeled with ReAsH, the fluorescence emission maximum wavelength of ReAsH is at 607 nm, which acts as an acceptor in GST-CCPGCC(ReAsH)-SNAP-25-EGFP (**P9-ReAsH**). ReAsH, without binding to CCPGCC, shows very low fluorescence emission at 607 nm when it is excited at 488 nm.

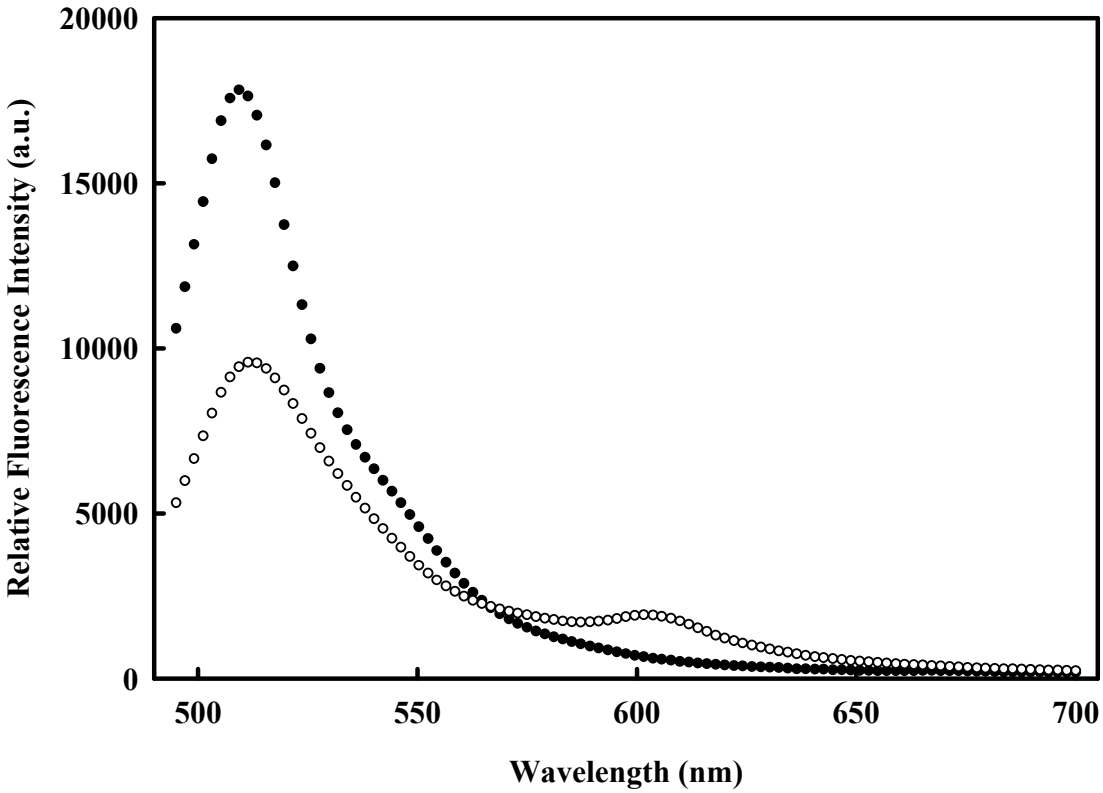

Figure 43. FRET of GST-CCPGCC-SNAP-25-EGFP (P9). The spectra were recorded in 10 mM MOPS buffer (pH 7.4), 150 mM NaCl, 100 μM TCEP, 1 mM β-mercaptoethanol, and 1 mM EDTA at 25 ºC. The fluorescence spectra were obtained with excitation at 488 nm. All samples contained 0.2 μM proteins. The spectra corresponded to: (●) emission spectrum of GST-CCPGCC-SNAP-25-EGFP (**P9**); (○) emission spectrum of GST-CCPGCC(ReAsH)-SNAP-25-EGFP (**P9-ReAsH**). The emission maximum wavelengths were 509 nm and 607 nm for EGFP and ReAsH, respectively. The fluorescence background of the buffer was subtracted in all cases.

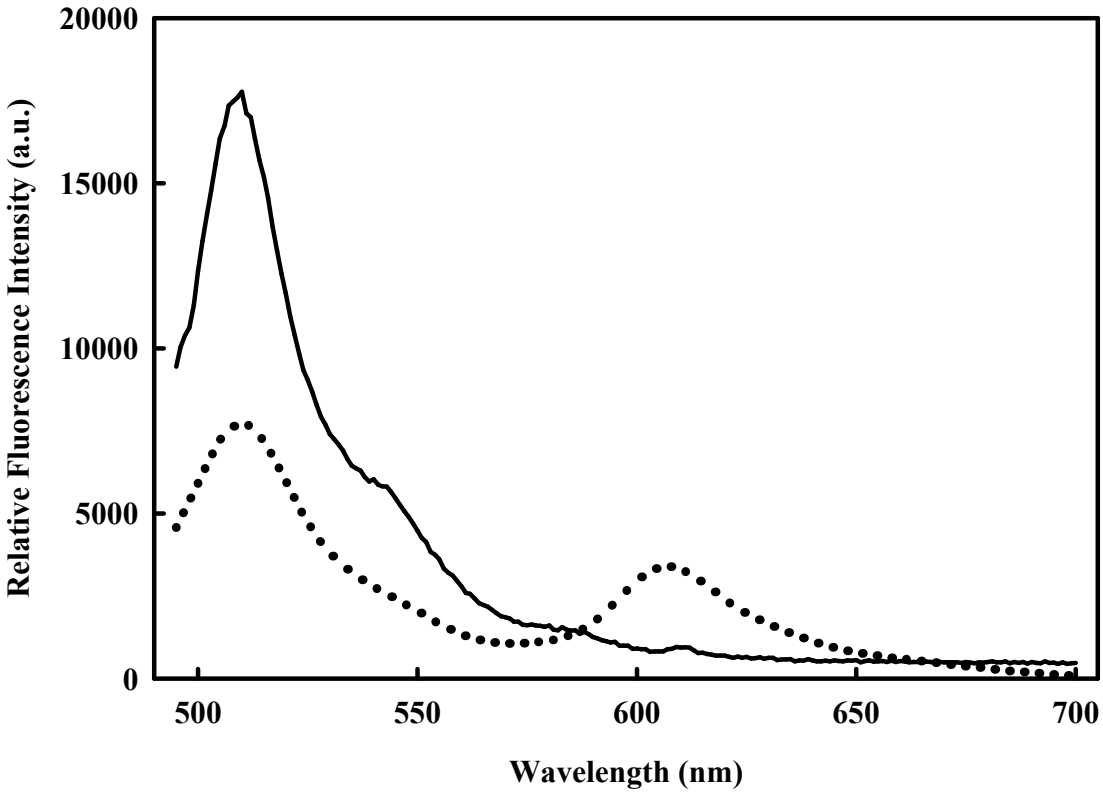

Figure 44. FRET of LC-bound GST-CCPGCC-SNAP-25-EGFP. The spectra were recorded in 10 mM MOPS buffer (pH 7.4), 150 mM NaCl, 100 μM TCEP, 1 mM β-mercaptoethanol, and 1 mM EDTA at 25 ºC. The excitation maximum wavelength was 488 nm. The solid line corresponded to the emission spectrum of the donor (EGFP) in the mixture of 0.2 μM GST-CCPGCC-SNAP-25-EGFP (**P9**) and 0.2 μM BoNT/A LC; the dotted line corresponded to the emission spectrum of the mixture of the double labeled 0.2 μM GST-CCPGCC(ReAsH)-SNAP-25-EGFP (**P9-ReAsH**) with 0.2 μM Zn^{2+}-depleted BoNT/A LC.

Figure 43 showed a typical set of fluorescence spectra obtained for the C-terminus of the SNAP-25 labeled with EGFP. When the N-terminal CCPGCC covalently bound to ReAsH, a decrease in the intensity of EGFP donor emission was observed, accompanied by an increase of the sensitized emission of ReAsH. The unbound free ReAsH itself was not fluorescent. So there should be little contribution from the ReAsH emission. The apparent distance from the C-terminus to the N-terminus of the SNAP-25 was calculated based on the EGFP fluorescence quenching percentage. The obtained energy transfer efficiency was (49.9 ± 1.3)%, corresponding to the apparent distance between the C-terminus and the N-terminus of the SNAP-25 which was 51.9 ± 0.6 Å.

When ReAsH covalently bound to CCPGCC at the N-terminus of the SNAP-25 in GST-CCPGCC-SNAP-25-EGFP, the fluorescent resonance energy transfer was determined in the complex of BoNT/A LC with SNAP-25. The binding of SNAP-25 to BoNT/A LC reached equilibrium in 2 h. The apparent distance between the C-terminus and the N-terminus of the SNAP-25 was calculated based on the EGFP fluorescence quenching percentage in the complex of BoNT/A LC and SNAP-25.

In the presence of 0.2 μM Zn^{2+}-depleted BoNT/A LC, the fluorescence intensity of donor emission decreased at 509 nm and the sensitized emission increased at 607 nm, which indicated an increase in energy transfer between EGFP and ReAsH, resulting in a shorter apparent distance between the C-terminus and the N-terminus of the SNAP-25 upon binding of BoNT/A LC (**Figure 44**). The obtained total fluorescence energy transfer efficiency was (54.9 ± 1.4)%. The real fluorescence energy transfer efficiency of the complex after normalization was (89.6 ± 1.4)%, which corresponded to the apparent distance between the C-terminus and the N-terminus of SNAP-25 which was 36.2 ± 1.1Å.

4.2.14 FRET and determination of apparent distance between the C-terminus and the N-terminus of the SNAP-25(A195S)

To confirm that FRET changes between EGFP and ReAsH in GST-CCPGCC-SNAP-25-EGFP (**P9**), SNAP-25(A195S) was introduced to GST-CCPGCC-SNAP-25(A195S)-EGFP (**P10**) to monitor the conformational change of SNAP-25(A195S) upon binding of active BoNT/A LC. GST-CCPGCC-SNAP-25(A195S)-EGFP (**P10**) was labeled with ReAsH to get GST-CCPGCC(ReAsH)-SNAP-25(A195S)-EGFP (**P10-ReAsH**) and the excess dye was removed by centrifugation.

GST-CCPGCC-SNAP-25(A195S)-EGFP (**P10**) could not be cleaved by active BoNT/A LC as confirmed by SDS-PAGE (**Figure 38**). In order to test the effects of BoNT/A LC binding to SNAP-25(A195S), the GST-CCPGCC-SNAP-25(A195S)-EGFP (**P10**) was incubated with ReAsH for 2 h at 25 ˚C to produce double labeled GST-CCPGCC(ReAsH)-SNAP-25(A195S)-EGFP (**P10-ReAsH**). The results are shown in **Figures 45** and **46**. The obtained fluorescence energy transfer efficiency was (30.3 ± 1.2)%, which corresponded to the apparent distance between the C-terminus and the N-terminus of the SNAP-25(A195S) which was 59.5 ± 0.6 Å. **Figure 46** showed a typical set of fluorescence spectra obtained for the SNAP-25(A195S) in GST-CCPGCC-SNAP-25(A195S)-EGFP (**P10**) with BoNT/A LC. The results were comparable with the SNAP-25 in GST-CCPGCC-SNAP-25-EGFP (**P9**) bound to the inactive BoNT/A LC. The obtained total energy transfer efficiency was (37.8 ± 1.3)%. The real energy transfer efficiency of the complex after normalization was (90.4 ± 1.3)%, which corresponded to the apparent distance between the C-terminus and the N-terminus of the SNAP-25 which was 35.7 ± 0.9 Å.

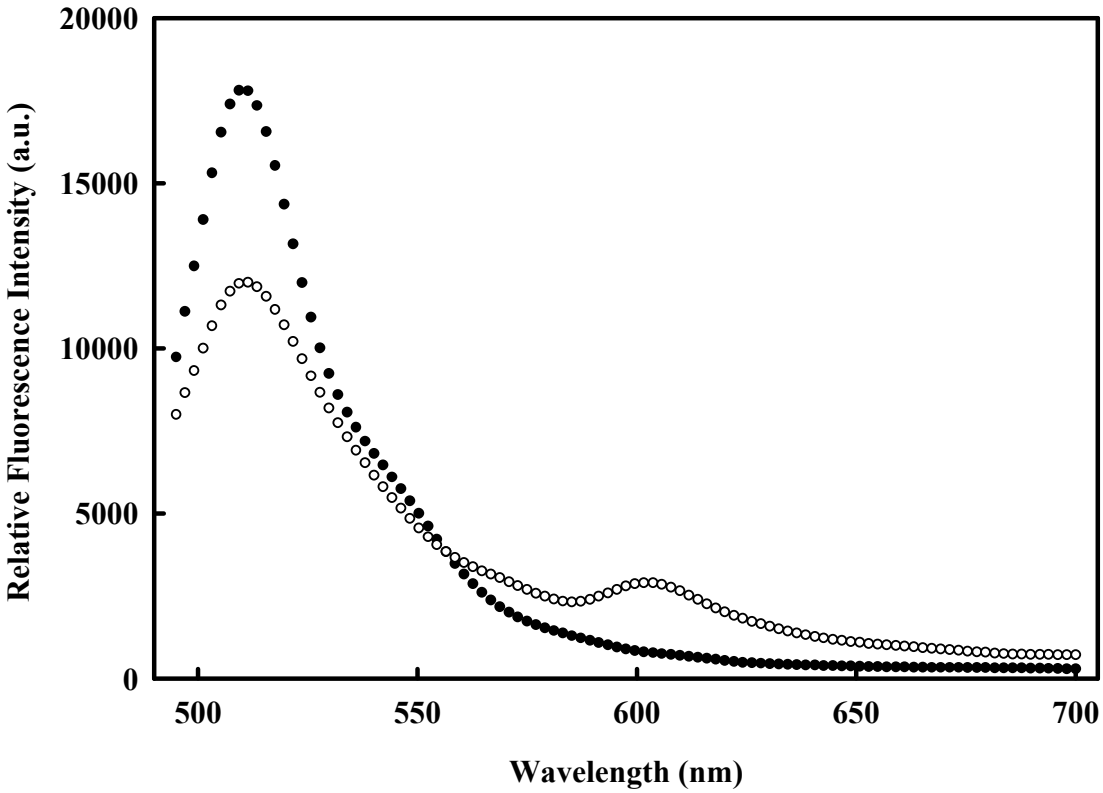

Figure 45. FRET of GST-CCPGCC-SNAP-25(A195S)-EGFP (P10). The spectra were recorded in 10 mM MOPS buffer (pH 7.4), 150 mM NaCl, 100 µM TCEP, 1 mM β-mercaptoethanol at 25 ºC. The fluorescence spectra were obtained with excitation at 488 nm. All samples contained 0.2 µM proteins. The spectra corresponded to: (●) emission spectrum of GST-CCPGCC-SNAP-25(A195S)-EGFP (**P10**); (○) emission spectrum of GST-CCPGCC(ReAsH)-SNAP-25(A195S)-EGFP (**P10-ReAsH**). The emission maximum wavelengths were 509 nm and 607 nm for EGFP and ReAsH, respectively. The fluorescence background of the buffer was subtracted in both cases.

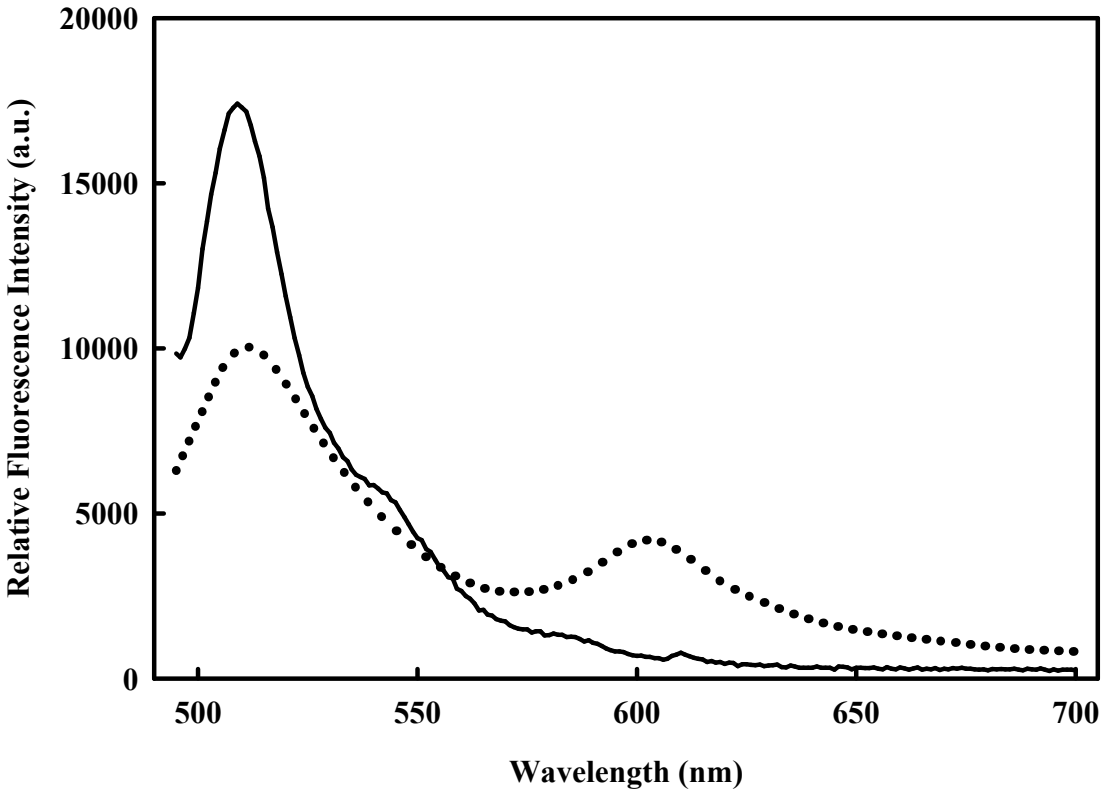

Figure 46. FRET of LC-bound GST-CCPGCC-SNAP-25(A195S)-EGFP. The spectra were recorded in 10 mM MOPS buffer (pH 7.4), 150 mM NaCl, 100 μM TCEP, and 1 mM β-mercaptoethanol at 25 ºC. The excitation wavelength was 488 nm. The solid line corresponded to the emission spectrum of donor (EGFP) in the mixture of 0.2 μM GST-CCPGCC-SNAP-25(A195S)-EGFP (**P10**) and 0.2 μM BoNT/A LC; the dotted line corresponded to the emission spectrum of the mixture of 0.2 μM GST-CCPGCC(ReAsH)-SNAP-25(A195S)-EGFP (**P10-ReAsH**) with 0.2 μM BoNT/A LC.

4.2.15 FRET and determination of apparent distance between the C-terminus and the D140 of the SNAP-25

In order to determine the distance between the C-terminus and the D140 of the SNAP-25, CCPGCC was inserted between D140 and A141 of the SNAP-25 by mutagenesis. The protein GST-SNAP-25(1-140)-CCPGCC-SNAP-25(141-206)-EGFP (**P11**) was used for FRET studies.

GST-SNAP-25(1-140)-CCPGCC-SNAP-25(141-206)-EGFP (**P11**) (0.2 μM) and GST-SNAP-25(1-140)-CCPGCC(ReAsH)-SNAP-25(141-206)-EGFP (**P11-ReAsH**) (0.2 μM) were incubated in 10 mM MOPS buffer (pH 7.4), 150 mM NaCl, 100 μM TCEP, 1 mM β-mercaptoethanol, and 1 mM EDTA for 2 h at 25 ˚C. The fluorescence intensity was recorded from 495 nm to 700 nm with an excitation maximum wavelength at 488 nm. The results are shown in **Figure 47**. The obtained fluorescence energy transfer efficiency was (53.7 ± 1.2)%, which corresponded to the apparent distance between the C-terminus and the D140 of the SNAP-25 was 50.6 ± 0.4 Å.

Similarly, SNAP-25 in GST-SNAP-25(1-140)-CCPGCC-SNAP-25(141-206)-EGFP (0.2 μM) (**P11**) and GST-SNAP-25(1-140)-CCPGCC(ReAsH)-SNAP-25(141-206)-EGFP (0.2 μM) (**P11-ReAsH**) bound to the 0.2 μM Zn^{2+}-depleted BoNT/A LC to from a stable binary complex. The results are shown in **Figure 48**. The obtained total fluorescence energy transfer efficiency was (54.7 ± 1.5)%. The real fluorescence energy transfer efficiency of the complex after normalization was (61.7 ± 1.5)%, which corresponded to the apparent distance between the C-terminus and the D140 of the SNAP-25 which was 47.9 ± 0.9 Å.

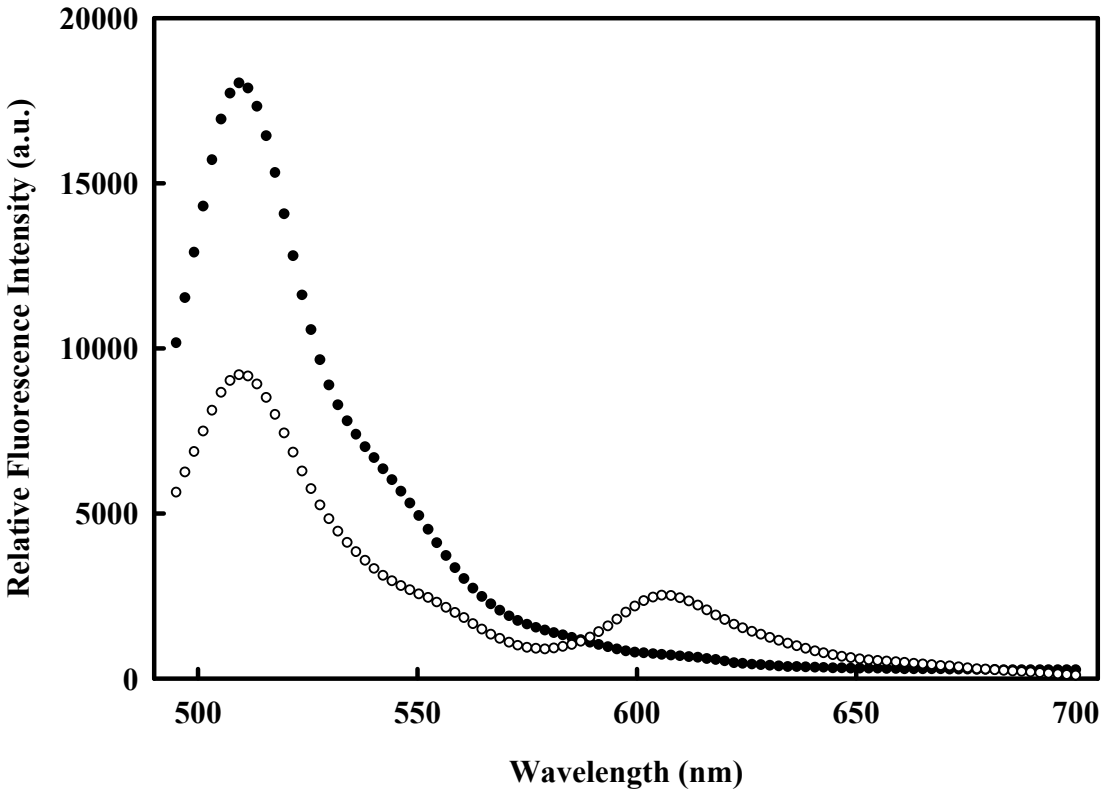

Figure 47. FRET of GST-SNAP-25(1-140)-CCPGCC-SNAP-25(141-206)-EGFP (P11). The spectra were recorded in 10 mM MOPS buffer (pH 7.4), 150 mM NaCl, 100 μM TCEP, 1 mM β-mercaptoethanol, and 1 mM EDTA at 25 ºC. The fluorescence spectra were obtained with excitation at 488 nm. All samples contained 0.2 μM proteins. The spectra corresponded to: (●) emission spectrum of EGFP in GST-SNAP-25(1-140)-CCPGCC-SNAP-25(141-206)-EGFP (**P11**); (○) emission spectrum of GST-SNAP-25(1-140)-CCPGCC(ReAsH)-SNAP-25(141-206)-EGFP (**P11-ReAsH**). The fluorescence background of the buffer was subtracted in both cases.

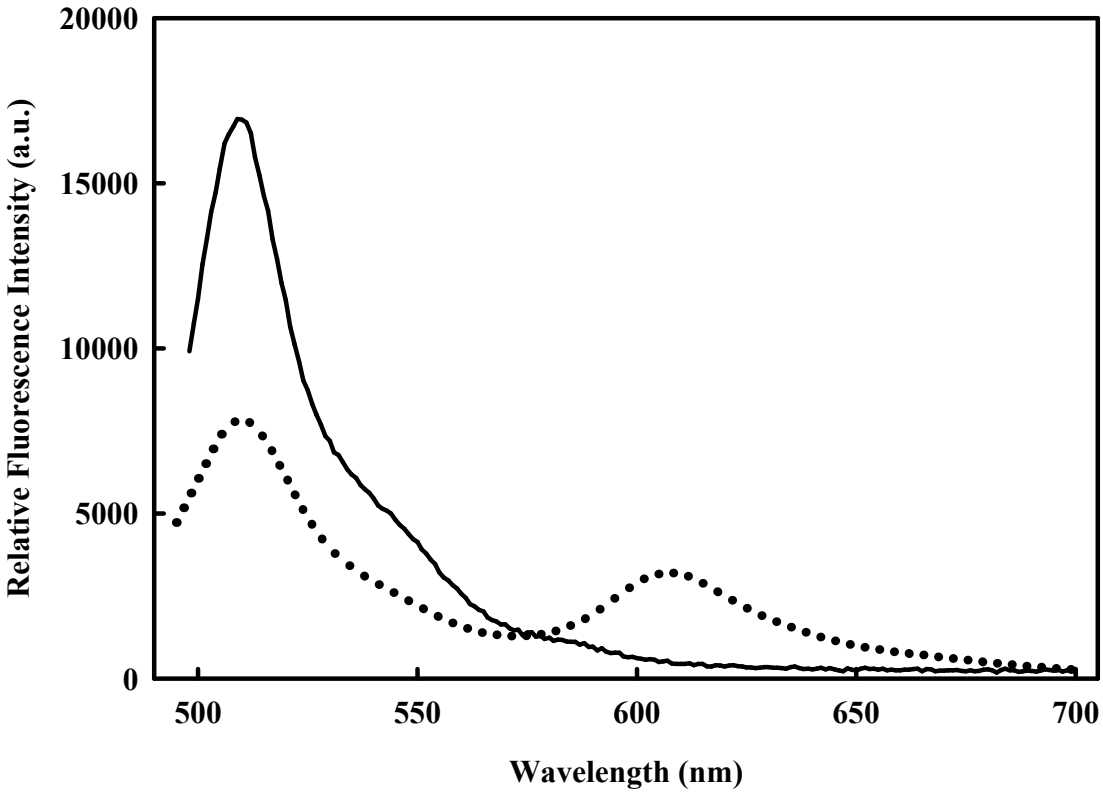

Figure 48. FRET of LC-bound GST-SNAP-25(1-140)-CCPGCC-SNAP-25(141-206)-EGFP. The spectra were recorded in 10 mM MOPS buffer (pH 7.4), 150 mM NaCl, 100 μM TCEP, 1 mM β-mercaptoethanol and 1 mM EDTA at 25 ºC. The fluorescence spectra were obtained with excitation at 488 nm. The solid line corresponded to the emission spectrum of donor (EGFP) in the mixture of 0.2 μM GST-SNAP-25(1-140)-CCPGCC-SNAP-25(141-206)-EGFP (**P11**) and 0.2 μM Zn^{2+}-depleted BoNT/A LC; the dotted line corresponded to the emission spectrum of the mixture of 0.2 μM GST-CCPGCC(ReAsH)-SNAP-25-EGFP (**P11-ReAsH**) and 0.2 μM Zn^{2+}-depleted BoNT/A LC.

4.2.16 FRET and determination of apparent distance between the C-terminus and the D140 of the SNAP-25(A195S)

In order to determine the distance between the C-terminus and the D140 of the SNAP-25(A195S), CCPGCC was inserted between D140 and A141 of the SNAP-25(A195S) by mutagenesis. The protein GST-SNAP-25(1-140)-CCPGCC-SNAP-25(141-206, A195S)-EGFP (**P12**) was used as FRET studies.

GST-SNAP-25(1-140)-CCPGCC-SNAP-25(141-206, A195S)-EGFP (**P12**) (0.2 μM) and GST-SNAP-25(1-140)-CCPGCC(ReAsH)-SNAP-25(141-206, A195S)-EGFP (**P12-ReAsH**) (0.2 μM) were incubated in 10 mM MOPS buffer (pH 7.4), 150 mM NaCl, 100 μM TCEP and 1 mM β-mercaptoethanol for 2 h at 25 ˚C. The fluorescence intensity was recorded from 495 nm to 700 nm with an excitation maximum wavelength at 488 nm. The results are shown in **Figure 49**. The obtained fluorescence energy transfer efficiency was (53.1 ± 1.3)%, corresponding to the apparent distance between the C-terminus and the D140 of the SNAP-25(A195S) which was 50.8 ± 0.5 Å.

Similarly, SNAP-25(A195S) in GST-SNAP-25(1-140)-CCPGCC-SNAP-25(141-206, A195S)-EGFP (**P12**) (0.2 μM) and GST-SNAP-25(1-140)-CCPGCC(ReAsH)-SNAP-25(141-206, A195S)-EGFP (**P12-ReAsH**) bound to the active 0.2 μM BoNT/A LC to from a stable complex. The results are shown in **Figure 50**. The obtained total energy transfer efficiency was (54.6 ± 1.5)%. The real energy transfer efficiency of the complex after normalization was (65.1 ± 1.5)%, which corresponded to the apparent distance between the C-terminus and the D140 of the SNAP-25(A195S) which was 46.7 ± 0.6 Å.

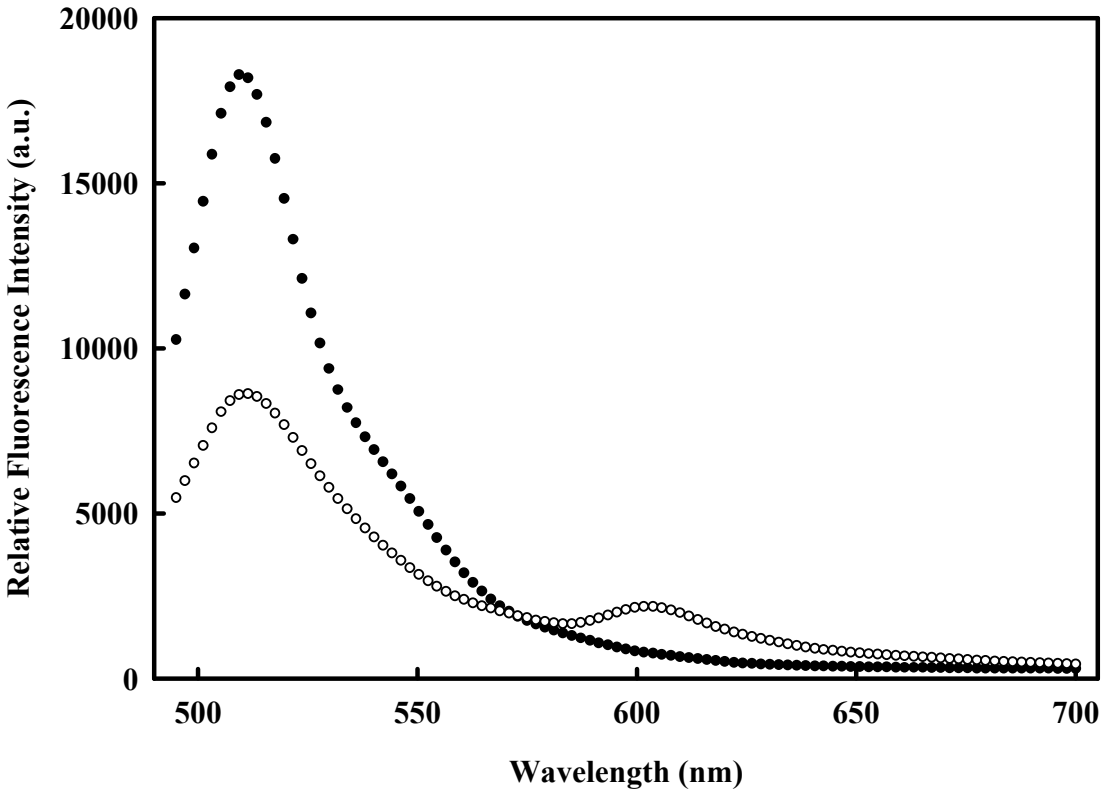

Figure 49. FRET of GST-SNAP-25(1-140)-CCPGCC-SNAP-25(141-206, A195S)-EGFP (P12). The spectra were recorded 10 mM MOPS buffer (pH 7.4), 150 mM NaCl, 100 μM TCEP and 1 mM β-mercaptoethanol at 25 ºC. The fluorescence spectra were obtained with excitation at 488 nm. The spectra corresponded to: (●) emission spectrum of 0.2 μM GST-SNAP-25(1-140)-CCPGCC-SNAP-25(141-206, A195S)-EGFP (**P12**); (○) emission spectrum 0.2 μM GST-SNAP-25(1-140)-CCPGCC(ReAsH)-SNAP-25(141-206, A195S)-EGFP (**P12-ReAsH**). The fluorescence background of the buffer was subtracted in both cases.

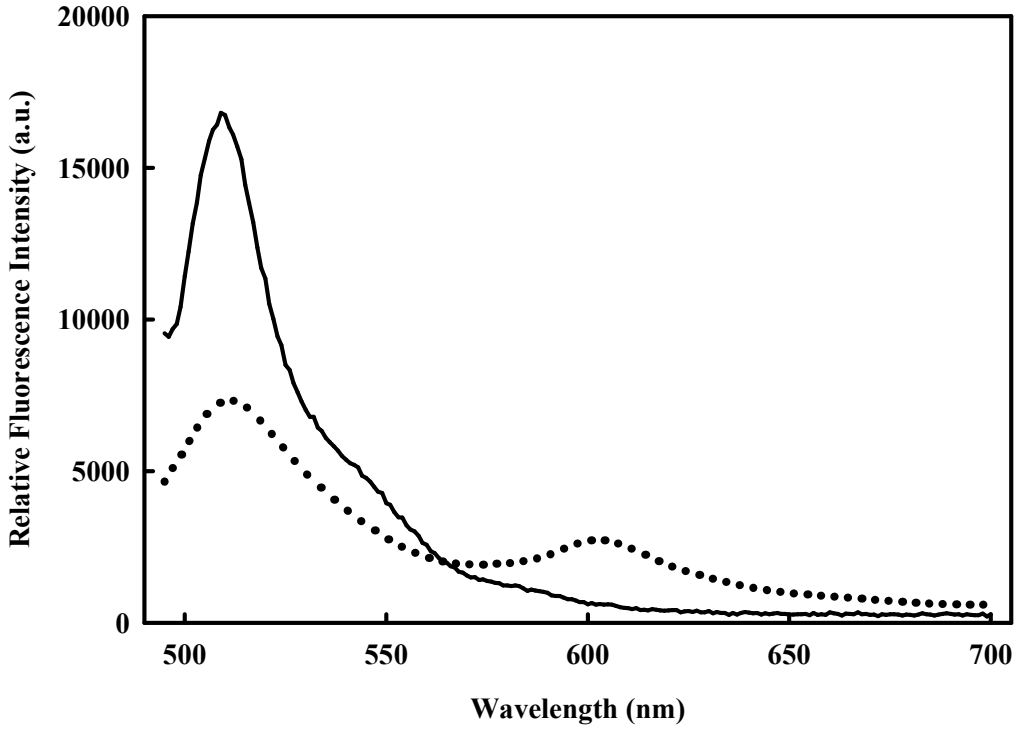

Figure 50. FRET of LC-bound GST-SNAP-25(1-140)-CCPGCC-SNAP-25(141-206, A195S)-EGFP. The spectra were recorded in 10 mM MOPS buffer (pH 7.4), 150 mM NaCl, 100 μM TCEP, and 1 mM mercaptoethanol at 25 ºC. The fluorescence spectra were obtained with excitation at 488 nm. The solid line corresponded to the emission spectrum of donor (EGFP) in the mixture of 0.2 μM GST-SNAP-25(1-140)-CCPGCC-SNAP-25(141-206, A195S)-EGFP (**P12**) and 0.2 μM BoNT/A LC; the dotted line corresponded to the emission spectrum of the mixture of 0.2 μM GST-SNAP-25(1-140)-CCPGCC(ReAsH)-SNAP-25(141-206, A195S)-EGFP (**P12-ReAsH**) and 0.2 μM BoNT/A LC.

4.2.17 FRET and determination of apparent distance between the N-terminus and the D140 of the SNAP-25

In order to determine the distance between the N-terminus and the D140 of the SNAP-25, CCPGCC was inserted between D140 and A141 of the SNAP-25 and EGFP was engineered at the N-terminus of the SNAP-25 by mutagenesis. The protein GST-EGFP-SNAP-25(1-140)-CCPGCC-SNAP-25(141-206) (**P14**) was used as FRET studies.

GST-EGFP-SNAP-25(1-140)-CCPGCC-SNAP-25(141-206) (**P14**) (0.2 μM) and GST-EGFP-SNAP-25(1-140)-CCPGCC(ReAsH)-SNAP-25(141-206) (**P14-ReAsH**) (0.2 μM) were incubated in 10 mM MOPS buffer (pH 7.4), 150 mM NaCl, 100 μM TCEP, 1 mM β-mercaptoethanol, and 1 mM EDTA for 2 h at 25 ˚C. The fluorescence intensity was recorded from 495 nm to 700 nm with an excitation maximum wavelength at 488 nm. The results are shown in **Figure 51**. The obtained fluorescence energy transfer efficiency was (22.9 ± 1.4)%, corresponding to the apparent distance between the N-terminus and the D140 of the SNAP-25 which was 63.5 ± 0.9 Å.

Similarly, SNAP-25 in GST-EGFP-SNAP-25(1-140)-CCPGCC-SNAP-25(141-206) (**P14**) (0.2 μM) and GST-EGFP-SNAP-25(1-140)-CCPGCC(ReAsH)-SNAP-25(141-206) (**P14-ReAsH**) (0.2 μM) bound to 0.2 μM Zn^{2+}-depleted BoNT/A LC to from a stable complex. The results are shown in **Figure 52**. The obtained total energy transfer efficiency was (15.8 ± 1.5)%. The real energy transfer efficiency of the complex after normalization was (36.6 ± 1.5)%, which corresponded to the apparent distance between the N-terminus and the D140 of the SNAP-25 which was 56.8 ± 0.7 Å.

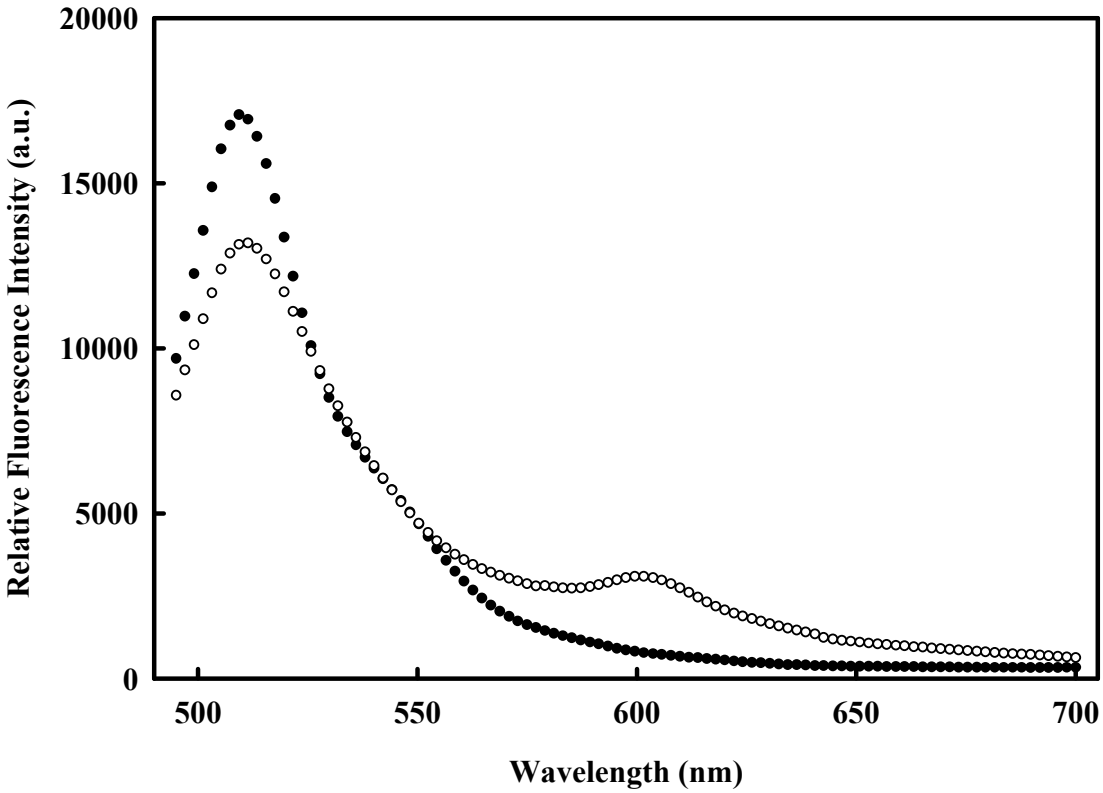

Figure 51. FRET of GST-EGFP-SNAP-25(1-140)-CCPGCC-SNAP-26(141-206) (P14). The spectral were recorded in 10 mM MOPS buffer (pH 7.4), 150 mM NaCl, 100 μM TCEP, 1 mM β-mercaptoethanol, and 1 mM EDTA at 25 ºC. The fluorescence spectra were obtained with excitation at 488 nm. The spectra corresponded to: (●) emission spectrum of 0.2 μM GST-EGFP-SNAP-25(1-140)-CCPGCC-SNAP-25(141-206) (**P14**); (○) emission spectrum of 0.2 μM GST-EGFP-SNAP-25(1-140)-CCPGCC(ReAsH)-SNAP-25(141-206) (**P14-ReAsH**). The fluorescence background of the buffer was subtracted in both cases.

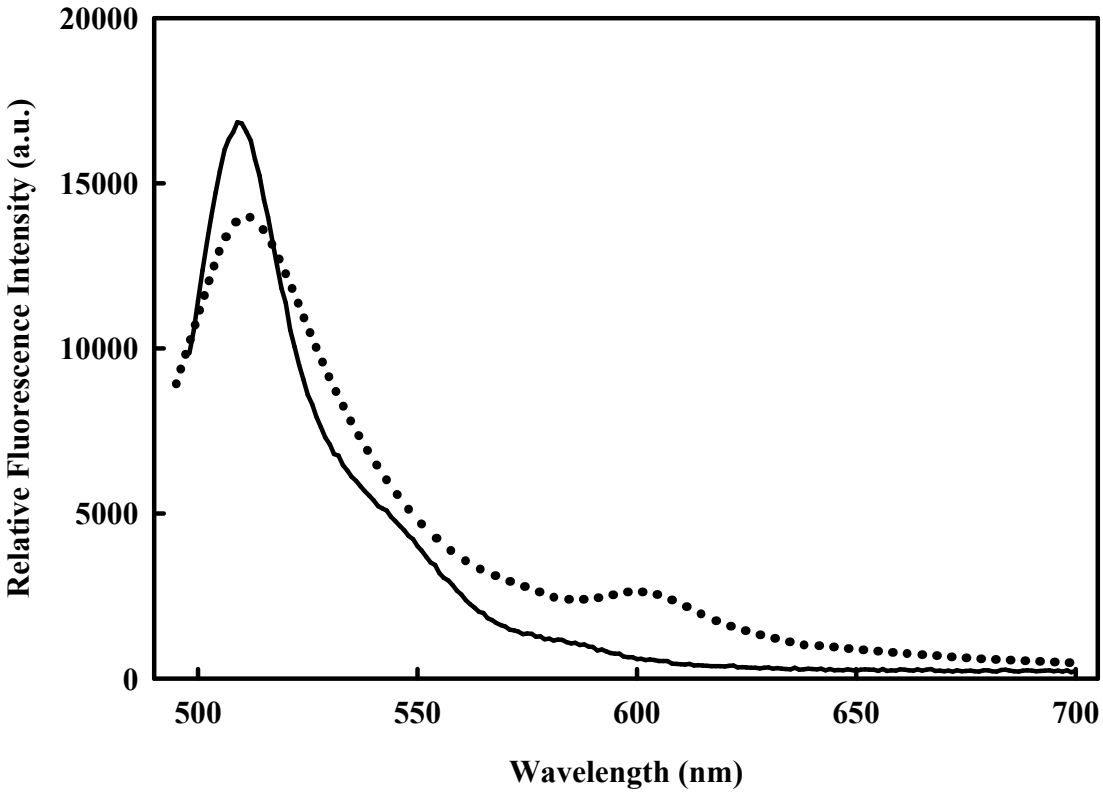

Figure 52. FRET of LC-bond GST-EGFP-SNAP-25(1-140)-CCPGCC-SNAP-25(141-206). The spectra were recorded in 10 mM MOPS buffer (pH 7.4), 150 mM NaCl, 100 μM TCEP, 1 mM β-mercaptoethanol and 1 mM EDTA at 25 ºC. The fluorescence spectra were obtained with excitation at 488 nm. The solid line corresponded to the emission spectrum of donor (EGFP) in the mixture of 0.2 μM GST-EGFP-SNAP-25(1-140)-CCPGCC-SNAP-25(141-206) (**P14**) and 0.2 μM Zn^{2+}-depleted BoNT/A LC; the dotted line corresponded to the emission spectrum of the mixture of 0.2 μM GST-EGFP-SNAP-25(1-140)-CCPGCC(ReAsH)-SNAP-25(141-206) (**P14-ReAsH**) and 0.2 μM Zn^{2+}-depeleted BoNT/A LC.

4.2.18 FRET and determination of apparent distance between the N-terminus and the D140 of the SNAP-25(A195S)

In order to determine the distance between the N-terminus and the D140 of the SNAP-25(A195S), CCPGCC was inserted between D140 and A141 of the SNAP-25 and EGFP was engineered at the N-terminus of the SNAP-25 by mutagenesis. The protein GST-EGFP-SNAP-25(1-140)-CCPGCC-SNAP-25(141-206, A195S) (**P15**) was used as FRET studies.

GST-EGFP-SNAP-25(1-140)-CCPGCC-SNAP-25(141-206, A195S) (**P15**) (0.2 μM) and GST-EGFP-SNAP-25(1-140)-CCPGCC(ReAsH)-SNAP-25(141-206, A195S)-EGFP (**P15-ReAsH**) (0.2 μM) were incubated in 10 mM MOPS buffer (pH 7.4), 150 mM NaCl, 100 μM TCEP, 1 mM β-mercaptoethanol, and 1 mM EDTA for 2 h at 25 ˚C. The fluorescence intensity was recorded from 495 nm to 700 nm with an excitation maximum wavelength at 488 nm. The results are shown in **Figure 53**. The obtained fluorescence energy transfer efficiency was (20.8 ± 1.5)%, which corresponded to the apparent distance between the N-terminus and the D140 of SNAP-25 which was 64.8 ± 0.9 Å.

Similarly, SNAP-25(A195S) in GST-EGFP-SNAP-25(1-140)-CCPGCC-SNAP-25(141-206, A195S) (**P15**) (0.2 μM) and GST-SNAP-25(1-140)-CCPGCC(ReAsH)-SNAP-25(141-206, A195S) (**P15-ReAsH**) (0.2 μM) bound to 0.2 μM active BoNT/A LC to form a stable complex. The results are shown in **Figure 54**. The obtained total energy transfer efficiency was (14.1 ± 1.4)%. The real energy transfer efficiency of the complex after normalization was (41.1 ± 1.4)%, which corresponded to the apparent distance between the N-terminus and the D140 of the SNAP-25 which was 55.0 ± 0.6 Å.

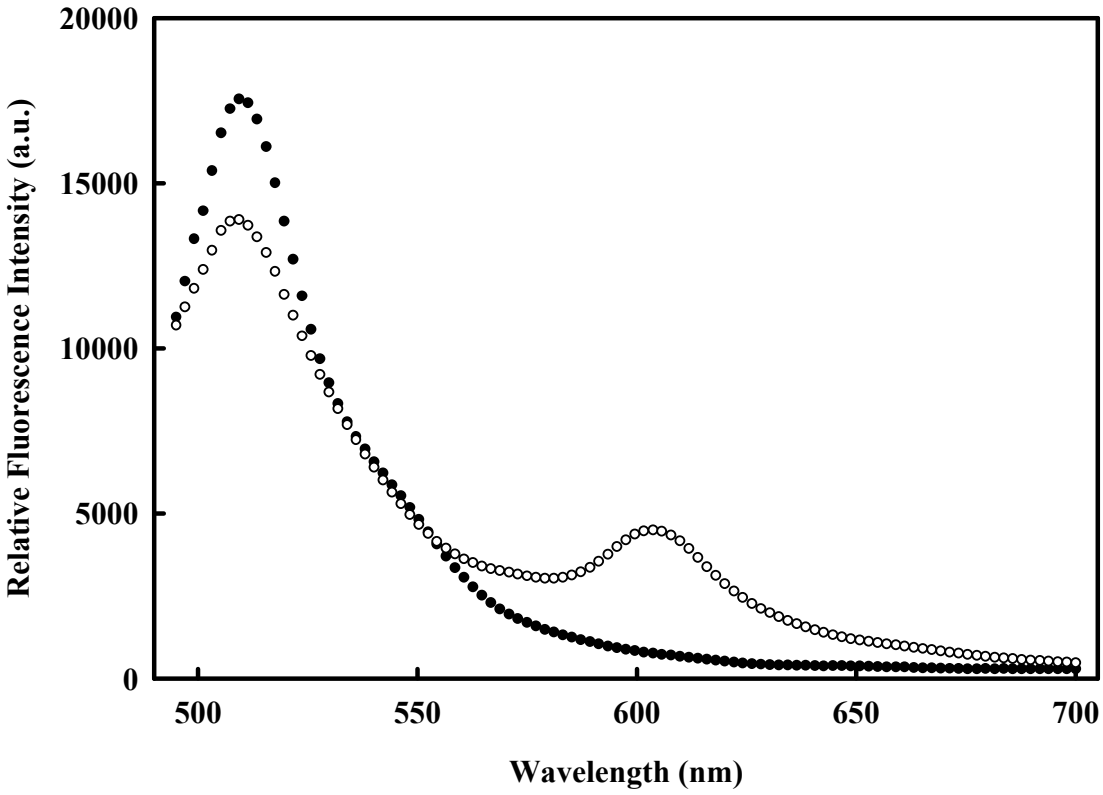

Figure 53. FRET of GST-EGFP-SNAP-25(1-140)-CCPGCC-SNAP-25(141-206, A195S) (P15). The spectra were recorded 10 mM MOPS buffer (pH 7.4), 150 mM NaCl, 100 μM TCEP, 1 mM β-mercaptoethanol, and 1 mM EDTA at 25 ºC. The fluorescence spectra were obtained with excitation at 488 nm. The spectra corresponded to: (●) emission spectrum of 0.2 μM GST-EGFP-SNAP-25(1-140)-CCPGCC-SNAP-25(141-206, A195S) (**P15**); (○) emission spectrum of 0.2 μM GST-EGFP-SNAP-25(1-140)-CCPGCC(ReAsH)-SNAP-25(141-206, A195S) (**P15-ReAsH**). The fluorescence background of the buffer was subtracted in both cases.

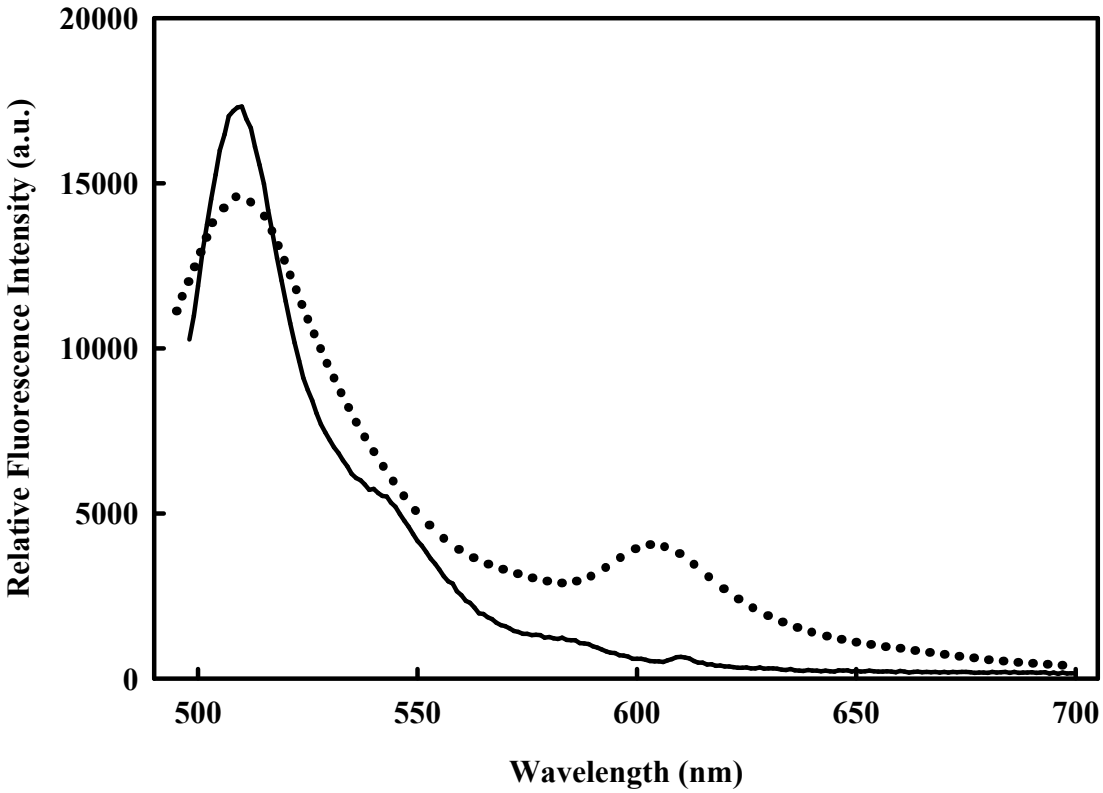

Figure 54. FRET of LC-bound GST-EGFP-SNAP-25(1-140)-CCPGCC-SNAP-25(141-206, A195S). The spectra were recorded in 10 mM MOPS buffer (pH 7.4), 150 mM NaCl, 100 μM TCEP 1 mM β-mercaptoethanol, and 1 mM EDTA at 25 ºC. The fluorescence spectra were obtained with excitation at 488 nm. The solid line corresponded to the emission spectrum of the mixture of 0.2 μM GST-EGFP-SNAP-25(1-140)-CCPGCC-SNAP-25(141-206, A195S) (**P15**) and 0.2 μM BoNT/A LC; the dotted line corresponded to the emission spectrum of the mixture of 0.2 μM GST-EGFP-SNAP-25(1-140)-CCPGCC(ReAsH)-SNAP-25(141-206, A195S) and 0.2 μM BoNT/A LC.

4.2.19 Summary of FRET and apparent distances of full length SNAP-25 in the absence and presence of BoNT/A LC

Based on the FRET, the energy transfer efficiency was obtained by the following **Equation 6**:

$$E = 1 - \frac{F_{DA}}{F_D} \qquad (6)$$

where, E represents the fluorescence energy transfer efficiency; F_{DA} represents the fluorescence intensity of EGFP in the CCPGCC with ReAsH; and F_D represents the fluorescence intensity of EGFP in the CCPGCC without ReAsH.

When BoNT/A LC (0.2 μM) and SNAP-25 (0.2 μM) were mixed, only 12.5% substrate formed SNAP-25-BoNT/A LC binary complex. 87.5% SNAP-25 and BoNT/A LC maintained in the mixture as free forms in the mixture based on the dissociation constant of SNAP-25 and BoNT/A LC (K_D = 1.2 μM) under this condition. Both SNAP-25 and SNAP-25-BoNT/A LC complex contributed to the fluorescence intensity.

The Förster resonance distance R_0 was obtained based on **Equation 4**. The spectral overlap of EGFP and ReAsH was obtained on **Equation 5**. The apparent distances between the probes were obtained by the **Equation 7**:

$$E = \frac{{R_0}^6}{{R_0}^6 + R^6} = 1 - \frac{F_{DA}}{F_D} \qquad (7)$$

The fluorescence energy transfer efficiencies and the apparent distances of double labeled SNAP-25 in the absence and presence of LC are summarized in **Table 4**.

Table 4. Summary of energy transfer efficiencies and apparent distances.

E indicates the fluorescence energy transfer efficiency; R represents the distance.

Data in parenthesis indicate the observed fluorescence energy transfer efficiency.

FRET		SNAP-25		SNAP-25(A195S)	
	LC	–	+	–	+
C → A	E(%)	49.9 ± 1.3	89.6 ± 1.4 (54.9)	30.3 ± 1.2	90.4 ± 1.3 (37.8)
	R(Å)	51.9 ± 0.6	36.2 ± 1.1	59.5 ± 0.6	35.7 ± 0.9
C → B	E(%)	53.7 ± 1.2	61.7 ± 1.5 (54.7)	53.1 ± 1.3	65.1 ± 1.5 (54.6)
	R(Å)	50.6 ± 0.4	47.9 ± 0.5	50.8 ± 0.5	46.7 ± 0.6
A → B	E(%)	22.9 ± 1.4	36.6 ± 1.5 (15.8)	20.8 ± 1.5	41.1 ± 1.4 (14.1)
	R(Å)	63.5 ± 0.9	56.8 ± 0.7	64.8 ± 0.9	55.0 ± 0.6

A: amino-terminus of SNAP-25

B: amino acid residue of D140 of SNAP-25

C: carboxyl-terminus of SNAP-25

4.2.20 Models of the tertiary structure of the SNAP-25

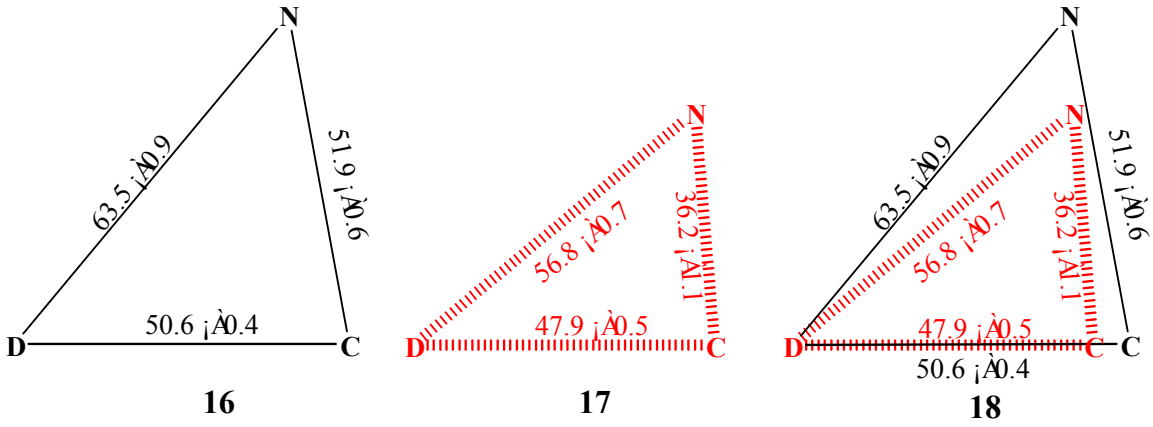

Figure 55. Models of the tertiary structure of SNAP-25 in the absence and presence of Zn^{2+}-depleted BoNT/A LC. The apparent distances were based on the fluorescence energy transfer efficiency. The solid lines represent the tertiary structure of the SNAP-25 (**16**) in the absence of BoNT/A LC, while the dashed lines represent the tertiary structure of the SNAP-25 (**17**) in the presence of Zn^{2+}-depleted BoNT/A LC. The superimposed structures of the SNAP-25 are shown in **18**.

In the presence of Zn^{2+}-depleted BoNT/A LC, the apparent distance between the N-terminus and the residue D140 and the C-terminal and the N-terminal domain (end to end) of SNAP-25 had a larger decrease from 63.5 to 56.8 Å and 51.9 to 36.2 Å, respectively. The apparent distance between the C-terminus and the D140 of the SNAP-25 had a smaller decrease from 50.6 to 47.9 Å. All the distance changes indicated that the conformation of SNAP-25 changed after binding to BoNT/A LC. The decreased distance indicated that the C-terminal residues may wrap around the BoNT/A LC, resulting in a shorter distance than that of unbound SNAP-25.

4.2.21 Models of the tertiary structure of the mutant SNAP-25(A195S)

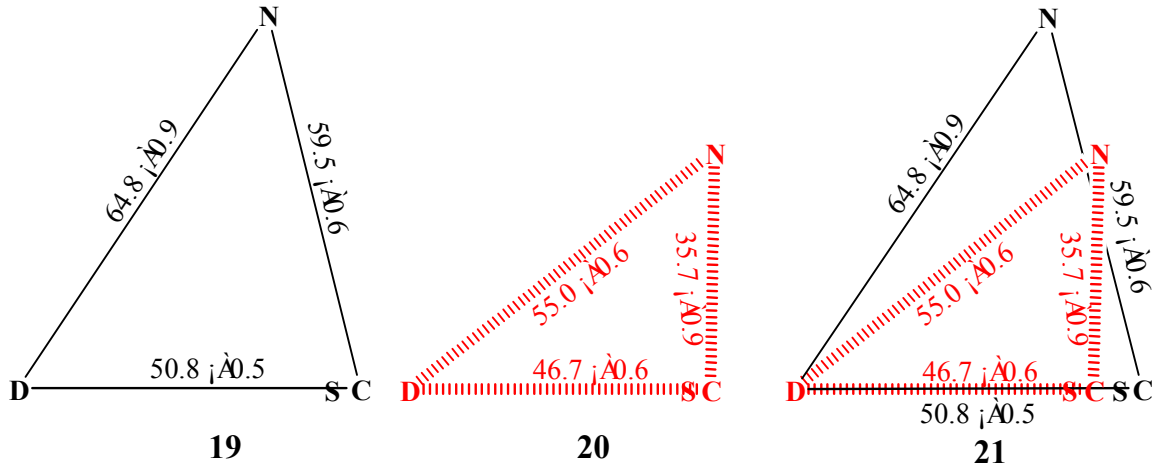

Figure 56. Models of the tertiary structure of the mutant SNAP-25(A195S) in the absence and presence of BoNT/A LC. The apparent distances were based on the fluorescence energy transfer efficiency. The solid lines represent the tertiary structure of the SNAP-25(A195S) (**19**) in the absence of BoNT/A LC, while the dashed lines represent the tertiary structure of the SNAP-25(A195S) (**20**) in the presence of active BoNT/A LC. The superimposed structures of the SNAP-25(A195S) are shown in **21**.

In the presence of BoNT/A LC, the apparent distance between the N-terminus and the D140 of the SNAP-25(A195S) decreased from 64.8 to 55.0 Å; the apparent distance between the C-terminus and the N-terminus of SNAP-25(A195S) sharply decreased from 59.5 to 35.7 Å; and the apparent distance between the C-terminus and the D140 decreased from 50.8 to 46.7 Å. All the distance changes indicated that the conformation of SNAP-25(A195S) changed after binding to active BoNT/A LC.

4.2.22 Time course of BoNT/A LC binding to GST-CCPGCC-SNAP-25-EGFP in the absence and presence of ReAsH

The co-crystal structure of the SNAP-25(141-204)-BoNT/A LC(E224Q, Y366F) complex (PDB: 1XTG) (25) shows that SNAP-25 wraps around the protease. The time course of the binding of SNAP-25 to LC was monitored in the absence and presence of ReAsH. The results are shown in **Figure 57**.

The GST-CCPGCC(ReAsH)-SNAP-25-EGFP (**P9-ReAsH**) had lower fluorescence intensity than that of GST-CCPGCC-SNAP-25-EGFP (**P9**) under the same conditions. The results suggested that the fluorescence energy transfer occurred between EGFP and ReASH in GST-CCPGCC(ReAsH)-SNAP-25-EGFP (**P9-ReAsH**). The fluorescence energy transfer efficiency was 50% since the fluorescence intensity of **P9-ReAsH** was only half of the intensity of **P9** at the same concentration.

The fluorescence intensity of both **P9** and **P9-ReAsH** decreased due to the binding of SNAP-25 to BoNT/A LC. The second order binding rates of **P9** and **P9-ReAsH** with BoNT/A LC were found to be 2408 and 2375 $M^{-1}\cdot s^{-1}$ (**Figure 57**), respectively. These results were similar with SNAP-25 and active BoNT/A LC binding rate constant (1875 $M^{-1}\cdot s^{-1}$) (**Figure 42**). The results indicate that CCPGCC-ReAsH doesn't affect the binding between the SNAP-25 and BoNT/A LC.

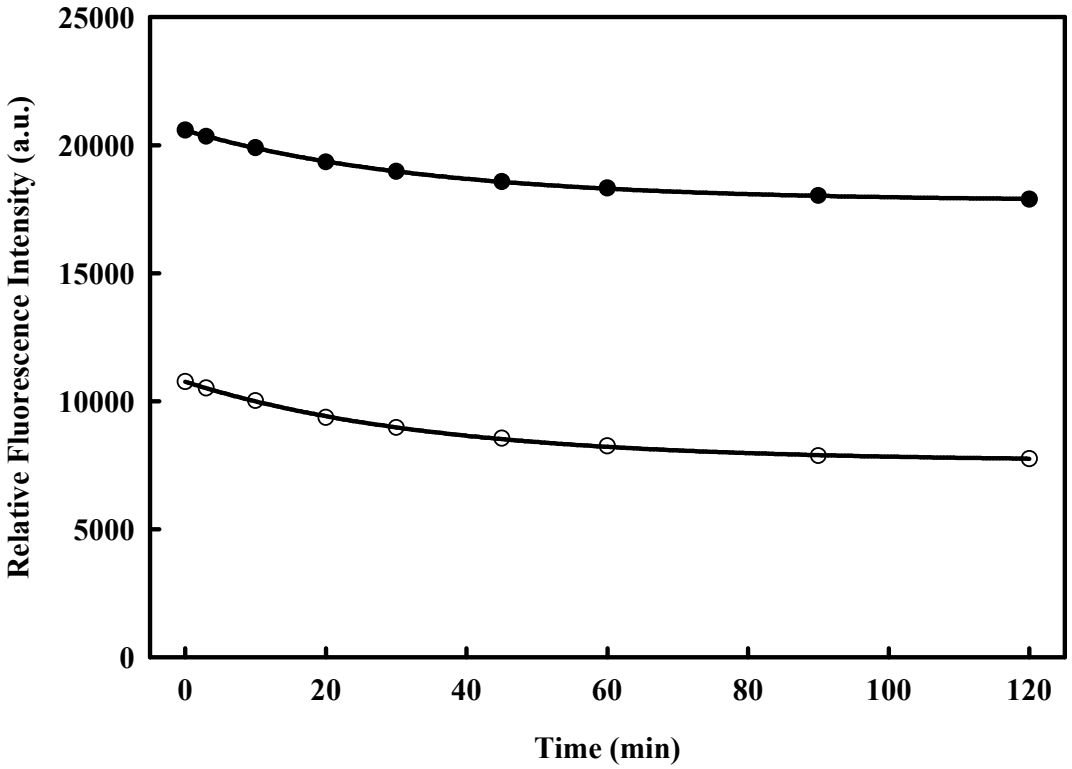

Figure 57. Time courses of BoNT/A LC binding to GST-CCPGCC-SNAP-25-EGFP in the absence and presence of ReAsH. To the protein samples containing GST-CCPGCC-SNAP-25-EGFP (**P9**) (0.2 μM) and GST-CCPGCC(ReAsH)-SNAP-25-EGFP (**P9-ReAsH**) (0.2 μM), Zn^{2+}-depleted BoNT/A LC (2.0 μM) was added phosphate buffer containing 20 mM potassium phosphate, pH 7.4, 100 mM NaCl, 0.3 mM TCEP, and 1 mM β–mercaptoethanol and 1 mM EDTA. The fluorescence spectra were obtained with excitation at 488 nm. The spectra corresponded to: (●) GST-CCPGCC-SNAP-25-EGFP (**P9**); (○) GST-CCPGCC(ReAsH)-SNAP-25-EGFP (**P9-ReAsH**).

4.2.23 Time course of BoNT/A LC binding to GST-SNAP-25(1-140)-CCPGCC(ReAsH)-SNAP-25(141-206)-EGFP and GST-EGFP-SNAP-25(1-140)-CCPGCC-SNAP-25(141-206)

In order to measure the effect of CCPGCC-ReAsH during SNAP-25 binding to BoNT/A LC, CCPGCC was genetically engineered between D140 and A141 of the SNAP-25 by mutagenesis. The protein GST-SNAP-25(1-140)-CCPGCC-SNAP-25(141-206) (**P11-ReAsH**) and GST-EGFP-SNAP-25(1-140)-CCPGCC-SNAP-25(141-206, A195S) (**P15-ReAsH**) were used as binding studies. The results are shown in **Figure 58**.

The obtained binding rate constants for the **P11-ReAsH** and the **P14-ReAsH** were 2398 and 2342 $M^{-1}\cdot s^{-1}$, respectively. The similar rate constants suggested that the EGFP didn't affect GST-SNAP-25(1-140)-CCPGCC-SNAP-25(141-206)-EGFP (**P11**) and GST-EGFP-SNAP-25(1-140)-CCPGCC-SNAP-25(141-206) (**P14**) binding to BoNT/A LC. While the conformation changed after the complex formation of the CCPGCC-ReAsH modified SNAP-25 and BoNT/ LC, the binding modes of SNAP-25 and LC were not affected by introducing CCPGCC between the D140 and A141 of the SNAP-25.

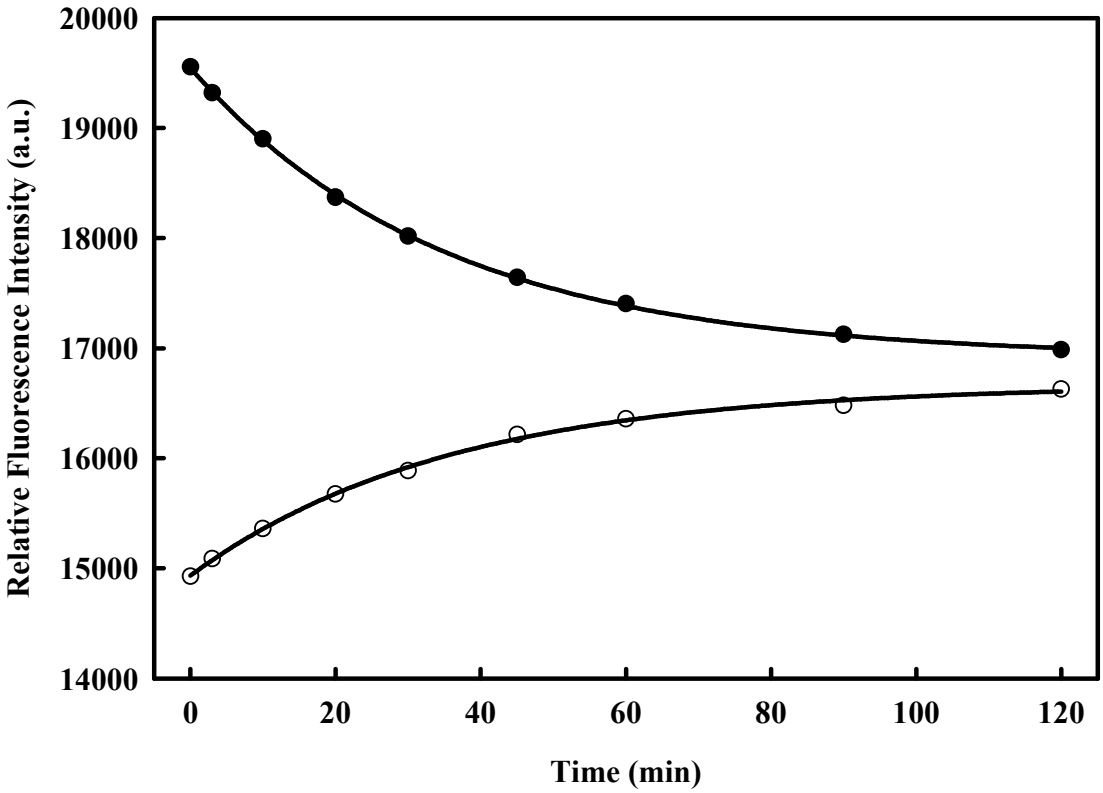

Figure 58. Time course of BoNT/A LC binding to P11-ReAsH and P14-ReAsH. To the samples containing GST-SNAP-25(1-140)-CCPGCC(ReAsH)-SNAP-25(141-206)-EGFP (**P11-ReAsH**) and GST-EGFP-SNAP-25(1-140)-CCPGCC(ReAsH)-SNAP-25(141-206) (**P14-ReAsH**), BoNT/A LC was added Zn^{2+}-depleted in phosphate buffer containing 20 mM potassium phosphate, pH 7.4, 100 mM NaCl, 0.3 mM TCEP, 1 mM β–mercaptoethanol, and 1 mM EDTA. The fluorescence spectra were obtained with excitation at 488 nm. The time courses corresponded to: (●) GST-SNAP-25(1-140)-CCPGCC(ReAsH)-SNAP-25(141-206)-EGFP (**P11-ReAsH**); (○) GST-EGFP-SNAP-25(1-140)-CCPGCC(ReAsH)-SNAP-25(141-206) (**P14-ReAsH**).

4.3 Discussion

The conformation of the intrinsically disordered protein SNAP-25 is of considerable importance to elucidating the mechanism of SNARE formation. Once SNAP-25 is cleaved by botulinum neurotoxin A, the helical bundle cannot be formed, resulting in membrane fusion failure. Although the co-crystal structure of the C-terminus of SNAP-25(141-204) with the BoNT/A LC(E224Q, Y366F) (25) is known, the high resolution structures of SNAP-25 or in the complex with BoNT/A LC are not yet available. Determining the distances between specific points on SNAP-25 can provide insights of the overall structural conformation of SNAP-25 after binding to BoNT/A LC. We used FRET to gain information of overall conformational changes of SNAP-25 and SNAP-25(A195S) in the absence and presence of BoNT/A LC.

FRET can be used as a molecular ruler to measure the distances between two fluorophores if each location can be specifically labeled with a donor and an acceptor. We chose two fluorescence probes, EGFP and CCPGCC-ReAsH, in the fusion protein with SNAP-25. While EGFP can be used as a donor probe, the arsenical ReAsH compound binds to a tetracysteine motif (CCPGCC) that can be introduced into specific sites within SNAP-25, providing an acceptor fluorescent probe.

The fluorescence energy transfer occurs between EGFP and ReAsH at a limited distance. Based on the fluorescence energy transfer efficiency, an apparent distance can be obtained. The Förster distance R_0 for the EGFP/ReAsH pair is 51.8 Å, making it appropriate for many structural studies in proteins. EGPF is itself a fluorescent protein, while CCPGCC is a non-fluorescent probe that develops much higher fluorescence intensity when covalently bound to ReAsH.

We engineered SNAP-25 with double labeled probes containing a CCPGCC motif either at the N-terminus or between D140 and A141, and EGFP either at the N-terminus or the C-terminus. This labeling strategy allowed us to monitor the conformational changes of SNAP-25 using FRET. We demonstrated that the clearly fluorescent quenching of the donor (EGFP) is accompanied by an increase in the acceptor (ReAsH).

Botulinum neurotoxin serotype A light chain (BoNT/A LC) is a zinc-dependent metalloprotease that can specifically cleave SNAP-25 between Q197 and R198. In order to determine the conformational changes of SNAP-25 upon binding with BoNT/A LC, we used Zn^{2+}-depleted BoNT/A LC to prevent the cleavage of SNAP-25. The distances were determined in the absence and presence of Zn^{2+}-depleted BoNT/A LC. Barbieri (28) reported that SNAP-25(A195S) can tightly bind to BoNT/A LC with a 6000-fold slower cleavage. Therefore, we used the A195S mutated SNAP-25 in the absence and presence of active BoNT/A LC to probe the conformational changes of SNAP-25(A195S) using FRET.

The apparent distances between the C-terminus and the N-terminus of SNAP-25 in GST-CCPGCC-SNAP-25-EGFP (**P9**) were found to be 51.9 ± 0.6 and 36.2 ± 1.1 Å in the absence and presence of Zn^{2+}-depleted BoNT/A LC, respectively. The distance between the C-terminus and the N-terminus of SNAP-25 lessens in the binary complex. The decreased distance is consistent with SNAP-25 wrapping around the BoNT/A LC. For the full-length unstructured SNAP-25, these results are the average distances in various orientations. BoNT/A LC may promote the folding of SNAP-25 during the binding process, resulting in a fully or partially structured SNAP-25. In order to rule out the effects of Zn^{2+}-depleted BoNT/A LC, we genetically engineered SNAP-25(A195S)

by mutagenesis. The apparent distances between the C-terminus and the N-terminus of SNAP-25(A195S) in GST-CCPGCC-SNAP-25(A195S)-EGFP (**P10**) were found to be 59.5 ± 0.6 and 35.7 ± 0.9 Å in the absence and presence of active BoNT/A LC, respectively. The decreased apparent distance provides more evidence that the full length SNAP-25 wraps tighter around the BoNT/A LC, thus resulting in a more structured or partially structured conformation.

The apparent distance, determined using FRET, between the C-terminus and the N-terminus (end to end) of SNAP-25 indicates that the conformation of SNAP-25 and the folding process of the full-length SNAP-25 differ. In order to determine the validity of the FRET, we genetically engineered SNAP-25 to contain a CCPGCC motif between D140 and A141 by mutagenesis in order to compare the apparent distance of SNAP-25 with that of the co-crystal structure of SNAP-25(141-204) with BoNT/A LC(E224Q, Y366F) (25). For the co-crystal structure of the complex, the distance between A141 and G204 is 40.2 Å. The apparent distances between the C-terminus and D140 of SNAP-25 in GST-SNAP-25(1-140)-CCPGCC-SNAP-25(141-206)-EGFP (**P11**) were determined to be 50.6 ± 0.4 and 47.9 ± 0.5 Å in the absence and presence of Zn^{2+}-depleted BoNT/A LC, respectively. The experimental results are slightly greater (47.9 Å) than for the co-crystal structure (40.2 Å) (25). The small difference may be due to the size contribution of EGFP and ReAsH-CCPGCC between the C-terminus and D140, both free and in the complex. The results demonstrate that the C-terminus of SNAP-25 binding to BoNT/A LC does not affect the conformation of the full-length SNAP-25. The apparent distances between the C-terminus and D140 of SNAP-25(A195S) in GST-SNAP-25(1-140)-CCPGCC-SNAP-25(141-206, A195S)-EGFP (**P12**) are determined to be 50.8 ± 0.5 and 46.7 ± 0.6 Å in the

absence and presence of active BoNT/A LC, respectively. The results suggest that SNAP-25(A195S) maintains a conformation similar to the wild-type SNAP-25.

The apparent distances between the N-terminal domain and D140 of SNAP-25 in GST-EGFP-SNAP-25(1-140)-CCPGCC-SNAP-25(141-206) (**P14**) were determined to be 63.5 ± 0.9 and 56.8 ± 0.7 Å in the absence and presence of Zn^{2+}-depleted BoNT/A LC, respectively. The apparent distance decreases after binding to BoNT/A LC, which suggests that the interactions between the N-terminus of SNAP-25 and BoNT/A LC adopt a different binding mode. When EGFP is located on the N-terminus of SNAP-25, the interaction effects between SNAP-25 and BoNT/A LC are weak, and the N-terminal domain of SNAP-25 may not affect the total conformation of the complex, thus resulting in only a small change of apparent distance. Similarly, the apparent distances between the N-terminal domain and D140 of SNAP-25(A195S) in GST-EGFP-SNAP-25(1-140)-CCPGCC-SNAP-25(141-206, A195S) (**P15**) were found to be 64.8 ± 0.9 and 55.0 ± 0.6 Å in the absence and presence of active BoNT/A LC, respectively. The results are consistent with those for GST-EGFP-SNAP-25(1-140)-CCPGCC-SNAP-25(141-206) (**P14**).

We kept the apparent distance of the C-terminus and D140 of SNAP-25 fixed and superimposed the other two distances. It is clear that the N-terminus of SNAP-25 and SNAP-25(A195S) has a larger change in apparent distance than the other locations on SNAP-25 (**18**) and SNAP-25(A195S) (**21**).

We investigated the time course of the fluorescence energy transfer between EGFP and ReAsH during SNAP-25 binding to BoNT/A LC. The lower donor fluorescence intensity of GST-CCPGCC(ReAsH)-SNAP-25-EGFP (**P9-ReAsH**) than that

of GST-CCPGCC-SNAP-25-EGFP (**P9**) is consistent with FRET. The fluorescence intensity of GST-CCPGCC(ReAsH)-SNAP-25-EGFP (**P9-ReAsH**) gradually decreases when binding to BoNT/A LC, which suggests that CCPGCC at the N-terminus of SNAP-25 and ReAsH do not affect the binding between SNAP-25 and LC. The binding rates determined for **P9** and **P9-ReAsH** with BoNT/A LC were 2408 and 2375 $M^{-1}\cdot s^{-1}$ (**Figure 57**), respectively. These results are similar to the SNAP-25 binding constant (1875 $M^{-1}\cdot s^{-1}$) with active BoNT/A LC (**Figure 42**). However, when CCPGCC exists within SNAP-25, interactions between SNAP-25 and LC may be different. Similarly, GST-SNAP-25(1-140)-CCPGCC-SNAP-25(141-206)-EGFP (**P11**) and GST-EGFP-SNAP-25(1-140)-CCPGCC-SNAP-25(141-206) (**P11**) revealed similar binding constants with BoNT/A LC. The results provide evidence that CCPGCC in the middle of SNAP-25 does not affect the binding mode between SNAP-25 and LC.

SNAP-25 binds to VAMP and syntaxin in the SNARE complex. In addition, SNAP-25 interacts with synaptotagmin, munc18, α-SNAP, and phospholipids during membrane fusion. Furthermore, SNAP-25 can be modified by acetylation, palmitoylation, and phosphorylation. These interactions may involve conformational changes of SNAP-25. The fluorescent derivatives of SNAP-25 synthesized in the present studies can be directly applied to SNAP-25 interacting proteins.

Chapter 5. Secondary structure of SNAP-25

5.1 Introduction

The highly conserved protein SNAP-25 is part of the SNARE complex. Previous work has demonstrated that SNAP-25 binds to syntaxin and synaptobrevin to form a stable four-helix bundle. The three proteins contain a considerable amount of α-helical components upon intertwining together. However, prior to the formation of the helical bundle, SNAP-25 is likely to be an intrinsically disordered protein (**Appendix A8**). The folding process of SNAP-25 has not yet been clarified.

We use circular dichroism (CD) spectroscopy to study the secondary structures of SNAP-25 and its N-terminus and C-terminus in the absence and presence of BoNT/A LC. Familiarity with these structures can help us fully understand the folding process during binding to other intrinsically disordered proteins.

.

5.2 Results

5.2.1 Construct of pGEX-SNAP-25, pGEX-SNAP-25(1-140) and pGEX-SNAP-25(141-206)

In order to determine the secondary structures of the SNAP-25, the plasmids expression SNAP-25(1-140), SNAP-25(141-206), and the full length SNAP-25(1-206) were constructed. After the expression and purification, the GST-tag was removed by PreScission™ protease from the corresponding GST fusion proteins. The schematic representation of SNAP-25 and its fragments are shown in **Figure 59**. The secondary structures of the N-terminus, the C-terminus, and the full-length of the SNAP-25 were determined by circular dichroism.

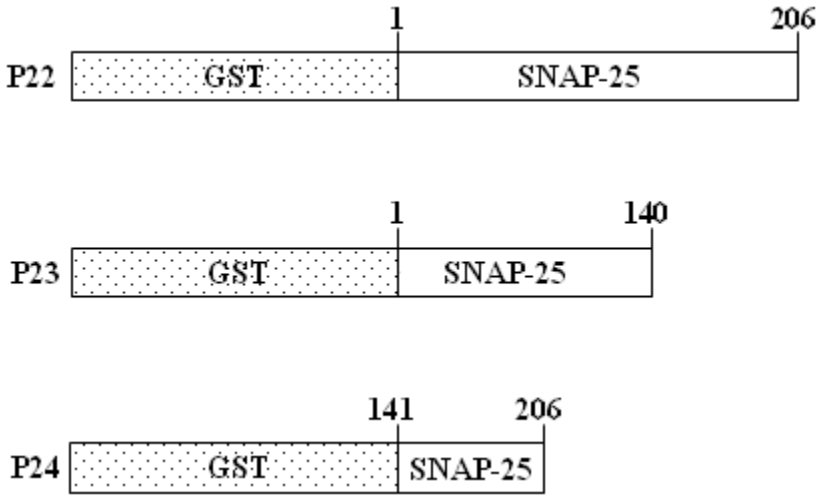

Figure 59. Schematic representation of the SNAP-25 with GST-tag. The numbers on the bar indicate the residue of SNAP-25. The GST can be removed by PreScission™ protease.

SNAP-25 cDNA was inserted into pGEX-6P-3 vector (**6**) (Amersham Biosciences) by using BamHI/NotI digestion, resulting in the pGEX-SNAP-25 (**22**) construct.

PCR for amplification of SNAP-25 was performed by using a 30 nucleotide forward primer (5'-CTGGGATCCATGGCCGAGGACGCAGACATG-3') and a 39 nucleotide reverse primer (5'-GTC*GCGGCCGC*TTTAACCACTTCCCAGCATCTTTG TTGC-3'). The underlined residues indicate the 5' BamHI site and the 3' NotI site, respectively. The plasmid pGEX-SNAP-25 (**22**) was obtained after the ligation. A 6-nucleotide linker GGATCC was introduced between the GST and the SNAP-25, which was expressed as Gly-Ser.

SNAP-25(1-140) cDNA was inserted into pGEX-6P-3 vector (**6**) (Amersham Biosciences) by using double restriction digestion of BamHI/NotI, resulting in the pGEX-

SNAP-25(1-140) (**23**). PCR for amplification of SNAP-25(141-206) was performed by using a 30 nucleotide forward primer (5'-CTGGGATCCATGGCCGAGGACGCAGACATG-3') and a 42 nucleotide reverse primer (5'-GTC*GCGGCCGC*TTTAATCATTTGTTACCCTGCGGATGAAGCC-3'). The underlined residues indicate the start codon and D140, respectively. The plasmid pGEX-SNAP-25(1-140) (**23**) was obtained after the ligation.

SNAP-25(141-206) cDNA (Clontech) was inserted into pGEX-6P-3 vector (**6**) (Amersham Biosciences) by using double restriction digestion of BamHI/NotI, resulting in the pGEX-SNAP-25(141-206) (**24**). PCR for amplification of SNAP-25(1-140) was performed by using a 30 nucleotide forward primer (5'-CTGGGATCCGCCCGGGAAAATGAGATGG-3') and a 39 nucleotide reverse primer (5'-GTC*GCGGCCGC*TTTAACCACTTCCCAGCATCTTTGTTGC-3'). The underlined residues indicate the A141 and the stop codon, respectively. The plasmid pGEX-SNAP-25(141-206) (**24**) was obtained after the ligation. All the final constructs were confirmed by DNA sequencing.

5.2.2 Expression of GST-SNAP-25, GST-SNAP-25(1-140) and GST-SNAP-25(141-206)

The plasmids (**22**, **23,** and **24**) were used to transform *E. coli* BL21(DE3)LysS. Cells were grown in LB broth containing 100 μg/ml ampicillin overnight at 37 ºC with shaking. The overnight culture was diluted 1:100 with LB broth containing 100 μg/ml ampicillin and incubated at 37 ºC until OD_{600nm} reached 0.6. The cells were subsequently induced with 1 mM IPTG and incubated at 37 ºC for an additional 4 h.

GST-fusion proteins were purified by affinity chromatography on glutathione-sepharose beads in the wash buffer (10 mM Phosphate, 150 mM NaCl, 1 mM EDTA, 1 mM DTT, 0.5% Triton X-100, pH 7.4). Proteins were eluted in the elution buffer with 10 mM reduced glutathione. The purified proteins were dialyzed against 1× PBS containing 10% polyethylene glycol (Sigma) and stored in 4 ˚C for cleavage.

The purified proteins were analyzed by SDS-PAGE. The results are shown in **Figure 61**.

The molecular weights of GST-SNAP-25, GST-SNAP-25(1-140), and GST-SNAP-25(141-206) were 51, 43, and 35 kD, respectively. The GST-tag is removed from the proteins in the following experiments.

5.2.3 Removal of GST from GST fusion proteins by PreScission

PreScission™ protease is a genetically engineered GST-tag fusion protein consisting of human rhinovirus 3C protease, which was specifically designed to facilitate removal of the protease by allowing simultaneous protease immobilization and cleavage of GST fusion proteins produced from the pGEX-SNAP-25. PreScission™ protease specifically cleaves between the Gln and Gly of the recognition sequence of Leu-Glu-Val-Leu-Phe-Gln-Gly-Pro, which is followed by the N-terminus of the SNAP-25.

The mixture of GST-SNAP-25 (**P22**) (400 μg in 200 μl) and PreScission™ protease (20 μl, 40 units) in cleavage buffer (10 mM Phosphate, pH 7.4, 150 mM NaCl, 1 mM EDTA, 1 mM DTT, 0.5% Triton X-100) was incubated at 4 ˚C for 16 h. The digested sample was loaded onto a column of glutathione agarose in wash buffer (10 mM phosphate, pH 7.4, 150 mM NaCl, 1 mM EDTA, 1 mM DTT, 0.5% Triton X-100) to remove the GST portion of the fusion protein and PreScission™ protease from the mixture. SNAP-25 in the flow through was collected and dialyzed against 1× PBS containing 10% polyethylene glycol (Sigma) for 3 h. The process of cleavage and purification of GST fusion proteins is summarized in **Figure 60**.

Using the same cleavage and purification method, SNAP-25(1-140) (**P23**) and SNAP-25(141-206) (**P24**) were obtained for the further secondary structure tests by circular dichroism. The proteins before and after the cleavage of GST were analyzed by SDS-PAGE. The results are shown in **Figure 61**.

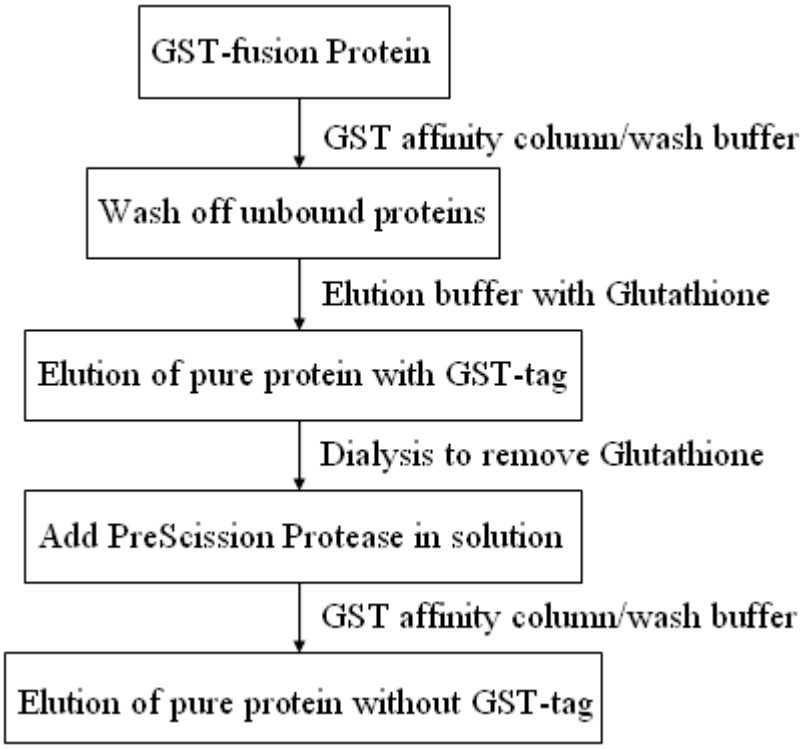

Figure 60. **Scheme of the operation of SNAP-25, SNAP-25(1-140), and SNAP-25(141-206).**

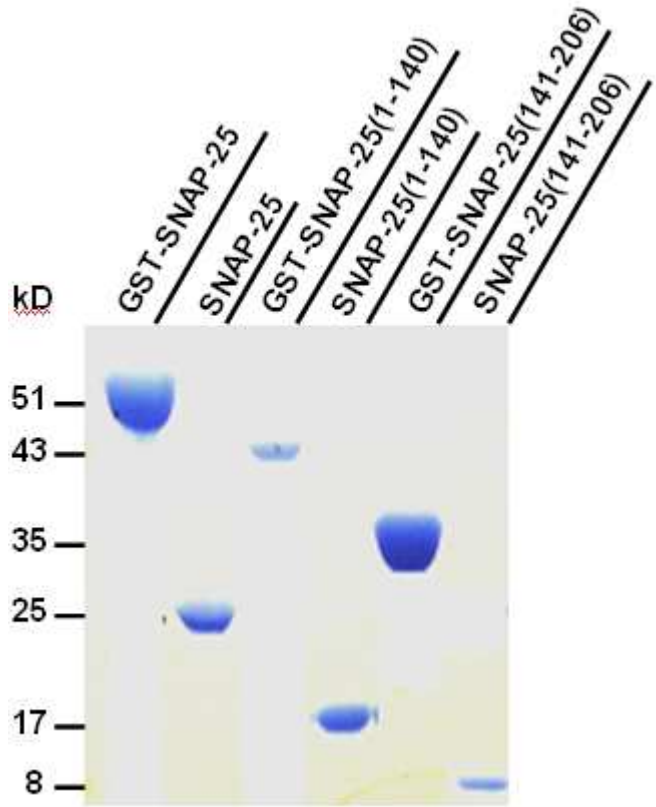

Figure 61. GST fusion proteins cleavage by PreScission™ protease.

The purified GST-SNAP-25 (**P22**), GST-SNAP-25(1-140) (**P23**), GST-SNAP-25(141-206) (**P24**), and corresponding GST- cleaved proteins (10 µl) were individually mixed with 20 µl Laemmli sample buffer (Bio-Rad) and denatured at 94 ˚C for 5 min and subjected to SDS-PAGE.

The results demonstrated that the GST-tag was removed by PreScission™ protease. The molecular weights of GST-SNAP-25, GST-SNAP-25(1-140), and GST-SNAP-25(141-206) were 51, 43, and 35 kD, respectively. After the GST-tag removed, the molecular weights of SNAP-25, SNAP-25(1-140), and SNAP-25(141-206) were 25, 17, and 8 kD, respectively.

5.2.4 CD spectra of SNAP-25(1-140), SNAP-25(141-206), and SNAP-25(1-206)

The proteins SNAP-25(1-140), SNAP-25(141-206), and SNAP-25(1-206) were incubated in the buffer containing 100 mM MOPS buffer (pH 7.2), 150 mM NaCl, and 100 μM TCEP, 1mM β-mercaptoethanol, and 1 mM EDTA. The ellipticities were recorded in millidegree. The results are shown in **Figure 62**.

The ellipticity can be converted into a mean residue ellipticity according to the following **Equation 8**:

$$[\theta] = \frac{100 \times \theta}{\text{number of amino acid} \times C \times l} (\text{deg} \cdot cm^2 \cdot dmol^{-1}) \qquad (8)$$

where, θ is observed ellipticity in degree; C is the molar concentration of protein in mol · L^{-1}; and l is the path length in cm.

The mean residue ellipticities based on the observed ellipticities of SNAP-25 and its fragments are shown in **Figure 63**. The results demonstrated that the full length SNAP-25, the N-terminus, and the C-terminus of the SNAP-25 (**P22R**) are intrinsically disordered proteins. SNAP-25(1-140) (**P23R**) had more α-helical components than that of SNAP-25(141-206) (**P24R**).

The fractional α-helical contents for the full length, the N-terminal and the C-terminal domain of SNAP-25, and their corresponding complex with BoNT/A LC were calculated by **Equation 9** using the assumption that for 100% α-helix the mean residue ellipticity, [θ], at 222 nm (20).

$$[\theta]_{222} = \frac{-36300}{\left(1 - \frac{2.57}{x}\right)} (\text{deg} \cdot cm^2 \cdot dmol^{-1}) \qquad (9)$$

where, x is the number of amino acids in the individual proteins.

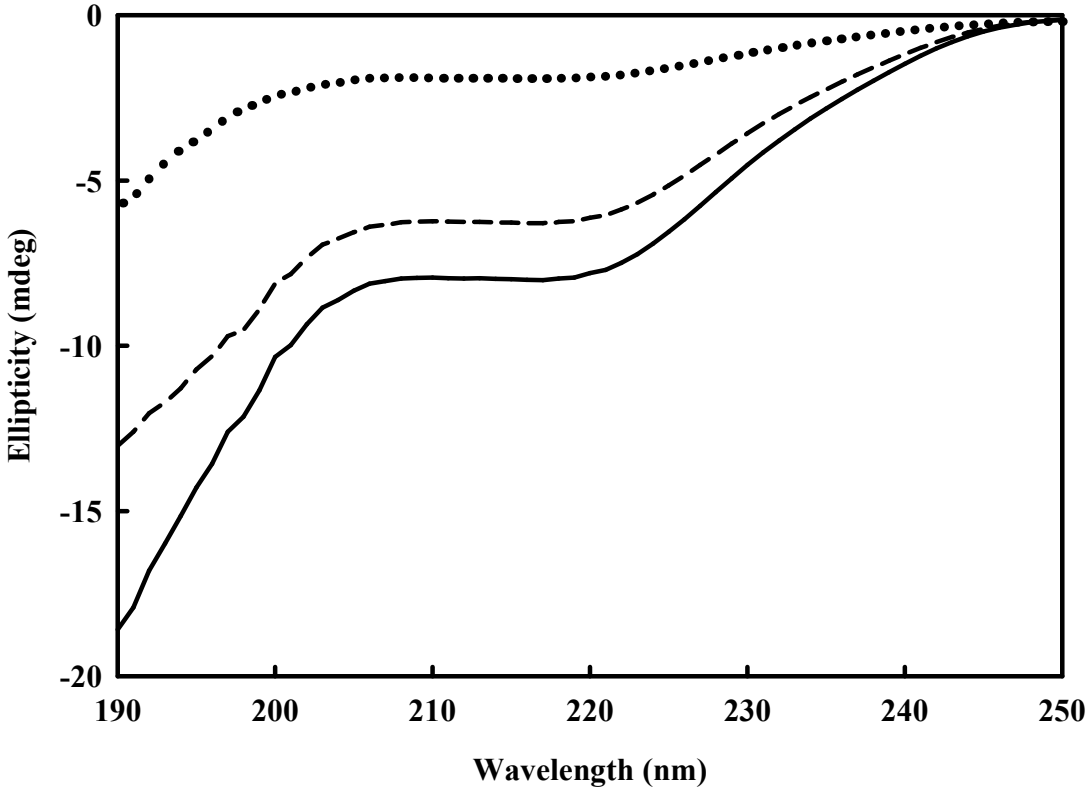

Figure 62. The ellipticities of SNAP-25(1-140) (P22R), SNAP-25(141-206) (P23R), and SNAP-25(1-206) (P24R) at 25 ˚C. The spectra corresponded to the C-terminal fragment of SNAP-25(141-206) (dotted line), the N-terminal fragment of SNAP-25(1-140) (dashed line), and the full length SNAP-25(1-206) (solid line). The concentrations for all proteins are 5.0 μM. The buffer background was subtracted in all cases.

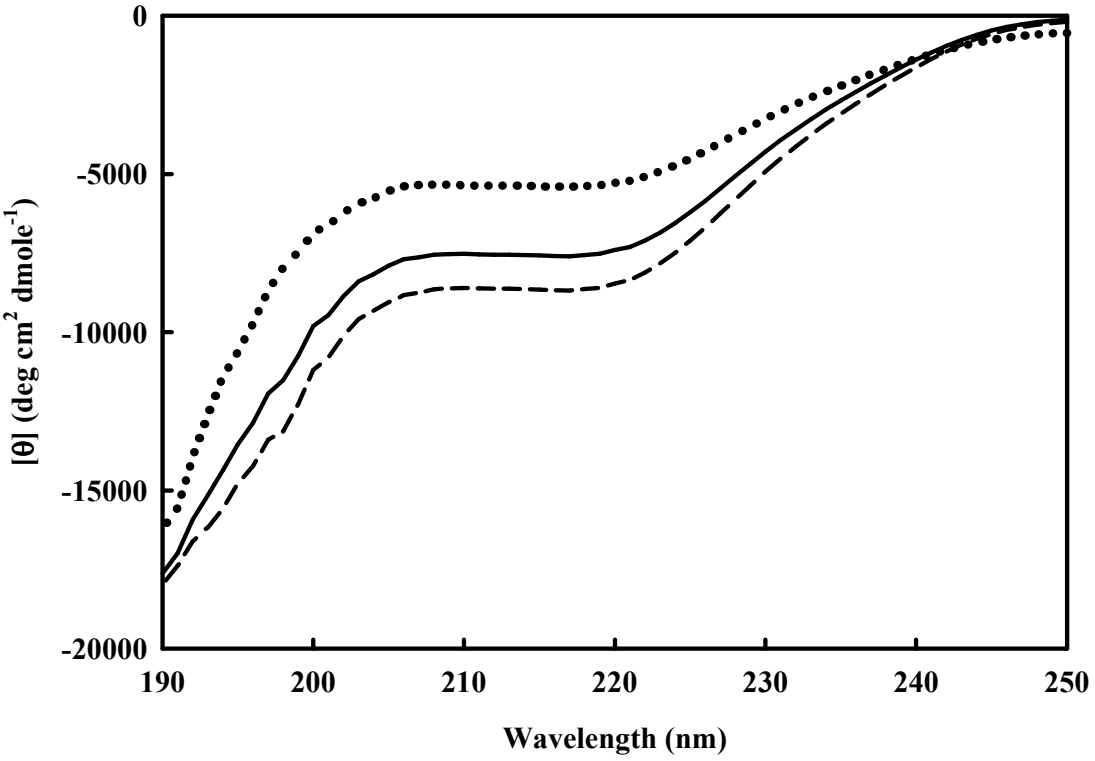

Figure 63. The mean residue ellipticity of SNAP-25(1-140), SNAP-25(141-206) and SNAP-25(1-206). The spectra corresponded to the C-terminal fragment of SNAP-25(141-206) (dotted line), the N-terminal fragment of SNAP-25(1-140) (dashed line), and the full length SNAP-25(1-206) (solid line). The concentrations for all proteins were 5.0 μM. The buffer background was subtracted in all cases. The α-helical contents from $[\theta]_{222}$ using **Equation 9** were found to be 14.5, 22.8, and 22.6% for SNAP-25(141-206), SNAP-25(1-140), and SNAP-25(1-206), respectively.

5.2.5 CD spectrum of the binary complex of SNAP-25 and LC

Full length SNAP-25 (5.0 μM) and BoNT/A LC (5.0 μM) were incubated at 4 °C overnight in buffer containing 100 mM MOPS buffer (pH 7.2), 150 mM NaCl, and 100 μM TCEP, 1mM β-mercaptoethanol, and 1 mM EDTA. The CD spectrum of the SNAP-25-BoNT/A LC complex was recorded in the same buffer at 25 ˚C. The theoretical mean residue ellipticity (20) of the mixture was obtained from the CD spectra of SNAP-25 and BoNT/A LC using the **Equation 10**:

$$[\theta]_{sum} = \frac{C_1 n_1 [\theta]_1 + C_2 n_2 [\theta]_2}{C_1 n_1 + C_2 n_2} \qquad (10)$$

where C_1 and C_2 are the respective molarity concentrations of SNAP-25 and BoNT/A LC; n_1 and n_2 are the numbers of amino acid residue of SNAP-25 and BoNT/A LC; and $[\theta]_1$ and $[\theta]_2$ are the observed mean residue ellipticities of the two proteins.

The recombinant SNAP-25 contained additional 5 residues, Gly-Pro-Leu-Gly-Ser, at the N-terminal of SNAP-25. The CD spectrum of the SNAP-25 was not affected by the additional 5 residues. The results are shown in **Figure 64**.

The relationship of mean residue ellipiticity and molar extinction coefficient can be converted using **Equation 11**:

$$[\theta] = 100\Delta\varepsilon\left(\frac{\ln 10}{4}\right)\left(\frac{180}{\pi}\right) = 3298.2\Delta\varepsilon \qquad (11)$$

CD data should be in per residue $\Delta\varepsilon$ ($M^{-1}\cdot cm^{-1}$) unit and the α-helix, β-strand, turn, and unordered motifs can be obtained using downloaded software SELCON3 (72).

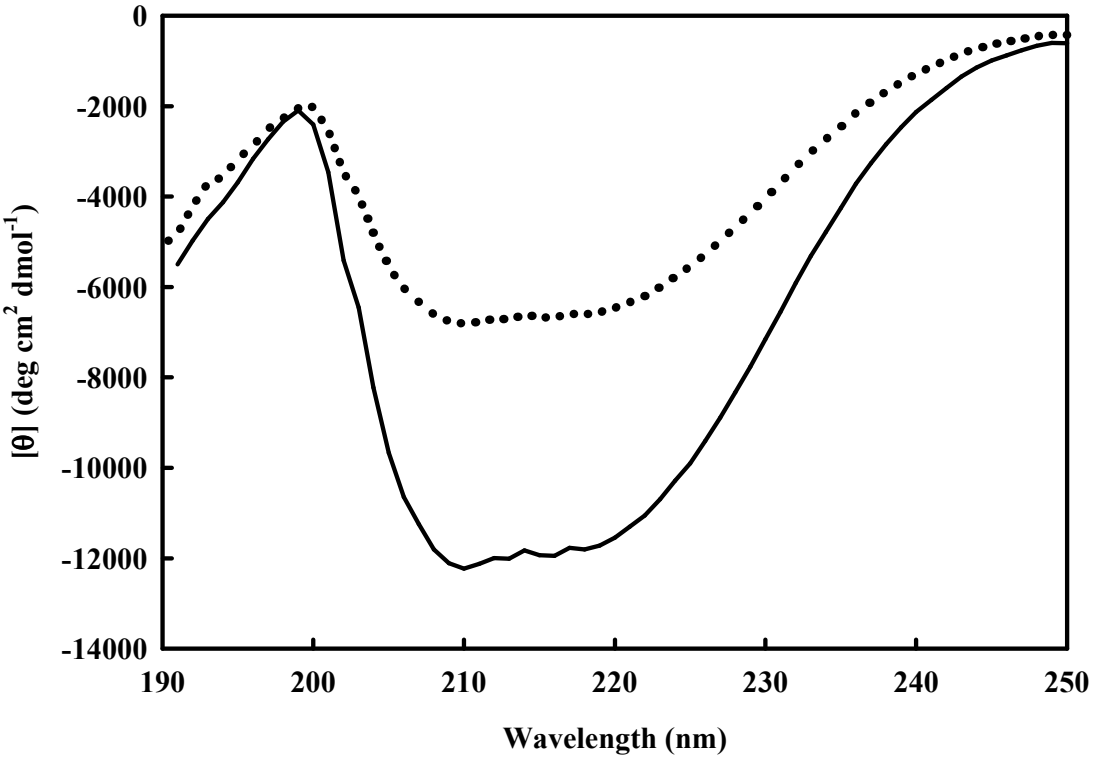

Figure 64. Calculated CD spectrum based on the summation of the CD spectra of SNAP-25 and BoNT/A LC and the experimentally observed CD spectrum of the complex of SNAP-25 and BoNT/A LC. The solid line is the experimentally observed CD spectrum. The dotted line is the calculated CD spectrum based on the free SNAP-25 and BoNT/A LC before binding using **Equation 8**. The results suggest that higher α-helical content was formed when SNAP-25 bound to BoNT/A LC when compared to the theoretically calculated. The α-helical contents of the SNAP-25-BoNT/A LC complex from $[\theta]_{222}$ using **Equation 9** were found to be 17.3 and 30.8% for the theoretically and experimentally observed results, respectively.

5.2.6 CD spectrum of the binary complex of SNAP-25(1-140) and BoNT/A LC

SNAP-25(1-140) (5.0 μM) and BoNT/A LC (5.0 μM) were incubated at 4 °C overnight in 10 mM phosphate buffer (pH 7.4), 150 mM NaCl, 1 mM TCEP, and 1 mM EDTA. Assume the SNAP-25(1-140) and BoNT/A LC had reached equilibrium and formed a 1:1 complex. The result is shown in **Figure 65**.

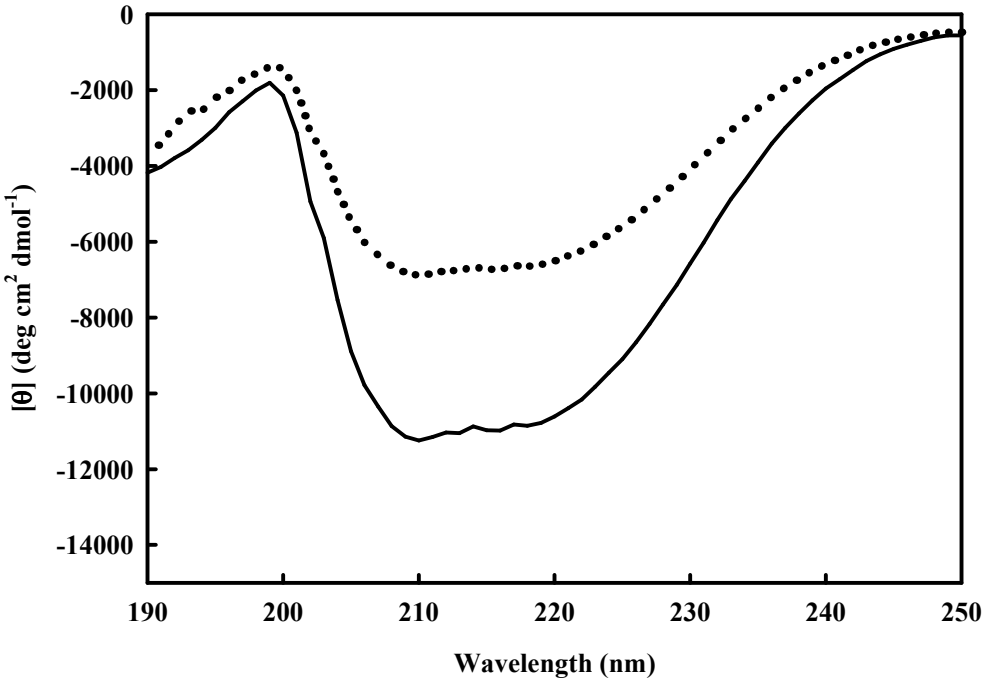

Figure 65. Changes in the CD spectra caused by interactions between SNAP-25(1-140) and BoNT/A LC at 25 °C. The solid line is the experimentally observed CD spectrum. The dotted line is the calculated CD spectrum based on the free SNAP-25 (1-140) and BoNT/A LC before binding using **Equation 8**. The results indicate that higher α-helical content formed when SNAP-25(1-140) bound to BoNT/A LC than was theoretically calculated. The α-helical contents of the SNAP-25(1-140)-BoNT/A LC complex from $[\theta]_{222}$ using **Equation 9** were found to be 15.5 and 28.5% for the theoretically and experimentally observed results, respectively.

5.2.7 CD spectrum of the binary complex of SNAP-25(141-206) and BoNT/A LC

SNAP-25(141-206) (5.0 μM) and BoNT/A LC (5.0 μM) were incubated at 4 °C overnight in 10 mM phosphate buffer, 150 mM NaCl, 1 mM EDTA, 1 mM TCEP, pH 7.4. SNAP-25(141-206) and BoNT/A LC had reached equilibrium and formed a 1:1 complex. The mean residue ellipticity of SNAP-25(141-206) was determined. The results are shown in **Figure 66**.

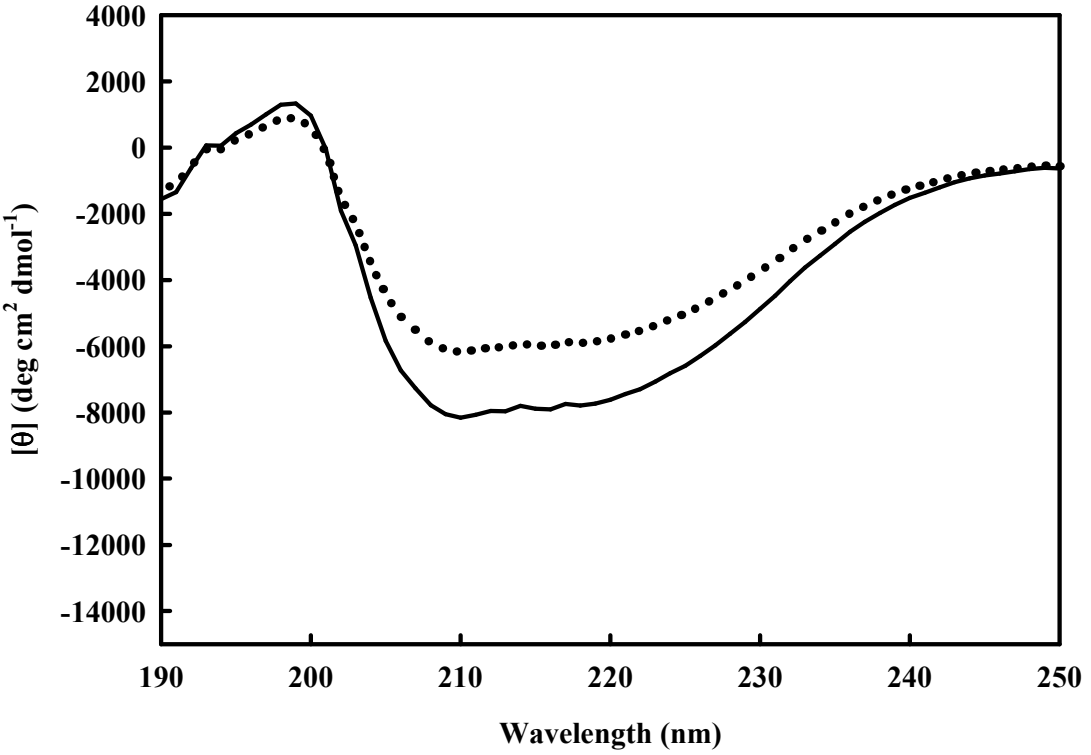

Figure 66. Changes in the CD spectra caused by interactions between SNAP-25(141-206) and BoNT/A LC at 25 °C. The solid line is the experimental observed CD spectrum. The dotted line is the calculated CD spectrum based on the free SNAP-25(141-206) and BoNT/A LC before binding using **Equation 8**. The results indicate that higher α-helical content (from 15.8 to 20.8%) formed when SNAP-25(141-206) bound to BoNT/A LC when compared to the theoretically calculated CD data.

5.2.8 Changes in the CD spectra caused by interactions among the SNAP-25(1-140), SNAP-25(141-206), and BoNT/A LC

The mixture of equimolar SNAP-25(1-140), SNAP-25(141-206), and BoNT/A LC were incubated at 4 °C overnight in 10 mM phosphate buffer, 150 mM NaCl, 1 mM EDTA, 1 mM TCEP, pH 7.4. Three proteins formed a ternary complex and reached equilibrium. The mean residue ellipticity was measured by CD. The results are shown in **Figure 67**.

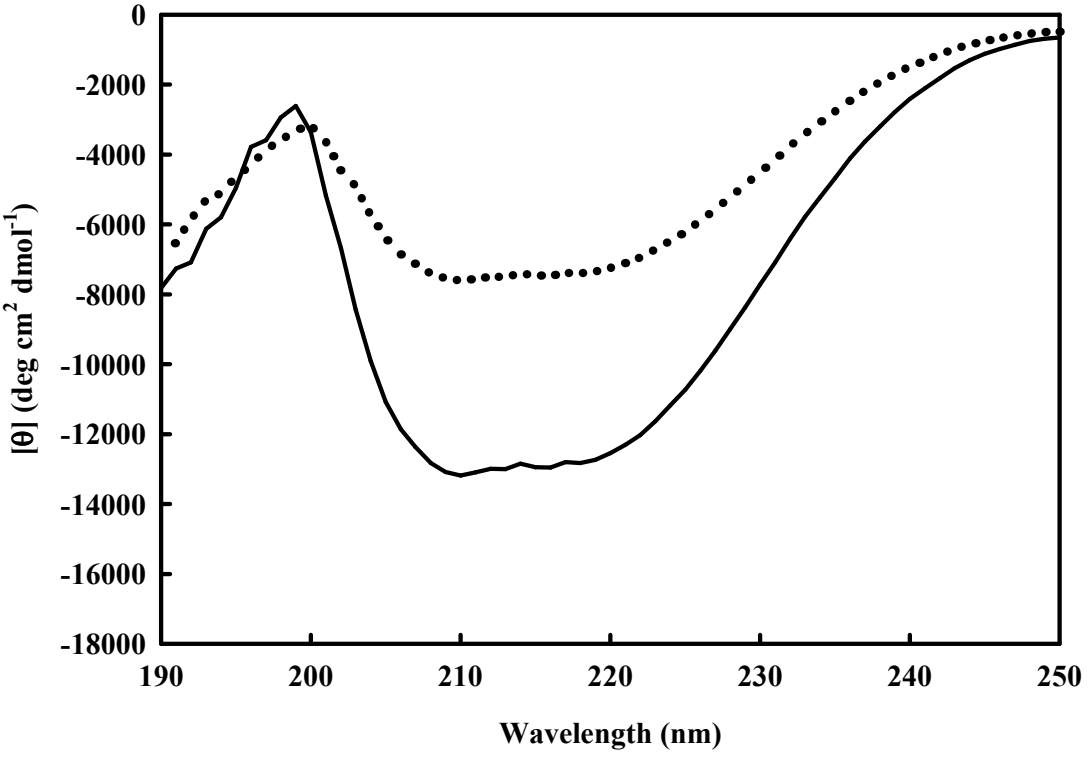

Figure 67. CD spectrum of the ternary complex of SNAP-25(1-140), BoNT/A LC, and SNAP-25(141-206). The solid line is the experimentally observed CD spectrum. The dotted line is the calculated CD spectrum based on the free SNAP-25(1-140), SNAP-25(141-206) and BoNT/A LC before binding using **Equation 8**. The results indicate that higher α-helical content in the ternary formation compared to the theoretically calculated.

The CD data in **Figure 63, 64, 65,** and **66** between 240 and 200 nm were analyzed using SELCON3 (72) using **Equation 11**. The results are shown in **Table 5**. FL, CT, and NT indicate the full length, the C-terminal, and the N-terminal domain of SNAP-25.

Table 5. Analysis of CD spectra using SELCON3 program

	α_R	α_D	β_R	β_D	T	U
BoNT/A LC	0.052	0.060	0.209	0.120	0.219	0.333
CT	0.032	0.074	0.195	0.114	0.231	0.318
CT-LC (Cal.)	0.078	0.090	0.163	0.100	0.190	0.275
CT-LC (Exp.)	0.103	0.118	0.189	0.107	0.203	0.261
NT	0.043	0.078	0.156	0.116	0.230	0.412
NT-LC (Cal.)	0.041	0.069	0.200	0.116	0.231	0.350
NT-LC (Exp.)	0.105	0.101	0.157	0.100	0.237	0.323
FL	0.015	0.087	0.182	0.120	0.222	0.365
FL-LC (Cal.)	0.041	0.065	0.191	0.115	0.234	0.373
FL-LC (Exp.)	0.125	0.119	0.154	0.100	0.232	0.316

α_R, regular α-helix; α_D, distorted α-helix;

β_R, regular β-strand; β_D, distorted β-strand; T, turn; U, unordered.

The results suggest that more α-helical components formed when SNAP-25 bound to LC, which were consistent with the direct calculation using **Equation 9**. The sum of α-helical contents of SNAP-25(141-206) increased from 16.8% to 22.1%. That is, the binary complex had 16 out of 71 amino acid residues involved in the α-helix formation, which corresponded to the α-exosite component, 152 to 167 amino acid residues of SNAP-25, in the co-crystal structure of SNAP-25(141-204)-BoNT/A LC(E224Q, Y366F) (25).

5.2.9 Construct of pGEX-CCPGCC-SNAP-25, pGEX-CCPGCC-SNAP-25(1-140), and pGEX-CCPGCC-SNAP-25(141-206)

The complex of SNAP-25(1-140) and BoNT/A LC displayed higher α-helical content than the individual proteins. The SNAP-25(141-206) showed similar results. These results suggested that the N-terminus of the SNAP-25 bound to BoNT/A LC and induced more α-helical content. In order to prove these results, new plasmids were constructed in order to demonstrate the N-terminus of the SNAP-25 binding to BoNT/A LC. CCPGCC was genetically inserted on the N-terminus of the SNAP-25, SNAP-25(1-140), and SNAP-25(141-206) by mutagenesis. The schematic representation of the CCPGCC-modified SNAP-25 and its fragments are shown in **Figure 68**.

The secondary structures of the CCPGCC-SNAP-25, CCPGCC-SNAP-25(1-140), and CCPGCC-SNAP-25(141-206) were measured by circular dichroism.

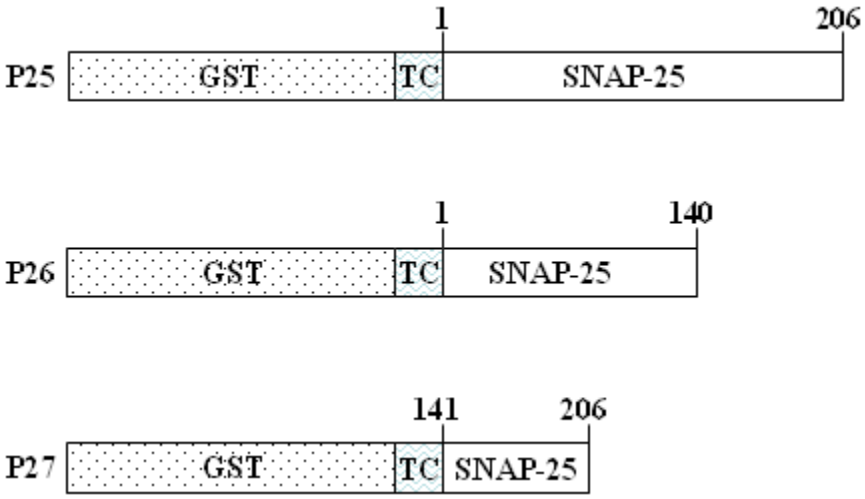

Figure 68. Schematic representation of the CCPGCC-SNAP-25, CCPGCC-SNAP-25(1-140), and CCPGCC-SNAP-25(141-206) with GST-tag. The numbers on the box indicated the residues of SNAP-25. TC represents the tetracysteine motif CCPGCC. The N-terminal GST-tag can be removed by PreScission^{TM} protease.

CCPGCC-SNAP-25 cDNA was inserted into pGEX-6P-3 vector (**6**) (Amersham Biosciences) by using BamHI/NotI digestion, resulting in the pGEX-CCPGCC-SNAP-25 (**25**) construct. PCR for amplification of CCPGCC-SNAP-25 was performed by using a 23 nucleotide forward primer (5'-GGGCTGGCAAGCCACGTTTGGTG-3') and a 39 nucleotide reverse primer (5'-GTC*GCGGCCGC*TTTAACCACTTCCCAGCATCTTTG TTGC-3'), pGEX-CCGPCC-SNAP-25-EGFP (**9**) was used as a template. The underlined residues indicate the stop codon of SNAP-25. The plasmid pGEX-CCPGCC-SNAP-25 (**25**) was obtained after the ligation. A six-nucleotide linker GGATCC was introduced between the GST and the CCPGCC-SNAP-25, which was expressed as Gly-Ser.

CCPGCC-SNAP-25(1-140) cDNA was inserted into pGEX-6P-3 vector (**6**) (Amersham Biosciences) by using BamHI/NotI digestion, resulting in the pGEX-

CCPGCC-SNAP-25(1-140) (**26**) construct. PCR for amplification of SNAP-25(1-140) was performed by using a 23 nucleotide forward primer (5'-GGGCTGGCAAGCCACGT TTGGTG-3') and a 42 nucleotide reverse primer (5'-GTC*GCGGCCGC*TTTAATCATT TGTTACCCTGCGGATGAAGCC-3'). pGEX-CCGPCC-SNAP-25-EGFP (**9**) was used as a template. The underlined residues indicate the last residue of D140 in the CCPGCC-SNAP-25. The plasmid pGEX-CCPGCC-SNAP-25(1-140) (**26**) was obtained after the ligation.

CCPGCC-SNAP-25(141-206) cDNA was inserted into pGEX-6P-3 vector (**6**) (Amersham Biosciences) by using BamHI/NotI digestion, resulting in the pGEX-CCPGCC-SNAP-25(141-206) (**27**) construct. PCR for amplification of SNAP-25(141-206) was performed by using a 30 nucleotide forward primer (5'-CTGGGATCCTGTTG TCCTGGCTGTTGCGCC-3') and a 39 nucleotide reverse primer (5'-GTC*GCGGCCGC* TTTAACCACTTCCCAGCATCTTTGTTGC-3'). pGEX-SNAP-25(1-140)-CCGPCC-SNAP-25(141-206)-EGFP (**11**) was used as a template. The underlined residues indicate the restricted digestion site of BamHI and the stop codon in the CCPGCC-SNAP-25(141-206), respectively. The plasmid pGEX-CCPGCC-SNAP-25(141-206) (**27**) was obtained after the ligation. All final constructs were confirmed by DNA sequencing.

5.2.10 Expression of CCPGCC-SNAP-25 and cleavage of GST-tag by PreScission protease

The GST-CCPGCC-SNAP-25 (**P25**) was expressed and purified with a GST-tag attached on the N-terminus of the SNAP-25. Similarly, GST-CCPGCC-SNAP-25(1-140) (**P26**) and GST-CCPGCC-SNAP-25(141-206) (**P27**) were expressed and purified. The GST-tag was removed by PreScission™ protease. After the cleavage, CCPGCC was located on the N-terminus of the SNAP-25 and its corresponding fragments: CCPGCC-SNAP-25(1-140) and CCPGCC-SNAP-25(141-206). The proteins were analyzed by SDS-PAGE. The results are shown in **Figure 69**.

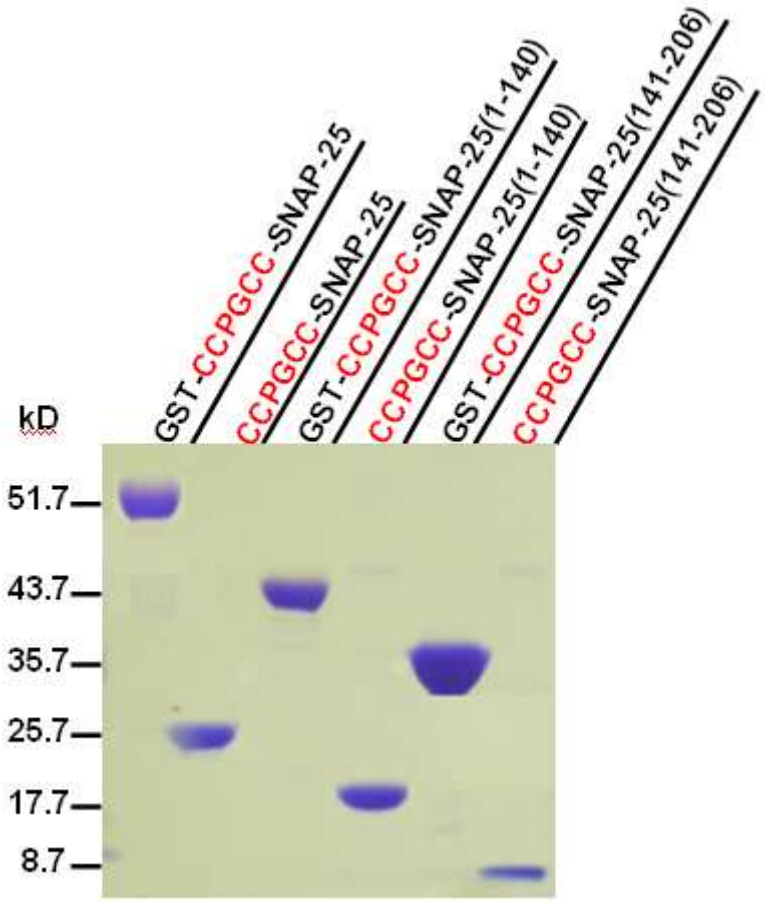

Figure 69. GST-CCPGCC-SNAP-25 cleavage by PreScission™ protease. The purified GST-CCPGCC-SNAP-25 (**P25**), GST-CCPGCC-SNAP-25(1-140) (**P26**), GST-CCPGCC-SNAP-25(141-206) (**P27**), and cleaved proteins were subjected to SDS-PAGE. The results suggested that the GST-tag had been removed by PreScission™ protease. The molecular weights of GST-CCPGCC-SNAP-25 (**P25**), GST-CCPGCC-SNAP-25(1-140) (**P26**), and GST-CCPGCC-SNAP-25(141-206) (**P27**) were 51.7, 43.7, and 34.7 kD, respectively. After the cleavage of GST-tag, the molecular weights of CCPGCC-SNAP-25 (**P25R**), CCPGCC-SNAP-25(1-140) (**P26R**), and CCPGCC-SNAP-25(141-206) (**P27R**) were 25.7, 17.7, and 8.7 kD, respectively.

5.2.11 Determination of secondary structure of CCPGCC-SNAP-25, CCPGCC-SNAP-25(1-140), and CCPGCC-SNAP-25(141-206) by circular dichroism

The proteins of CCPGCC-SNAP-25(1-206) (**P25R**), CCPGCC-SNAP-25(1-140) (**P26R**), and CCPGCC-SNAP-25(141-206) (**P27R**) were diluted in 100 mM MOPS buffer (pH 7.2), 150 mM NaCl, 100 μM TCEP, 1 mM β-mercaptoethanol, and 1 mM EDTA. The ellipicity of the proteins were measured by CD. The results are shown in **Figure 70**.

The mean residue ellipticities based on the observed ellipticities of CCPGCC-SNAP-25 and its fragments are shown in **Figure 71**.

The results demonstrate that CCPGCC-SNAP-25(1-206) (**P25R**), CCPGCC-SNAP-25(1-140) (**P26R**), and CCPGCC-SNAP-25(141-206) (**P27R**) are disordered proteins. The obtained α-helical content for CCPGCC-SNAP-25(141-206) (**P27R**), CCPGCC-SNAP-25(1-140) (**P26R**), and CCPGCC-SNAP-25(1-206) (**P25R**) were 18.1%, 26.5%, and 24.6%, respectively. CCPGCC-SNAP-25(1-140) (**P26R**) had higher α-helical content than that of CCPGCC-SNAP-25(141-206) (**P27R**), while full-length (**P25R**) had less α-helical content than the CCPGCC-SNAP-25(1-140) (**P26R**). However, all three proteins did not display minima at 208 and 222 nm.

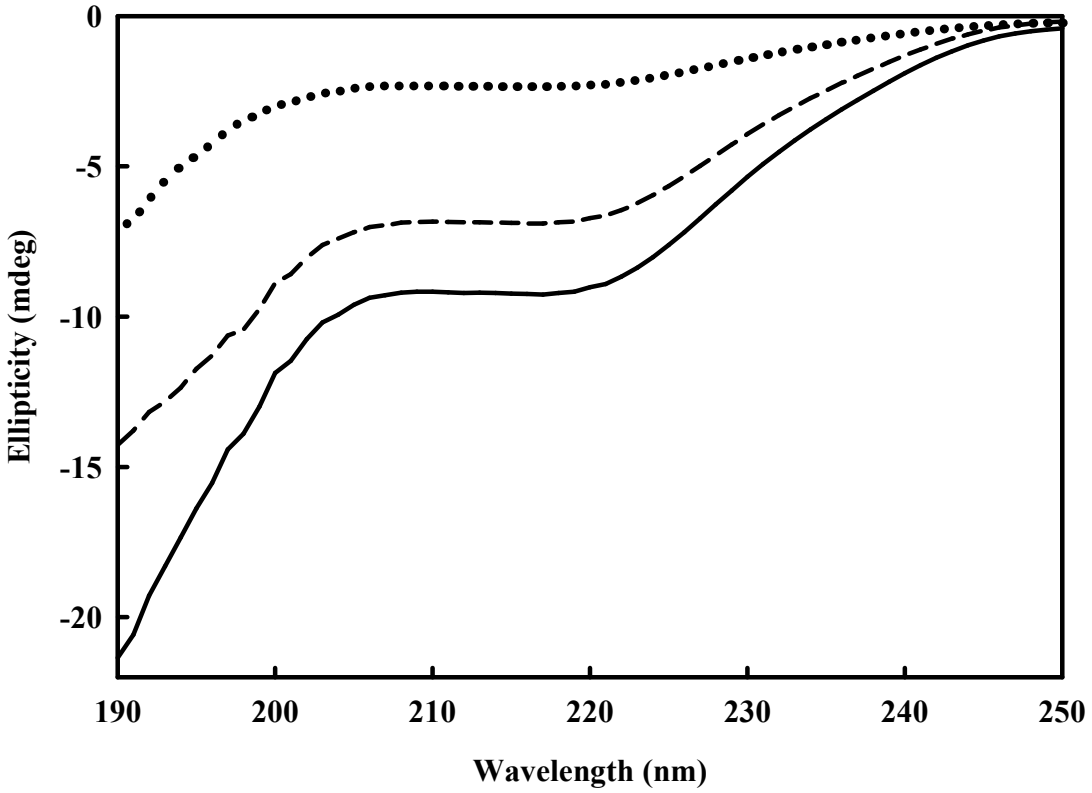

Figure 70. The ellipticity of CCPGCC-SNAP-25(141-206) (P27R), CCPGCC-SNAP-25(1-140) (P26R), and CCPGCC-SNAP-25(1-206) (P25R). The circular dichroism spectra were monitored at 25 ˚C from 190 to 250 nm in 10 mM MOPS buffer (pH 7.4), 150 mM NaCl, 100 μM TCEP, 1 mM β-mercaptoethanol, and 1 mM EDTA. The spectra corresponded to the CCCPGCC-SNAP-25(141-206) (**P27R**) (dotted line), CCPGCC-SNAP-25(1-140) (**P26R**) (dashed line), and CCPGCC-SNAP-25(1-206) (**P25R**) (solid line). The concentrations for all proteins are 5.0 μM. The buffer background was subtracted in all cases.

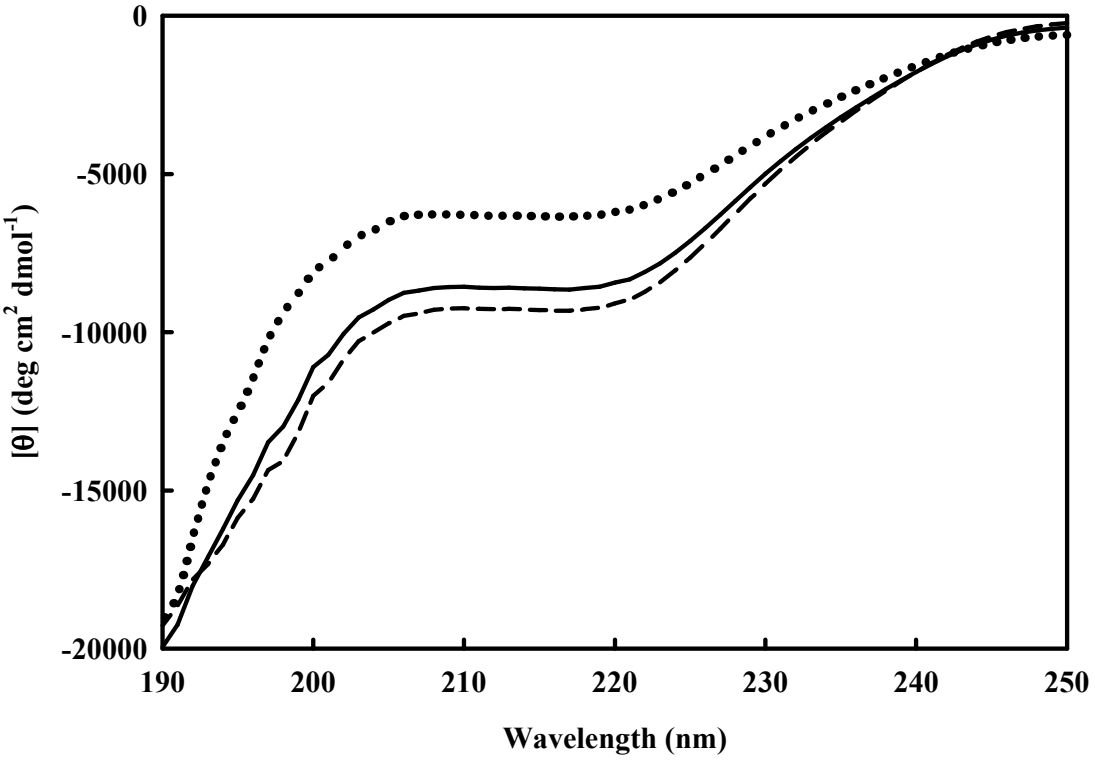

Figure 71. The mean residue ellpticity of CCPGCC-SNAP-25(141-206) (P27R), CCPGCC-SNAP-25(1-140) (P26R), and CCPGCC-SNAP-25(1-206) (P25R). The circular dichroism was monitored at 25 ˚C from 190 to 250 nm in 100 mM MOPS buffer (pH 7.4), 150 mM NaCl, 100 μM TCEP, 1 mM β-mercaptoethanol, and 1 mM EDTA. The spectra corresponded to CCPGCC-SNAP-25(141-206) (**P27R**) (dotted line) CCPGCC-SNAP-25(1-140) (**P26R**) (dashed line), and CCPGCC-SNAP-25(1-206) (**P25R**) (solid line). The concentrations for all proteins are 5.0 μM. The buffer background was subtracted in all cases. The α-helical contents from $[\theta]_{222}$ using **Equation 9** were found to be 17.0, 24.5, and 22.7% for CCPGCC-SNAP-25(141-206), CCPGCCSNAP-25(1-140), and CCPGCC-SNAP-25(1-206), respectively.

5.2.12 Time course of CCPGCC-SNAP-25(1-140) binding to Zn^{2+}-depleted BoNT/A LC

To characterize the process of binary complex of CCPGCC-SNAP-25(1-140) (**P26R**) and BoNT/A LC, we measured the ellipticity changes with time. Equimolar amounts (5.0 μM) of CCPGCC-SNAP-25(1-140) (**P26R**) and BoNT/A LC were incubated in 100 mM MOPS buffer (pH 7.4), 150 mM NaCl, 100 μM TCEP, 1 mM β-mercaptoethanol, and 1 mM EDTA. The binary complex formation was monitored by changes in ellipticity. The results are shown in **Figure 72**.

Based on the X-ray crystallization results, the conformation of BoNT/A LC does not change upon binding of SNAP-25 (25). All the ellipticity changes can be attributed to changes in CCPGCC-SNAP-25. Apparently, the α-helical content of CCPGCC-SNAP-25(1-140) (**P26R**) increased binding to BoNT/A LC. Similarly, the process of binary complex of CCPGCC-SNAP-25(141-206) binding to BoNT/A LC was monitored using the same method. The results are shown in **Figure 73**. Higher α-content was formed once CCPGCC-SNAP-25(141-206) bound to BoNT/A LC. The results indicated that two different conformations were formed between unbound CCPGCC-SNAP-25 and bound CCPGCC-SNAP-25. The binding process between CCPGCC-SNAP-25 and BoNT/A LC was very slow and tight, which is consistent with the fluorescence binding studies. These results are biologically intriguing, since they imply that other factors must play critical roles in accelerating association.

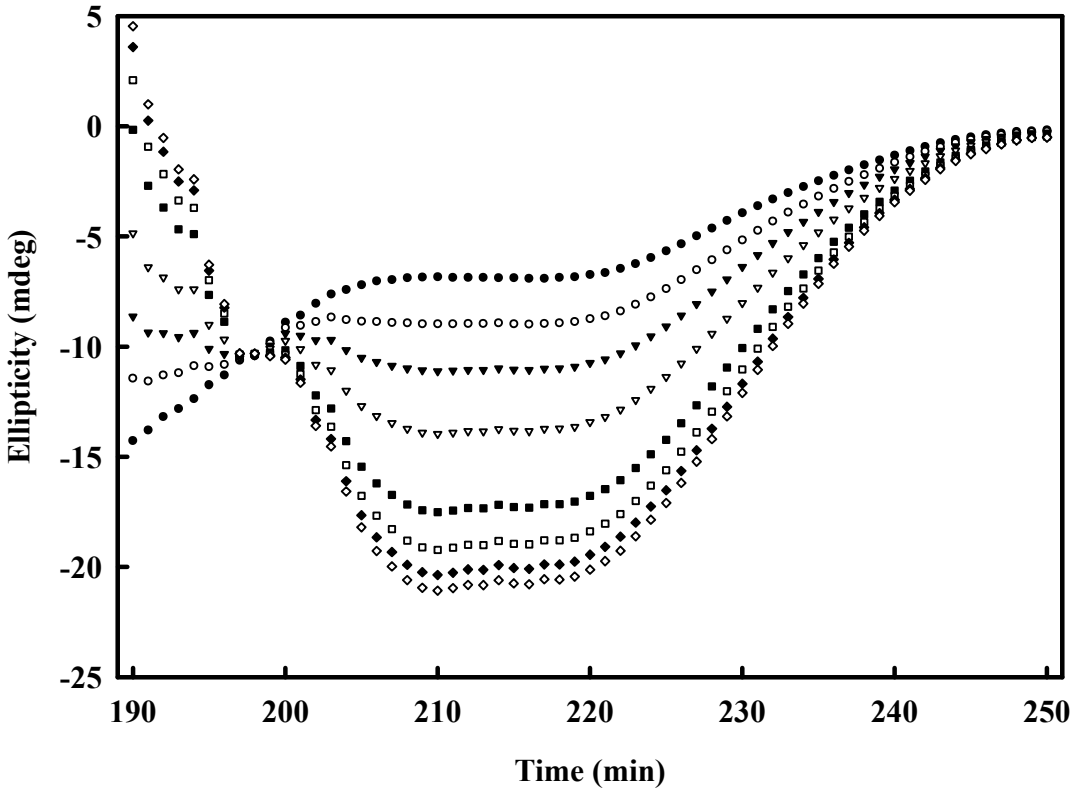

Figure 72. Binary complex formation of CCPGCC-SNAP-25(1-140)-BoNT/A LC. The CD spectra were monitored under a specific time at 25 ˚C. Proteins were mixed at a concentration of 5.0 μM each. The ellipticity of BoNT/A LC was subtracted in all cases. The spectra corresponded to (●) 0 min, (○) 4 min, (▼) 16 min, (▽) 40 min, (■) 60 min, (□) 80 min, (◆) 100 min, and (◇) 120 min, respectively.

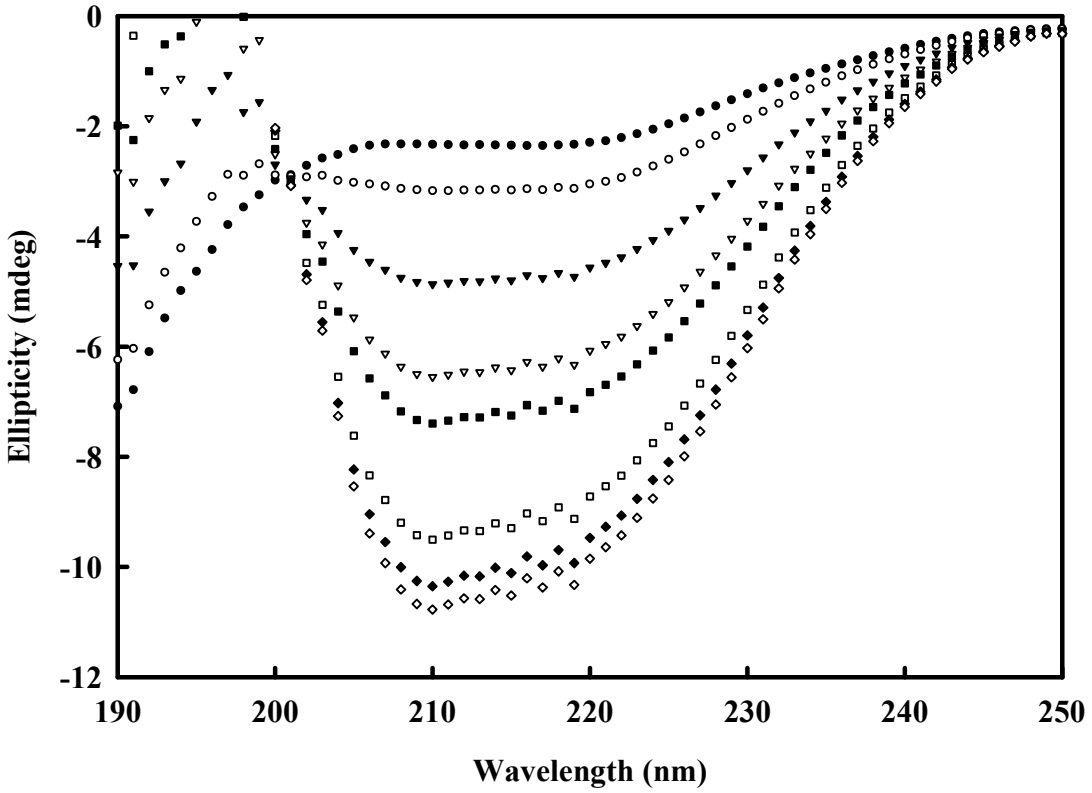

Figure 73. Binary complex formation of the CCPGCC-SNAP-25(141-206)-BoNT/A LC. The CD spectra were monitored under a specific time at 25 ˚C. Proteins were mixed at a concentration of 5.0 μM each. The ellipticity of BoNT/A LC was subtracted in all cases. The spectra corresponded to (●) 0 min, (○) 4 min, (▼) 16 min, (▽) 40 min, (■) 60 min, (□) 80 min, (◆) 100 min, and (◇) 120 min, respectively.

5.2.13 Kinetics analysis of SNAP-25 binding to BoNT/A LC by circular dichroism

The rate constant, k, for the formation of each binary or ternary complex was calculated by fitting kinetic data to a second order reaction equation A + B → P for a simplified case in which $[A]_0 = [B]_0$.

The results can be obtained using **Equations 12-14** (23):

$$\frac{1}{[A]} = \frac{1}{[A]_0} + kt \tag{12}$$

$$\alpha = \frac{\Delta\theta}{\Delta\theta_{\max}} = \frac{\theta_t - \theta_0}{\theta_\infty - \theta_0} = 1 - \frac{[A]}{[A]_0} = 1 - \frac{1}{[A]_0 kt + 1} = \frac{[A]_0 kt}{[A]_0 kt + 1} \tag{13}$$

$$\theta_t = \theta_0 + \frac{(\theta_\infty - \theta_0)([A]_0 kt)}{([A]_0 kt + 1)} \tag{14}$$

$$t = 0, \theta_t = \theta_0$$

where θ_0, θ_t, and $\theta_{\max}$ are the ellipticity in the initial time t = 0, in the process of folding with time t, and in the end of folding with $t = \infty$, respectively. $[A]_0$ is the initial concentration of fragment of SNAP-25 in molar units (M), k is the rate constant with unit $M^{-1} \cdot s^{-1}$, and t is the time since mixing in min. For the CD kinetic experiments, θ_0 was calculated as the ellipticity value of appropriate SNAP-25 fragments without binding to BoNT/A LC.

The results are shown in **Figure 74**.

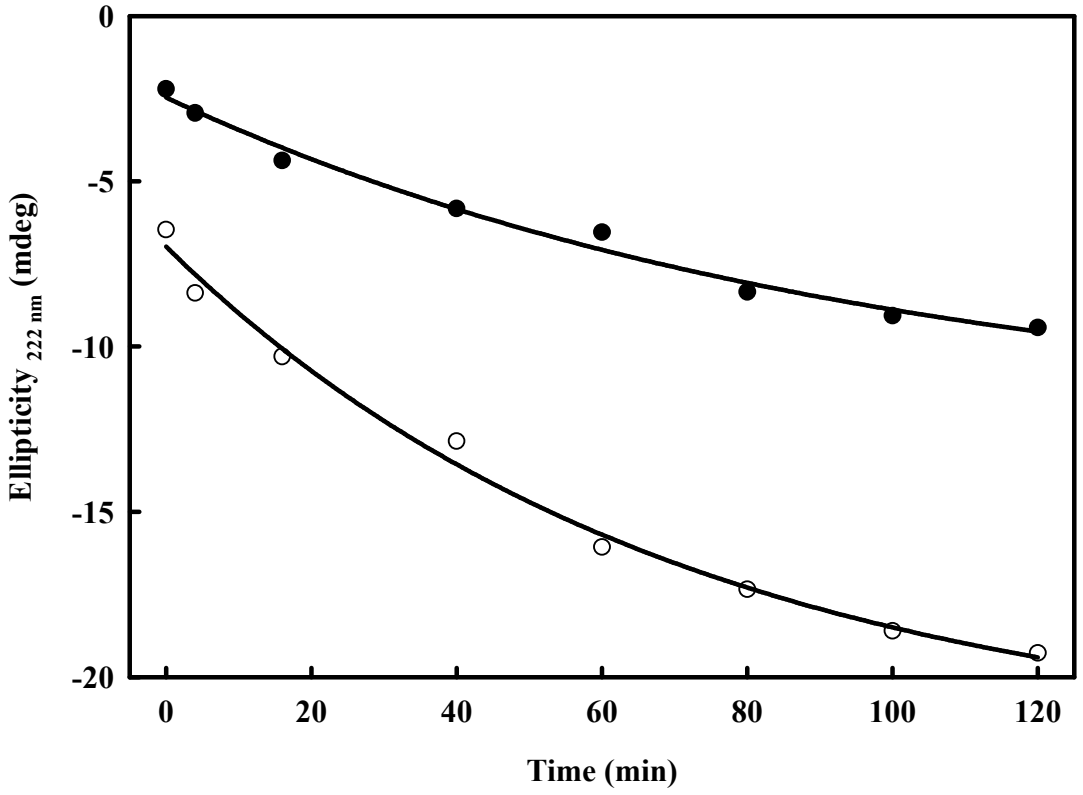

Figure 74. Slow formation of the binary complex between CCPGCC-SNAP-25(1-140), CCPGCC-SNAP-25(141-206), and BoNT/A LC. Equimolar (5.0 μM) mixtures of N-terminal or C-terminal of SNAP-25 bound to BoNT/A LC (5.0 μM). The ellipticity was monitored at 25 °C at 222 nm in 10 mM MOPS buffer (pH 7.4), 150 mM NaCl, 100 μM TCEP, 1 mM β-mercaptoethanol, and 1 mM EDTA. The BoNT/A LC ellipticties were subtracted in all cases. The time courses corresponded to (●) CCPGCC-SNAP-25(141-206) and (○) CCPGCC-SNAP-25(1-140). The obtained rate constants using **Equation 13** for CCPGCC-SNAP-25(141-206) and CCPGCC-SNAP-25(1-140) were 173.3 and 236.7 $M^{-1} \cdot s^{-1}$, respectively.

5.2.14 Excitation and emission of CCPGCC(FlAsH)-SNAP-25(1-140) and CCPGCC(ReAsH)-SNAP-25(141-206)

The fluorescence spectra of FlAsH and ReAsH were determined in the buffer containing 100 mM MOPS (pH 7.4), 150 mM NaCl, 100 μM TCEP, and 1 mM β-mercaptoethanol. For FlAsH, the excitation maximum wavelength was 508 nm and the emission maximum wavelength was 528 nm; while for ReAsH bound to CCPGGCC, the maximum excitation wavelength was 597 nm and the emission maximum wavelength was 607 nm. The results are shown in **Figure 75**.

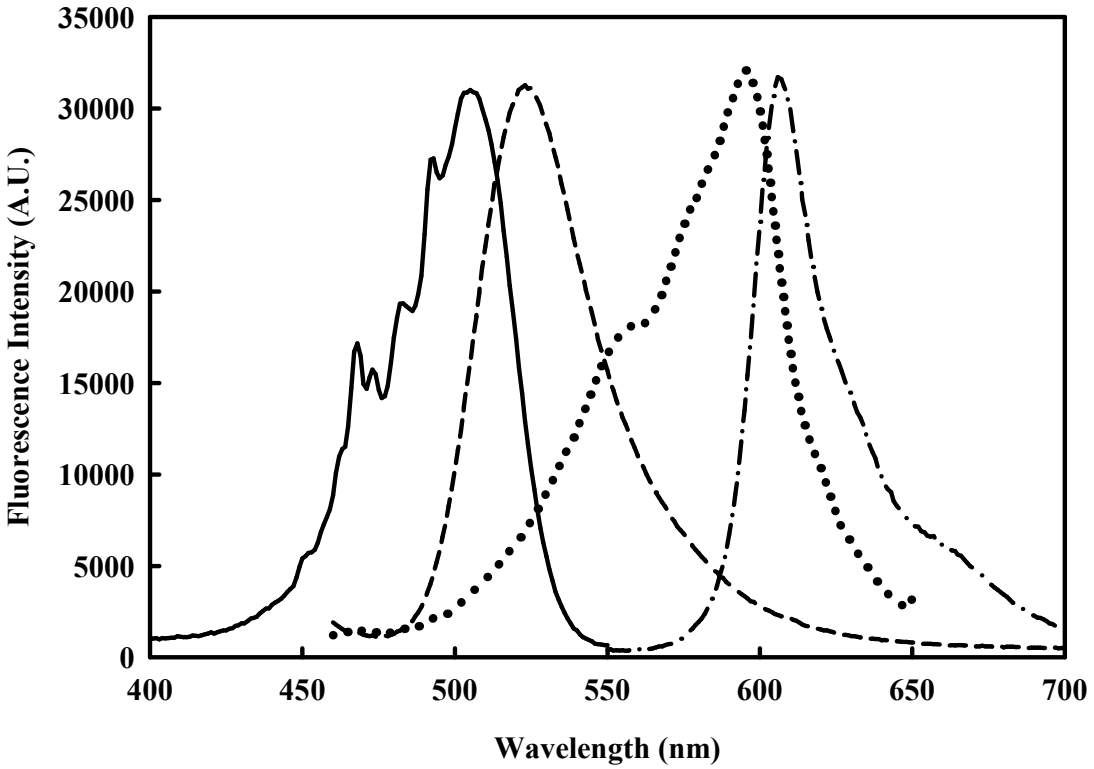

Figure 75. The excitation and emission spectra of CCPGCC(FlAsH)-SNAP-25(1-140) and CCPGCC(ReAsH)-SNAP-25(141-206). The spectra correspond to the excitation (solid line) and emission (short dashed line) spectra of FlAsH bound to CCPGCC-SNAP-25(1-140), with the emission wavelength at 560 nm and excitation wavelength at 450 nm, respectively. The dotted line and dash-dot lines represent the excitation and emission of ReAsH bound to CCPGCC-SNAP-25(141-206), with the emission wavelength at 660 nm and excitation wavelength at 540 nm.

5.2.15 Binding of CCPGCC(FlAsH)-SNAP-25(1-140), CCPGCC(FlAsH)-SNAP-25(141-206), and CCPGCC(FlAsH)-SNAP-25(1-206) to BoNT/A LC

The CCPGCC-FlAsH fluorescence of modified SNAP-25 (0.2 μM) in 100 mM MOPS buffer (pH 7.2), 150 mM NaCl, 100 μM TCEP, 1 mM β-mercaptoethanol, and 1 mM EDTA was monitored with varying concentrations of Zn^{2+}-depleted BoNT/A LC after 2 h incubation at 25 ˚C. The results are shown in **Figure 76**.

The fluorescence emission maximum wavelength was at 528 nm, which was the characteristic wavelength of FlAsH covalently bound to CCPGCC. The fluorescence intensity increased with an increasing amount of Zn^{2+}-depleted BoNT/A LC addition to the solution of CCPGCC(FlAsH)-SNAP-25, CCPGCC(FlAsH)-SNAP-25(1-140), or CCPGCC-SNAP-25(141-206).

The results demonstrated that CCPGCC-SNAP-25(1-140), CCPGCC-SNAP-25(141-206), and CCPGCC-SNAP-25 bound to BoNT/A LC tightly. It is well known that the C-terminal SNAP-25 can bind to BoNT/A LC. However, the results demonstrated that CCPGCC-SNAP-25(1-140) could specifically bind to BoNT/A LC. The full length SNAP-25 bound to BoNT/A LC with the N-terminus and the C-terminus of the SNAP-25.

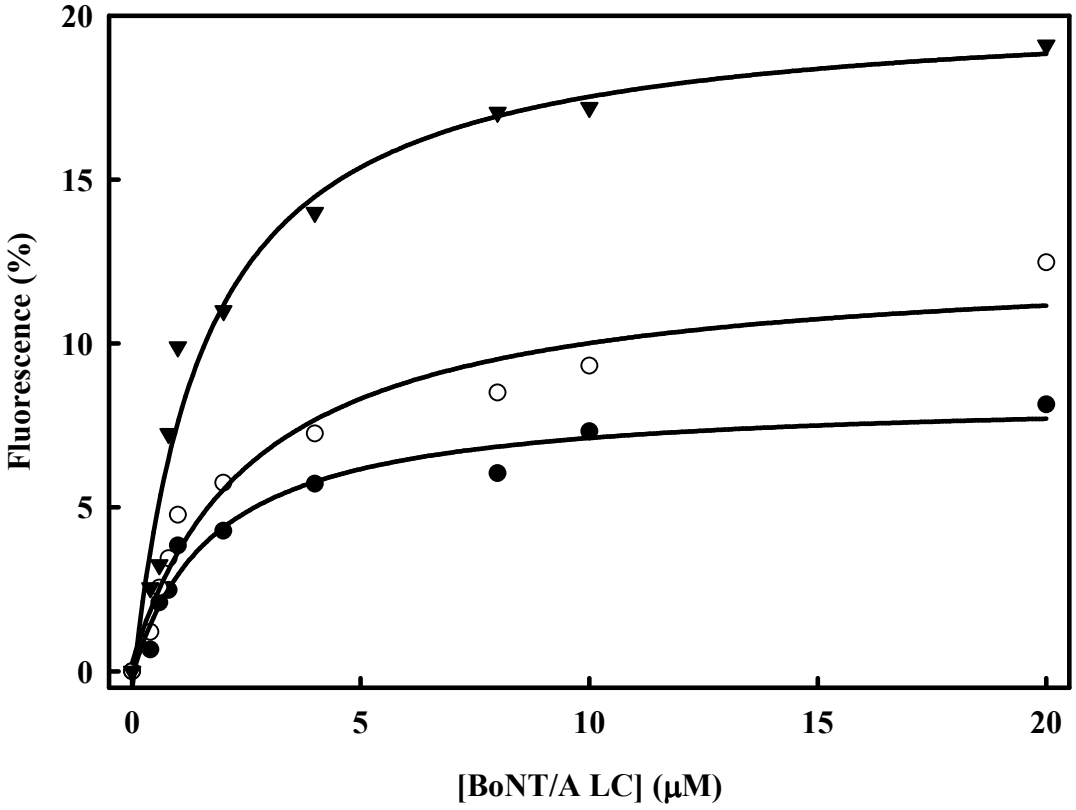

Figure 76. Fluorescence titration of BoNT/A LC with CCPGCC(FlAsH)-SNAP-25(1-140), CCPGCC(FlAsH)-SNAP-25(141-206), and CCPGCC(FlAsH)-SNAP-25(1-206). The titrations corresponded to (●) CCPGCC(FlAsH)-SNAP-25(1-140), (○) CCPGCC(FlAsH)-SNAP-25(141-206), and (▼) CCPGCC(FlAsH)-SNAP-25(1-206). The fluorescence intensity was measured at 528 nm. The changes of the fluorescence intensity with increasing concentration of BoNT/A LC were analyzed as described in Material and Methods. Solid lines were fitted lines to the Schatchard equation (**Equation 1**). The obtained K_D values for CCPGCC(FlAsH)-SNAP-25(1-140) (**P26R-FlAsH**), CCPGCC(FlAsH)-SNAP-25(141-206) (**P27R-FlAsH**), and CCPGCC(FlAsH)-SNAP-25(1-206) (**P25R-FlAsH**) were 1.8, 1.5, and 1.2 μM, respectively.

5.2.16 Time based assay of CCPGCC(FlAsH)-SNAP-25(1-140) in the presence of BoNT/A LC—k_{on} between the N-terminus of the SNAP-25 and BoNT/A LC

The fluorescence intensity of the CCPGCC-SNAP-25(1-140) (**P26R**) modified with FlAsH was monitored with time after the addition of BoNT/A LC in 100 mM MOPS buffer (pH 7.2), 150 mM NaCl, 100 μM TCEP, 1 mM β-mercaptoethanol, and 1 mM EDTA. The fluorescence intensity of FlAsH was monitored immediately after mixing BoNT/A LC to SNAP-25. Both binding and conformational changes processes occurred during the formation of complex. The results are shown in **Figure 77**.

Plotting the apparent first order constants against the concentration of BoNT/A LC, a straight line was obtained. The slope of the straight line corresponded to the secondary rate constant. The result is shown in **Figure 78**.

These results demonstrated that the N-terminus of the SNAP-25 bound to BoNT/A LC with a very slow rate, which was consistent with the previous Peptide C binding to BoNT/A LC.

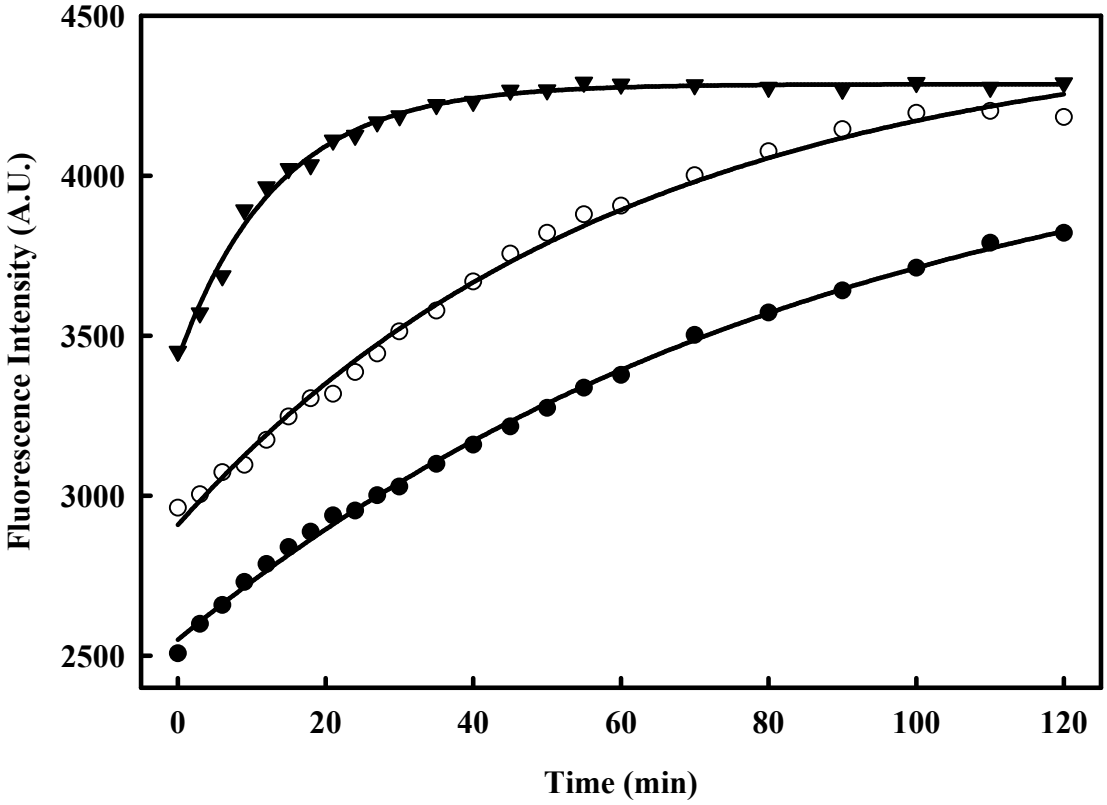

Figure 77. Time courses of the BoNT/A LC binding to CCPGCC-SNAP-25(1-140). The spectra corresponded to the concentration of BoNT/A LC (●) 1.0 μM, (○) 4.0 μM, and (▼) 20.0 μM. The time courses were fitted according to first order reaction kinetics and provided pseudo-first order rate constants of 0.0111 ± 0.0006, 0.0167 ± 0.0012, and 0.0744 ± 0.0031 min^{-1} in the presence of 1, 4, and 20 μM BoNT/A LC, respectively.

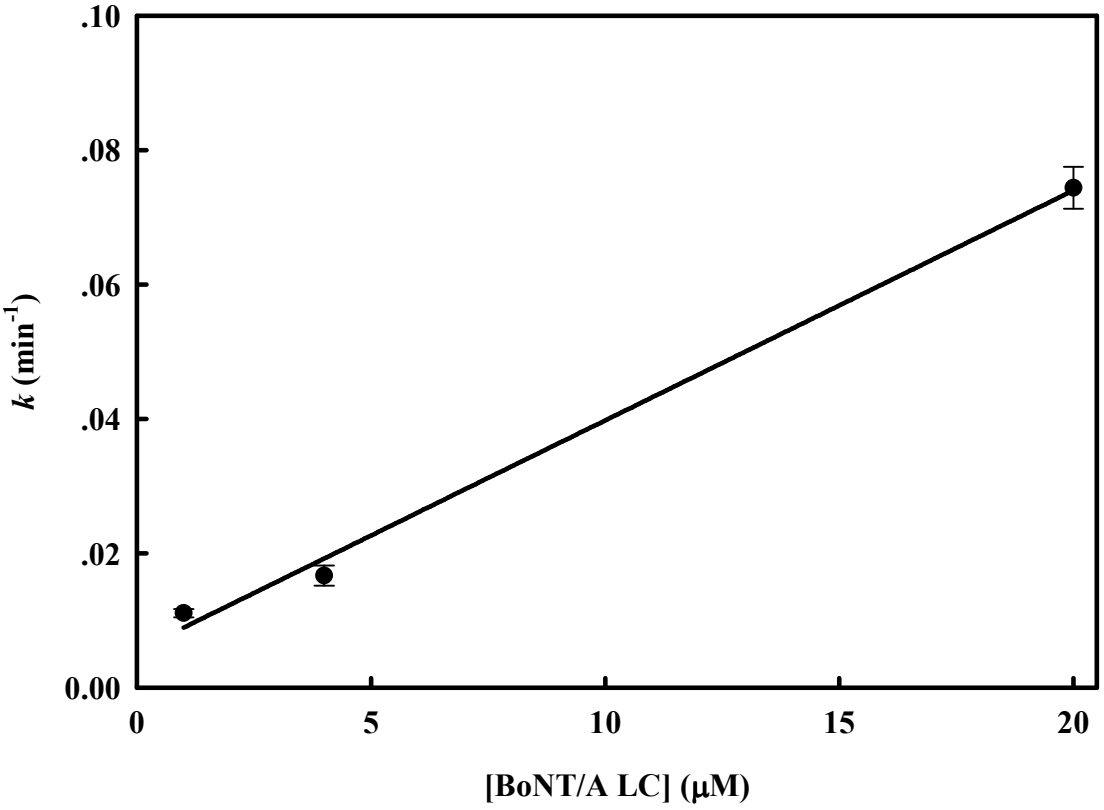

Figure 78. The secondary rate constant of the BoNT/A LC binding to CCPGCC-SNAP-25(1-140) (P26R). Plotting the apparent first order constants against the concentration of BoNT/A LC, a straight line was obtained. The slope of the straight line corresponded to the secondary rate constant. The obtained secondary rate constant was $0.0034 \pm 0.0002\ \mu M^{-1} \cdot min^{-1}$, corresponding to be $56.7\ M^{-1} \cdot s^{-1}$.

5.2.17 Fluorescence of CCPGCC(FlAsH)-SNAP-25(1-140) and CCPGCC(ReAsH)-SNAP-25(141-206) in the absence and presence of BoNT/A LC

CCPGCC-SNAP-25(1-140) (**P26R**) labeled with FlAsH with an emission maximum wavelength at 528 nm and CCPGCC-SNAP-25(141-206) (**P27R**) labeled with ReAsH with an emission maximum wavelength at 597 nm bound to BoNT/A LC to form an individually stable binary complex. Can both the N-terminal and the C-terminal domain of SNAP-25 bind to LC to form a ternary complex or not? We measured the fluorescence intensity of **P26R-FlAsH** and **P27R-ReAsH** bound to BoNT/A LC. The results are shown in **Figure 79 and 80**.

The binary complex with **P27R-ReAsH** was an acceptor and the **P26R-FlAsH** was a donor. When CCPGCC-SNAP-25(1-140) (**P26R-FlAsH**) and CCPGCC-SNAP-25(141-206) (**P27R**) bound to BoNT/A LC to form a ternary complex, FRET occurred between FlAsH and ReAsH. The emission of fluorescence intensity was monitored with excitation maximum at 480 nm and continuous emission scan from 495 nm to 700 nm. 0.2 μM CCPGCC(ReAsH)-SNAP-25(141-206) (**P27R-ReAsH**) was added to the binary complex and incubated at 25 ˚C for 2 h. The emission of fluorescence intensity was monitored with excitation maximum at 480 nm and continuous emission scan from 495 nm to 700 nm. The fluorescence resonance energy transfer (FRET) occurred between FlAsH and ReAsH. Fluorescence intensity decreases FlAsH, accompanied by an increase of ReAsH due to FRET. The fluorescence energy transfer efficiency was 47%, which provided evidence of the ternary complex of CCPGCC(FlAsH)-SNAP-25(1-140)-BoNT/A LC-CCPGCC(ReAsH)-SNAP-25(141-206).

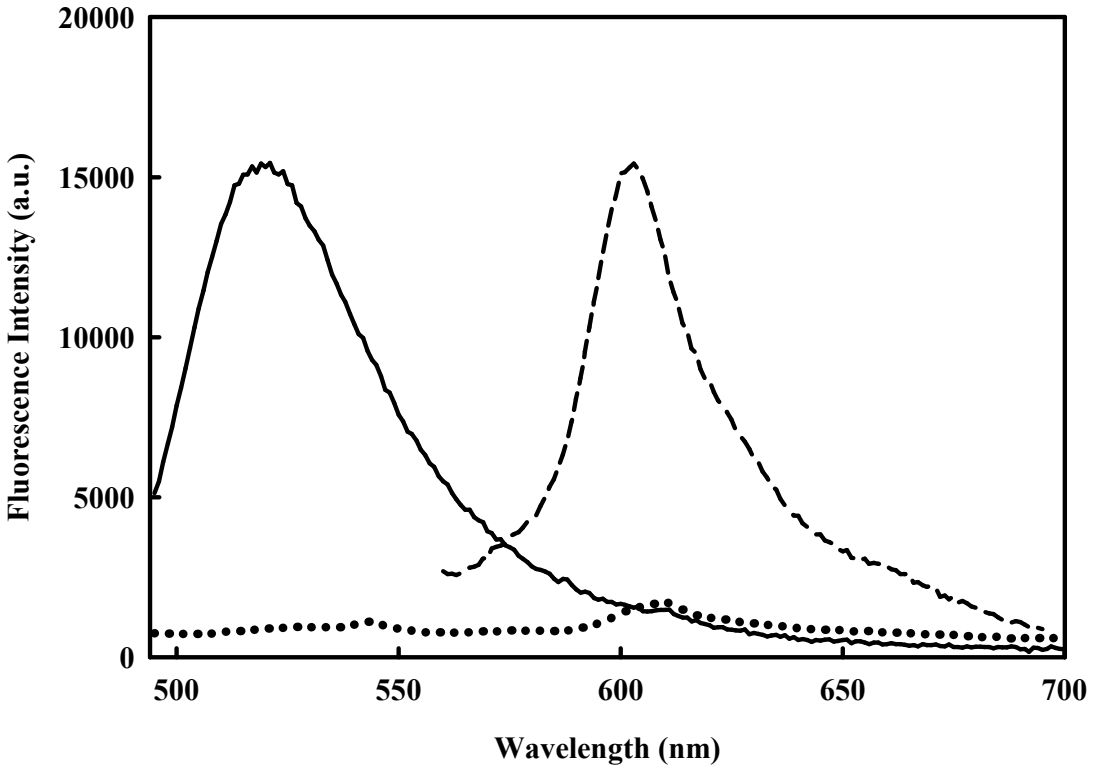

Figure 79. Fluorescence emission spectra of CCPGCC(FlAsH)-SNAP-25(1-140) and CCPGCC(ReAsH)-SNAP-25(141-206) in the absence of BoNT/A LC. The spectra were recorded at 25 ˚C. The buffer background was subtracted in all cases. The solid line corresponded to the mixture of CCPGCC(FlAsH)-SNAP-25(1-140) (**P26R-FlAsH**) and CCPGCC(ReAsH)-SNAP-25(141-206) (**P27R-ReAsH**); the dotted line corresponded to the emission of CCPGCC(ReAsH)-SNAP-25(141-206) (**P27R-ReAsH**) with excitation maximum wavelength at 480 nm; and the dashed line corresponded to the emission of CCPGCC(ReAsH)-SNAP-25(141-206) (**P27R-ReAsH**) with excitation maximum wavelength at 580 nm in the mixture. All samples contained 0.2 μM proteins.

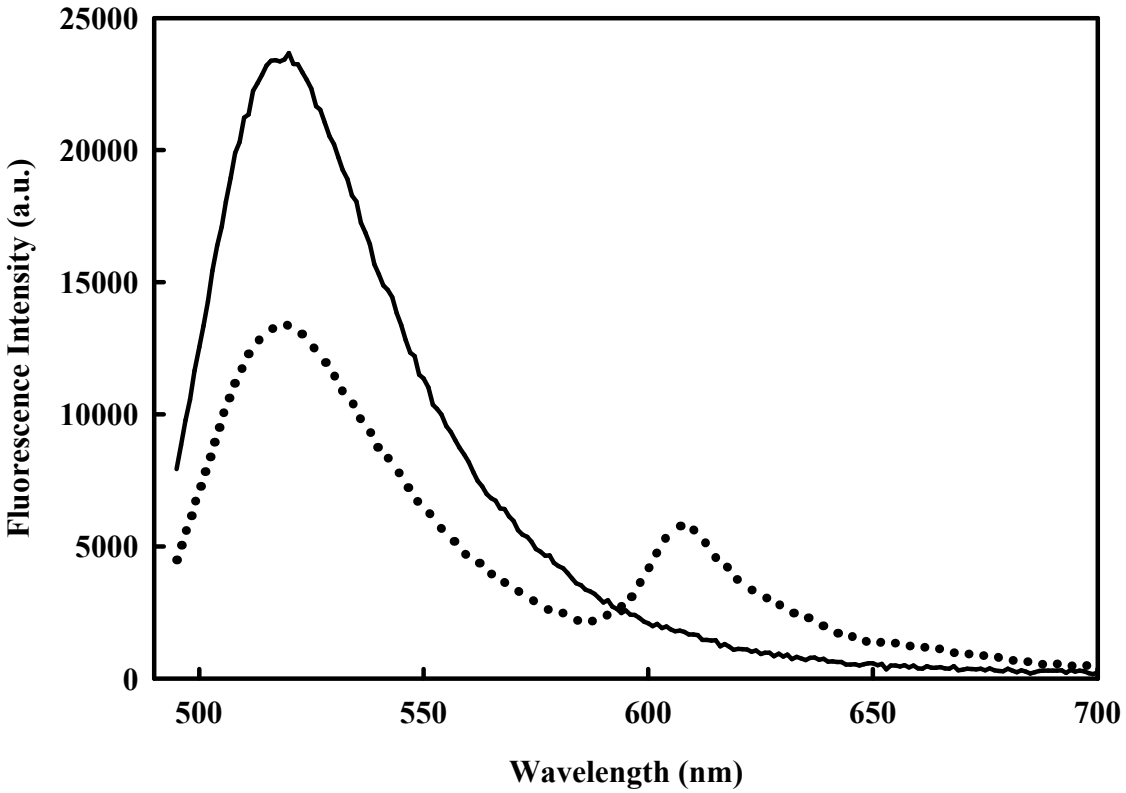

Figure 80. Fluorescence emission spectra of CCPGCC(FlAsH)-SNAP-25(1-140) and CCPGCC(ReAsH)-SNAP-25(141-206) in the presence of BoNT/A LC. The spectra were recorded with an excitation maximum wavelength of 480 nm at 25 ˚C. To a mixture of 0.2 μM CCPGCC(FlAsH)-SNAP-25(1-140) (**P26R-FlAsH**), 0.2 μM BoNT/A LC was added and incubated at 25 ˚C for 2 h. Then, 0.2 μM CCPGCC(ReAsH)-SNAP-25(141-206) (**P27R-ReAsH**) was added into the binary complex and incubated at 25 ˚C for 2 h. The buffer background was subtracted in all cases. The solid line corresponded to the binary complex of CCPGCC(FlAsH)-SNAP-25(1-140) (**P26R-FlAsH**) in the presence of BoNT/A LC and the dotted line corresponded to the ternary complex of CCPGCC(FlAsH)-SNAP-25(140)-BoNT/A LC-CCPGCC(ReAsH)-SNAP-25(141-206).

5.3 Discussion

SNAP-25 plays a key role in membrane fusion (2). BoNT/A can specifically cleave SNAP-25 and block membrane fusion. The conformation of SNAP-25 is important to understanding the membrane fusion process.

We investigated the binding of the full-length, the N-terminal, and the C-terminal domains of SNAP-25 to BoNT/A LC. The binary complex of SNAP-25(1-140)-BoNT/A LC, SNAP-25(141-206)-BoNT/A LC and the ternary complex SNAP-25(1-140)-BoNT/A LC-SNAP-25(141-206) displayed a large increase in α-helical content, indicating that the folding and complex formation of SNAP-25 are linked. We engineered SNAP-25 and its N-terminal and C-terminal fragments with CCPGCC modification on the N-terminus of each protein. The CD data demonstrated that the formation of a binary complex between CCPGCC-SNAP-25(1-140) (**P26R**) and BoNT/A LC was associated with an increase in α-helical content, which presumably mainly occurred in SNAP-25. The results were similar for CCPGCC-SNAP-25(141-206) (**P27R**) and BoNT/A LC. The dissociation constant obtained by monitoring the fluorescence intensity changes of FlAsH ranged between 1.0 and 2.0 μM. The results indicate that not only the C-terminal domain, but also the N-terminal domain of SNAP-25 participate in binding to BoNT/A LC.

Higher α-helical components indicate a slow formation for the N-terminus and the C-terminus of SNAP-25 and BoNT/A LC. The second order rate constants obtained for CCPGCC-SNAP-25(141-206) and CCPGCC-SNAP-25(1-140) were 173.3 and 236.7 $M^{-1} \cdot s^{-1}$, respectively (**Figure 74**), compared with the N-terminal binding constant of 56.7 $M^{-1} \cdot s^{-1}$ (**Figure 78**). The results suggest that the binding process is slower than the folding process. Only correctly folded SNAP-25 is able to bind to BoNT/A LC slowly and tightly.

This folding and binding mode may be used to investigate other intrinsically disordered proteins.

How does the N-terminus of SNAP-25 bind to LC? What are the binding sites between LC and the N-terminal domain of SNAP-25? The answers to these questions are not clearly explained in the literature. It is possible to conclude that the linker domain binds to BoNT/A LC, as the linker domain is flexible in its overall conformation. The N-terminus of SNAP-25 is known to form one of the four helices bundles in the SNARE complex (2). The linker domain between residues 85 and 140 may change the conformation and bind to BoNT/A LC.

In order to prove that the N-terminus of SNAP-25 binds to BoNT/A LC, we investigated the ternary complex among the N-terminal and the C-terminal domain of SNAP-25 and BoNT/A LC. The N-terminal domain of SNAP-25 was labeled with CCPGCC-FlAsH. A binary complex of CCPGCC(FlAsH)-SNAP-25(1-140)-BoNT/A LC was formed in the presence of BoNT/A LC. The fluorescence intensity of the FlAsH (acceptor) was monitored in this binary complex. A ternary complex was obtained by incubating CCPGCC(ReAsH)-SNAP-25(141-206) with the binary complex. An apparent fluorescence resonance energy transfer (FRET) was observed. The FlAsH fluorescence intensity decreased with an emission maximum wavelength at 528 nm, accompanied by an increase at emission maximum wavelength at 607 nm. The results suggest that three components form a ternary complex and that the distance between the N-terminus and D140 of SNAP-25 was in the energy transfer range. This method may be used to investigate the conformational changes of other intrinsically disordered proteins.

Chapter 6. Summary

SNAP-25 assembles with syntaxin and synaptobrevin to form a four-helix bundle of the SNARE complex, which plays a key role in exocytosis of synaptic vesicles. Botulinum neurotoxins specifically cleave one of the SNARE proteins, resulting in an inhibition of membrane fusion. Small molecule inhibitors can be used to block the toxin's activity. The C-terminus of SNAP-25 wraps around the botulinum neurotoxin serotype A light chain (BoNT/A LC) (25), but it is unknown how the N-terminal domain of SNAP-25 responds to the presence of BoNT/A LC.

We developed a method to investigate the conformational changes of SNAP-25 in the absence and presence of Zn^{2+}-depleted BoNT/A LC, using fluorescence resonance energy transfer (FRET) between EGFP (green) and CCPGCC-ReAsH (red) at specific locations. We measured the apparent distances between the C-terminus and the N-terminus, the C-terminus and residue D140, and the N-terminus and residue D140, based on the fluorescence energy transfer efficiency. SNAP-25(A195S) was used to further test the tertiary structures in the absence and presence of BoNT/A LC. The secondary structures of the SNAP-25 fragments were measured by CD. The results suggest that a higher α-helical content form when the N-terminus and the C-terminus binds to BoNT/A LC. The N-terminus of SNAP-25 specifically binds to BoNT/A LC with a slow and tight binding. As an intrinsically disordered protein, SNAP-25's folding process was determined to be slightly faster than the binding process, which suggests that only correctly folded protein binds with BoNT/A LC.

For the inhibition studies, the present studies demonstrate that QAQ is evidently able to bind to Zn^{2+}-free BoNT/A LC and the peptide-BoNT/A LC complexes. The QAQ

inhibition of the protease activity is not due to chelation, nor to the removal of zinc ion from BoNT/A LC. QAQ binds at a hydrophobic pocket of BoNT/A LC. Molecular modeling studies of the QAQ-BoNT/A LC complex in the absence of the peptide have shown that QAQ may be coordinated by the Zn^{2+} in BoNT/A LC, while in the presence of the peptide, QAQ may not interact strongly with the Zn^{2+} in the Peptide-BoNT/A LC complex. Long peptides, such as Peptide C and C1, were found to bind very slowly and tightly to BoNT/A LC. The slow and tight binding of the long peptide could conceivably allow for a new approach in the design of peptide inhibitors. The insights gained regarding the interactions of quinolinols and peptides with the zinc protease of BoNT/A should aid in the general development of inhibitors of metalloproteases.

Appendix

A.1 Binding mode of QAQ to BoNT/A LC

All the experimental results suggested that QAQ was a non-competitive inhibitor, which bound to the BoNT/A LC and the complex of BoNT/A LC and substrate. The process was illustrated in **Figure A1**.

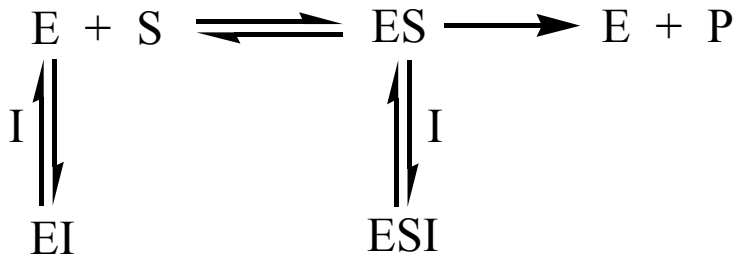

Figure A1. Diagram of non-competitive inhibitor and enzyme relationship. E, S and I represent the protease BoNT/A LC, SNAP-25 and QAQ, respectively. EI is the binary complex of SNAP-25-BoNT/A LC, which is shown in **Figure A3**. ESI represents the ternary complex of SNAP-25-BoNT/A LC-QAQ, which is shown in **Figure A4**.

A.2 Model of kinetics in the presence of two inhibitors

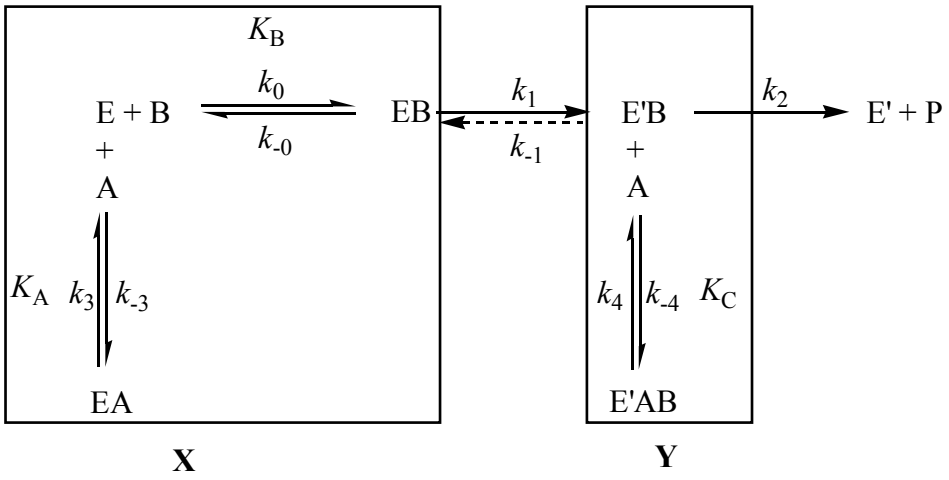

$$K_B = \frac{k_{-0}}{k_0} = \frac{[E][\mathrm{B}]}{[\mathrm{EB}]}, \text{ then } [E] = \frac{K_B[\mathrm{EB}]}{[\mathrm{B}]}$$

$$K_A = \frac{k_{-3}}{k_3} = \frac{[E][\mathrm{A}]}{[\mathrm{EA}]}, \text{ then } [EA] = \frac{[E][\mathrm{A}]}{\mathrm{K_A}} = \frac{[A]}{K_A} \cdot \frac{K_B[EB]}{[B]} = \frac{K_B[A][EB]}{K_A[B]}$$

$$\mathrm{X} = [E] + [EA] + [EB] = \frac{K_B[EB]}{[B]} + \frac{K_B[A][EB]}{K_A[B]} + [EB]$$

$$\mathrm{X} = \left(\frac{K_B}{[B]} + \frac{K_B[A]}{K_A[B]} + 1 \right) [EB]$$

$$[EB] = \frac{K_A[B][E_0]}{K_A K_B + K_B[A] + K_A[B]} \qquad \text{(A1)}$$

$$K_C = \frac{[E'B][A]}{[E'AB]}$$

$$\mathrm{Y} = [E'B] + [E'AB] = [E'B] + \frac{[E'B][A]}{K_C} = \left(1 + \frac{[A]}{K_C} \right) [E'B]$$

$$[E'B] = \frac{\mathrm{Y}}{1+\frac{[A]}{K_C}} = \frac{K_C \cdot \mathrm{Y}}{K_C + [A]} \qquad \text{(A2)}$$

$$\mathbf{X} \underset{k_{-1}}{\overset{k_1}{\rightleftharpoons}} \mathbf{Y} \xrightarrow{k_2} \mathrm{E'} + \mathrm{P}$$

$$[E]_0 = [X] + [Y]$$

$$v = \frac{d[P]}{dt} = k_2[Y] = k_1[X'] - (k_{-1} + k_2)[Y'] = k_1[EB] - (k_{-1} + k_2)[E'B] \qquad \text{(A3)}$$

(A1) and (A2) were induced into equation (A3):

$$v = k_1\left(\frac{K_A[B]}{K_A K_B + K_B[A] + K_A[B]}\right)[X] - (k_{-1} + k_2)\left(\frac{K_C}{K_C + [A]}\right)[Y]$$

In this equation: A stands for the inhibitor QAQ, B stands for Peptide C.

$$[X] + [Y] \approx [E]_0 = 0.2$$

$$k_1 = k_{\mathrm{on}} = 0.0046, \quad k_{-1} = k_{off} = 0.0046 \times 0.0249 = 1.15 \times 10^{-4}, \quad k_2 \to 0$$

$$K_A = 0.02,\ K_B = 0.025,\ K_C = 4.0$$

$$y = 0.0046 \times \left(\frac{0.02 \times [B]}{0.02 \times 0.025 + 0.025x + 0.02 \times [B]}\right)[X] - \left(\frac{0.000115 \times 4}{4 + x}\right)[0.2 - X]$$

Plotting the fluorescence against the concentration of inhibitors, a slow binding model can be obtained.

A.3 Binding mode of QAQ to BoNT/A LC

Geometrically minimized binding mode of QAQ obtained using the QM/MM method. This compound has very few rotatable bonds, hence it possesses restricted conformations that reduce the number of potential binding modes it may assume in the enzyme's catalytic active site. The results are shown in **Figure A3**.

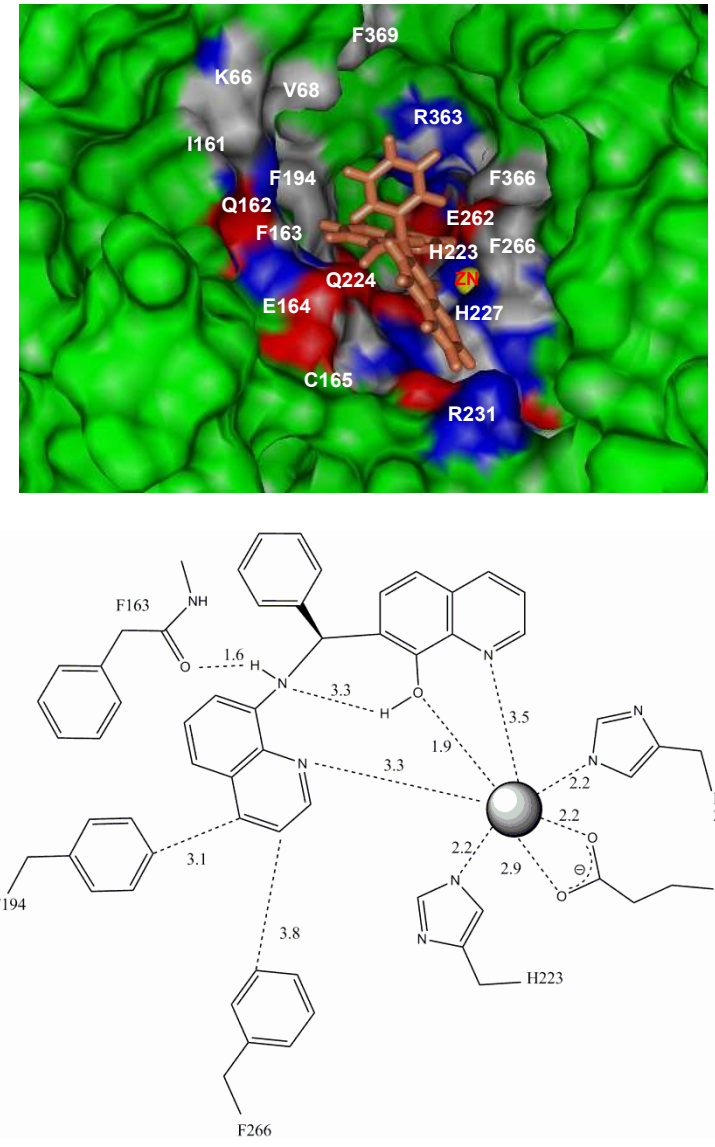

Figure A3. The binding mode of QAQ with BoNT/A LC from QM/MM simulations.

The oxygen and nitrogen atoms of the 8-hydroxyquinoline are within the distance of 2.0 and 3.5 Å, respectively, from the catalytic Zn^{2+}. The hydroxyl moiety may displace the water molecule that is used during catalysis. The benzene ring of the ligand points toward a hydrophobic pocket formed by the aromatic residues F366 and F369, and the non-polar residues L256 and V68. The cationic center of K66 is located near the centroid normal of the π system of the benzene ring but the ring plane is slightly twisted. However, the distance between ε-amino group and the aromatic ring system is within 4.5 Å and thus falls within the cation-π contact distance with the ring. The quionline moiety that is buried deep in the pocket forms a stacking interaction with H223, and is surrounded by hydrophobic ring clusters such as F163, F194 and F266. The 8-hydroxyquinoline ring is stacked with H227, makes hydrophobic contacts with the carbon atoms of E164, and cation-π contacts with R231. The cation-π interactions could make important contributions to increased affinity. The results show the binding mode of QAQ to BoNT/A LC with the distance to neighboring residues and Zn^{2+} and with the hydrophobic pocket binding the benzene ring.

The QAQ quinolinol ring N and hydroxyl O are 3.5 and 5.7 Å, respectively, away from the Zn^{2+} in the active site and could not chelate the Zn^{2+}. Quinolinol exocyclic N is hydrogen bonded to the carboxyl O of Asp370. Phe163 and Phe184 form a hydrophobic wall surrounding the quinolinol and quinoline rings. QAQ was thus deep in the hydrophobic pocket near the active site of BoNT/A LC in the presence of SNAP-25.

A.4 Binding mode of QAQ to the SNAP-25-BoNT/A LC complex

The binding mode of QAQ to the SNAP-25-BoNT/A LC complex (PDB 1XTG) was similarly examined by QM/MM method. The results are shown in **Figure A4**. The results indicate that the active site pocket in BoNT/A LC bound to SNAP-25 and the cavity can accommodate QAQ. However, the binding mode is different from that of the BoNT/A LC without peptide.

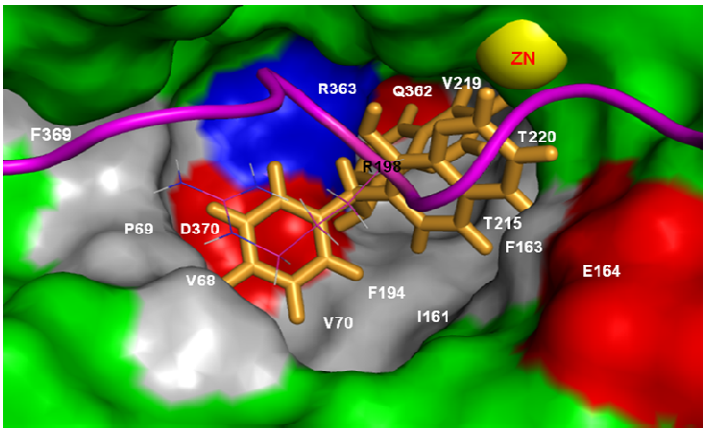

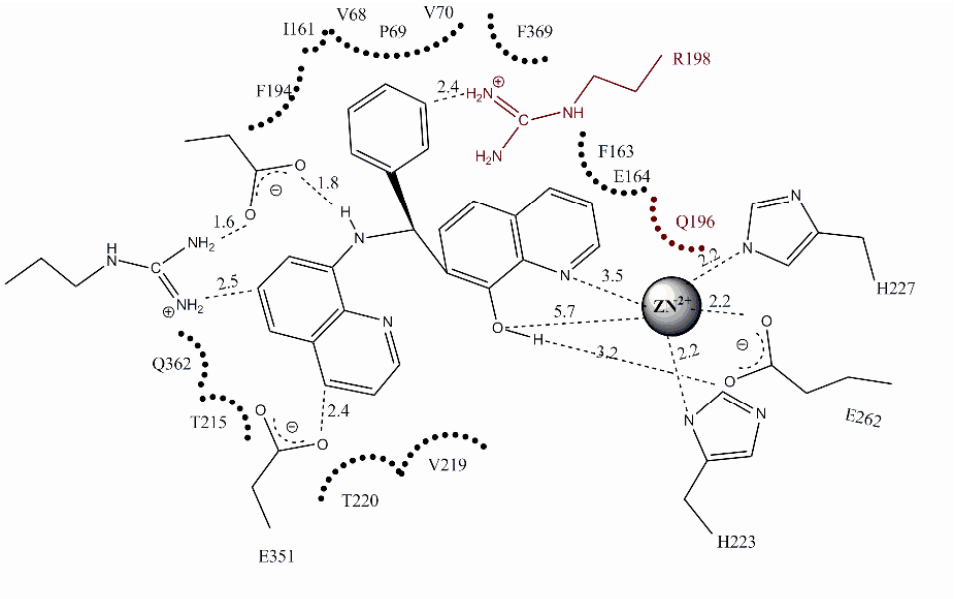

Figure A4. The binding mode of QAQ to the SNAP-25(141-204)-BoNT/A LC complex.

A.5 PAR assay

The chromophoric chelator 4-(2-pyridylazo)resorcinol (PAR) was used for the assessment of the metal ion content in metalloproteins (131). Botulinum neurotoxin serotype A light chain (BoNT/A LC) is a zinc metalloprotease. The method is very sensitive to the concentration of zinc ions in solution. The absorbance of the free PAR and the complex of PAR-Zn^{2+} was 416 nm (ε = 33, 700 $M^{-1}\cdot cm^{-1}$) and 497 nm (ε = 46, 700 $M^{-1}\cdot cm^{-1}$), respectively. The concentration of Zn^{2+} in the buffer can be determined based on band-shift of PAR in an excess of PAR. The method is shown in **Figure A5**.

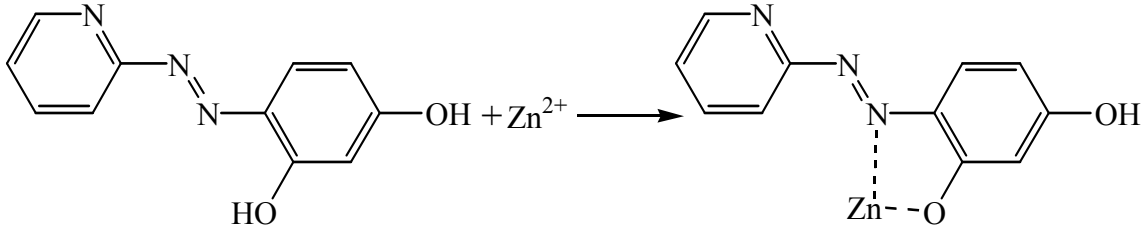

4-(2-pyridylazo)resorcinol (PAR) PAR-Zn^{2+} complex

Figure A5. Schematic diagram of PAR assay.

A.6 Peptide inhibitors from mRNA display

The substrate recognition by the catalytic domain is unusual in that it requires a minimum number of amino acids as substrates for cleavage. BoNT/A LC is a zinc-protease and CRATKML can bind to the active site, resulting in the inhibition of the protease. Zinc-chelator can bind to the Zn^{2+} located in the active site of protease. mRNA display approach allows libraries containing more than 10^{13} independent peptides to be constructed entirely *in vitro*, providing the highest sequence diversity. We designed the mRNA library containing a constant region with HHHHHHCRATKML to isolate peptides that bind to BoNT/A LC.

This method overcomes several limitations in the phage display such as folding, poor expression and display. High affinity peptide inhibitors in an mRNA-peptide library were screened for binding to the BoNT/A LC. The mRNA display library construction is shown in **Figure A6.1**.

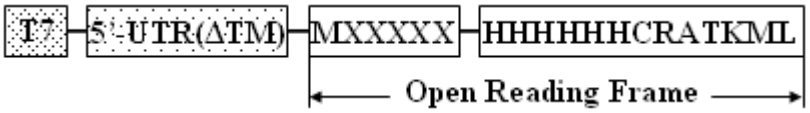

Figure A6.1 Library of mRNA display. The template of mRNA display library contains the following fragments: A T7 promoter is present at the 5' end to allow large-scale synthesis of mRNA *in vitro* using T7 polymerase. A 5'untranslated region of tobacco mosaic virus [5'UTR (ΔTMV)] is used to provide efficient translation initiation. The start codon ATG (AUG in mRNA) which indicates the initiation of protein synthesis following a variable region contains 3,200,000 (20^5) random nucleotide sequences. A constant region can encode HHHHHHCRATKML, which is essential for binding to protease. X represents a random amino acid.

The amino acid sequence CRATKML, derived from the C-terminus of the SNAP-25, was a known inhibitor of BoNT/A, which was incorporated into the constant region of the templates to screen for new inhibitors with improved inhibition efficiency. The HHHHHH region acts as the chelator for the zinc atom at the active site of the light chain. Five random amino acid residues were added in this template to increase the peptide diversity. So the library had an expected degeneracy of 3,200,000, which was reasonably small and contains all peptide sequences at significant concentrations for screening.

In the selection cycle, the double stranded DNA templates containing random sequences were transcribed, generating a pool of mRNA templates. These templates were then ligated to a flexible DNA oligonucleotide containing puromycin. Translation of these ligated templates *in vitro* produced a covalent bond between the mRNA and the peptide it encodes attached by means of their C terminus to puromycin. These fusions were then converted into mRNA-peptide fusions and selectively purified with an affinity matrix. The biotin tagged BoNT/A LC was immobilized on monomeric streptavidin, and incubated with the pool of mRNA-displayed peptides. Consequently, peptides that bound the light chain with high affinity were also immobilized while low affinity peptides flew through. Upon elution of the light chain with biotin-tag at native conditions, mRNA-peptides that bound to the BoNT/A LC with high affinity were simultaneously eluted, serving as template for reverse transcription and polymerase chain reaction (RT-PCR) amplification. The overall procedures of mRNA display are shown in **Figure A6.2**.

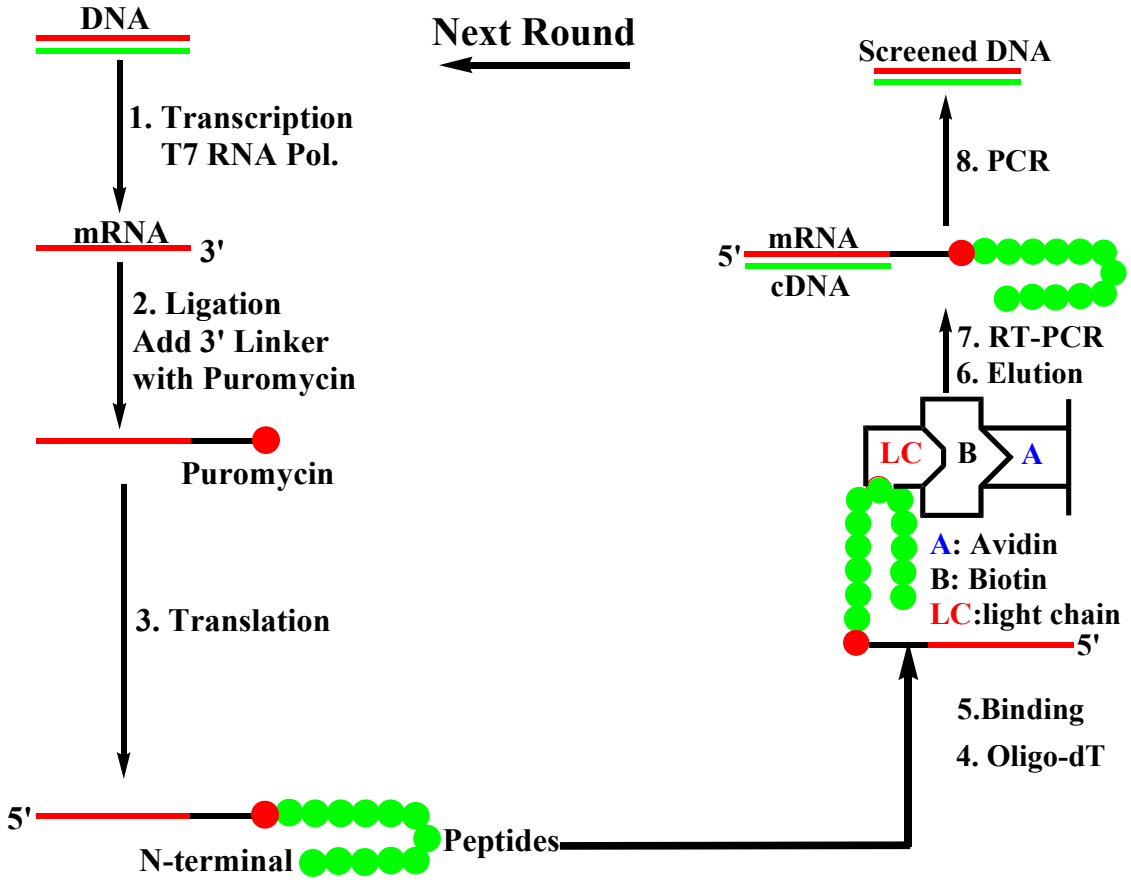

Figure A6.2 mRNA display. The library of dsDNA sequences was transcribed to generate mRNA (step 1), which was ligated to a puromycin oligonucleotide (step 2) and used in a translation reaction (step 3). The mRNA-peptide was sieved using the BoNT/A LC after the purification (step 4) and binding (step 5). The high affinity peptides with the light chain were eluted (step 6) and the cDNA-peptides were obtained using RT-PCR (step 7). PCR was used to regenerate the full-length DNA construct for the next round selection cycles (step 8).

The RT-PCR products were composed of double stranded DNA sequences of an enriched pool of peptides and amino acid residues of the peptides that bound to the BoNT/A LC were determined upon cloning the PCR products and sequencing a representative set of clones. To select for high affinity binding peptides to the BoNT/A LC, the library of mRNA displayed peptides were subjected to three cycles of binding to immobilized BoNT/A LC. The cycle was repeated and the stringency after each successive cycle was increased by gradually decreasing the incubation time between BoNT/A LC and the peptide library as well as increasing the extent of washing to select for high affinity peptides.

The DNA template contained a T7 promoter, a 5'-untranslated region of tobacco mosaic virus 5'-UTR (ΔTMV) and an open reading frame (ORF). The sense strand of DNA library template (TAATACGACTCACTATAACAATTACTATTTACAATTACA ATGNNSNNSNNSNNSNNSCACCATCACCATCACCACTGCCGCGCCACCAAGAT GCTG) was amplified using polymerase chain reaction (PCR) with the sense primer (5'-GGATCC TAATACGACTCACTATAACAATTACTATTTACAATTACA-3') and the antisense primer (5'-TAACATCTTTGTTGCTCTGCA-3'). The resulting double stranded DNA template were used to generate mRNA using *in vitro* transcription by T7 RNA polymerase according to manufactures instructions (Ambion). The transcripts were purified by polyacrylamide gel electrophoresis in TBE-Urea gel. The mRNA were excised from the gel, gel crushed and mRNA eluted overnight in 50 mM sodium acetate, pH 4.5, 20 M EDTA and 200 M KCl with shaking at 4 ºC. The sample was then centrifuged at 4 ºC and the supernatant, containing the mRNA transcripts, was ethanol precipitated twice. The purified mRNA transcripts were ligated to a phosphorylated

DNA-puromycin linker [5'dA21$(C9)_3$dACAdCP-3', C9 = triethylene glycol phosphate, P = Puromycin] via a DNA splint (5'TTTTTTTTTTTAACATCTTTGT-3') using T4 DNA ligase to generate an mRNA fusion template for *in vitro* translation. The flexible linker and splint were synthesized by QIAGEN and the ligation reaction was carried in a 1 : 0.3 : 1.1 ratio of mRNA, linker and splint with 1.6 U of T4 DNA ligase per picomole of mRNA template for 2 h at 25 °C. Ligated products were purified by 15% TBE-Urea gel (Invitrogen) electrophoresis and used as template for *in vitro* translation with rabbit recticulocyte lysate (Novagen) under optimized conditions according to manufactures instructions. After translation, magnesium acetate was added to the reaction mixture at a 50 mM final concentration and incubated overnight at −20 ºC to maximize mRNA−peptide puromycin fusion formation. mRNA-peptide fusion consists of a peptide sequence covalently linked via its C terminus to the 3' end of its own messenger RNA. The displayed mRNA-peptide fusion was purified from the translation mixture using an oligo-dT chromatography column (New England Biolabs).

Purified biotin-tagged BoNT/A light chain was immobilized on Softlink monomeric avidin (Promega) and incubated with the displayed peptides for 60 min in buffer (25 mM Hepes, pH 8.0, 250 mM NaCl, 1 mM DTT and 0.1% triton X-100). The mixture was loaded onto a chromatography column and washed 10 times with 10 volumes of the same buffer. mRNA-peptide bound to the light chain was eluted off the column with 5 mM biotin in the same buffer.

The enriched library was subjected to more rounds of screening to select for high affinity binding peptides. In the second and third round the enriched libraries of peptides were incubated for 30 and 10 min, respectively, with the immobilized light chain. After

each round the mRNA sequences with bound peptides were reverse transcribed and amplified by RT-PCR, cloned into the TOPO vector (Invitrogen). Colonies were chosen at random from the plate for sequencing. After three-round screening, a few of peptide inhibitors were selected. The sequences are summarized in **Table A6**.

Table A6 Peptide sequences from mRNA display.

code	Round 1	Round 2	Round 3
1	M S W K E L	M S W K E L	M S W K E L (4)
2	M R Q A S A	M R T I D M	M R T I D M
3	M R Q D A R	M R A D G R	M R Q D A R (4)
4	M Q A A M P	M Q M S W V (2)	M R V R W E
5	M V Q S A S	M V L Q S G	M V L Q S G
6	M W Q D R L	M W Q D R L	M W H V N L
7	M A P V S W	M A V L K E	M H E M G L
8	M G P T S G	M D R S I Q	M R H H A K
9	M P M A T W	M E W L W R	M R W L G K
10	M R S T F L	M G Q V G A	M S Q M V A
11	M R F C N A	M G V D L L	M T L K Q V
12	M W M V S G	M H S T Y L	M V P R D H

The number in the parenthesis indicates the numbers of peptides appeared in the same round. The constant region containing HHHHHHCRATKML is not included at the 3'end of the peptides.

The screened peptides are potential inhibitor with tighter binding than that of CRATKML. The further inhibition can be screened using enzyme-linked immunosorbent assay (ELISA). However, the peptides showed insignificant inhibition *in vivo*. The results suggest that peptide may be degraded before binding to the active site of protease *in vivo*. The results directed us to screen the non-peptide small molecule inhibitors to block the activity of BoNT/A LC.

A.7 Synthesized small molecules inhibitors with quinolinol scaffold

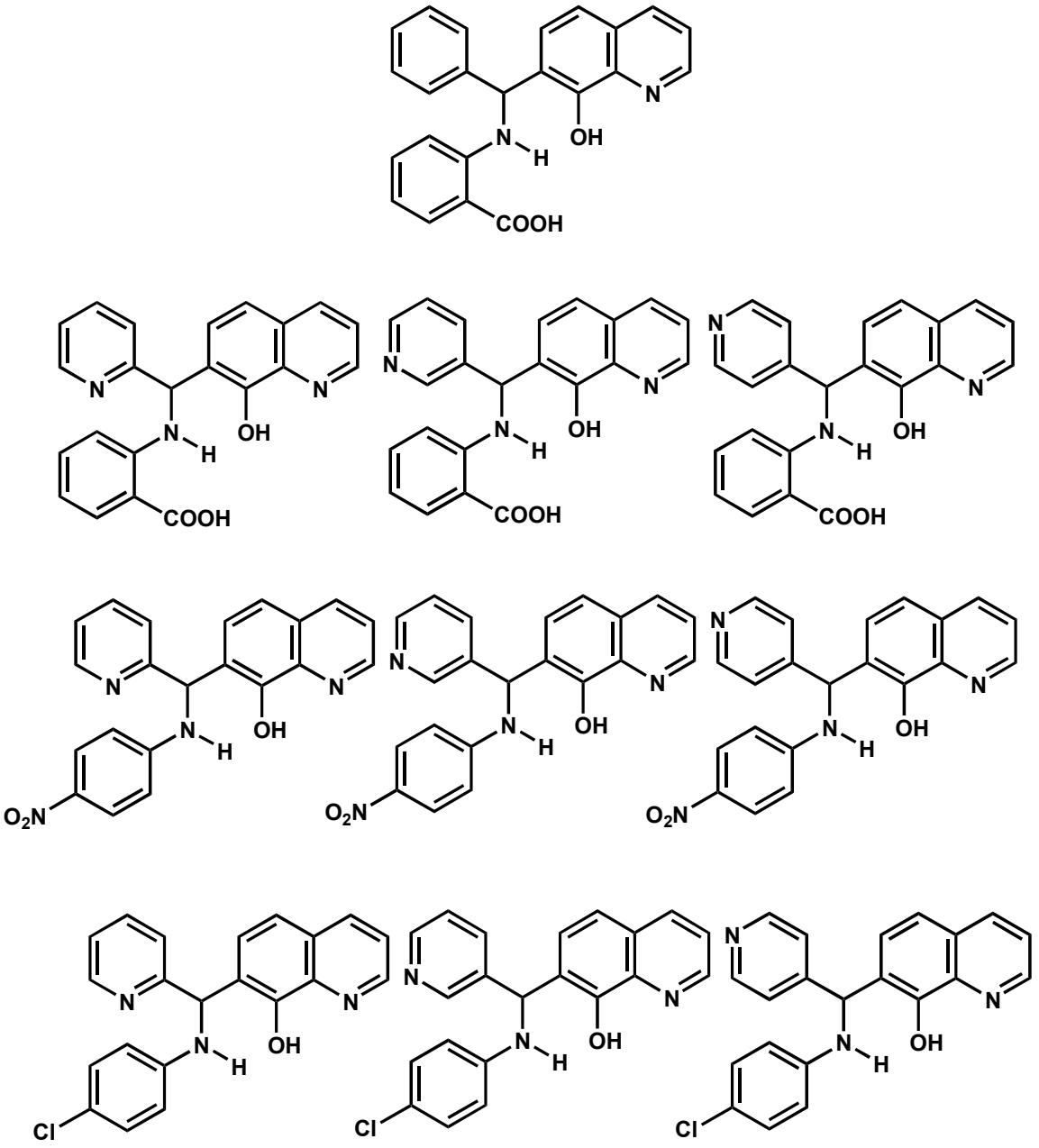

Figure A7. Synthesized small molecule inhibitors with quinolinol scaffold.

The small molecule inhibitors (**Figure A7**) were synthesized in order to screen a second generation inhibitors of BoNT/A LC, which were supposed to show better inhibition than that of QAQ. The results suggested that the inhibitors were not better than

QAQ based on the catalytic efficiency (K_i) against BoNT/A LC *in vitro*. We tried to measure the fluorescence energy transfer between the anthranilic acid moiety of the inhibitor and the tryptophans of BoNT/A LC when the inhibitor binding to BoNT/A LC. However, it was difficult to measure the interactions between the inhibitor and BoNT/A LC since the background of fluorescence intensity increased more than that of fluorescence quenching. We realized that the anthranilic acid might be hydrolyzed before it bound to BoNT/A LC. So the binding and hydrolyzation of anthranilic acid moiety became complicated in this case. But the idea of fluorescence energy transfer leads us to design the fluorescence probes in the substrate of BoNT/A LC.

A.8 Predictor of naturally disordered regions (PONDR) prediction of SNAP-25

"Access to PONDR® was provided by Molecular Kinetics (6201 La Pas Trail - Ste 160, Indianapolis, IN 46268; 317-280-8737; E-mail: main@molecularkinetics.com). VL-XT is copyright©1999 by the WSU Research Foundation, all rights reserved. PONDR® is copyright©2004 by Molecular Kinetics, all rights reserved."

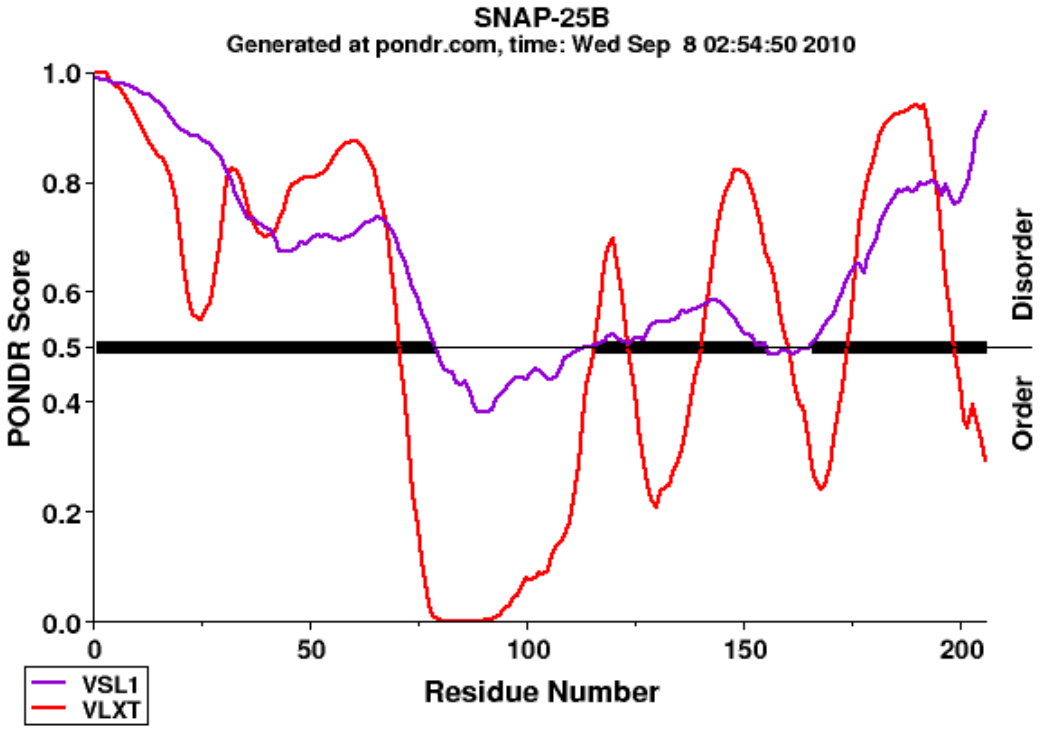

Figure A8. Prediction of intrinsically disordered domains of SNAP-25.

The output of a residue value exceeds 0.5, the residue is considered disordered. The prediction indicates that the N-terminal domain of SNAP-25 is a disordered region, which is expected to be more difficult to get crystallized. The linker region of the SNAP-25 is an ordered domain based on the prediction. The ordered and disordered domains can help us to predict the possible conformations of SNAP-25.

Chapter 7. Bibliography

1. Südhof T. C.; Rothman, J. E. Membrane fusion: grappling with SNARE and SM proteins. *Science* **2009**, *323*, 474-477.
2. Sutton, R. B.; Fasshauer, D.; Jahn, R.; Brunger, A. T. Crystal structure of a SNARE complex involved in synaptic exocytosis at 2.4 Å resolution. *Nature* **1998**, *395*, 347-353.
3. Schiavo, G.; Rossetto, O.; Catsicas, S.; De Laureto, P. P.; DasGupta, B. R.; Benfenati, F.; Montecucco, C. Identification of the nerve terminal targets of botulinum neurotoxin serotypes A, D. and E. *J. Biol. Chem.* **1993**, *268*, 23784-23787.
4. Bennett, M. K.; García-Arrarás, J. E.; Elferink, L. A.; Peterson, K.; Fleming, A. M.; Hazuka, C. D.; Scheller, R. H. The syntaxin family of vesicular transport receptors. *Cell* **1993**, *74*, 863-873.
5. Fernandez, U.; Ubach, J.; Dulubova, I.; Zhang, X.; Südhof T. C.; Rizo, J. Three-dimensional structure of an evolutionarily conserved N-terminal domain of syntaxin 1A. *Cell* **19983**, *94*, 841-849.
6. Lerman, J. C.; Robblee, J.; Fairman, R.; Hughson, F. M. Structural analysis of the neuronal SNARE protein syntaxin-1A. *Biochemistry* **2009**, *53,* 3478-3486.
7. Milsura, K. M.; Scheller, R. H.; Weis, W. I. Three-dimensional structure of the neuronal-Sec1-syntaxin 1a complex.. *Nature* **2000**, *404*, 355-362.
8. Han, X.; Wang, C. –T.; Bai, J.; Chapman, E. R.; Jackson, M. B. Transmembrane segments of syntaxin line the fusion pore of Ca^{2+}-triggered exocytosis. *Science* **2004**, *304*, 289-292.

9. Stein, A.; Weber, G.; Wahl, M. C.; Jahn, R. Helical extension of the neuronal SNARE complex into the membrane. *Nature* **2009**, *460*, 525-528.

10. Baumert, M.; Maycox, P. R.; Navone, F.; De Camilli, P.; Jahn, R. Synaptobrevin: an integral membrane protein of 18000 daltons in small synaptic vesicles of rat brain. *EMBO J.* **1989**, *8*, 379-384.

11. Hanson, M. A.; Stevens, R. C. Cocrystal structure of synaptobrevin-II bound to botulinum neurotoxin type B at 2.0 Å resolution. *Nat. Struc. Biol.* **2000**, *7,* 687-792.

12. Bark, I. C.; Hahn, K. M.; Ryabinin, A. E.; Wilson, M. C. Differential expression of SNAP-25 protein isoforms during divergent vesicle fusion events of neural development. *Proc. Natl. Acad. Sci. USA* **1995**, *92*, 1510-1514.

13. Hodel A.; SNAP-25. *Int. J. Biochem. Cell Biol.* **1998,** *30,* 1069-1073.

14. Blasi, J.; Chapman, E. R.; Link, E.; Binz, T.; Yamasaki, S.; Camilli, P. D.; Südhof, T. C.; Niemann, H.; Jahn, R. Botulinum neurotoxin A selectively cleaves the snaptic protein SNAP-25. *Nature* **1993,** *365,* 1601-63.

15. Binz, T.; Blasi, J.; Yamasaki, S.; Baumeister, A.; Link, F.; Sudhof, T. C.; Jahn, R.; Niemann, H. Proteolysis of SNAP-25 by types E and A botulinal neurotoxins. *J. Biol. Chem.* **1994,** *269,* 1617-1620.

16. Lane, S. R.; Liu, Y. Characterization of the palmitoylation domain of SNAP-25. *J. Neurochem.* **1997,** *69,* 1864-1869.

17. Veit, M.; Sollner, T. H.; Rothman, J. E. Multiple palmitoylation of synaptotagmin and the *t*-SNARE SNAP-25. *FEBS Lett.* **1996,** *385,* 119-123.

18. Nagy, G.; Milosevic, I.; Mohrmann, R.; Wiederhold, K.; Walter, A. M.; Sørensen, J. B. The SNAP-25 linker as an adaptation toward fast exocytosis. *Mol. Biol. Cell* **2008,** *19,* 3769-3781.

19. Gonzalo, S.; Greentree, W. K.; Linder, M. E. SNAP-25 is targeted to the plasma membrane through a novel membrane-binding domain. *J. Biol. Chem.* **1999,** *274,* 21313-21318.

20. Fasshauer, D.; Bruns, D.; Shen, B.; Jahn, R.; Brünger, A. T. A structural change occurs upon binding of syntaxin to SNAP-25. *J. Biol. Chem.* **1997,** *272,* 4582-4590.

21. Fasshauer, D.; Margittai, M. A transient N-terminal interaction of SNAP-25 and syntaxin nucleates SNARE assembly. *J. Biol. Chem.* **2004,** *279,* 7613-7621.

22. Weninger, K.; Bowen, M. E.; Choi, U. B.; Chu, S.; Brünger, A. T. Accessory proteins stabilize the acceptor complex for synaptobrevin, the 1:1 syntaxin/SNAP-25 complex. *Structure* **2008,** *16,* 308-320.

23. Nicholson, K. L.; Munson, M.; Miller, R. B.; Filip, T. J.; Fariman, R.; Hughson, F. M. Regulation of SNARE complex assembly by an N-terminal domain of the t-SNARE Sso1p. *Nat. Stuct. Biol.* **1998,** *5,* 793-802.

24. Xiao, W.; Poirier, M. A.; Bennett, M. K.; Shin, Y. –K. The neuronal t-SNARE complex is a parallel four-helix bundle. *Nat. Stuct. Biol.* **2001,** *8,* 308-311.

25. Breidenbach, M. A.; Brünger, A. T. Substrate recognition strategy for botulinum neuroxoin serotype A. *Nature* **2004,** *432,* 925-929.

26. Washbourne, P.; Pellizzari, R.; Baldini, G.; Wilson, M. C.; Montecucco, C. Botulinum neurotoxin types A and E require the SNARE motif in SNAP-25 for proteolysis. *FEBS Lett.* **1997,** *418,* 1-5.

27. O'Sullivan, G. A.; Mohammed, N.; Foran, P. G.; Lawrence, G. W.; Dolly, J. O. Rescue of exocytosis in botulinum toxin A-poisoned chromaffin cells by expression of cleavage-resistant SNAP-25: identification of the minimal essential C-terminal residues. *J. Biol. Chem.* **1999,** *274,* 36897-36904.

28. Chen, S.; Barbieri, J. T. Unique substrate recognition by botulinum neurotoxins serotype A and E. *J. Biol. Chem.* **2006,** *281,* 10906-10911.

29. Dong, M.; Tepp, W. H.; Johnson, E. A.; Chapman, E. R. Using fluorescent sensors to detect botulinum neurotoxin activity *in vitro* and in living cells. *Proc. Natl. Acad. Sci. USA* **2004**, *101*, 14701-14706.

30. Boldt, G. E.; Kennedy, J. P.; Janda, K. D. Identification of a potent botulinum neurotoxin A protease inhibitor using in situ lead identification chemistry *Org. Lett.* **2006,** *8,* 1729-1732.

31. Chen, S.; Kim, J. P.; Barbieri, J. T. Mechanism of substrate recognition by botulinum neurotoxin serotype A. *J. Biol. Chem.* **2007,** *282,* 9621-9627.

32. Chen, S.; Barbieri, J. T. Multiple pocket recognition of SNAP-25 by botulinum neurotoxin serotype E. *J .Biol. Chem.* **2007,** *282,* 9621-9627.

33. Pires-Alves, M.; Ho, M.; Aberle, K. K.; Janda, K. D.; Wilson, B. A. Tandem fluorescent proteins as enhanced FRET-based substrates for botulinum neurotoxin activity. *Toxicon* **2009,** *53,* 392-399.

34. Simpson, L. L. Molecular pharmacology of Botulinum Toxin and Tetanus Toxin. *Annu, Rev. Pharmacol. Toxicol*. 1986, 26, 427-453.

35. Bossi, P.; Garin, D.; Guihot, A.; Gay, F.; Crance, J. M.; Debord, T.; Autran, B.; Bricaire, F. Bioterrorism: management of major biological agents. *Cell. Mol. Life Sci.* **2006,** *63,* 2196-2212.

36. Turton, K.; Chaddock, J. A.; Acharya, K. R. Botulinum and tetanus neurotoxins: structure, function and therapeutic utility. *Trend. Biochem. Sci.* **2002**, *27*, 552-558.

37. Lacy, D. B.; Tepp, W.; Cohen, A. C.; DasGupta, B. R.; Stevens, R. C. Crystal structure of botulinum neurotoxin type A and implications for toxicity. *Nat. Struct. Biol.* **1998,** *5,* 898-902.

38. Segelke, B.; Knapp, M.; Kadkhodayan, S.; Balhorn, R.; Rupp, B. Crystal structure of clostridium botulinum neurotoxin protease in a product-bound state: evidence for noncanonical zinc protease activity. *Proc. Natl. Acad. Sci. USA* **2004**, *101*, 6888-6893.

39. Fu, Z.; Chen, S.; Baldwin, M. R. Boldt, G. E.; Crawford, A.; Janda, K. D.; Barbieri, J. T.; Kim, J. –J. Light chain of botulinum neurotoxin serotype A: structural resolution of a catalytic intermediate. *Biochemistry* **2006,** *45,* 8903-8911.

40. Swaminathan S.; Eswaramoorthy, S. Structural analysis of the catalytic and binding sites of *Clostridium botulinum* neurotoxin B. *Nat. Struct. Biol.* **2000**, *7*, 693-699.

41. Jin, R.; Sikorra, S.; Stegmann, C. M.; Pich, A.; Binz, T.; Brunger, A. T. Structural and biochemical studies of botulinum neurotoxin serotype C1 light chain protease: implications for dual substrate specificity. *Biochemistry* **2007,** *46,* 10685-10693.

42. Arndt, J. W.; Cai, Q.; Christian, T.; Stevens, R. C. Structure of Botulinum neurotoxin type D light chain at 1.65 Å resolution: repercussions for VAMP-2 substrate specificity. *Biochemistry* **2006,** *45,* 3255-3262.

43. Agarwal, R.; Eswaramoorthy, S.; Kumaran, D.; Binz, T.; Swaminathan, S. Structural analysis of botulinum neurotoxin type E catalytic domain and its mutant Glu212→Gln reveals the pivotal role of the Glu212 carboxylate in the catalytic pathway. *Biochemistry* **2004,** *43,* 6637-6644.

44. Agarwal, R.; Binz, T.; Swaminathan, S. Structural analysis of botulinum neurotoxin serotype F light chain: implications on substrate binding and inhibitor design. *Biochemistry* **2005,** *44,* 11758-11765.

45. Arndt, J. W.; Yu, W.; Bai, F.; Stevens, R. C. Crystal structure of botulinum neurotoxin type G light chain: serotype divergence in substrate recognition. *Biochemistry* **2005,** *44,* 9574-9580.

46. Schiavo, G.; Rossetto, O.; Santucci, A.; DasGupta, B. R.; Montecucco, C. Botulinum neurotoxins are zinc proteins. *J. Biol. Chem.* **1992,** *267,* 23479-23483.

47. Simpson, L. L. Identification of the major steps in botulinum toxin action. *Ann. Rev. Pharmacol. Toxicol.* **2004,** *44,* 167-193.

48. Schiavo, G.; Benfenati, F.; Poulain, B.; Rossetto, O.; de Laureto, P. P.; DasGupta, B. R.; Montecucco, C. Teanus and botulinum-B neurotoxins block

neurotransmitter release by proteolytic cleavage of synaptobrevin. *Nature* **1992,** *359,* 832-835.

49. Schiavo, G.; Shone, C. C.; Bennett, M. K.; Scheller, R. H.; Montecucco, C. Botulinum neurotoxin type C cleaves a single Lys-Ala bond within the carboxyl-terminal region of syntaxins. *J. Biol. Chem.* **1995,** *270,* 10566-10570.

50. Schiavo, G.; Rossetto, O; Catsicas, S.; de Laureto, P. P.; DasGupta, B. R.; Benfenati, F.; Montecucco, C. Identification of the nerve terminal target of botulinum neurotoxin serotypes A, D, and E. *J. Biol. Chem.* **1993,** *268,* 23784-23787.

51. Schmidt, J. J.; Stafford, R. G. Botulinum neurotoxin serotype F: identification of substrate recognition requirements and development of inhibitors with low nanomolar affinity. *Biochemistry* **2005,** *44,* 4067-4073.

52. Schiavo, G.; Malizio, C.; Trimble, W. S.; de Laureto, P. P.; Milan, G.; Sugiyama, H. Johnson, E. A.; Montecucco, C. Botulinum G neurotoxin cleaves VAMP/synaptobrevin at a single Ala-Ala peptide bond. *J. Biol. Chem.* **1994,** *269,* 20213-20216.

53. Zuniga, J. E.; Schmidt, J. J.; Fenn, T.; Burnett, J. C.; Arac, D.; Gussio, R.; Stafford, R. G.; Badie, S. S.; Bavari, S.; Brunger, A. T. A potent peptidomimetic inhibitor of botulinum neurotoxin serotype A has a very different conformation than SNAP-25 substrate. *Structure* **2008,** *16,* 1588-1597.

54. Silvaggi, N. R.; Wilson, D.; Tzipori, S.; Allen, K. N. Catalytic features of the botulinum neurotoxin A light chain revealed by high resolution structure of an inhibitory peptide complex. *Biochemistry* **2008,** *47,* 5736-5745.

55. Eswaramoorthy, S.; Kumaran, D.; Swaminathan, S. A novel mechanism for *clostridium botulinum* neurotoxin inhibition. *Biochemistry* **2002,** *41,* 9795-9802.

56. Arnon, S. S.; Schechter, R.; Inglesby, T. V.; Henderson, D. A.; Bartlett, J. G.; Ascher, M. S.; Eitzen, E.; Fine, A. D.; Hauer, J.; Layton, M.; Lillibridge, S.; Osterholm, M. T.; O'Toole, T.; Parker, G.; Perl, T. M.; Russell, P. K.; Swerdlow, D. L.; Tonat, K. Botulinum Toxin as a biological weapon: medical and public health management. *J. Am. Med. Assoc.* **2001,** *285,* 1059-1070.

57. Garcia-Rodriguez, C.; Levy, R.; Arndt, J. W.; Forsyth, C. M.; Razai, A.; Lou, J.; eren, I.; Stevens, R. C.; Marks, J. D. Molecular evolution of antibody cross-reactivity for two subtypes of type A botulinum neurotoxin. *Nat. Biotechnol.* **2006,** *25,* 107-116.

58. Nowakowski, A.; Wang, C.; Powers, D. B.; Amersdorfer, P.; Smith, T. J.; Montgomery, V. A.; Sheridan, R.; Blake, R.; Smith, L. A.; Marks, J. D. Potent neutralization of botulinum neurotoxin by recombinant oligoclonal antibody. *Proc. Natl. Acad. Sci. USA* **2002**, *99*, 11346-11350.

59. Amersdorfer, P.; Wong, C.; Smith, T.; Chen, S.; Deshpande, S.; Sheridan, R.; Marks, J. D. Genetic and immunological comparison of anti-botulinum type A antibodies from immune and non-immune human phage libraries. *Vaccine* **2002**, *20,* 1640-1648.

60. Schmidt, J. J.; Stafford, R. G.; Bostian, K. A. Type A botulinum neurotoxin proteolytic activity: development of competitive inhibitors and implications for substrate specificity at the S_1' binding subsite. *FEBS Lett.* **1998,** *435,* 61-64.

61. Schmidt, J. J.; Stafford, R. G. A high-affinity competitive inhibitor of type A botulinum neurotoxin protease activity. *FEBS Lett.* **2002,** *532,* 423-426.

62. Yiadom, K. P. A. B.; Muhie, S.; Yang, D. C. H. Peptide inhibitors of botulinum neurotoxin by mRNA display. *Biochem. Biophys. Res. Commun.* **2005,** *335,* 1247-1253.

63. Burnett, J. C.; Schmidt, J. J.; McGrath, C. F.; Nguyen, T. L.; Hermone, A. R.; Panchal, R. G.; Vennerstrom, J. L.; Kodukula, K.; Zaharevitz, D. W.; Gussio, R.; Bavari, S. Conformational sampling of the botulinum neurotoxin serotype A light chain: implications for inhibitor binding. *Bioorg. Med. Chem.* **2005,** *13,* 333-341.

64. Kumaran, D.; Rawat, R.; Ahmed, S. A.; Swaminathan, S. Substrate binding mode and its implication on drug design for botulinum neurotoxin A. *PLoS Pathog.* **2008,** *4,* e1000165.

65. Boldt, G. E.; Kennedy, J. P.; Janda, K. D. Identification of a potent botulinum neurotoxin A protease inhibitor using in situ lead identification chemistry. *Org. Lett.* **2006,** *8,* 1729-1732.

66. Silvaggi, N. R.; Boldt, G. E.; Hixon, M. S.; Kennedy, J. P.; Tzipori, S.; Janda, K. D.; Allen, K. N. Structures of *clostridium botulinum* neurotoxin serotype A light chain complexed with small-molecule inhibitors highlight active-site flexibility. *Chem. Biol.* **2007,** *14,* 533-542.

67. Silvaggi, N. R.; Wilson, D.; Tzipori, S.; Janda, K. D.; Allen, K. N. Catalytic features of the botulinum neurotoxin A light chain revealed by high resolution structure of an inhibitory peptide complex. *Biochemistry* **2008,** *47,* 5736-5745.

68. Čapková, K.; Yoneda, Y.; Dickerson, T. J.; Janda, K. D. Synthesis and structure-activity relationships of second-generation hydroxamate botulinum neurotoxin A protease inhibitors. *Bioorg. Med. Chem. Lett.* **2007,** *17,* 6463-6466.

69. Čapková, K.; Hixon, M. S.; Pellett, S.; Barbieri, J. T.; Johnson, E. A.; Janda, K. D. Benzylidene cyclopentenediones: first irreversible inhibitors against botulinum neurotoxin A's zinc endopeptidase. *Bioorg. Med. Chem. Lett.* **2010,** *20,* 206-208.

70. Stowe, G. N.; Šilhár, P.; Hixon, M. S.; Silvaggi, N. R.; Allen, K.; N.; Moe, S. T.; Jacobson, A. R.; Barbieri, J. T.; Janda, K. D. Chirality holds the key for potent inhibition of the botulinum neurotoxin serotype A protease. *Org. Lett.* **2010,** *12,* 756-759.

71. Hanson, M. A.; Oost, T. K.; Sukonpan, C.; Rich, D. H.; Stevens, R. C. Structural basis for BABIM inhibition of botulinum neurotoxin type B protease. *J. Am. Chem. Soc.* **2000,** *122,* 11268-11269.

72. Sreerama, N.; Woody, R. W. Estimation of protein secondary structure from circular dichroism spectra. *Anal. Biochem.* **2000,** *287,* 252-260.

73. Burnett, J. C.; Schmidt, J. J.; Stafford, R. G.; Panchal, R. G.; Nguyen, T. L.; Hermone, A. R.; Vennerstrom, J. L.; McGrath, C. F.; Lane, D. J.; Sausville, E. A.; Zaharevitz, D. W.; Gussio, R.; Bavari, s. Novel small molecule inhibitors of botulinum neurotoxin A metalloprotease activity. *Biochem. Biophys. Res. Commun.* **2003,** *310,* 84-93.

74. Burnett, J. C.; Opsenica, D.; Sriraghavan, K.; Panchal, R. G.; Ruthel, G.; Hermone, A. R.; Nguyen, T. L.; Kenny, T. A.; Lane, D. J.; McGrath, C. F.; Schmidt, J. J.; Vennerstrom, J. L.; Gussio, R.; Šolaja, B. A.; Bavari, S. A refined

pharmacophore potent 4-amino-7-chloroquinonline-based inhibitors of the botulinum neurotoxin serotype A metalloprotease. *J. Med. Chem.* **2007,** *50,* 2127-2136.

75. Šolaja, B. A.; Opsenica, D.; Smith, K. S.; Milhous, W. K.; Terzić, N.; Opsenica, I.; Burnett, J. C.; Nuss, J.; Gussio, R.; Bavari, S. Novel 4-aminoquinolines active against chloroquine-resistant and sensitive *P. falciparum* strains that also inhibit botulinum serotype A. *J. Med. Chem.* **2008,** *51,* 4388-4391.

76. Moe, S. T.; Thompson, A. B.; Smith, G. M.; Fredenburg, R. A.; Stein, R. L.; Jacobson, A. R. Botulinum neurotoxin serotype A inhibitors: Small-molecule mercaptoacetamide analogs. *J. Med. Chem.* **2009,** *17,* 3072-3079.

77. Burnett, J. C.; Wang, C.; Nuss, J. E.; Nguyen, T. L.; Hermone, A. R.; Schmidt, J. J.; Gussio, R.; Wipf, P.; Bavari, S. Pharmacophore-guided lead optimization: The rational design of a non-zinc coordinating, sub-micromolar inhibitor of the botulinum neurotoxin serotype a metalloprotease. *Bioorg. Med. Chem. Lett.* **2009,** *19,* 5811-5813.

78. Burnett, J. C.; Ruthel, G.; Stegmann, C. M.; Panchal, R. G.; Nguyen, T. L.; Hermone, A. R.; Stafford, R. G.; Lane, D. J.; Kenny, T. A.; McGrath, C. F.; Wipf, P.; Stahl, A. M.; Schmidt, J. J.; Gussio, R.; Brunger, A. T.; Bavari, S. Inhibition of metalloprotease botulinum serotype A from a pseudo-peptide binding mode to a small molecule that is active in primary neurons. *J. Biol. Chem.* **2007,** *282,* 5004-5014.

79. Park, J. G.; Sill, P. C.; Makiyi, E. F.; Garcia-Sosa, A. T.; Millard, C. B.; Schmidt, J. J.; Pang, Y. –P. Serotype-selective, small-molecule inhibitors of the zinc

endopeptidase of botulinum neurotoxin serotype A. *Bioorg. Med. Chem. Lett.* **2006,** *14,* 395-408.

80. Tang, J.; Park, J. W.; Millard, C. B.; Schmidt, J. J.; Pang, Y. P. Computer-aided lead optimization: improved small-molecule inhibitor of the zinc endopeptidase of botulinum neurotoxin serotype A. *PLoS ONE* **2007,** *2,* e761.

81. Kumaran, D.; Rawat, R.; Ludivico, M. L.; Ahmed, S. A.; Swaminathan, S. Structure- and substrate-based inhibitor design for *Clostidium botulinum* neurotoxin serotype A. *J. Biol. Chem.* **2008,** *283,* 18883-18891.

82. Young, W. B.; Sprengeler, P.; Shrader, W. D.; Li, Y.; Rai, R.; Verner, E.; Jenkins, T.; Fatheree, P.; Kolesnikov, A.; Janc, J. W.; Cregar, L.; Elrod, K.; Katz, B. Generation of potent coagulation protease inhibitors utilizing zinc-mediated chelation. *Bioorg. Med. Chem. Lett.* **2006,** *16,* 710-713.

83. Eubanks, L. M.; Hixon, M. S.; Jin, W.; Hong, S.; Clancy, C. M.; Tepp, W. H.; Baldwin, M. R.; Malizio, C. J.; Goodnough, M. C.; Barbieri, J. T.; Johnson, E. A.; Boger, D. L.; Dickerson, T. J.; Janda, K. D. An *in vitro* and *in vivo* disconnect uncovered through high-throughput identification of botulinum neurotoxin A antagonists. *Proc. Natl. Acad. Sci. USA* **2007**, *104*, 2602-2607.

84. Čapková K.; Salzameda, N. T.; Janda, K. D. Invstigations into small molecule non-peptideic inhibitors of the botulinum neurotoxins. *Toxicon* **2009,** *54,* 575-582.

85. Cordingley, M. G.; Callahan, P. L.; Sardana, V. V.; Garsky, V. M.; Colonno, R. J. Substrate requirements of human rhinovirus 3C protease for peptide cleavage in vitro. *J. Biol. Chem.* **1990**, *265*, 9062-9065.

86. Tsien, R. Y. The green fluorescent protein. *Annu. Rev. Biochem.* **1998,** *67,* 509-544.

87. Zimmer, M. Green fluorescent protein (GFP): applications, structure, and related photophysical behavior. *Chem. Rev.* **2002,** *102,* 759-782.

88. Yang, F.; Moss, L. G.; Phillips, G. N. Jr. The molecular structure of green fluorescent protein. *Nat. Biotechol*. **1996**, *14*, 1246-1251.

89. Ganesan, S.; Ameer-beg, S. M.; Ng, T. T. C.; Vojnovic, B.; Wouters, F. S. A dark yellow fluorescent protein (YFP)-based resonance energy-accepting chromoproein (REACh) for Förster resonance energy transfer with GFP. *Proc. Natl. Acad. Sci. USA* **2006**, *103*, 4089-4094.

90. Madani, F.; Lind, J.; Damberg, P.; Adams, S. R.; Tsien, R. Y.; Gräslund, A. O. Hairpin structure of a Biarsenical—tetracysteine motif determination by NMR spectroscopy. *J. Am. Chem. Soc.* **2009,** *131,* 4613-4615.

91. Wilkins, B. J.; Yang, X.; Cropp, T. A. Photochemical control of FlAsH labeling of proteins. *Bioorg. Med. Chem. Lett.* **2009,** *19,* 4296-4298.

92. Coleman, B. M.; Nisbet, R. M.; Han, S.; Cappai, R.; Hatters, D. M.; Hill, A. F. Conformational detection of prion protein with biarsenical labeling and FlAsH fluorescence. *Biochem. Biophys. Res. Commun.* **2009,** *380,* 564-568.

93. Krishnan, B.; Gierasch, L. M. Cross-stand split tetra-cys motifs as structure sensors in a β-sheet protein. *Chem. Biol.* **2008,** *15,* 1104-1115.

94. Chaumont, S.; Khakh, B. S. Patch-clamp coordinated spectroscopy shows $P2X_2$ receptor permeability dynamics require cytosolic domain rearrangements but not Panx-1 channels. *Proc. Natl. Acad. Sci. USA* **2008,** *105,* 12063-12068.

95. Turville, S. G.; Aravantinou, M.; Stössel, H.; Romani, N.; Robbiani, M. Resolution of *de novo* HIV production and trafficking in immature dendritic cells. *Nat. Methods* **2008,** *5,* 75-85.

96. Granier, S.; Kim, S.; Shafer, A. M.; Ratnala, V. R. P.; Fung, J. J.; Zare, R. N.; Kobilka, B. Structure and conformational changes in the C-terminal domain of the β2-adrenoceptor: insights from fluorescence resonance energy transfer studies. *J. Biol. Chem.* **2007,** *282,* 13895-13905.

97. Hoffmann, C.; Zürn, A.; Bünemann, M.; Lohse, M. J. Conformational changes in G-protein-coupled receptors—the quest for functionally selective conformations is open. *Br. J. Pharmcol.* **2008,** *153,* S358-S366.

98. Erster, O.; Eisenstein, M.; Liscovitch, M. Ligand interaction scan: a general method for engineering ligand-sensitive protein alleles. *Nat. Methods* **2007,** *4,* 393-395.

99. Blommel, P. G.; Fox, B. G. Fluorescence anisotropy assay for proteolysis of specifically labeled fusion proteins. *Anal. Biochem.* **2005,** *336,* 75-86.

100. Griffin, B. A.; Adams, S. R.; Tsien, R. Y. Specific covalent labeling of recombinant protein molecules inside live cells. *Science* **1998,** *281,* 269-272.

101. Luedtke, N. W.; Dexter, R. J.; Fried, D. B.; Schepartz, A. Surveying polypeptide and protein domain conformation and association with FlAsH and ReAsH. *Nat. Chem. Biol.* **2007,** *3,* 779-784.

102. Liu, B. archer, C. T.; Burdine, L.; Gillette, T. G.; Kodadek, T. Label transfer chemistry for the characterization of protein-protein interactions. *J. Am. Chem. Soc.* **2007,** *129,* 12348-12349.

103. Archer, C. T.; Burdine, L.; Liu, B.; Ferdous, A.; Johnston, S. A.; Kodadek, T. Physical and functional interactions of monoubiquitylated transactivators with the proteasome. *J. Biol. Chem.* **2008,** *283,* 21789-21798.

104. Romantsov, T.; Battle, A. R.; Hendel, J. L.; Martinac, B.; Wood. J. M. Protein Localization in *Escherichia coli* Cells: Comparison of the Cytoplasmic Membrane Proteins ProP, LacY, ProW, AqpZ, MscS, and MscL. *J. Bacteriol.* **2010,** *192,* 912-924.

105. Navaroli, D. M.; Melikian, H. E. Insertion of tetracysteine motifs into dopamine transporter extracellular domains. *PLoS One* **2010,** *5,* e9113.

106. Copeland, M. F.; Flickinger, S. T.; Tuson, H. H.; Weibel, D. B. Studying the dynamics of Flagella in multicellular communities of *Escherichia coli* by using biarsenical dyes. *Appl. Environ. Microbiol.* **2010,** *76,* 1241-1250.

107. Zhang, X. –Y.; Bishop, A. C. Site-specific incorporation of allosteric-inhibition sites in a protein tyrosine phosphatase. *J. Am. Chem. Soc.* **2007,** *129,* 3812-3813.

108. Zhang, X. –Y.; Bishop, A. C. Engineered inhibitor sensitivity in the WPD loop of a protein tyrosine phosphatase. *Biochemistry* **2008,** *47,* 4491-4500.

109. Bishop, A. C.; Chen, V. L. Brought to life: targeted activation of enzyme function with small molecules. *J. Chem. Biol.* **2009,** *2,* 1-9.

110. Brandt, T.; Petrovich, M.; Joerger, A. C.; Veprintsev, D. B. Conservation of DNA-binding specificity and oligomerisation properties within the p53 family. *BMC Genomics* **2009,** *10,* 628-641.

111. Andersen, M. A.; Schmitz-Salue, R.; Jakobs, S. Short tetracysteine tags to β-tubulin demonstrate the significance of small labels for live cell imaging. *Mol. Biol. Cell* **2004,** *15,* 5616-5622.

112. Gaietta, G. M.; Giepmans, B. N. G.; Deerinck, T. J.; Smith, W. B.; Ngan, L.; Llopis, J.; Adams, S. R.; Tsien, R. Y.; Ellisman, M. H. Golgi twins in late mitosis revealed by genetically encoded tags for live cells imaging and correlated electron microscopy. *Proc. Natl. Acad. Sci. USA* **2006,** *103,* 17777-17782.

113. Yan, P.; Xiong, Y.; Chen, B.; Negash, S.; Squier, T. C.; Mayer, M. U. Fluorophore-assisted light inactivation of calmodulin involves singlet-oxygen mediated cross-linking and methionine oxidation. *Biochemistry* **2006,** *45,* 4736-4748.

114. Mayer, M. U.; Shi, L.; Squier, T. C. One-step, non-denaturing isolation of an RNA polymerase enzyme complex using an improved multi-use affinity probe resin. *Mol. Biosyst.* **2005,** *1,* 53-56.

115. Chen, B.; Cao, H.; Yan, P.; Mayer, U.; Squier, T. Identification of an orthogonal peptide binding motif for biarsenical multiuse affinity probes. *Bioconjugate Chem.* **2007,** *18,* 1259-1265.

116. Wang, T.; Yan, P.; Squier, T. C.; Mayer, M. U. Prospecting the proteome: identification of naturally occurring binding motifs for biarsenical probes. *Chem. Bio. Chem.* **2007,** *8,* 1937-1940.

117. Hoffmann, C.; Gaietta, G.; Bünemann, M.; Adams, S. R.; Oberdorff-Maass, S.; Behr, B.; Vilardaga, J. –P.; Tsien, R. Y.; Ellisman, M. H.; Lohse, M. J. A FlAsH-

based FRET approach to determine G protein—coupled receptor activation in living cells. *Nat. Methods* **2005,** *2,* 171-176.

118. Maier-Peuschel, M.; Frölich, N.; Dees, C.; Hommers, L. G.; Hoffmann, C.; Nikolaev, V. O.; Lohse, M. J. A fluorescence resonance energy transfer-based M_2 Muscarinic receptor sensor reveals rapid kinetics of allosteric modulation. *J. Biol. Chem.* **2010,** *285,* 8793-8800.

119. Lin, M. Z.; Wang, L. Selective labeling of proteins with chemical probes in living cells. *Physiology* **2008,** *23,* 131-141.

120. Martin, B. R.; Giepmans, B. N. G.; Adams, S. R.; Tsien, R. Y. Mammalian cell–based optimization of the biarsenical-binding tetracysteine motif for improved fluorescence and affinity. *Nat. Biotechnol.* **2005,** *23,* 1308-1314.

121. Giepmans, B. N. G.; Adams, S. R.; Ellisman, M. H.; Tsien, R. Y. The fluorescent toolbox for assessing protein location and function. *Science* **2006,** *312,* 217-224.

122. Adams, S. R.; Campbell, R. E.; Gross, L. A.; Martin, B. R.; Walkup, G. K.; Yao, Y.; Llopis, J.; Tsien, R. Y. New biarsenical ligands and tetracysteine motifs for protein labeling in vitro and in vivo: synthesis and biological applications. *J. Am. Chem. Soc.* **2002,** *124,* 6063-6076.

123. Kumar, K. P.; Chatterji, D. Resonance energy transfer study on the proximity relationship between the GTP binding site and the Rifampicin binding site of *Escherichia coli* RNA polymerase. *Biochemistry* **1990,** *29,* 317-322.

124. Chowdhury, R. P.; Chatterji, D. Estimation of Foster's distance between two ends of Dps protein from mycobacteria: distance heterogeneity as a function of oligomerization and DNA binding. *Biophys. Chem.* **2007,** *128,* 19-29.

125. Adams, S. R.; Tsien, R. Y. Preparation of the membrane-permeant biarsenicals FlAsH-EDT_2 and ReAsH-EDT_2 for fluorescent labeling of tetracysteine-tagged proteins. *Nat. Protoc*. **2008**, *3*, 1527-1534.

126. Kukreja, R.; Singh, B. Biologically active novel conformational state of botulinum, the most poisonous poison. *J. Biol. Chem.* **2005,** *280,* 39346-39352.

127. Roxas-Duncan, V.; Enyedy, I.; Montgomery, V. A.; Eccard, V. S.; Carrington, M. A.; Lai, H.; Gul, N.; Yang, D. C. H.; Smith, L. A.; Yang, D. C. H. Identification and biochemical characterization of small-molecule inhibitors of Clostridium botulinum neurotoxin serotype A. *Antimicrob. Agents Chemother.* **2009**, *53,* 3478-3486.

128. Lai, H.; Feng, M.; Roxas-Duncan, V.; Dalshanamurthy, S.; Smith, L. A.; Yang, D. C. H. Quinolinal and peptide inhibitor of zinc protease in botulinum neurotoxin A: Effects of zinc ion and peptides on inhibition. *Arch. Biochem. Biophys.* 2009, *491,* 75-84.

129. Jones, J. G.; Poole, J. B.; Tomkinson, J. C.; Williams, R. J. P. The relationship between proton dissociation constants and the stability constants of complex ions. *J. Chem. Soc.* **1958,** 2001-2009.

130. Hunt, J. B.; Neece, S. H.; Ginsburg, A. The use of 4-(2-pyridylazo)resorcinol in studies of zinc release from *Escherichia coli* aspartate transcarbamoylase. *Anal. Biochem.* **1985,** *146,* 150-157.

131. Säbel, C. E.; Shepherd, J. L.; Siemann, S. A direct spectrophotometric method for the simultaneous determination of zinc and cobalt in metalloproteins using 4-(2-pyridylazo)resorcinol. *Anal. Biochem.* **2009,** *391,* 74-76.